Provenance of Late Paleozoic and Mesozoic sediment to key Arctic basins: implications for the opening of the Arctic Ocean

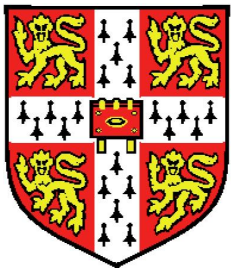

Jenny Eide Omma

Department of Earth Sciences

University of Cambridge

A thesis submitted for the degree of

Doctor of Philosophy

September 2009

Declaration

This thesis is my own work and contains nothing which is the outcome of work done in collaboration, except where specified in the text and acknowledgments. It does not exceed the page limit set by the degree committee of Earth Sciences and Geography and does not contain work that has been submitted for any degree, diploma or other qualification at another University.

Jenny Eide Omma
Gonville and Caius College, 2009

Abstract

The Arctic region is dominated by the Arctic Ocean, which contains two deep oceanic basins and is surrounded by the shallow shelves of Alaska, the Canadian Arctic Islands, Greenland, Scandinavia and the Russian Arctic. The Arctic Ocean basins, the Amerasia and Eurasia basins, formed by rifting and spreading during Cretaceous and Tertiary time. Whilst the tectonic history of the Eurasia Basin is fairly well understood, there is great uncertainty surrounding the opening history of the Amerasia Basin. It is unclear how various Arctic plates were juxtaposed prior to Amerasia Basin formation and when and how they separated.

The most commonly cited model for Amerasia Basin opening involves clockwise rotation of Arctic Alaska and the East Siberian Shelf away from the Canadian Arctic Islands during Early Cretaceous time. Other Amerasia Basin opening models reject the rotation hypothesis and suggest the oceanic basin may have formed by a variety of different mechanisms.

This project aims to test Amerasia Basin opening models by utilizing the provenance of Late Paleozoic and Mesozoic clastic sediments on the northern margins of the sedimentary basins surrounding the Amerasia Basin. Sediment from the northern Sverdrup Basin, Svalbard, the southwestern Barents Shelf and Taimyr are studied using petrography, heavy mineral analysis, mineral chemistry of garnet and tourmaline and zircon geochronology.

The results of this work show that two main areas acted as a sediment source to the northern Sverdrup Basin and Barents Shelf (including Svalbard) during Mesozoic time: the Uralian Orogen and Baltic Shield. A rotational model for the opening of the entire Amerasia Basin is not supported by these findings. Instead, a more complicated Amerasia Basin opening history is envisaged, possibly including large areas of continental crust flooring the Central Arctic Ocean.

Acknowledgments

I thank my supervisors, Robert Scott, Andrew Morton and Nick McCave for their valuable contributions and guidance throughout the project. Vicky Pease provided additional supervision, which was greatly appreciated.

The project was made possible through the funding from Total Norge AS, coordinated by Henri-Christian Mathieu and Jean-Jacque Biteau. I warmly thank them for their contribution and gratefully acknowledge additional funding from the University of Cambridge. The CASP Arctic Project subscribing companies also provided generous funds for the research, for which I am very thankful.

There are many people at CASP who have provided support throughout the project and to whom I owe great thanks. Christine Brouet-Menzies, Andrew Whitham and Robert Scott arranged my studentship. Clive Johnson and Mary Rodger organized fieldwork logistics. Stewart Sinclair, Jamie Stewart, Benoit Vautravers and Almar de Ronde provided computer support. Tina Walker dealt with my complicated accounts. All my colleagues at CASP have made it a very pleasant place to work and this has been greatly appreciated.

I have analysed samples from several external organizations, without which this project would not have been possible. I gratefully acknowledge these collaborators. Simon Kelly of CASP provided Cambridge Spitsbergen Expedition samples, collected by John Parker and Simon Kelly. Ashton Embry of the Geological Survey of Canada provided Axel Heiberg Island samples. Steve Matthews, Gary Pelka and Sandy Phillips of BP facilitated a sampling trip to Anchorage, Alaska to sample cores. John Reeder and Susan Browne of the Minerals Store, Eagle River, Alaska provided access to additional core samples.

Thin sections were prepared by Keith Gray of the Department of Earth Sciences, University of Cambridge and John Coundon of Petrotech. Heavy mineral separates were prepared by Lee Clarke of Palynoservices.

Sample analysis was carried out in several laboratories and I thank all those who taught me to use the analytical equipment required. Martin Whitehouse,

Lev Ilyinsky and Kerstin Lindén provided help at the Nordsim ionprobe facility in Stockholm. Andy Carter of University College London provided help with LAICPMS analysis. Stephen Reed and Martin Walker provided help with the scanning electron microscope at the Department of Earth Sciences, University of Cambridge. Andy Buckley and Chiara Petrone provided help with the electron microscope at the Department of Earth Sciences, University of Cambridge.

I have been encouraged during the course of this project by the many useful discussions from peers and colleagues. Thanks to Peter Friend, Bob White and Bryan Lovell for giving helpful feedback on the project. Thanks to George Morris for company on two Arctic Canada field seasons and to Robert Duller for company and help in Anchorage, Alaska.

I would like to thank my friends for making my time in Cambridge very enjoyable. Warmest thanks go to my family for their constant care and support. I also owe the greatest thanks to Alex, whose help and support has been invaluable throughout the entire project.

Contents

List of Figures

List of Tables

Chapter 1

Introduction

1.1 Project rationale

The Arctic region is an area of increasing geopolitical importance. Rapid climate change is affecting Arctic sea-ice distribution and disturbing Arctic ecosystems, indigenous populations and global weather patterns. A recent assessment by the United States Geological Survey estimated that the Arctic contains more than 20% of the world's recoverable petroleum resources (Bird *et al.*, 2008). This hydrocarbon potential, along with other economic opportunities presented by an increasingly ice-free Arctic region, has intensified territorial disputes between countries bordering the Arctic Ocean. These countries (Russia, Norway, Denmark, Canada and USA) are presently submitting territorial claims under the UN Convention on the Law of the Sea. Sovereignty of offshore areas will be rewarded for the 'natural prolongation' of a country's continental shelf and thus geological studies in the region strongly affect political realities. This is particularly important as many fundamental issues of Arctic tectonic evolution remain unresolved. Jurassic-Recent spreading formed the Arctic Ocean, but the geometry and timing of this spreading and thus the pre-Jurassic plate configuration remain unclear.

1.2 Project aims

This thesis examines the validity of published Arctic Ocean opening models by applying sediment provenance techniques to Late Paleozoic-Mesozoic sediments in key Arctic basins: the Sverdrup Basin, the Barents Shelf including Svalbard and the Taimyr Peninsula (Fig. 1.1). These sediments may in part have been derived from the area now occupied by the Arctic Ocean. Sediment provenance techniques utilize the study of the mineral assemblages of clastic sediment to gain information

on the transport pathways and source areas of a sediment. This can ultimately provide clues about the sediment source areas and plate configurations at the time of deposition.

1.3 Thesis outline

Chapter 2 reviews the Archean to Recent tectonic history of the Arctic region. The uncertainty surrounding the Mesozoic opening of the Arctic Ocean is discussed and models of the opening of the Arctic Ocean are presented and evaluated. Published provenance studies in the Arctic region are outlined.

Chapter 3 describes the analytical techniques used in this study: sediment petrography, heavy mineral analysis, single mineral geochemistry and zircon geochronology.

Chapter 4 discusses the depositional setting and provenance of Mesozoic sediments on Axel Heiberg Island, northern Sverdrup Basin, Canadian Arctic Islands. Fieldwork was carried out on northwestern Axel Heiberg Island in 2007. Outcrop samples collected by Ashton Embry of the Geological Survey of Canada are also included in this study.

Chapter 5 discusses the Mesozoic depositional setting and provenance of sediments from the Barents Shelf using samples from two areas: Svalbard and the southwestern Barents Shelf. The Svalbard study is based on outcrop samples collected during Cambridge Spitsbergen Expedition field seasons. The Barents Shelf study uses hydrocarbon core samples collected from the Norwegian Petroleum Institute core facility in Stavanger, Norway.

Chapter 6 discusses the depositional setting and provenance of Late Paleozoic and Mesozoic samples from the Taimyr Peninsula, Arctic Russia. This study uses outcrop samples collected by CASP geologists and Per Möller of Lund University.

Chapter 7 combines and discusses the results presented in chapters 4 to 6 and offers constraints on Arctic Ocean opening models.

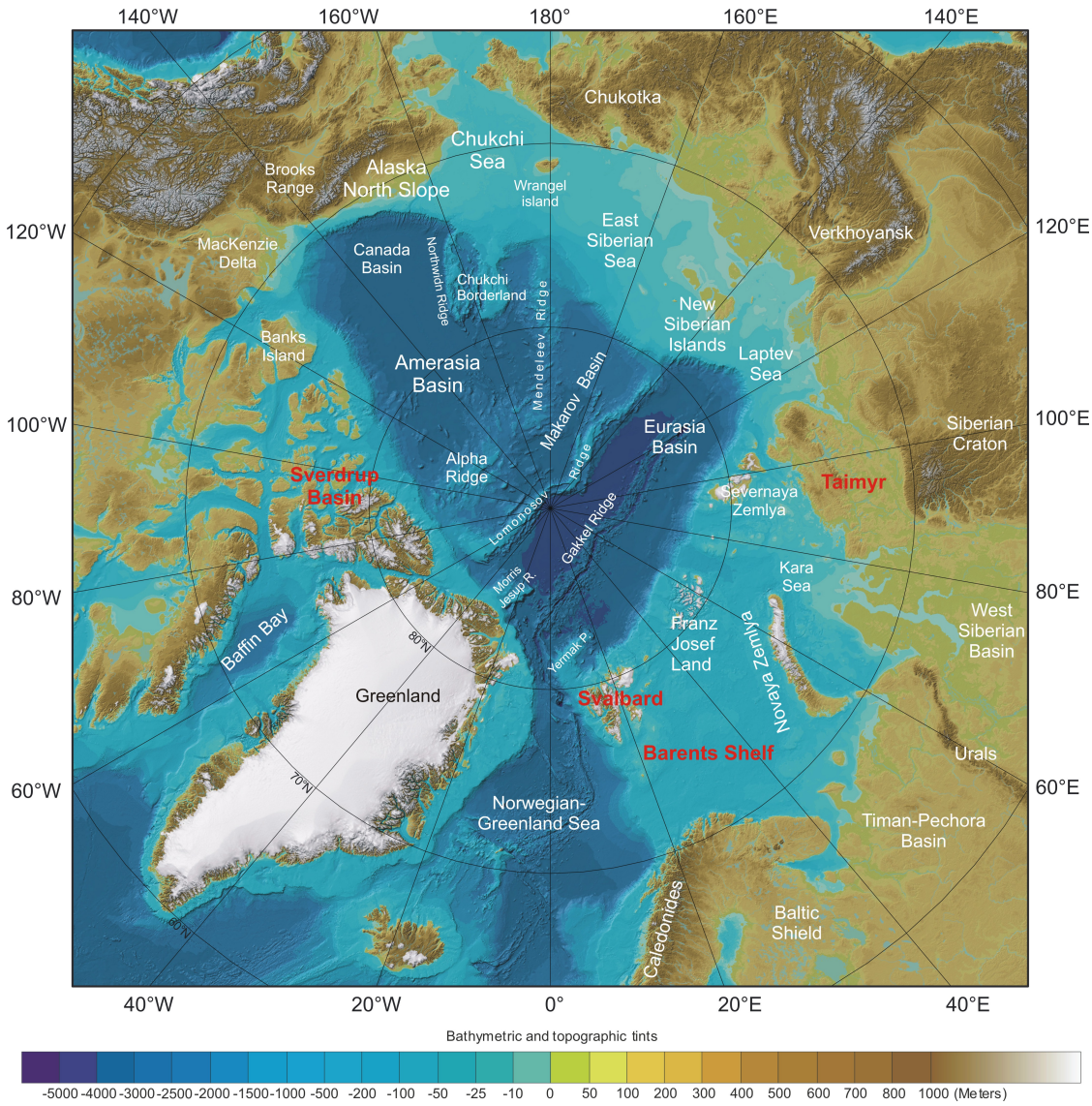

Figure 1.1: Location map of the Arctic region. Bathymetry and topography are from the IBCAO Arctic Bathymetry database (Jakobsson *et al.*, 2008). Study areas are indicated in red.

Chapter 2

Tectonic history of the Arctic region

2.1 Introduction

The Arctic region is dominated by the Arctic Ocean, which is almost entirely surrounded by the continental shelves of Alaska, Arctic Canada, Greenland, the Barents Shelf and the Russian Arctic Shelf (Fig. 1.1). The Arctic Ocean can be divided into two deep-water oceanic basins: the Amerasia and Eurasia basins, which are separated by the submarine Lomonosov Ridge.

Fundamental questions of Arctic tectonics remain unanswered due to lack of data. Outstanding questions include the location of major plate boundaries, affinities of key Arctic terranes, nature and extent of tectonic events and the presence or absence of continental crust in the Arctic Ocean basins (Fig. 2.1). Harrison (2005) provides a detailed review Arctic tectonic evolution and Lawver *et al.* (1990) review Arctic Ocean opening models as of 1990. Grantz *et al.* (2009) present a map of tectonic elements and sedimentary successions of the Arctic.

This section introduces the main points of Arctic tectonic evolution, outlines the physical characteristics of Arctic bathymetric features and presents Arctic Ocean opening models. The role of sediment provenance for constraining Arctic region tectonic evolution is explained.

2.2 Precambrian shield areas

The oldest exposed continental blocks in the Arctic region are Late Archean (3100-2600 Ma) and include the Rae and Slave terranes of Laurentia, the Kola and Karelia terranes of the Baltic Shield and the Magan and Daldyn terranes of the

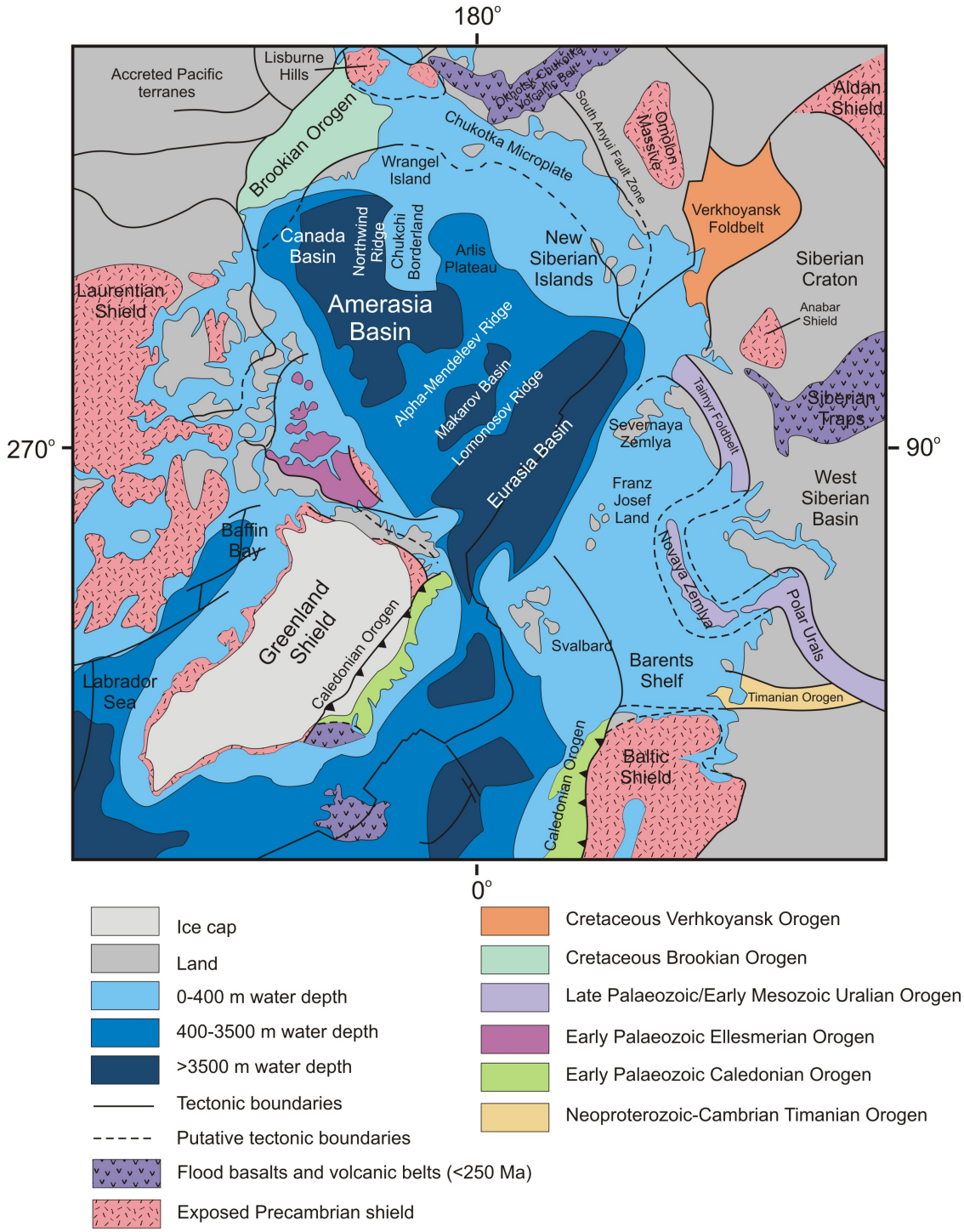

Figure 2.1: Tectonic map of the Arctic region. Bathymetry and topography are modified after the IBCAO Arctic Bathymetry database (Jakobsson *et al.*, 2008). Plate boundaries and geological features are modified after Harrison (2005). Neoproterozoic and younger orogenic belts on land are shown with different shadings.

eastern Russian Anabar Shield (Fig. 2.2). These areas preserve some of the oldest rocks on Earth, for example the early Archean Amitsoq gneiss and Isua sequence in southwest Greenland (Nutman *et al.*, 1996). The important Arctic cratons, Siberia, Baltica and Laurentia, were amalgamated by late Paleoproterozoic time (1800 Ma) (Harrison, 2005) (Fig. 2.2). The nature and affinity of some Arctic Precambrian shield areas is not well understood, including the Barents-Kara block (underlying large parts of the Barents Shelf/Kara Sea), the Pearya terrane (northern Ellesmere Island), the basement underlying the North Slope of Alaska and the Chukchi Shelf and basement underlying much of northeastern Russia, east of the Verkhoyansk mountains (Fig. 2.1).

2.3 Rodinia: Mesoproterozoic to Neoproterozoic tectonic evolution

Large areas of the Siberia, Baltica and Laurentia cratons are covered by Meso-Neoproterozoic sediments. In the Arctic region these sediments were largely undeformed during Meso- and Neoproterozoic time. The exception is sediments found on the Pearya terrane (northern Ellesmere Island), Svalbard, East Greenland, Taimyr and Norway where strata are highly deformed, metamorphosed and intruded by 1100-950 Ma felsic plutonic rocks. This deformation is linked with the 1200-950 Ma Grenville Orogeny, which continued along southern Scandinavia and Labrador through to the southwestern United States as part of the amalgamation of the Rodinia supercontinent (Rivers, 1997).

Rodinia assembled between 1300 and 900 Ma during a series of worldwide orogenic events (Li *et al.*, 2008). The precise configuration of Arctic terranes within the Rodinia supercontinent is not well known. Least controversial is the restoration of West Greenland onto the eastern margin of Laurentia, a position it held until Cretaceous rifting opened the Labrador Sea and Baffin Bay (Harrison, 2005). In most models, Baltica is reconstructed to a position along the southeast margin of Greenland and the Barents-Kara block to the northeast margin of Greenland. There is much debate regarding the position of the Siberia craton within the Rodinia supercontinent (Li *et al.*, 2008). Some models reconstruct the northern-eastern margin of Siberia to the western margin of Laurentia (e.g. Sears & Price, 2003) (Fig. 2.2). Other authors, for example Condie & Rosen (1994), place the northern and eastern margin of Siberia north of the Canadian Arctic Islands in the Late Proterozoic. Palaeomagnetic data do not constrain the distance between Laurentia and Siberia during Meso- and Neoproterozoic time. This opens the possibility that

other terranes were located between the two cratons, for example Arctida (Zonenshain *et al.*, 1990) or other Arctic terranes, including northern Alaska, Chukchi Peninsula, Wrangel Island, the New Siberian Islands and the northern Kara block. The position of these blocks within Rodinia is not well understood (Li *et al.*, 2008 and references therein).

The break-up of Rodinia was initiated in Neoproterozoic time (around 825 Ma) and lasted until approximately 570 Ma (Li *et al.*, 2008). In the Arctic region, the emplacement of three major dyke swarms at 780 Ma (Tzetzotene swarm, northwestern Laurentia), 723 Ma (Franklin swarm, northern Laurentia) and 615 Ma (Balto-Scandian swarm, Scandinavia and northern Newfoundland) are attributed to the breakup of Rodinia (Harrison, 2005) (Fig. 2.2). Rift-related sedimentation occurred during Late Neoproterozoic time and deposition of thick sediment wedges developed on Cambrian and younger post-Rodinia continental margins. Many early Paleozoic margins developed stable shelf depositional environments while other margins were being deformed in the concurrent assembly of the Gondwanaland and Pangaea supercontinents in Neoproterozoic though Paleozoic time (600-250 Ma) (Li *et al.*, 2008).

2.4 Pangaea: Neoproterozoic to Paleozoic tectonic evolution

During Neoproterozoic through Paleozoic time several orogenic events contributed to the formation of the Pangaea supercontinent in the Arctic region: the Timanian, Caledonian, Ellesmerian and Uralian events. The precise interrelationship between these tectonic events is poorly understood and major questions about the real extent of each orogeny, the timing, geodynamics and deformation mechanisms remain unanswered.

Timanian Orogeny

The first orogenic event associated with the amalgamation of Pangaea in the Arctic region was the Late Neoproterozoic-Cambrian Timanian Orogeny (600-575 Ma). The orogen extends for at least 3000 km, from the Varanger Peninsula of northern Norway to the South Ural mountains in Kazakhstan. In this event, crust of unknown affinity was accreted to the northern margin of Baltica (Siedlecka *et al.*, 2004). Crust of the Timanide Orogen crops out in the Timan Range of northwestern Russia, sections of the Urals mountain chain, Novaya Zemlya and coastal

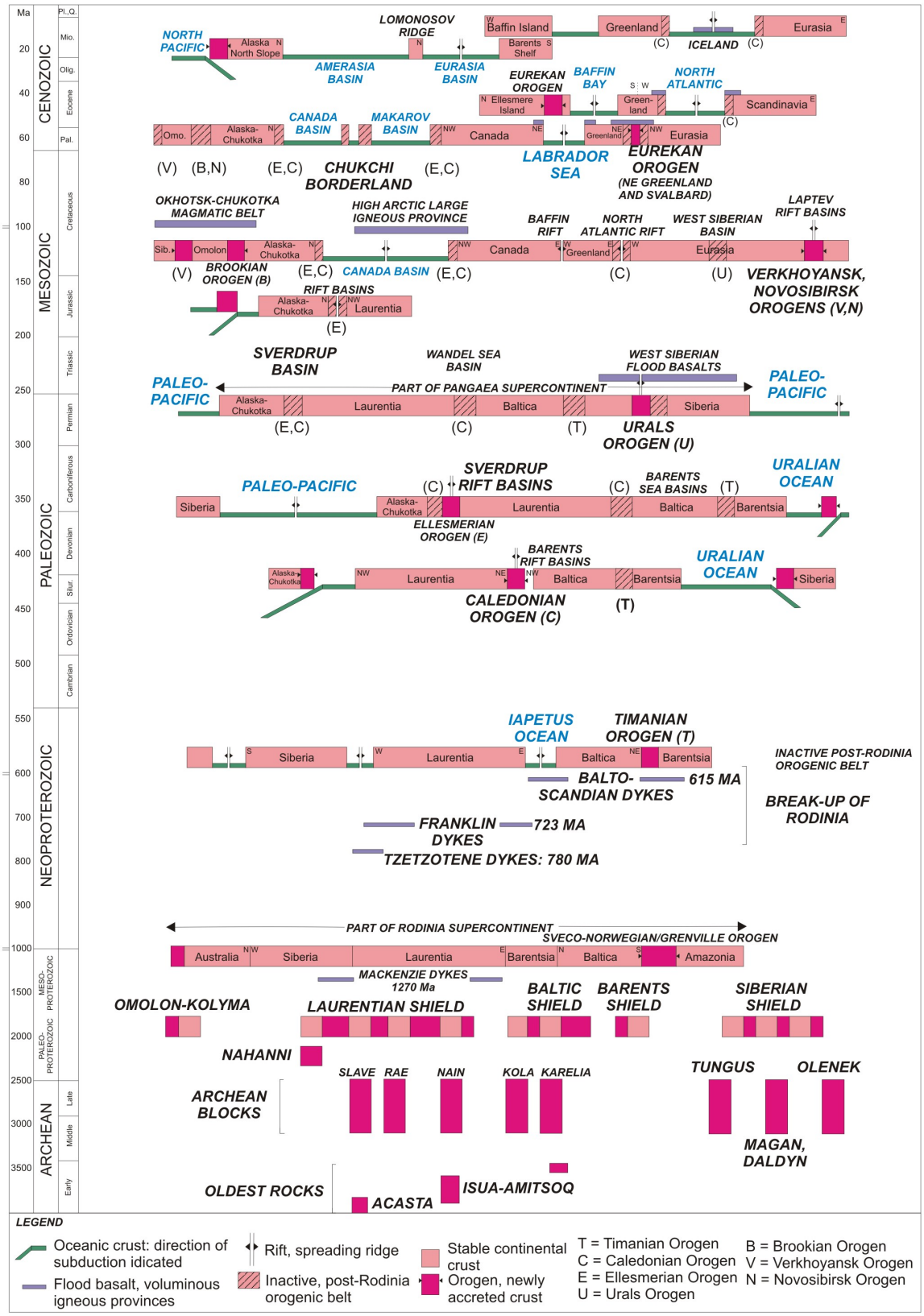

Figure 2.2: Tectonic evolution of the Arctic region from Archean time to present modified after Harrison (2005).

regions of the Barents Sea in Russia and Norway, and underlies the Timan-Pechora Basin and parts of the Barents Shelf (Gee & Pease, 2004).

Caledonian Orogeny

During late Early Silurian to late Early Devonian time (the Scandian phase of the Caledonian Orogeny) the western margin of Baltica collided with the eastern margin of Laurentia (Lawver *et al.*, 2002). In this event, Pearya and possibly Chukotka were amalgamated to Laurentia, forming Laurussia (Lawver *et al.*, 2002).

There is uncertainty over how far the Caledonian Orogeny continues into the Arctic region. Many authors have proposed that the orogeny connects to the Innutian Orogen (formed by the Devonian-Carboniferous Ellesmerian Orogeny and the Cenozoic Eurekan Orogeny). Ziegler (1988, 1989) suggested that the orogens were directly linked, through the Svalbard Archipelago. Doré (1991) and Gudlaugsson *et al.* (1998) suggested a bifurcation of the Caledonian Orogeny, with one strand continuing northeastwards across the Barents Shelf and another strand connecting to the Innutian Orogen via Svalbard.

McKerrow *et al.* (2000) proposed to expand the Caledonian Orogeny of northwestern Europe to include all Late Cambrian to Late Devonian tectonic events associated with the closure of the Iapetus Ocean between Laurussia in the northwest and Baltica and Avalonia in the southeast and east. The Iapetus Ocean in the Arctic region continued as far as Arctic Alaska. Kos'ko *et al.* (1993) suggested that the Scandian Orogeny led to the suturing of Chukotka and Arctic Alaska. Evidence of Scandian-age deformation may also be seen in Arctic Alaska, as evidenced by a strongly deformed sequence of Ordovician and Silurian sediments (Carter & Laufield, 1975), overlain by steeply dipping, unmetamorphosed Middle (perhaps Lower) Devonian redbeds (Moore *et al.*, 1994).

Ellesmerian deformation

During Late Devonian-Early Carboniferous time, a tectonic event along the northern margin of Laurussia produced the Ellesmerian Orogeny (Trettin, 1991), affecting East and North Greenland, Svalbard, the Canadian Arctic Islands, Arctic Alaska and possibly other Arctic regions. The extent, nature and precise timing of the Ellesmerian Orogeny are all poorly understood, as is the correlation of events between regions (e.g. Thorsteinsson & Tozer, 1970; Trettin, 1991; Higgins *et al.*, 2000). The geodynamic cause of the so-called orogeny is uncertain, and we have an incomplete understanding of which plates were involved in the collision. The

Ellesmerian Orogeny correlates in age to the Svalbardian phase of the Caledonian Orogeny (McKerrow *et al.*, 2000) although it is disputed whether the Ellesmerian Orogeny is older and thus is the same event as the Scandian phase of the Caledonian Orogeny, as suggested by Lawver *et al.* (2002); McKerrow *et al.* (2000); Ziegler (1988, 1989). For example, the emplacement of Pearya onto the northern margin of Laurentia (today forming northern Ellesmere Island) regarded as an Ellesmerian event, occurred during late Early Silurian to Late Silurian time (Trettin, 1991).

Uralian Orogeny

During Carboniferous time, closure of the Uralian Ocean between Baltica and the Kasakhstan plate and the closure of the paleo-Asian Ocean between the Kasakhstan plate and Siberia formed the Eurasia continent (Hamilton, 1970; Zonenshain *et al.*, 1984). The Uralian Orogen stretches more than 4000 km from the Aral Sea in the south to the Taimyr Peninsula in the north, with variations in geometry and age of deformation along the length of the orogen. In particular, in Novaya Zemlya and the Taimyr Peninsula, deformation continued into early Mesozoic time (Inger *et al.*, 1999).

At the Permo-Triassic boundary (252 Ma), the Siberian flood basalts were formed and several kilometres of volcanic rocks were extruded over a vast area in less than two million years (Reichow *et al.*, 2009). Mafic extrusive and intrusive rocks of this event are found on the Siberian Platform, the Western Siberian lowlands and the Taimyr Peninsula (Kamo *et al.*, 2003). The West Siberian Basin formed during Early Triassic time on the accreted terranes involved in the Uralian collision (Hamilton, 1970; Zonenshain *et al.*, 1984).

2.5 Mesozoic-Cenozoic tectonic evolution

During Mesozoic and Cenozoic time, the current plate tectonic framework in the Arctic region became established. The most important tectonic events were widespread rifting (leading to the opening of the Arctic Ocean basins) and the growth of several important Cretaceous to Cenozoic orogenic events affecting Arctic landmasses. Cenozoic uplift and erosion took place as a result of complex plate interactions and later glaciations.

Amerasia Basin formation

The Amerasia Basin is generally considered to be of Jurassic-Cretaceous age, although the formation of the basin is not well understood. The spreading geometries are controversial, data are sparse and there is no easily interpretable pattern of magnetic anomalies or an active spreading centre. Furthermore, fundamental questions remain about the nature and origin of component features in the basin. Section 2.7 covers the evolution of the Amerasia Basin in detail. The opening of the Amerasia Basin is the main concern of this thesis.

Eurasia Basin formation

During Late Cretaceous time, central Atlantic seafloor spreading propagated into the Labrador Sea and Baffin Bay (Lawver *et al.*, 2002). During Cenozoic time, spreading also commenced between Norway and Greenland, continuing northwards to form the Eurasia Basin.

The Eurasia Basin is bounded by the Laptev, Barents-Kara and North Greenland margins and by the Lomonosov Ridge. The basin contains the ultra slow spreading Gakkel Ridge, a continuation of the North Atlantic spreading system (e.g. Eldholm *et al.*, 1990; Kristoffersen, 1990, 2000) (Fig. 2.1). The opening history of the Eurasia Basin is reasonably well constrained by a pattern of linear magnetic anomalies in oceanic crust (Karasik, 1968; Vogt *et al.*, 1979a; Glebovsky *et al.*, 2000) (Fig. 2.4). Spreading commenced on the Gakkel Ridge in Palaeocene-Eocene time (∼55 Ma; anomaly 24R or 25R) (Glebovsky *et al.*, 2000; Brozena, 2003), rendering the Lomonosov Ridge a microcontinental fragment. Reconstructing the Lomonosov Ridge back to the Barents-Kara margin shows the extremely good fit of this bathymetric feature along most of its 1700 km length (Fig. 2.3). However, the fit of the reconstructed Lomonosov Ridge is poor at the Laptev margin of the Eurasia Basin, possibly explained by the presence of several large transform faults (Scott *et al.*, 2004).

Cretaceous to Cenozoic events

During Late Jurassic time, the Arctic Alaska plate became the Arctic Alaska composite terrane by the accretion of Pacific terranes from the south, an accretion that is still ongoing (Plafker & Berg, 1994). The Brooks Range-Novosibirsk-Chukchi Orogen was formed by the mid Cretaceous collision between the Arctic Alaska and Chukotka terranes with Pacific terranes, closing the South Anyui Basin and forming the South Anyui Suture (Harrison, 2005). It stretches from northern Yukon,

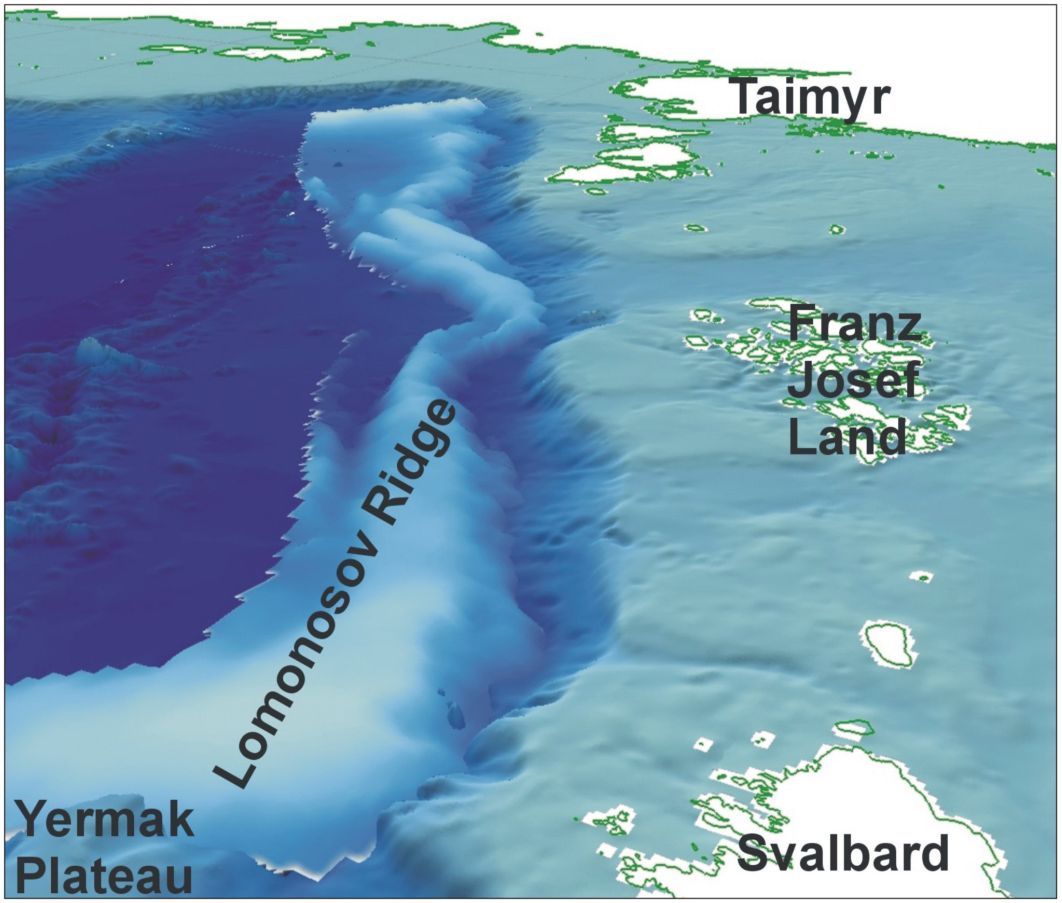

Figure 2.3: Restoration of the Lomonosov Ridge against the Barents/Kara Shelf, on a 3D bathymetric map, showing an excellent fit prior to the opening of the Eurasia Basin. The ridge was reconstructed in 3D GIS using Brozena (2003) magnetic anomaly picks and a finite rotation pole for 55 Ma (Scott *et al.*, 2004).

the Brooks Range of Northern Alaska, and fold belts in the Russian Far East, although the exact extent of the orogen under the Arctic shallow shelves is unclear (Plafker & Berg, 1994). The Verkhoyansk fold belt can be traced along the eastern margin of the Siberian craton from the Sea of Okhotsk to the Lena Delta (Fig. 2.1). This fold belt was formed by the accretion of the Kolyma-Omolon terrane to the Siberian craton during Early Cretaceous to early Late Cretaceous time (Harrison, 2005).

The occurrence of Early Cretaceous igneous activity in several Arctic areas (Svalbard, Franz Josef Land, De Long Islands, Canadian Arctic Islands) has been interpreted as a large igneous province centred on the Alpha Ridge (Maher, 2001; Tarduno, 1998). Geochronological and stratigraphic evidence suggests that there

were two main pulses of igneous activity, in Barremian and Albian time (Maher, 2001).

The thin-skinned Eurekan Orogeny formed during late Paleocene-Eocene time in Svalbard, North Greenland and the northern Canadian Arctic Islands, from Ellesmere to Prince Patrick Island (e.g. Thorsteinsson & Tozer, 1970; Trettin, 1991). It represents the tectonic response to the northward movement of the Greenland plate during seafloor spreading in the Labrador Sea between 62 and 33 Ma and on North Atlantic and Arctic ridges between 57 and 33 Ma (e.g. Thorsteinsson & Tozer, 1970; Trettin, 1991).

2.6 Amerasia Basin bathymetric features

The Amerasia Basin comprises all features to the west of the Lomonosov Ridge, including the Canada and Makarov basins, Chukchi Borderland and the Alpha-Mendeleev Ridge. The geometry and timing of Amerasia Basin formation is a topic of long-standing debate. The basin does not contain an active spreading centre and the complex geophysical signature suggests that the opening mechanism is not simple (Fig. 2.4). A wide variety of opening models have been proposed, the most important of which are outlined below. In order to understand the opening of the Amerasia Basin, we must have an overview of the important bathymetric features in the basin.

Lomonosov Ridge

The Lomonosov Ridge is a ∼1700 km long, narrow ridge that divides the Arctic Ocean into the Eurasia and Amerasia basins (Fig. 1.1). The ridge trends from offshore Ellesmere Island to the north of the New Siberian Islands, approximately via the North Pole with a ridge crest at 500 m depth. The ridge is 45-150 km wide. The Lomonosov Ridge was originally part of the Barents/Kara margin and rifted off to form a microcontinental sliver as a result of the opening of the Eurasia Basin in Paleocene-Eocene to Recent time (Fig. 2.3).

Ridge morphology (IBCAO digital bathymetric grid, Jakobsson *et al.*, 2000, 2008), velocity profiles (ARCTIC'91 reflection data, Jokat *et al.*, 1992, 1995) and sampling (piston core samples, Grantz *et al.*, 2001) corroborate the continental nature of the ridge. The Lomonosov Ridge is composed of a series of sub-parallel ridges, interpreted as fault blocks (Jokat *et al.*, 1992, 1995). Change in character along the ridge may also be attributed to changes in basement type, as would be

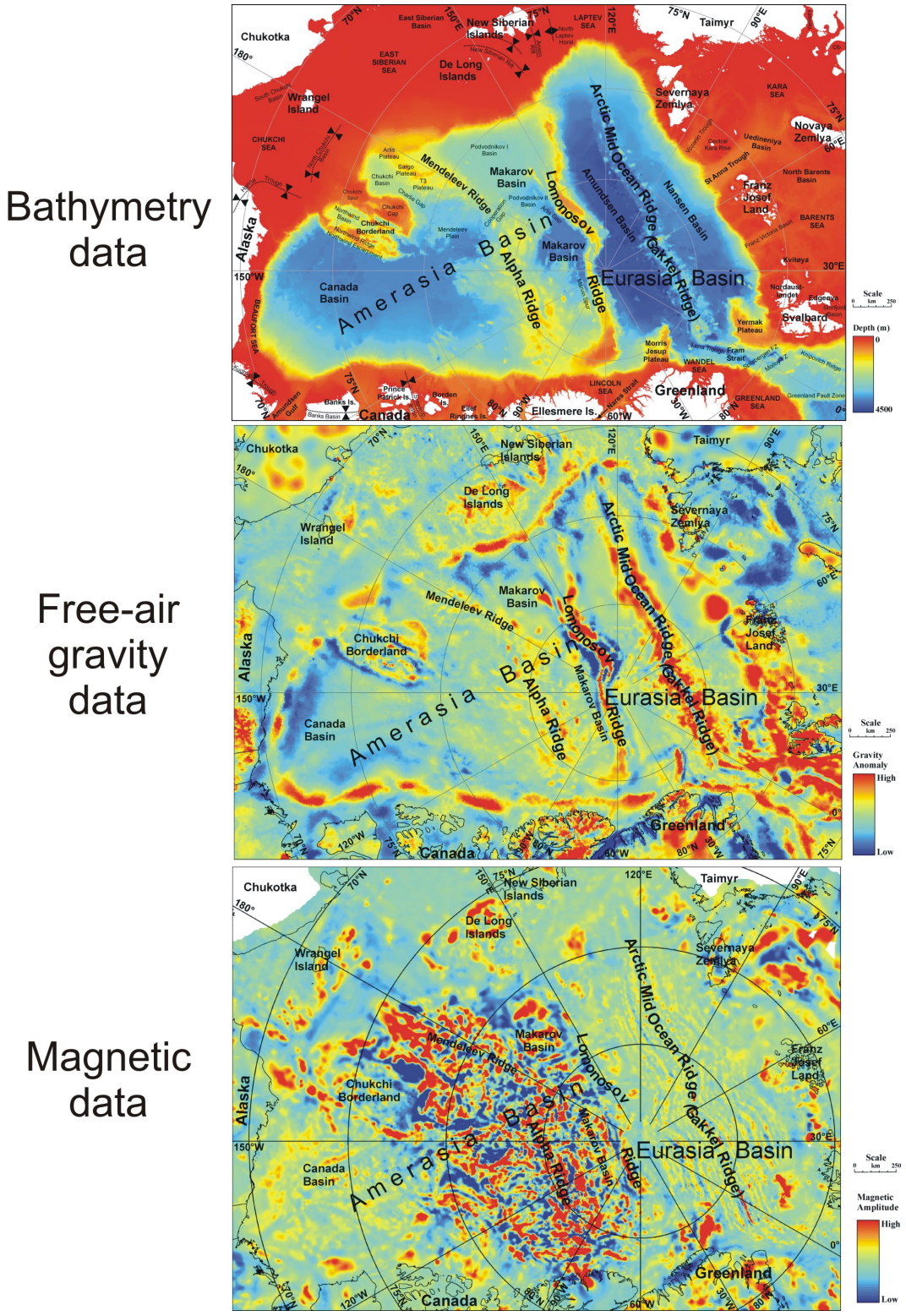

Figure 2.4: Bathymetry, free-air gravity and magnetic datasets for the Arctic region. The bathymetry dataset is modified after Jakobsson *et al.* (2000). The free-air gravity dataset is compiled from the Arctic Gravity Project (Forsberg & Kenyon, 2004). The magnetic dataset is compiled from unpublished data from Glebovsky and Kovacs (Scott *et al.*, 2004).

expected from extrapolation from the adjacent Barents/Kara margin (Scott *et al.*, 2004).

The Lomonosov Ridge is covered by an approximately 500 m thick package of subhorizontal strata (Jokat *et al.*, 1992, 1995). Dipping but parallel strata can be seen overlying tilted fault blocks.

Makarov-Podvodnikov Basin

The Makarov-Podvodnikov Basin is a triangular basin that lies between the Lomonosov and Alpha-Mendeleev ridges and has a free-air gravity signal similar to these ridges (Figs. 1.1 and 2.4). Evidence from prograding sediment wedges suggests the Makarov-Podvodnikov Basin is older than the Eurasia Basin. Poor data resolution does not allow the identification of any possible extinct spreading ridges, although many workers consider the basin to be underlain by thick oceanic crust (e.g. Weber & Sweeney, 1990). The basin has a variable water depth, deepening abruptly stepwise from the Siberian margin. The age and nature of the basin are disputed and are intimately linked with the nature of the Alpha-Mendeleev Ridge (e.g. Lawver & Muller, 1994). Absence of clear magnetic anomalies, seismic data and basement samples do not allow the elimination of the possibility of continental crust in the basement, in particular in areas close to the Siberian margin (e.g. Lebedeva-Ivanova *et al.*, 2003).

Alpha-Mendeleev Ridge

The Alpha-Mendeleev Ridge crosses the entire Amerasia Basin and subdivides it into the Canada and Makarov-Podvodnikov basins (Fig. 1.1). The ridge is between 250 and 800 km wide and has an overall kinked morphology and variable bathymetry, composed of numerous isolated peaks and ridges in a number of orientations. The ridge is undoubtedly the most controversial bathymetric feature in the Arctic Ocean. It has been interpreted as:

1. an extinct spreading centre (e.g. Hall, 1970; Vogt & Ostenso, 1970; Ostenso & Wold, 1971).

2. an extinct island arc system (e.g. Herron *et al.*, 1974).

3. an oceanic plateau produced by hot-spot volcanism (e.g. Vogt *et al.*, 1979b; Lawver & Muller, 1994; Lawver *et al.*, 1984, 1990, 2002; Forsyth *et al.*, 1986; Grantz *et al.*, 1998, 2001; Jokat, 2003; Weber & Sweeney, 1990).

4. a continental crust fragment, containing various amounts of mafic volcanism (e.g. King *et al.*, 1966; Sweeney, 1990; Green *et al.*, 1984; Weber & Sweeney, 1990; Zonenshain *et al.*, 1990; Johnson *et al.*, 1994; Astafurova *et al.*, 2003; Kaban'kov *et al.*, 2003; Kaminsky *et al.*, 2003; Zamanskii *et al.*, 2003; Zatzepin *et al.*, 2003).

There is little evidence in support of a spreading centre origin for the Alpha-Mendeleev Ridge. Evidence from the rest of the Amerasia Basin suggests that the basin is Cretaceous age and the ridge is too elevated for a spreading centre of this age. There is also no evidence in support of an island arc origin for the ridge. No arc-related volcanism has been found, no trench has been imaged and the ridge contains right-angle bends, not compatible with an arc.

The interpretation that the ridge is an oceanic plateau produced by hot-spot volcanism is favoured by many researchers. They point to the thick crust of the ridge (up to 37 km thick) and relatively uniform, high crustal velocities, the proven presence of basalt, and geophysical and morphological similarities with the Greenland-Iceland-Faroes Ridge. There is abundant Cretaceous basaltic volcanism around the margins of the Arctic Ocean (e.g. Maher, 2001; Tarduno, 2003; Damaske & Estrada, 2003; Villeneuve & Williamson, 2003) in support of this interpretation. Some workers (e.g. Lawver & Muller, 1994; Lawver *et al.*, 2002) interpret the Alpha-Mendeleev Ridge as the Cretaceous expression of the Iceland plume.

However, it is still plausible that the Alpha-Mendeleev Ridge contains continental crust. The ridge has a complex bathymetry and gravity signature, and a morphology that is similar to an extensional regime, showing apparent rift flanks. The overall shape and orientation of the ridge is similar to the continental Lomonosov Ridge, further evidence for a an attenuated continental crust origin (Scott *et al.*, 2004).

Canada Basin

The Canada Basin is an approximately triangular basin bounded by Arctic Alaska, the western Canadian Arctic margin, the Northwind Ridge and the Alpha Ridge (Fig. 1.1). The crust underlying the basin has not been sampled directly. However, it is generally assumed to be a Cretaceous oceanic basin on the basis of cessation of northerly derived sedimentation onto Arctic Alaska, age of interpreted break-up unconformities and eruption of large volumes of volcanics in the Arctic region (HALIP) (e.g. Lawver & Muller, 1994). The Canada Basin can be subdivided

into the southern and northern Canada Basin. The southern Canada Basin is relatively uniform, with a deep, smooth floor. Here, gravity data show a faint but distinctive low running across the centre of the basin, which has been interpreted as an extinct spreading centre (Laxon & McAdoo, 1994). The northern Canada Basin lies in the central Arctic Ocean region. It has a more complex bathymetry than the southern Canada Basin and magnetic anomalies that are similar to that of the Alpha-Mendeleev Ridge. The gravity low can not be imaged in this portion of the basin (Fig. 2.4).

Chukchi Borderland

The Chukchi Borderland projects out into the Canada Basin at a high angle to the East Siberian Shelf (Fig. 1.1). It is a complex feature containing a number of component ridges and basins oriented perpendicular to the trend of the shelf margin. The Northwind Ridge provides an abrupt border to the Canada Basin, sharply rising 3000 m above the Canadian Abyssal Plain. It is generally considered to be composed of extended continental crust, but its original location prior to the opening of the Amerasia Basin is disputed. Grantz *et al.* (1993) showed seismic reflection profiles that indicated that the ridge and trough bathymetry was formed by Tertiary extension of continental crust. Grantz *et al.* (1998) recorded Cambrian to Miocene age sediments in piston cores from the Northwind Ridge and suggested that the stratigraphic sequence was very similar to the succession of the Canadian Arctic Islands.

2.7 Amerasia Basin opening models

The opening history of the Amerasia Basin is greatly disputed. Numerous models have been proposed since the acceptance of the theory of plate tectonics in the 1960s. The nearly-continuous ice cover of the Arctic Ocean inhibits data collection such that at present there is not sufficient evidence to allow the confirmation of any one model. The sections below summarize the most important Amerasia Basin opening models.

Initiation of rifting that formed the Amerasia Basin is estimated by the oldest age of sediments found in the rift margin grabens on the edges of the basin. The sediments flooring the Dinkum Graben, on the Alaska North Slope, are estimated as ?Hettangian-?Sinemurian in age, suggesting that rifting was initiated in Early Jurassic time (e.g. Hubbard *et al.*, 1987). Grabens in the Canadian Arctic Islands contain sediments estimated to be as old as Toarcian age (Harrison *et al.*, 1999).

Spreading in the southern Canada Basin is believed to have ceased before the Cretaceous normal magnetic superchron at ca. 120 Ma (near the beginning of Aptian time), as the magnetic anomaly stripes continue right up to the putative extinct spreading centre (Laxon & McAdoo, 1994).

Alaska Rotation models

In its simplest form, dubbed the 'Simple Alaska Rotation Model' (Scott *et al.*, 2004), the rotational model suggests the Amerasia Basin opened as a Jurassic-Cretaceous rotation of the Alaska-Chukotka block away from the Canadian Arctic Islands around a pole situated in the Mackenzie Delta region (Fig. 2.5). Carey (1955, 1958) characterized the bend in the trend between the Canadian Rockies and the Alaska Range as an orocline. The good bathymetric fit between Arctic Alaska and Arctic Canada led Hamilton (1967, 1968) and Tailleur (1973) to suggest the rotation of northern Alaska away from the Canadian Arctic margin, accommodated by strike-slip motion between Siberia and the Chukchi Shelf. At present, many workers support some variant of the 'Alaska Rotation Model'.

The following is implicit in the 'Simple Alaska Rotation Model':

- the continental margins of the Alaska North Slope, East Siberian Shelf and Canadian Arctic Islands are passive margins formed by rifting in the Early Cretaceous.
- the Canada and Makarov basins are of similar age and opened with a similar geometry.
- the Alpha-Mendeleev Ridge is oceanic and the product of a hotspot.
- the Makarov side of the Lomonosov Ridge is bounded by a curved dextral transform fault that continues onto the Russian Arctic Shelf.
- the Alaska North Slope and East Siberian Shelf were part of the same tectonic plate prior to the opening of the basin.

Data presented in support of this model include:

- a good bathymetric fit between the Alaska North Slope and the Canadian Arctic margin (Carey, 1958; Hamilton, 1967, 1968).
- interpreted similarities of Devonian-Cretaceous strata between the Alaska North Slope and the Canadian Arctic margin (Embry, 1990), including the Northwind Ridge of the Chukchi Borderland (Grantz *et al.*, 1998).

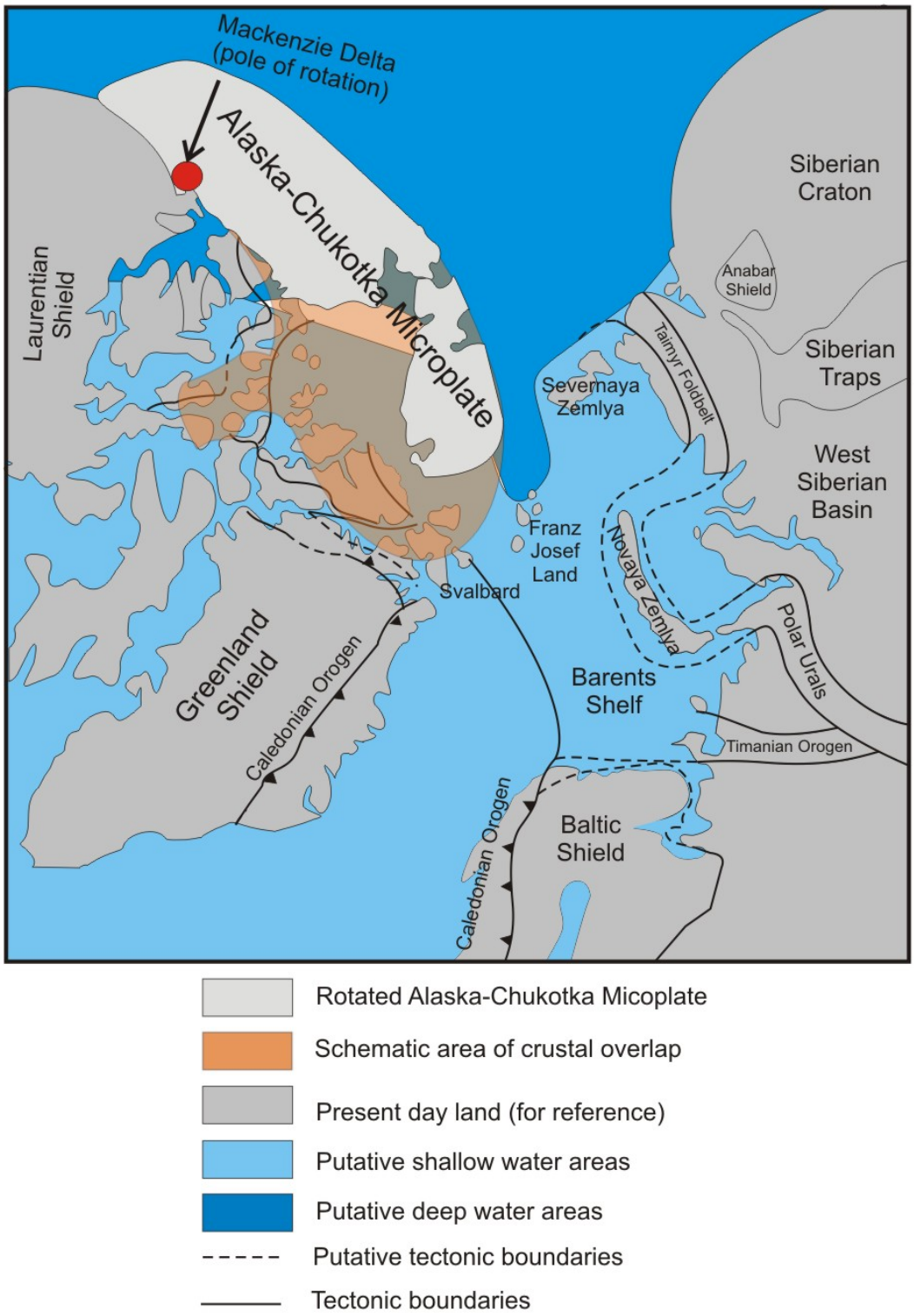

Figure 2.5: Rotation model for the development of the Amerasia Basin modified after Miller *et al.* (2006). The figure shows the pre-rift, Early Jurassic geometry predicted by the 'Simple Alaska Rotation Model'. The model suggests a 66° rotation of the 1000 m contour of the Canadian side about a pole in the Mackenzie Delta (69.1°N, 130.5°W), along a strike slip system following the Lomonosov Ridge in its pre-rift position along the Barents Shelf.

- a fan of lineated seafloor magnetic anomalies in the Canada Basin, converging towards the Mackenzie Delta (Brozena *et al.*, 1998) and along the axis of these anomalies, free air gravity interpretations showing apparent buried spreading centre in the Canada Basin (Laxon & McAdoo, 1994).
- palaeomagnetic data from a Valangian sandstone of the Kuparuk River Formation suggest 66° rotation of the North Slope away from the Canada margin (Halgedahl & Jarrad, 1987).
- the trend of the Alpha-Mendeleev Ridge approximates to a small circle around a pole of rotation in the Mackenzie Delta region, compatible with it being an oceanic hotspot trail created during rotational opening.
- the trend of the Lomonosov Ridge approximates to a small circle around the same pole, with interpretation as a major dextral strike-slip fault.

There are obstacles to this model:

- the Chukchi Borderland is an attenuated continental fragment that prevents a snug fit between the Alaskan North Slope and the Canadian Arctic margin prior to rotational opening. The sense of extension of the Chukchi Borderland is perpendicular to what would be expected from the simple rotation mechanism.
- there is no evidence for a strike-slip mechanism operating along the continental Lomonosov Ridge and there is no known analogue for a strike-slip fault of this scale.
- the Alpha-Mendeleev Ridge has a morphology which is similar to the continental Lomonosov Ridge: it contains sharp bends and structural traces in a wide variety of orientations.
- the data presented for the extinct spreading centre and magnetic anomalies are not clear, nor is the evidence for 66° rotation as the paleomagnetic data are not robust.
- the rift-drift unconformities along the North Alaska and Canadian Arctic margins are under debate, but many workers believe the Alaskan rift-drift unconformity to be 130 Ma (Late Hauterivian age) and the Canadian rift-drift unconformity to be 100 Ma (post-Albian age) suggesting that the two regions may not be conjugate margins.

- the magnetic anomalies in the Amerasia Basin are more complicated than would be expected from the 'Simple Alaska Rotation Model'.

Many of the more complex rotation models seek to address these problems as well as other unresolved issues. Some workers have rejected the idea of rotation altogether (e.g. Herron *et al.*, 1974; Lane, 1997; Cecile *et al.*, 2001).

Non-rotational spreading models

Lane (1997) suggested that the Amerasia Basin formed in three stages by non-rotational spreading, about a north-trending spreading centre in the Canada Basin, with the Chukchi Borderland reconstructing adjacent to the present-day Mackenzie Delta (Fig. 2.6). Implicit in this model is that Arctic Alaska and the Canada Arctic Islands were adjacent areas of the same margin, not conjugate margins separated by an ocean basin (Lane, 1997).

The basis for this new interpretation of the opening of the Amerasia Basin was a critical review by Lane (1997) of the evidence presented in support of the rotation models for the opening of the Amerasia Basin and the conclusion that the evidence suggested that a rotational opening was unnecessary and unlikely.

Similarities in Middle and Late Paleozoic stratigraphy and tectonic setting between Arctic Alaska and the Canadian Arctic Islands have been presented as evidence in favour of a rotational opening of the Amerasia Basin (e.g. Embry, 1989, 1990). However, Lane (1997) argued that the tectonic histories in these areas are too different to be considered correlative. In particular, he commented that during Devonian orogenesis, Arctic Alaska was undergoing extension and forming a south-facing continental margin, whilst the Canadian Arctic Islands were undergoing shortening (Moore *et al.*, 1994; Trettin, 1991).

One outstanding issue regarding the rotation hypothesis was highlighted by Lane (1997). Many workers believe the Alaskan rift-drift unconformity to be 130 Ma (Late Hauterivian age) and the Canadian rift-drift unconformity to be 30 million years younger, 100 Ma (post-Albian age), which, if true, casts doubt on whether the two margins were conjugate prior to the formation of the Canada Basin. The important point here is that the uncertainty regarding the age of the rift-drift transitions of these margins does not allow any clear conclusions on the tectonic evolution of the margins to be reached.

Lane (1997) noted that the crustal structure of the Central Beaufort Sea margin shows a 150-200 km offset in the continent-ocean boundary. The trend of the offset can be traced for 350 km into the Canada Basin, called the Beaufort Fracture

Zone. The angle of this fracture zone, and associated ocean spreading, were not interpreted to be compatible with the model of rotational opening of the Canada Basin.

Furthermore, Lane (1997) commented that northern Yukon and the northern North West Territories do not show the substantial Cretaceous shortening expected from the rotational opening of the Canada Basin, as is seen in the Pyrenees, where it is associated with the rotational opening of the Bay of Biscay (Roest & Srivastava, 1991).

Central Arctic Landmass models

An important and unresolved question regarding the evolution of the Amerasia Basin concerns the amount of continental crust in the central Arctic region. The Amerasia Basin is bathymetrically complex and a multistage opening history is plausible, which may increase the likelihood that microcontinents are present within the basin.

In order to explain the presence of northerly derived sediments in several Arctic basins, a central Arctic landmass has been depicted on many pre-Cretaceous palaeogeographic reconstructions. Tailleur (1973) proposed the existence of a landmass north of Arctic Alaska in the Paleozoic and Mesozoic, 'Barrovia', that acted as the source of the northerly derived Ellesmerian Sequence to the Alaska North Slope. Embry (1982, 1989) proposed the existence of an extensive landmass in the central Arctic, 'Crockerland', that acted as a sediment source for the Sverdrup Basin from Carboniferous to Middle Jurassic time (Fig. 2.7). He proposed that this landmass also acted as a sediment source for the Barents Shelf and the Chukchi Sea in the Paleozoic and Mesozoic. 'Crockerland' is the name used by most western scientists referring to a hypothesized central Arctic landmass. Zonenshain & Natapov (1987, 1989) proposed the existence of a similar central Arctic landmass, 'Arctida', based on palaeomagnetic and faunal evidence (Fig. 2.8). 'Arctida' is the name used by most Russian scientists when referring to a hypothesized central Arctic landmass.

Miller *et al.* (2006) presented a pre-Cretaceous Arctic region reconstruction, placing the Chukotka region close to the Arctic Russian regions of Taimyr and West Siberian Basin. In this model the Alpha-Mendeleev Ridge is composed of stretched continental crust, which was separated from the Lomonosov Ridge (and ultimately the Barents Shelf) by rifting. The complex ridge and basin morphology suggests that the central Arctic region rifted in several orientations.

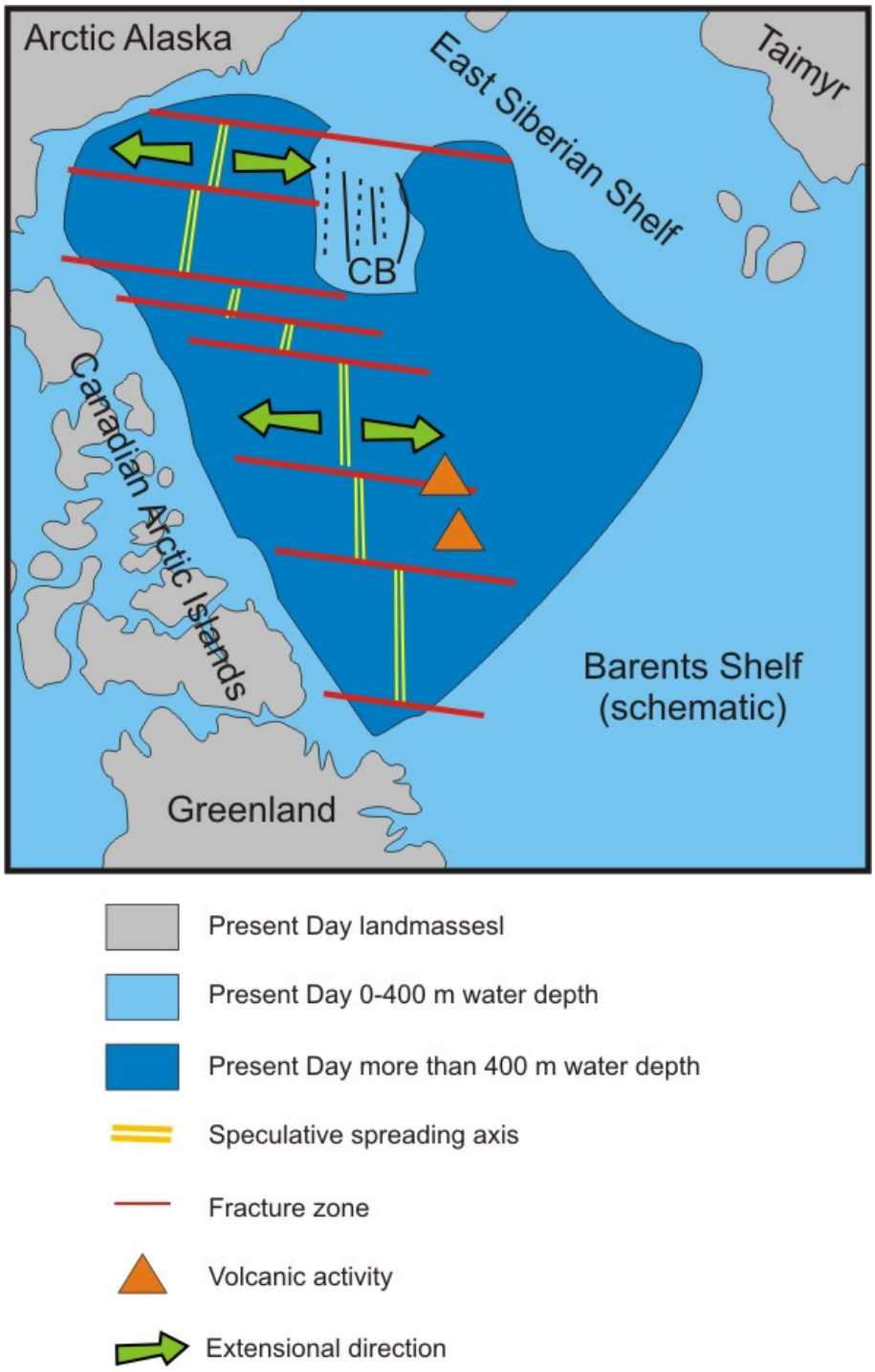

Figure 2.6: Non-rotational model for the development of the Amerasia Basin modified after Lane (1997), showing orthogonal spreading in the Canada Basin, removing the Chukchi Borderland from the Mackenzie Delta region (dashed and solid lines indicate extensional structures observed on the Chuckchi Borderland). Volcanic activity represents the formation of the Alpha-Mendeleev Ridge. CB = Chukchi Borderland.

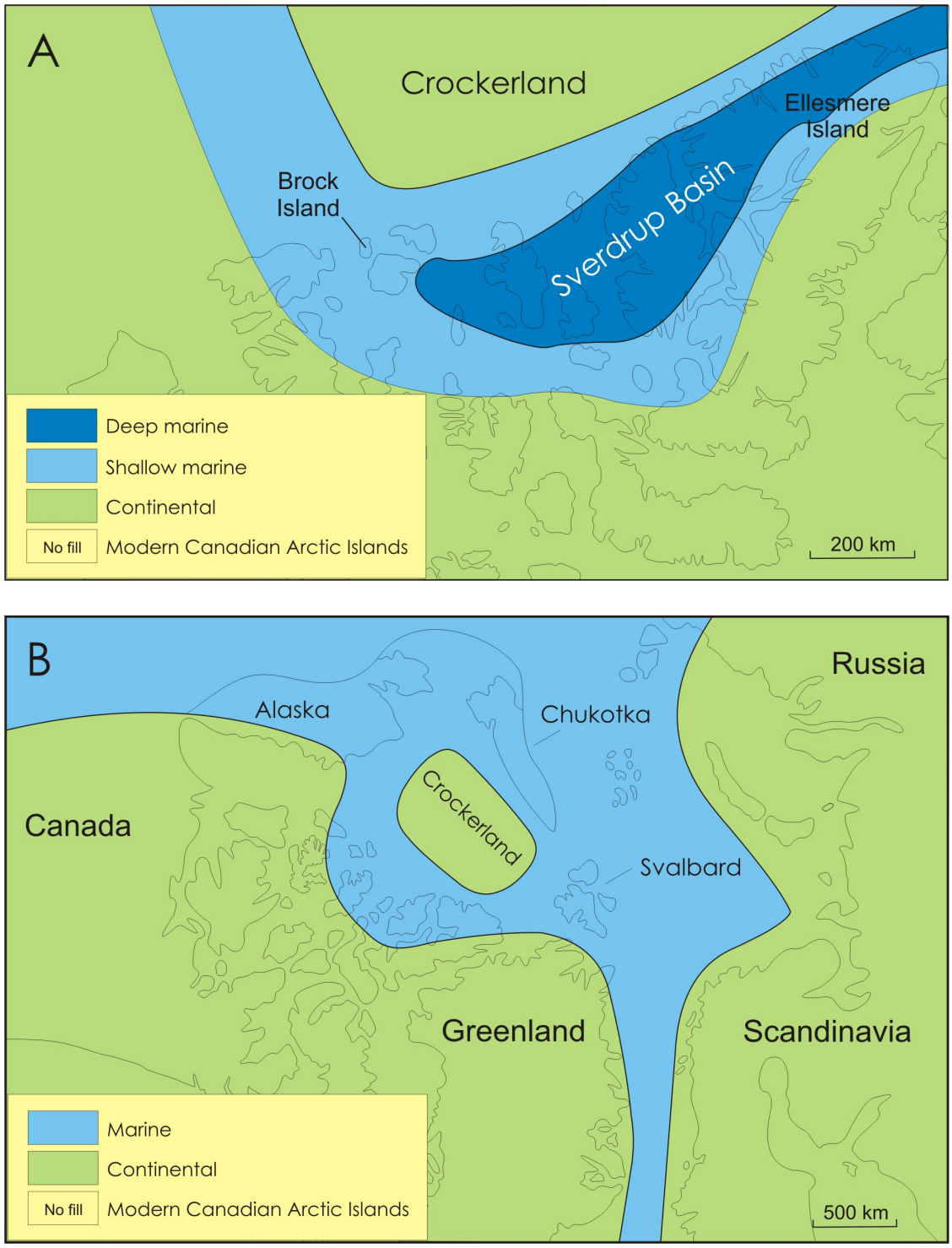

Figure 2.7: Paleogeographical reconstruction featuring Crockerland, modified from Embry (1992). (A) The Canadian Arctic Islands in the late Paleozoic-Jurassic. Crockerland is hypothesized to lie northwest of the Sverdrup Basin, from offshore Ellesmere Island in the east to Brock Island in the west. (B) Paleogeographical reconstruction for the Arctic region in Early Mesozoic time incorporating the hypothesized central Arctic landmass, Crockerland. In this reconstruction Crockerland could act as a source of sediment for the Sverdrup Basin, North Greenland, Svalbard, Chukotka and Alaska.

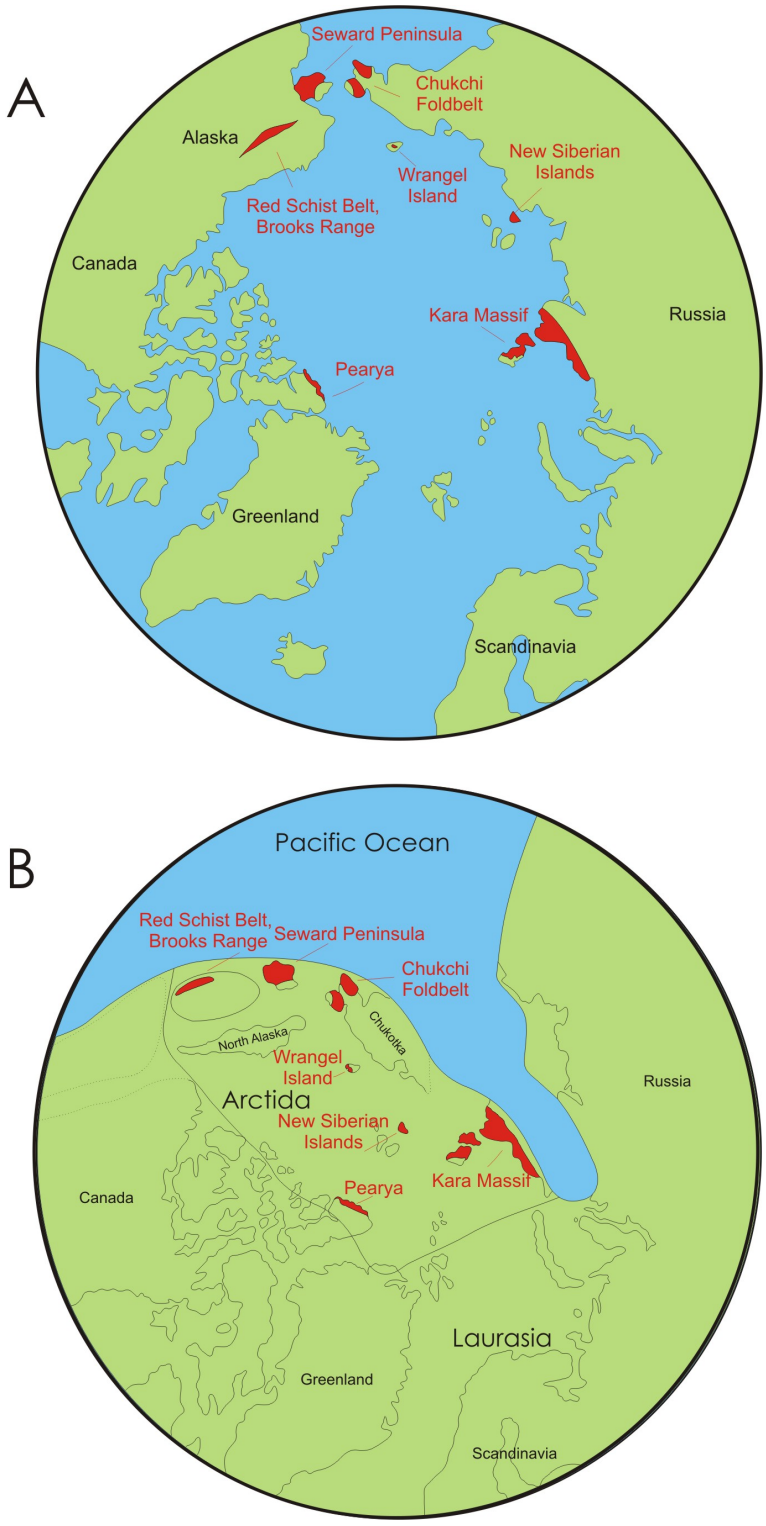

Figure 2.8: Paleogeographical reconstruction featuring Arctida. (A) Circum Arctic map showing the present positions (in red) of the remnant of the proposed Arctic paleo-landmass, Arctida. (B) Early Mesozoic palaeogeographic reconstruction of the Arctic region showing the position of the proposed paleo-landmass, Arctida, modified after Zonenshain & Natapov (1987, 1989).

2.8 Testing Amerasia Basin opening models with sediment provenance

Sediment provenance studies represent a valuable method for testing Amerasia Basin opening models. Some geographic areas are key: the Sverdrup Basin, Svalbard/Barents Shelf and Taimyr Peninsula.

Sverdrup Basin

The Sverdrup Basin contains northerly derived sediments of Late Carboniferous to Middle Jurassic age, deposited along the northern flank of the basin (Embry, 1992). These sediments are more than 2000 m thick and cover tens of thousands of square kilometres; evidence of a fairly large northern source terrain. These sediments thin towards the northwest, away from the axis of the Sverdrup Basin. The 'Simple Alaska Rotation Model' predicts that the succession is sourced from the East Siberian Shelf. The non-rotational spreading models suggest the same. The central Arctic landmass models suggest that the source of sediment would be a hypothesized central Arctic landmass, possibly of Baltica or Siberia affinity depending on the continuation of these terranes into the Central Arctic Ocean.

Svalbard/Barents Shelf

Svalbard and the Barents Shelf contain Mesozoic age sediments derived from the northwest, north and northeast. These sediments typically record deposition in deltaic environments (Harland, 1997). There is a wide range of possible sources for this sediment, including crust of Laurentia, Siberia and Baltica affinity.

Taimyr Peninsula

The absence of preserved sediment spanning most of the Late Palaeozoic to mid Mesozoic interval is compatible with exposure of the Taimyr and Severnaya Zemlya for almost the entire period during which a central Arctic landmass is considered to have existed. However, the absence of preserved sediment does not exclude the possibility that sediment was deposited and then eroded in these areas. Northerly derived, unconsolidated, Jurassic-Cretaceous sediments are found in northern areas of Taimyr and the provenance of this sediment was studied in this project.

2.9 Arctic region provenance studies

There are a limited number of published provenance studies of Paleozoic-Mesozoic Arctic region sediments. The studies are summarized below, and findings from the studies are discussed in more detail in chapters 4-7, where appropriate.

McNicoll *et al.* (1995) presented U-Pb zircon age data for 31 zircon grains from the northwesterly derived Devonian clastic wedge from several locations across the Canadian Arctic Islands. The zircons showed a mixture of Archean and Proterozoic ages, with one Silurian grain. The radiometric data provided a very good fit with the Scandinavian Caledonides, although the authors decided that derivation from the East Greenland Caledonides was more likely.

Mørk *et al.* (1999) analysed 180 Triassic sandstone samples from across the Barents Shelf, including Novaya Zemlya, Franz Josef Land, the Timan-Pechora Basin and Svalbard, using petrological, mineral-chemical and Sm-Nd bulk isotopic methods. Conclusions were drawn concerning the source areas of the samples, with sources including the Polar Urals, Baltic Caledonides and Shield, and poorly-understood northern source areas.

Grantz *et al.* (2001) presented sedimentological and U-Pb zircon age data from Triassic-Cretaceous sediments collected in two piston cores from the Eurasian margin of the Lomonosov Ridge. A 250 Ma zircon age peak in the samples suggests sediment derivation from the Taimyr Peninsula prior to the opening of the Eurasia Basin.

Miller *et al.* (2006) U-Pb analysed detrital zircons from twelve Triassic samples from seven circum-Arctic localities, in order to test Amerasia Basin opening models. The authors concluded that the Chukotka region was more closely related to the Taimyr Peninsula and Verkhoyansk, and not to the Canadian Arctic, prior to the opening of the Amerasia Basin.

Røhr *et al.* (2008) presented U-Pb zircon age data and Hf-isotope results of Early Cretaceous sandstones from the Wandel Sea Basin, North Greenland. The samples showed a wide range of zircon ages, with significant peaks at 1.0-1.1 and 1.8-2.0 Ga. The U-Pb and Hf data were all consistent with Greenland as the source of the sediment.

Chapter 3

Sediment Provenance Methodology

3.1 Introduction

In this study, sediment provenance analysis of sandstones is used to assess the Mesozoic tectonic evolution of three Arctic regions: the Sverdrup Basin, Barents Shelf and Taimyr Peninsula. This section describes the methods for each of the analytical techniques employed: petrography, heavy mineral analysis, single grain chemistry of garnet and tourmaline and zircon dating using U-Pb isotopes. All analytical data are found on the accompanying CD.

3.2 Controls on sandstone composition

Sandstone composition provides information about the rock type and tectonic setting of a sediment (Dickinson, 1970). However, the processes acting throughout the sedimentary cycle obscure this information. These processes include weathering, mechanical abrasion, hydraulic sorting during transport and diagenesis (Fig. 3.1). An understanding of these factors is vital in order to evaluate source-specific characteristics of the sediment.

Weathering

Physical and chemical weathering occur in the source terrain during alluvial storage and at the depositional site. Weathering rates are controlled by the presence of water, biological activity and temperature. Chemical weathering, in particular, greatly affects the mineralogical assemblage of the detritus, breaking down less

stable minerals such as feldspar, olivine, pyroxene and amphibole (Bateman & Catt, 1985; Johnsson *et al.*, 1991). The intensity of chemical weathering is determined by the rate of sediment transport, which is largely controlled by relief and climate. Chemical weathering is most intense in tropical climates and less intense in arid climates (e.g. Basu, 1985).

Mechanical abrasion

During transport, mechanical abrasion reduces grain size by fracturing and rounding, preferentially affecting minerals with a low mechanical stability (low hardness and presence of cleavage planes) (van Andel, 1959). This process appears to have little effect on mineral assemblages during river transport (e.g. Savage & Potter, 1991; van Andel, 1950) but is more important in shallow marine environments, where wave and current action abrades minerals (e.g. Savage *et al.*, 1988).

Hydraulic processes

Physical sorting of grains is controlled by the hydrodynamic conditions during transport and deposition. The concept of hydraulic equivalence, introduced by Rubey (1933), states that grains with the same settling velocity (based on grain size and density) are hydraulically equivalent and will normally be transported and deposited together. Hydraulic equivalence is a function of grain size and grain density. However, this relationship does not always hold true. Other factors, including grain shape, are also thought to be important (e.g. Morton & Hallsworth, 1999; van Andel, 1950).

Diagenesis

Burial changes the mineralogy assemblage of sand, preferentially dissolving less stable minerals and authigenically forming new minerals. In sandstones, we observe grain surface etching and disappearance of mineral species with increasing depth. Factors affecting mineral dissolution during burial include mineral stability, pore fluid composition and temperature, porefluid circulation and time (Morton & Hallsworth, 2007).

3.3 Petrography

This study utilizes point counting of thin sections in order to assess sandstone composition and maturity, providing information on the environment of deposi-

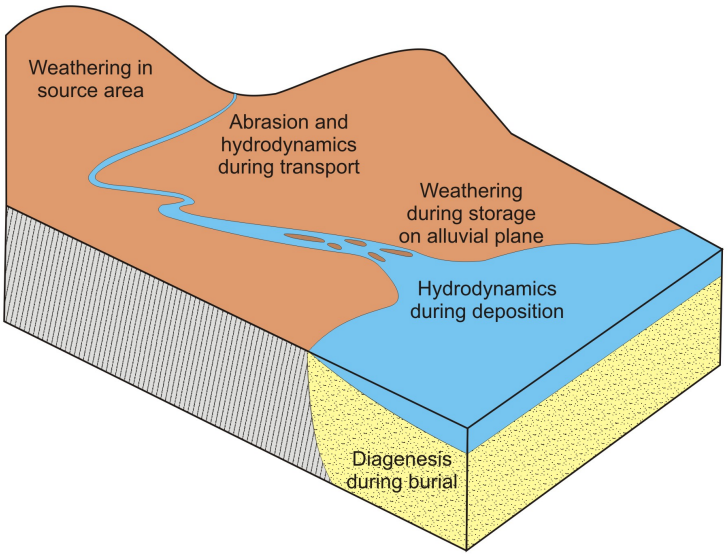

Figure 3.1: Processes operating during the sedimentary cycle to modify the composition of source rocks, modified after Morton & Hallsworth (1994).

tion and sediment provenance. Petrographic analysis of sandstone focusses on the following framework grains: quartz, feldspar and lithic fragments, although other constituents are also recorded. The framework grain types plotted during point counting are presented in Table 3.1.

Quartz

Quartz has a high resistance to physical and chemical corrosion and becomes concentrated in the sedimentary cycle. Quartz is the most abundant grain type in sandstones and can be subdivided into several types based on the number of crystals in the grain, the shape of crystal boundaries and the nature of extinction (Table 3.1). The type of quartz grain present in a sediment provides provenance information (Basu, 1985; Smyth *et al.*, 2008) (Table 3.2).

Quartz is an important primary constituent of many igneous rocks, for example granites, tonalites and rhyolites. Intermediate igneous rocks contain less quartz and basic rocks usually contain less than 5% quartz (Deer *et al.*, 1992). Quartz is also an important constituent of metamorphic rocks and forms as a secondary mineral in hydrothermal veins and as cement in sediments. Siliceous sediments (e.g. chert) form in a variety of sedimentary environments.

Quartz grains	
Qt	Total quartz grains (Qt = Qm + Qp2-3 + Qp>3)
Qm	Monocrystalline quartz (Qm = Qmnu + Qmu)
Qmnu	Monocrystalline quartz, non-undulatory
Qmu	Monocrystalline quartz, undulatory (extinction angle > 5 degrees)
Qp	Polycrystalline quartz (Qp = Qp2-3 + Qp>3)
Qp2-3	Polycrystalline quartz, 2-3 subgrains
Qp>3	Polycrystalline quartz, 4 or more subgrains
Qc	Chert (subgrains <30 μm)
Feldspar grains	
F	Total feldspar grains (F = P + K)
P	Plagioclase
K	Alkali feldspar
Lithic fragments	
L	Total unstable lithic fragments (L = Lpl + Lsst + Lm + Lv + Ls + Lun)
Lt	Total lithic fragments (Lt = L + Qp2-3 + Qp>3 + Qc)
Lpl	Plutonic lithic fragments
Lsst	Sandstone lithic fragments
Lm	Metamorphic lithic fragments
Lv	Volcanic lithic fragments
Ls	Sedimentary lithic fragments
Lun	Unknown lithic fragments

Table 3.1: Framework grain types used for petrography, modified after Dorsey (1988).

Quartz type	Grain shape	Colour	Polycrystalline	Undulosity	Inclusions	Other common textures
Plutonic	Anhedral and euhedral. Mono- or polycrystalline. Grain boundaries straighter than metamorphic rocks	Milky white to translucent	< 3 crystal units per grain	Weak < 5 degrees	Fluid inclusions common	Mineral inclusions, melt reaction textures, granophyric growth with feldspar
Plutonic (hypabyssal)	Euhedral, monocrystalline	Clear	Not common	Weak < 5 degrees to non-undulose	May be absent	Melt reaction textures may occur
Volcanic	Euhedral, monocrystalline, composite and aggregate grains	Clear	Microcrystalline aggregates may appear to be polycrystalline	Commonly non-undulose	Melt inclusions common	Skeletal grains, melt reaction textures, and bipyramidal grain shape
Metamorphic	Anhedral, sutured or irregular	Milky white to translucent	> 3 crystal units per grain. Most abundant in low-grade metamorphic rocks	> 5 degrees	Fluid inclusions common, often needlelike	Mortar texture, pressure fringes, foliation
Hydrothermal	Euhedral	Milky white to translucent		Undulose	Fluid inclusions common	Elongate, comb texture
Chert	Rounded or anhedral. Crypto- or microcrystalline or fibrous	Variable				May have similar look to volcanic quartz

Table 3.2: Quartz species found in sandstones, modified after Smyth *et al.* (2008).

Feldspar

Feldspar is the second most abundant grain type in sandstones and is ubiquitous in igneous rocks, with the exception of ultrabasic and rare alkaline rocks. There are two feldspar solid solution series: alkali feldspars and plagioclase (Fig. 3.2).

Alkali feldspar (K) is an important constituent of alkali and felsic igneous rocks: granites, granodiorites, syenites and their volcanic equivalents, as well as pegmatites and felsic-intermediate gneisses (Deer *et al.*, 1992). Plagioclase (P) is the primary constituent in most mafic and intermediate lavas and their plutonic equivalents, as well as many metamorphic rocks (Deer *et al.*, 1992).

The chemical weathering of all feldspars is relatively rapid, such that the presence of feldspar is indicative of a sediment showing rapid erosion and sediment transport rates (Johnsson *et al.*, 1988). Alkali feldspar is more resistant to chemical weathering than plagioclase (Deer *et al.*, 1992).

Lithic fragments

Several species of lithic fragments can be observed in sandstones (Table 3.1). Lithic fragments are of great importance as they directly reflect the sediment source rock. Many lithic grains are unstable and break down rapidly in the sedimentary cycle (e.g. volcanic, low-grade metamorphic and mudstone fragments). Chert and polycrystalline quartz are examples of stable lithic fragments.

Other constituents

Other sandstone constituents include micas and clays, heavy minerals, phosphate, glauconite, fossils, plant fragments, cement and pore spaces. These constituents are counted during sandstone petrography but are not plotted in the ternary classification diagrams (Fig. 3.2).

Point counting method

Thin sections were made by John Coundon of Petrotech Ltd and Keith Gray of the Department of Earth Sciences, University of Cambridge. The sections were treated with potassium cobaltinitrate, staining potassium feldspars yellow to aid identification.

For this work, the petrographic composition of sand-sized sediments in thin section were estimated by point counting 300 grains using a Nikon Optiphot2 microscope, Nikon DS-Fi1 photographic system and digital point counting stage with

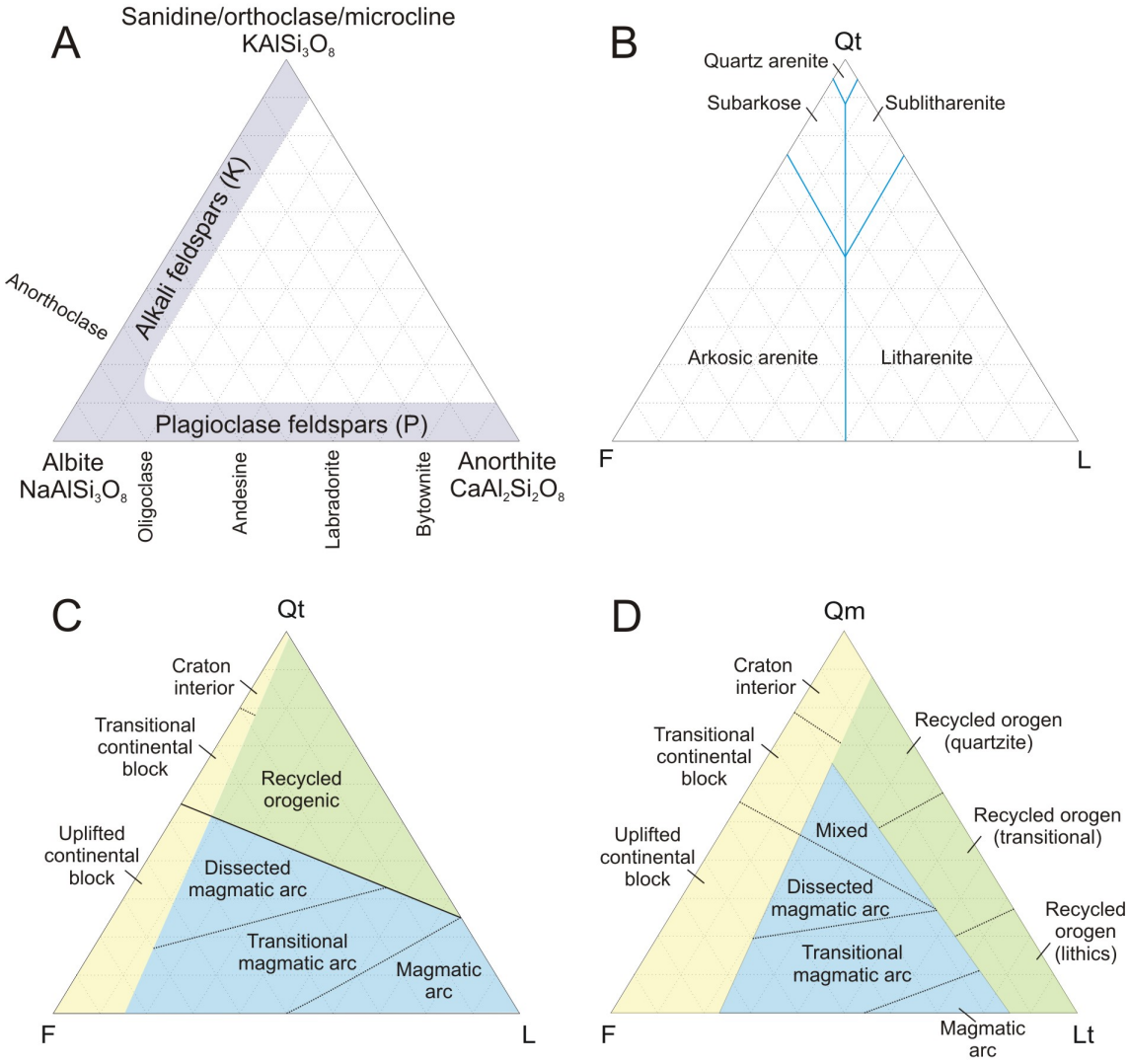

Figure 3.2: Feldspar and framework grains ternary diagrams used in this study. (A) Feldspar ternary diagram illustrating the feldspar solid solution series, modified from Deer *et al.* (1992). (B) QtFL sandstone classification plot, modified after Pettijohn *et al.* (1987). (C-D) QtFL and QmFLt diagrams showing tectonic setting source areas, modified after Dickinson & Suczek (1979).

PetrogLite software. Each grain was assigned to a category within the Gazzi-Dickinson QFL petrographic scheme and plotted on QtFL and QmFLt ternary diagrams (Dickinson & Suczek, 1979) (Fig. 3.2).

3.4 Heavy mineral analysis

Analysis of heavy minerals allow more specific provenance conclusions to be reached than analysis of framework grains. Mange & Maurer (1992) describe more than 50 non-opaque heavy mineral species, many of which have restricted paragenesis, thus providing important provenance information.

Heavy mineral analysis was commonly used in the first half of the 20^{th} century (e.g. Rubey, 1933; van Andel, 1950). Questions regarding the reliability of heavy mineral analysis, due to the factors modifying the mineral assemblages during the sedimentological cycle outlined in Section 3.2, led the technique to fall out of use. Since the 1980s, renewed research has been ongoing to address these concerns. These methods are outlined below.

Controls on heavy mineral assemblages

The main processes that overprint heavy mineral assemblages are chemical weathering, mechanical abrasion, hydrodynamic fractionation and diagenesis (Morton & Hallsworth, 1999).

Chemical weathering modifies the heavy mineral assemblage of a sediment both at source and during alluvial storage or deposition in marginal marine or non-marine environments. Table 3.3 outlines a selection of published studies illustrating the effect of soil formation on heavy mineral assemblages. The results show a good degree of consistency and an approximate order of mineral stability. During soil formation, it is likely that the ratio of stable to less stable minerals will increase, though this process is not considered to reduce the diversity of heavy mineral species in an assemblage significantly (Morton & Hallsworth, 1999).

Much work has been carried out to determine the relative mechanical stability of heavy minerals during transport. This process was long thought to be important for modifying heavy mineral assemblages (e.g. Dietz, 1973; Thiel, 1940, 1945; van Andel, 1959). However, there is no evidence from natural studies that this process greatly alters the heavy mineral assemblage (e.g. Morton & Smale, 1991; van Andel, 1950).

Dryden and Dryden (1946)	Lemcke et al (1953)	Bateman and Catt (1985)
Crystalline schist	Calcareous sandstones	Aeolian coversands
Zircon	Staurolite, Rutile, Tourmaline, Zircon	Andalusite, Kyanite, Rutile, Staurolite, Titanite, Tourmaline, Zircon
Sillimanite		
Monazite		
Kyanite	Epidote, Kyanite	
Calcic amphibole	Calcic amphibole	
Staurolite	Apatite	
Garnet	Garnet	Garnet
Orthopyroxene		Epidote
		Calcic amphibole, Clinopyroxene, Orthopyroxene
		Apatite

Table 3.3: Relative stability of translucent heavy minerals in weathering profiles, simplified from Morton & Hallsworth (1999). The most stable minerals are at the top of the list.

Hydraulic sorting of minerals during transport and deposition is an important modifier of heavy mineral assemblages (Morton & Hallsworth, 1999). To compensate for fractionation of assemblages due to hydraulic sorting, minerals with similar hydraulic behaviour (similar settling velocity) are studied.

Post-depositional diagenesis is an important factor for modifying heavy mineral assemblages (e.g. Morton, 1984; Morton & Hallsworth, 2007). Table 3.4 shows the relative stabilities of heavy minerals in deeply buried sandstones (Morton & Hallsworth, 2007).

Conventional heavy mineral analysis

Heavy mineral data provide valuable provenance information when potential modifying factors are accounted for. It is best to study minerals that are relatively stable in the sedimentary cycle. Stable minerals with similar hydraulic and diagenetic behaviour are studied and the ratios between the mineral pairs are recorded. The mineral ratios used for this study are outlined in Table 3.5.

Most stable
Rutile, Anatase, Brookite, Zircon, Apatite
Tourmaline, Monazite, Spinel
Garnet, Chloritoid
Allanite
Staurolite
Sodic amphibole
Kyanite
Titanite
Epidote
Calcic amphibole, Andalusite, Sillimanite
Sodic pyroxene
Orthopyroxene, Clinopyroxene
Olivine
Least stable

Table 3.4: Heavy mineral order of stability in deeply buried sandstones, modified from Morton & Hallsworth (2007).

Index	Mineral pair	Definition
ATi	apatite-tourmaline	100 x apatite count/(total apatite plus tourmaline)
GZi	garnet-zircon	100 x garnet count/(total garnet plus zircon)
RuZi	rutile-zircon	100 x rutile count/(total rutile plus zircon)
CZi	chrome spinel-zircon	100 x chrome spinel count/(total chrome spinel plus zircon)

Table 3.5: Provenance-sensitive mineral pairs, from Morton & Hallsworth (1994). The minerals are hydraulically similar, stable heavy minerals.

Varietal studies

Further provenance information can be acquired by detailed analysis of individual mineral species: varietal studies. Crystal morphology, colour and internal structure are indicators of petrogenesis and can therefore be used in provenance studies. Equally important is the acquisition of single mineral chemistry by electron microprobe analysis (Morton, 1985). This study utilizes mineral chemistry data from garnet and tourmaline and U-Pb data from zircon. These techniques will be discussed in detail in the next sections.

Heavy mineral method

Sample preparation for heavy mineral analysis was carried out by Lee Clark of Palynoservices, Aberdeen, UK. The sandstones were disaggregated with a hammer

and subsequently with a pestle and mortar. The grains were cleaned with soapy water and by ultrasonic probe. The cleaned grains were sieved to collect the 63-125 μm size fraction. The sieves were washed thoroughly between each sample to minimize contamination. The separation of heavy and light minerals from the 63-125 μm size fraction was done using the heavy liquid bromoform (specific gravity of 2.89 g/cm^3). The heavy mineral residues of the 63-125 μm size fraction were mounted on a petrographic slide using Canada Balsam.

3.5 Mineral chemistry

Microbeam analysis of single heavy mineral species is becoming an increasingly important technique in sediment provenance studies (Mange & Morton, 2007). Garnet and tourmaline analysis have been carried out for this study.

Mineral chemistry method

From the 63-125 μm heavy mineral size fraction separate, garnet and tourmaline grains were hand-picked under a binocular microscope, mounted in epoxy resin and polished to reveal grain centres. Electron-microprobe analyses of randomly selected grains were performed with a CAMECA SX-100 instrument at the Department of Earth Sciences, University of Cambridge. Wherever possible, at least 60 grains were analysed per sample. Each garnet grain was analysed for Mg, Si, Na, Al, Fe, Ca, Ti, Cr, Mn and Ni. Each tourmaline grain was analysed for Mg, Si, Na, Al, Fe, Ca, Ti, Cr, Mn, K and F.

Garnet chemistry

Garnet chemistry has been widely used as a sediment provenance tool since it was pioneered by Morton (1985) (e.g. Hartley & Otava, 2001; Mørk, 1999; Takeuchi, 1994). Garnet is a common component of many heavy mineral assemblages. It is relatively stable during weathering and burial diagenesis (Morton, 1984; Morton & Hallsworth, 2007) and shows a wide range of major element compositions (Morton, 1985) (Fig. 3.3). Garnet is a common mineral in a variety of metamorphic rocks and is also present in plutonic igneous rocks, pegmatites, ultramafic rocks and some felsic volcanics (Deer *et al.*, 1992) (Table 3.6). Morton *et al.* (2004) and Mange & Morton (2007) presented a classification system for garnets, allowing source rock information to be gained from the mineral chemistry of garnet grains (Fig. 3.3, Table 3.6).

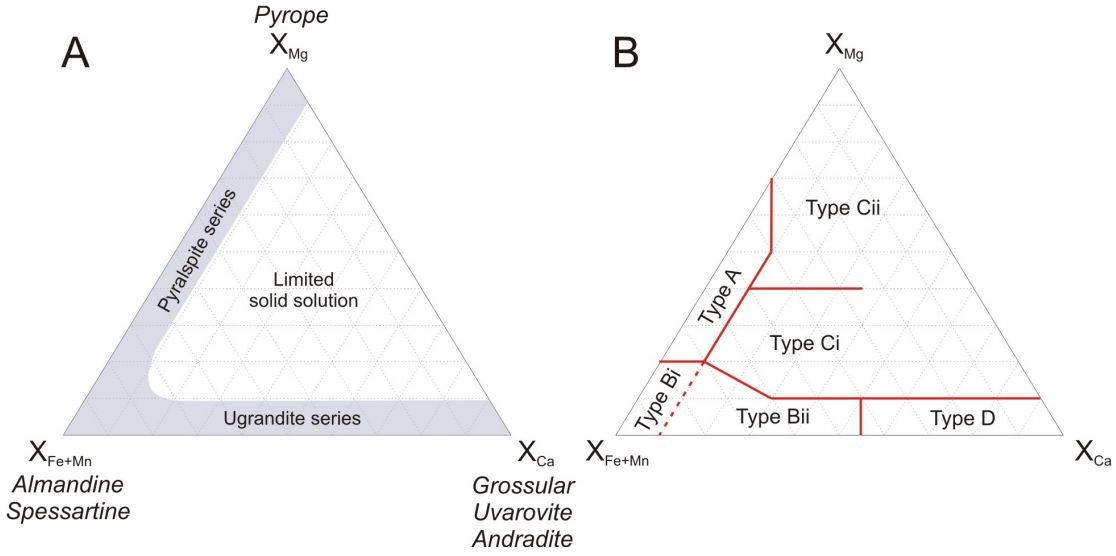

Figure 3.3: Garnet solid solution series. (A) Most naturally occurring garnets correspond to the general formula $(Mg,Fe^{2+},Mn,Ca)_3(Al,Cr,Ti,Fe^{3+})_2Si_3O_{12}$ (Deer *et al.*, 1992). There are two main garnet series: pyralspite (pyrope, almandine, spessartine) $[(Mg,Fe^{2+},Mn)_3Al_2Si_3O_{12}]$ and ugrandite (grossular, andradite, uvarovite) $[Ca_3(Al,Cr,Ti,Fe^{3+})_2Si_3O_{12}]$ (Deer *et al.*, 1992). There is continuous solid solution within these two series, but limited solid solution outside the compositional range of the series. Garnets with true end-member compositions are rare and names are assigned corresponding to the dominant ions. (B) Garnet classification system presented by Morton *et al.* (2004), showing the link between garnet chemistry and sediment source lithology. Classification of the fields are summarized in Table 3.6.

Although garnet is relatively stable during burial, it undergoes dissolution by high-temperature porefluids (Morton, 1984; Morton & Hallsworth, 2007). The stability of garnet is controlled by its composition and high-Ca garnets are less stable than low-Ca garnets (e.g. Morton & Hallsworth, 2007). Garnet populations that have been modified by dissolution during deep burial can be recognized by petrographic observation of their etched surface textures and data should be interpreted with this in mind (e.g. Turner & Morton, 2007).

Tourmaline chemistry

Tourmaline is a complex borosilicate with a large compositional range, making it a very useful provenance indicator. Tourmaline is a common accessory mineral in a wide range of rock types and is stable in weathering and diagenetic environments. Tourmaline forms in granitoid intrusive rocks and their associated aplites,

Garnet Type	Geochemical characteristics	Source lithologies	Differentiating source lithologies
A	High Mg, low Ca	High grade (granulite facies) metasedimentary rocks and charnokites or intermediate-acidic igneous rocks from magmas at deep crustal levels	Distinguish by integration of heavy mineral data with garnet geochemistry
B	Low Mg, variable Ca	Amphibolite facies metasedimentary rocks and gneisses (Bi or Bii) or intermediate-acidic igneous rocks (Bi)	Garnets from intermediate-acidic rocks commonly rich in Mn and have low Ca (Bi). Can also distinguish by integration of heavy mineral data with garnet geochemistry
C	High Mg, high Ca	High grade mafic (Ci) and ultramafic (Cii) gneisses	n.a.
D	High Fe^{3+}, high Ca	Contact/thermally metamorphosed calcareous sediments (in particular, skarns) or low grade metabasic rocks	Distinguish by integration of heavy mineral data with garnet geochemistry

Table 3.6: Classification of garnet species on the basis of major element chemistry (Morton *et al.*, 2004, and references therein).

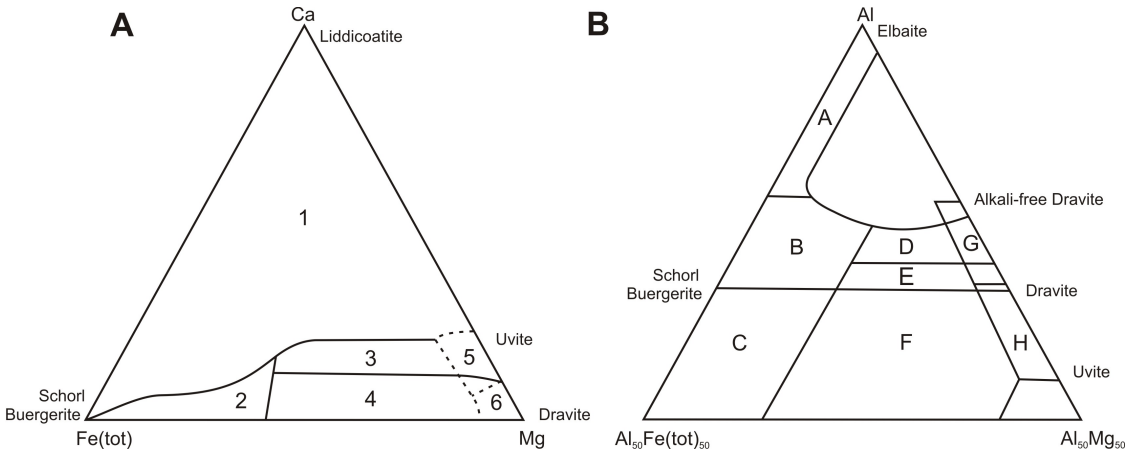

Figure 3.4: Classification of tourmaline species on the basis of major element chemistry (Henry & Dutrow, 1992; Henry & Guidotti, 1985). (A) Field 1, Li-rich granitoids, pegmatites and aplites. Field 2, Li-poor granitoids, pegmatites and aplites. Field 3, Ca-rich metapelites, metapsammites and calcsilicates. Field 4, Ca-poor metapelites, metapsammites and quartz tourmaline rocks. Field 5, Metacarbonates. Field 6, Metapyroxenites. (B) Field A, Li-rich granitoids, pegmatites and aplites. Field B, Li-poor granitoids, pegmatites and aplites. Field C, Hydrothermally-altered granitic rocks. Field D, Aluminous metapelites and metapsammites. Field E, Al-poor metapelites and metapsammites. Field F, Fe^{3+}-rich quartz-tourmaline rocks, calc-silicates and metapelites. Field G, Low-Ca ultramafics. Field H, Metacarbonates and metapyroxenites. Tourmaline has the general formula $XY_3Z_6(T_6O_{18})(BO_3)_3V_3W$ (Hawthorne & Henry, 1999).

pegmatites and hydrothermal aureoles. It also forms in metamorphic rocks with a wide range of bulk compositions and at virtually all grades. It may also form authigenically during the late stages of diagenesis (Henry & Guidotti, 1985). Henry & Guidotti (1985) and Henry & Dutrow (1992) demonstrated that tourmaline mineral chemistry provides information about its petrogenesis and can be represented by two ternary diagrams (Fig. 3.4).

3.6 Zircon geochronology

Zircon forms mainly during major crust-forming and crust-modifying events (tectonogenic events). Zircon is a common accessory mineral in nature and occurs in a wide variety of sedimentary, igneous and metamorphic rocks. It is present as an accessory mineral in a large range of rock types, predominantly felsic-intermediate igneous and high-grade metamorphic rocks, but also in more mafic and lower grade metamorphic rocks (Hoskin & Schaltegger, 2003, and references therein). Zircon

($ZrSiO_4$) incorporates uranium atoms (^{235}U and ^{238}U) as impurities in the lattice during crystallization (Finch & Hanchar, 2003 and references therein). The uranium atoms decay ultimately to lead (^{207}Pb and ^{206}Pb). This process allows measurement of the age of crystallization of the zircon grain.

The extremely high mechanical and chemical stability of zircon allows it to pass through the sedimentary cycle generally without loss of the original isotopic information (Morton & Hallsworth, 1999). The ability to date specific zones within individual zircon grains, and the ease of dating large numbers of samples with modern scientific instruments, makes zircon geochronology a very important technique in sediment provenance studies.

Zircon geochronology method

From the 63-125 μm heavy mineral size fraction separate, zircon grains were handpicked under a binocular microscope, mounted in epoxy resin and polished to reveal grain centres. Sample spots were chosen by interrogation of Scanning Electron Microscope (SEM) and cathodoluminescence (CL) photographs, using a JEOL JSM-820 SEM at the Department of Earth Sciences, University of Cambridge.

SIMS U-Pb analyses were performed using a CAMECA IMS 1270 ion-microprobe at the Nordsim facility, Swedish Museum of Natural History, Stockholm. Analytical procedures followed those of Whitehouse *et al.* (1999) and Whitehouse & Kamber (2005). All data were corrected for common lead where appropriate, using the model lead compositions of Stacey & Kramers (1975), anchored to 0 Ma. Pb/U calibration was performed relative to the Geostandards zircon 91500 (Wiedenbeck *et al.*, 1995). Data reduction was performed using the NordAge software suite, developed by M.J. Whitehouse. Ages were calculated using the decay constants of Steiger & Jäger (1977).

LA-ICP-MS U-Pb analyses were performed using a New Wave 213 aperture imaged frequency quintupled laser ablation system coupled to an Agilent 750a quadrupole-based ICP-MS. Real time data were processed using GLITTER. Pb/U calibration was performed relative to the Plešovice zircon standard (Sláma *et al.*, 2008) and NIST 612 silicate glass (Pearce *et al.*, 1997). All data were corrected for common lead where appropriate, using the ^{208}Pb method assuming a common Pb composition from the age-dependent Pb model of Cumming & Richards (1975).

Concordia diagrams were made using ISOPLOT/Ex 3.00 (Ludwig, 2003). Histograms and probability density distribution plots were made using AgeDisplay (Sircombe, 2004). Ages younger than 1200 Ma are $^{206}Pb/^{238}U$ ages. Ages older than 1200 Ma are $^{207}Pb/^{206}Pb$ ages.

3.7 Time scale and geographical positions

This study uses the Geological Time Scale 2004 (Gradstein *et al.*, 2004). Map, fieldwork and sample localities are quoted in the Decimal Degree coordinate system and projected using a North Pole Stereographic Projection. All directions given in the text refer to present-day orientations, unless otherwise specified.

3.8 Samples used in this study

Three main study areas are discussed in this thesis: northern Sverdrup Basin, Barents Shelf (including Svalbard) and Taimyr. In total, 57 samples were studied for sediment provenance. Of these samples, there are 28 from the Sverdrup Basin, 21 from Svalbard and the Barents Shelf and eight from Taimyr. Fig. 1.1 shows the regions studied. Fig. 3.5 shows the stratigraphic positions of these samples alongside simplified Late Paleozoic-Mesozoic stratigraphic columns for the regions. The full sample list is included in the accompanying CD.

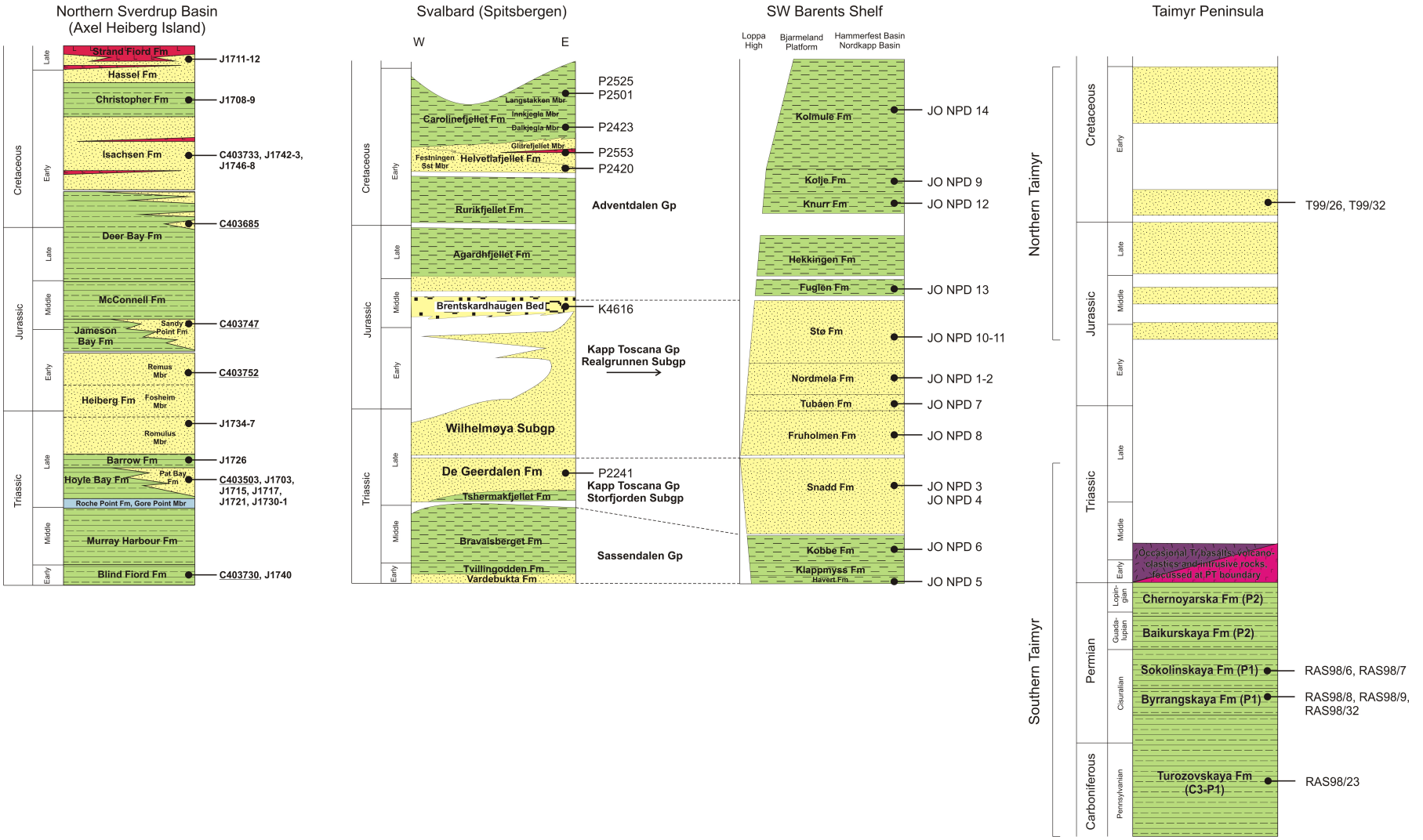

Figure 3.5: Sample stratigraphy for samples used in this study. Approximate stratigraphical positions of the samples are shown beside simplified tectonostratigraphic columns. The tectonostratigraphic columns are modified from Embry (1991a,b) (Sverdrup Basin), Harland (1997) (Svalbard and the Barents Shelf) and Inger *et al.* (1999) (Taimyr Peninsula). A complete list of samples is found on the Appendix CD.

Chapter 4

Composition and provenance of Mesozoic sandstones on northwestern Axel Heiberg Island, Canadian Arctic Islands

In this chapter, 28 Mesozoic sandstone samples from northwestern Axel Heiberg Island are studied to evaluate the sediment characteristics, sediment dispersal patterns and source areas to the northern Sverdrup Basin. Three distinctive provenance types are identified in the petrography, heavy mineral and zircon data (sand types 1-3). Early Triassic, Late Triassic and Middle Jurassic samples (sand type 1) are dominated by apatite grains and young (Permo-Triassic) zircons and are inferred to be derived from the region of Taimyr/Polar Urals, the New Siberian Islands or some unexposed source submerged beneath the Arctic Ocean. An Early Jurassic sample (sand type 2) is dominated by late Neoproterozoic to Silurian zircons, which correlate with the Caledonian and Timanian orogens on the Barents Shelf. Late Jurassic-Cretaceous samples (sand type 3) are dominated by garnet grains and Meso-, Paleoproterozoic and Archean age zircons. This succession may be derived from the Canada-Greenland Shield, the northerly derived Devonian clastic wedge or directly from another Proterozoic-Archean terrane in the Arctic region (most likely Baltica).

4.1 Introduction

The Sverdrup Basin, situated in the Canadian Arctic Islands, is a NE-SW trending basin, approximately 1300 km long and 400 km wide (Fig. 4.1). The basin was a

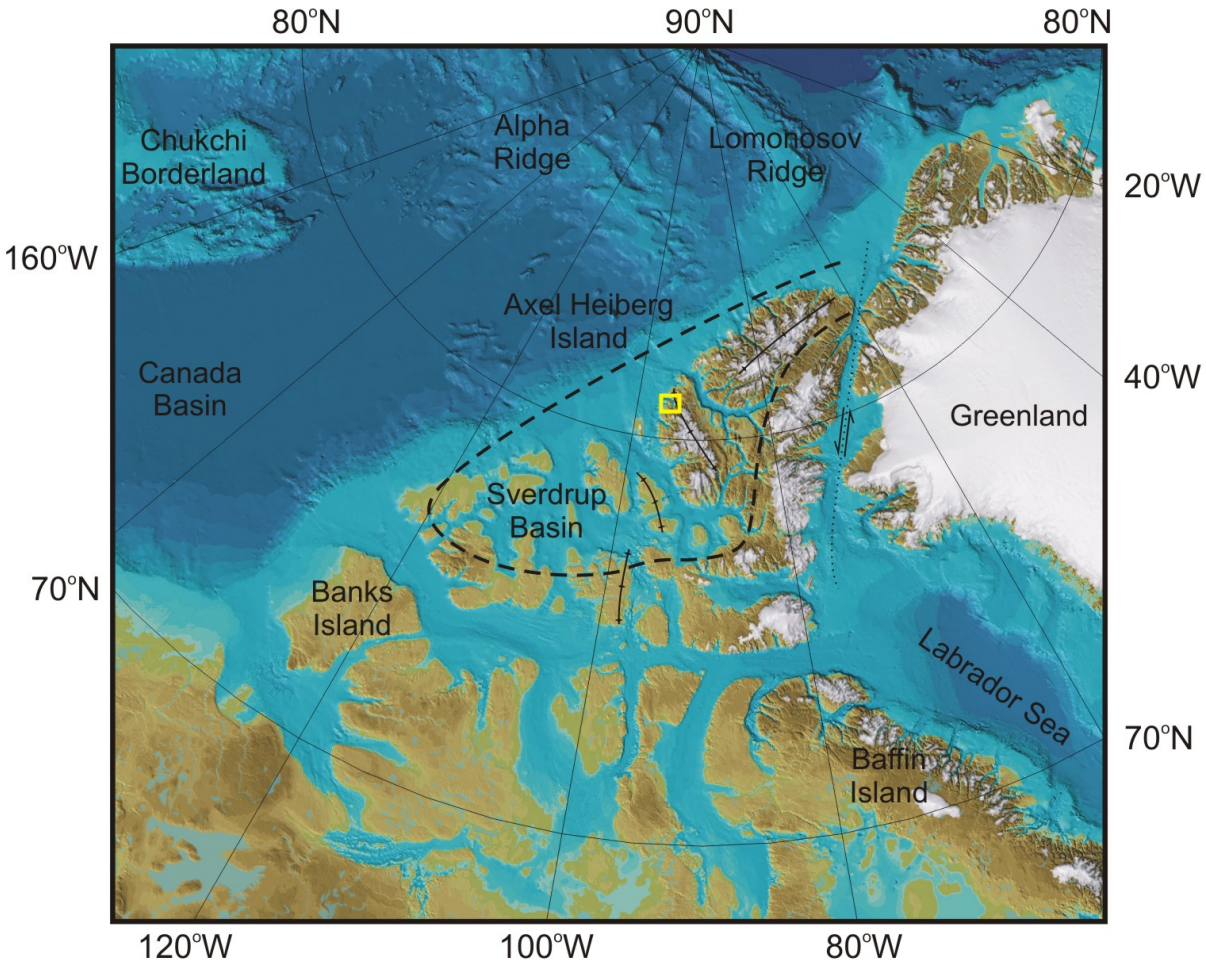

Figure 4.1: Regional setting of the Canadian Arctic Islands, showing the outline of the Sverdrup Basin (dashed). The basin lies at the northern margin of North America (Laurentia) and is bounded by Greenland and the Labrador Sea to the east, Banks Island to the west and the Arctic Ocean to the north. This topographic view shows the mountainous nature of the eastern Sverdrup Basin. The yellow box shows the area discussed (Fig. 4.2). Bathymetry and topography are from the IBCAO Arctic Bathymetry database (Jakobsson *et al.*, 2008).

major depocentre from Carboniferous to early Cenozoic time and contains a near complete succession composed almost entirely of clastic sedimentary rocks, reaching 9 km thick in the basin centre (Embry, 1991a). As a result of Eurekan deformation, the entire sequence is exposed on northwestern Axel Heiberg Island (Fig. 4.2).

This investigation of Mesozoic sandstones in the Sverdrup Basin provides constraints on the provenance of Mesozoic clastic sediment to the Sverdrup Basin and provides suggestions about the tectonic evolution of the Arctic region prior to the opening of the Arctic Ocean in late Mesozoic and Cenozoic time. This contribution represents the first Sverdrup Basin sediment provenance study, including detrital zircon ages, of a suite of stratigraphically constrained samples along a relatively continuous section.

4.2 Geological setting

The Sverdrup Basin formed by rifting in mid Carboniferous to Early Permian time, on the site of the Late Devonian-Early Carboniferous Ellesmerian deformation belt, possibly caused by extensional collapse of the deformation belt (Thorsteinsson & Tozer, 1970). The Ellesmerian event affected the northern margins of Alaska, North America (Laurentia) and Greenland, producing E-W and NE-SW trending folds, subparallel to the basin axis. However, the geodynamic cause of this compressional tectonism is poorly understood (Higgins *et al.*, 2000). The Late Paleozoic sedimentary fill in the basin comprises basal red beds and minor volcanic rocks, overlain by marine evaporites and carbonates and finally terrigenous clastic sediment (Davies & Nassichuk, 1991).

From Early Permian through Early Jurassic time, the Sverdrup Basin underwent thermal subsidence and most of the sedimentary succession was deposited (Davies & Nassichuk, 1991; Embry, 1991a). The Mesozoic fill in the basin is almost exclusively clastic sediment, with minor carbonates and volcanic rocks. Embry (1991a) subdivided the succession into 30 transgressive-regressive cycles, with subaerial unconformity cycle boundaries visible at the basin margins and submarine unconformity cycle boundaries in the basin centre. The regressive cycles typically consist of marine shale and siltstone coarsening up to shallow marine and deltaic sandstones (Embry, 1991a).

Source areas for the Mesozoic succession contained in the Sverdrup Basin are assumed to have lain to the south, east and northwest (Embry, 1991a, 1992). The landmasses to the immediate east and south currently expose Lower Paleozoic and Proterozoic carbonate and clastic rocks and Precambrian crystalline basement rocks

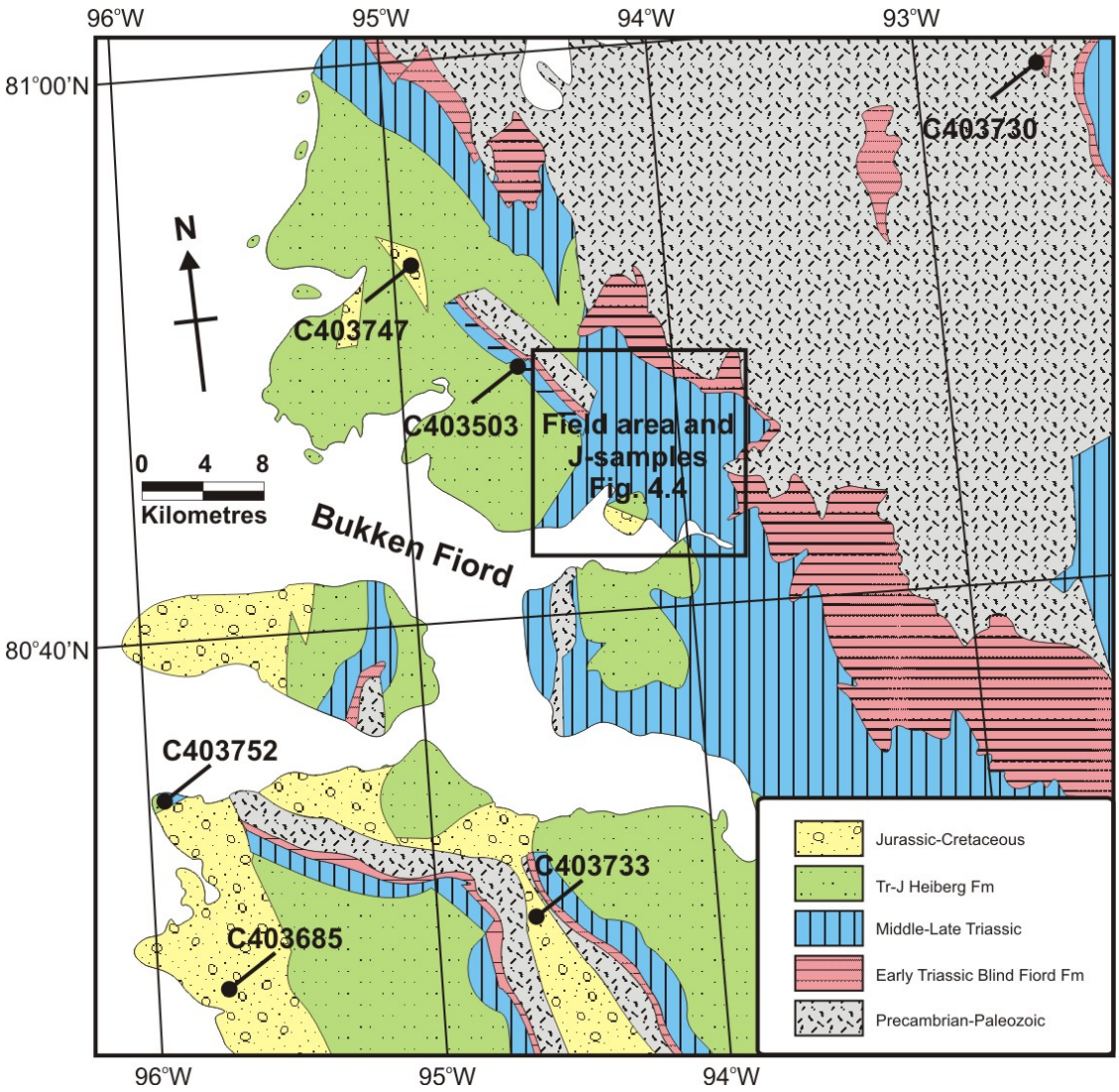

Figure 4.2: Simplified geological map of northwest Axel Heiberg Island, modified after Mayr *et al.* (2002), showing locations of Geological Survey of Canada (GSC) samples (C-samples) and the 2007 field area north of Bukken Fiord. The region contains abundant sills and dykes, which are not shown on the map.

of the Canada-Greenland Shield (Patchett *et al.*, 2004). Until Early Cretaceous time, much of the shield area is thought to have been covered by Middle-Late Devonian clastic wedge deposits transported onto the North American landmass following the mid Paleozoic Ellesmerian event (Patchett *et al.*, 2004 and references therein). Embry (1992) proposed that a cratonic source area to the northwest of the Sverdrup Basin, 'Crockerland', supplied sediment to the basin intermittently from Late Carboniferous through Middle Jurassic time. This inferred northerly derived succession thins towards the northwest where shallower-water facies are preserved (Embry, 1991a). The northerly derived clastic rocks are composed of very fine- to fine-grained sandstone, siltstone and shale, deposited in a variety of deep marine to nearshore settings. The succession is more than 2000 m thick and covers tens of thousands of square kilometres, indicating an extensive northern source (Embry, 1992).

Rifting of the Sverdrup Basin recommenced in Middle Jurassic time, forming a significant unconformity in Aalenian time, interpreted to represent the initiation of rifting in the proto-Amerasia Basin (Embry, 1991a). Two Early Cretaceous unconformities are interpreted to mark the onset of major rifting and seafloor spreading in the Amerasia Basin (Hauterivian age) and cessation of Canada Basin seafloor spreading (mid Cenomanian age) (Embry, 1991a). Igneous activity in the northeastern Sverdrup Basin is interpreted to be associated with these Early Cretaceous (and younger) tectonic events, forming the Sverdrup Basin Magmatic Province (Embry, 1991a; Villeneuve & Williamson, 2006). Basalt lava flows interbedded with Cretaceous clastic rocks and associated hypabyssal intrusive rocks were intruded into older sediments. Villeneuve & Williamson (2006) reviewed the Sverdrup Basin Magmatic Province and reported at least three episodes of magmatic activity: (1) magma intrusion during Barremian time (129-127 Ma), (2) flood basalt eruption with associated intrusions during Cenomanian time (98-92 Ma) and (3) emplacement of tholeitic lava flows in the Strand Fiord Formation during Santonian time (85.7-81.2 Ma). Note however that the Strand Fiord Formation has been dated as Cenomanian-Turonian on the basis of biostratigraphic data (Embry, 1991a).

A Maastrictian unconformity is interpreted to represent the onset of the Eurekan orogeny (Embry, 1991a). This mainly Paleocene-Eocene event was characterized by a series of intraplate deformation events caused by plate reorganizations linked to the opening of Baffin Bay, the North Greenland Sea and the Eurasia Basin (Okulitch & Trettin, 1991). The orogeny mainly affected eastern parts of the Sverdrup Basin (Ellesmere and Axel Heiberg Islands) and Late Paleozoic and

Mesozoic strata in the western Sverdrup Basin were only mildly deformed (Trettin, 1991).

Sverdrup Basin Mesozoic succession

Figure 4.3 shows a simplified Mesozoic stratigraphic column for northwest Axel Heiberg Island. The Early Triassic Blind Fiord Formation forms the entire Lower Triassic succession of the northern Sverdrup Basin, reaching a thickness of 1300 m in the basin centre (Embry, 1991a). Unconformably overlying Permian strata, the Blind Fiord Formation is composed of three members, with shale at the base, coarsening up to siltstone, with minor sandstone in the north. It is interpreted to represent slope and basin fill deposits (Embry, 1986) and on the basis of facies evidence and sediment geometry is interpreted to be northerly derived on Axel Heiberg Island (Embry, 1992).

The Murray Harbour Formation was deposited following a sea level rise at the beginning of the Middle Triassic. It consists of organic-rich shale, calcareous siltstone and minor very fine-grained calcareous sandstone in the upper part, interpreted to be of offshore origin (Embry, 1991a).

The Hoyle Bay Formation records an influx of large volumes of clastic sediment from the northwest during Carnian time. The formation is composed of shale and calcareous siltstone and has been interpreted to have been deposited in an outer shelf to slope setting (Embry, 1984). The Pat Bay Formation interfingers and conformably overlies the Hoyle Bay Formation and consists of very fine- to fine-grained calcareous sandstone, interpreted as nearshore-shallow marine and basinal sands (Embry, 1991a). As these two formations are interbedded, the name Hoyle Bay Formation will be used for both units.

The Norian Barrow Formation conformably overlies the Hoyle Bay Formation and contains shale and siltstones interpreted as prodelta and offshore marine shelf/slope deposits (Embry, 1984, 1991a).

The Norian-earliest Toarcian Heiberg Formation conformably overlies the Barrow Formation and is subdivided into the Romulus (lowest), Fosheim (middle) and Remus (highest) members, comprising sandstones of shallow marine shelf, fluvial-deltaic plain and delta front origin, respectively (Embry, 1991a). The sediment source for the deltas of the Heiberg Formation is believed to have been to the east and south of the Sverdrup Basin (Embry, 1991a).

The Toarcian-Aalenian Sandy Point Formation is an upward-coarsening succession of glauconitic very fine- to fine-grained sandstone, interpreted as shallow

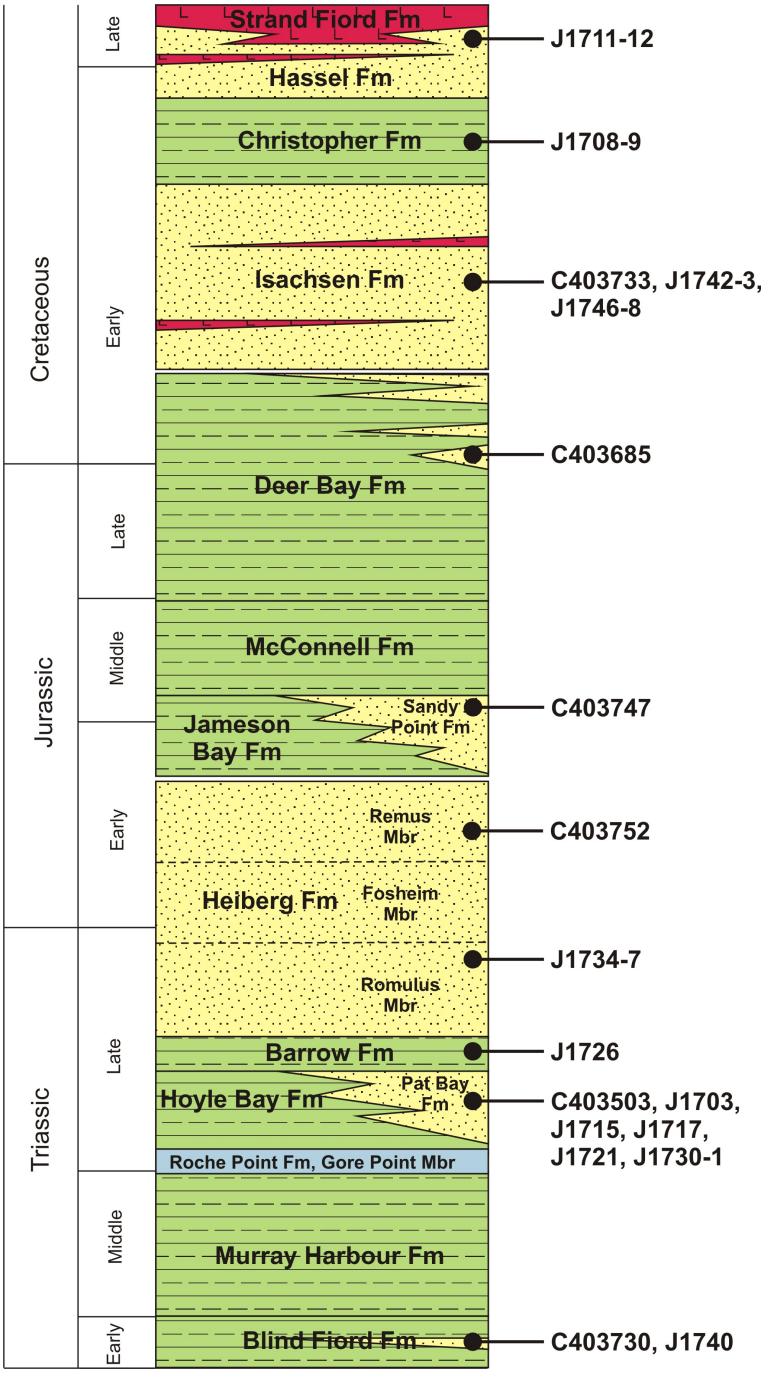

Figure 4.3: Simplified stratigraphic column for northwest Axel Heiberg Island, modified after Embry (1991a). Stratigraphic positions of the samples are shown. Three igneous events are shown, after Villeneuve & Williamson (2006): Barremian age basalt flows in the Isachsen Formation, Cenomanian age basalt flows in the Hassel Formation and the Santonian age Strand Fiord Formation.

marine shelf origin (Embry, 1991a). The sandstones become more shale-rich towards the southwest, implying a sediment source to the north (Embry, 1992).

The Berriasian-Valangian Deer Bay Formation is interpreted to represent outer shelf shale, with minor very fine-grained sandstone and siltstone, and on facies evidence is thought to have been sourced from the east and south of the Sverdrup Basin (Embry, 1991a).

The Valangian-Aptian Isachsen Formation consists of sandstone containing rounded quartzite pebbles and coal and minor shale and siltstone, interbedded with basalt flows and pyroclastics, interpreted to have been deposited in a deltaic environment (Embry & Osadetz, 1988).

The late Aptian-early Cenomanian Christopher Formation consists of shale, siltstones and minor volcanic sandstone, of prodelta to offshore marine origin. The Albian-Cenomanian Hassel Formation contains sandstone, with minor siltstone and shale, of deltafront origin and is interbedded with basalt flows of the Strand Fiord Formation containing mainly subaerial basalt flows and pyroclastic material. Minor coal, shale and conglomerate are associated with the igneous material.

4.3 Samples and methods

Twenty eight Mesozoic samples from northwestern Axel Heiberg Island are discussed in this chapter (Fig. 4.3). Samples with a J-prefix were collected during 2007 fieldwork around Bukken Fiord, northwestern Axel Heiberg Island (Figs. 4.2 and 4.4). Samples with a C-prefix were provided by Ashton Embry of the Geological Survey of Canada (GSC) and were collected during 1996 and 1999 field seasons to northwestern Axel Heiberg Island. The samples were analysed for petrography, heavy mineral analysis, garnet and tourmaline chemistry and SIMS zircon analysis (Table 4.1) following analytical methods outlined in Chapter 3.

4.4 Bukken Fiord area fieldwork observations

Fieldwork was carried out in the Bukken Fiord area, northwestern Axel Heiberg Island, during June-July 2007 (Fig. 4.4). Figure 4.5 shows views of the study area from the base camp north of Bukken Fiord. The study area is characterized by a succession of Triassic and Cretaceous south-southwest dipping strata, separated by a fault system. Figure 4.6 shows panoramic views of the strata encountered in the study area.

Sample	Formation	Age	Petro-graphy	HM analysis	Garnet chemistry	Tourmaline chemistry	Zircon dating
J1712	Strand Fiord	K1-K2	y	y		y	
J1711	Strand Fiord	K1-K2	y				
J1709	Christopher	K1	y	y		y	
J1708	Christopher	K1	y	y	y	y	
J1707	Christopher	K1	y				
C403733	Isachsen	K1	y	y	y	y	
J1748	Isachsen	K1	y				
J1747	Isachsen	K1	y	y			
J1746	Isachsen	K1	y	y			
J1743	Isachsen	K1	y	y	y	y	
J1742	Isachsen	K1	y				
C403685	Deer Bay	J3	y	y	y	y	y
C403747	Sandy Point	J2	y	y		y	y
C403752	Heiberg	J1	y	y		y	y
J1737	Heiberg	T3-J1	y	y		y	
J1736	Heiberg	T3-J1	y	y		y	
J1735	Heiberg	T3-J1	y				
J1734	Heiberg	T3-J1	y				
J1726	Barrow	T3-J1	y	y			
C403503	Hoyle Bay	T3	y	y		y	y
J1731	Hoyle Bay	T3	y				
J1730	Hoyle Bay	T3	y				
J1721	Hoyle Bay	T3	y	y		y	
J1717	Hoyle Bay	T3	y	y			
J1715	Hoyle Bay	T3	y	y		y	
J1703	Hoyle Bay	T3	y				
C403730	Blind Fiord	T1	y	y			y
J1740	Blind Fiord	T1	y				

Table 4.1: Overview of analyses performed on the Axel Heiberg samples. The samples are listed in stratigraphic order, with the youngest samples at the top. The stratigraphic position of the C-samples in relation to the J-samples is not always clear. J-samples were collected during June-July 2007 fieldwork. C-samples are Geological Survey of Canada samples, collected by Ashton Embry during 1996 and 1999 fieldseasons. HM = Heavy mineral. Y=sample analysis done.

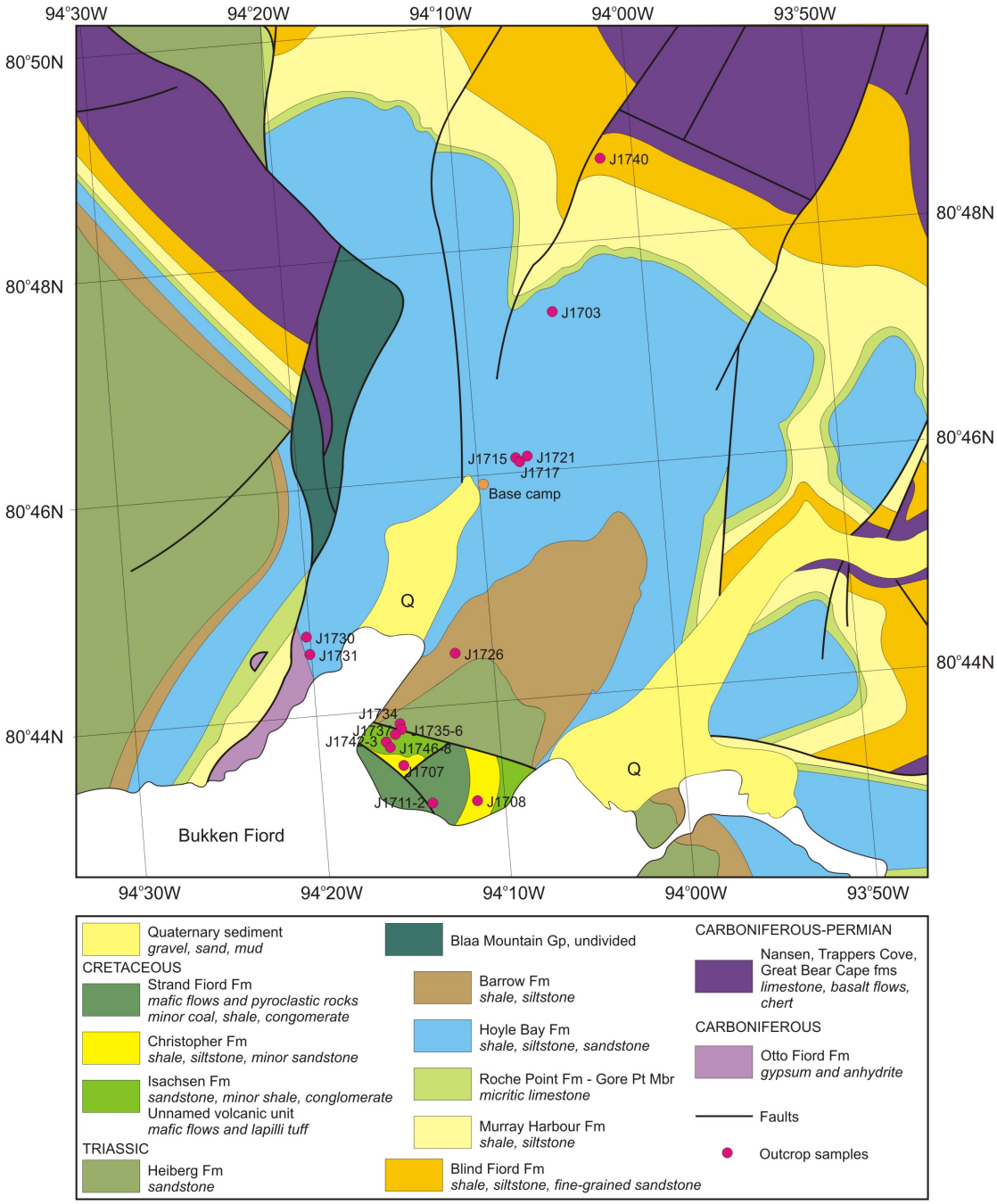

Figure 4.4: Bukken Fiord field localities, shown on a geological map modified after Mayr *et al.* (2002). Abundant sills and dykes, present mainly in the Hoyle Bay Formation, are not mapped. Jurassic units, present elsewhere on Axel Heiberg Island, are not exposed in the Bukken Fiord area. These units include the Fosheim and Remus members of the Heiberg Formation, Jameson Bay Formation, Sandy Point Formation, McConnell Formation and Deer Bay Formation.

Northwestern Axel Heiberg Island shows abundant structural complexity, mainly related to the Eurekan Orogeny. For the Bukken Fiord area, Mayr *et al.* (2002) depict a number of NE-SW faults. One such fault was observed in the main valley of the study area (just west of 94°10W), showing a near-vertical, dextral strike-slip geometry (Figs. 4.4 and 4.6). No repetition of strata were seen within the study area but additional structural complications should not be ruled out, as poor exposure due to frost shattering and dislocated scree on slopes may mask complexity.

The Triassic succession (and in particular the Hoyle Bay Formation) contains abundant Cretaceous hypabyssal sills and lesser dykes, often capping hills and inhibiting erosion of Triassic strata (Fig. 4.6). These volcanic rocks are not indicated on the geological maps of the area (Mayr *et al.*, 2002). There is little published information concerning the biostratigraphic dating of the succession and the samples discussed here are assigned formation names on the basis of the Geological Survey of Canada 1:125,000 scale geological map of the region (Mayr *et al.*, 2002). Palaeontological samples were collected by the Axel Heiberg field party and subsequently analysed by Simon Kelly of CASP (Kelly *et al.*, 2008). The collection of accurate orientation data was made made difficult by close proximity to the magnetic North Pole, rendering a magnetic compass useless.

Triassic succession

The Bukken Fiord area exposes an apparently continuous Triassic succession from the Early Triassic Blind Fiord Formation, through the Blaa Mountain Group (Murray Harbour, Roche Point, Hoyle Bay, Barrow formations), to the Late Triassic Heiberg Formation (Romulus Member) (Fig. 4.4). On the basis of mean dip of 15-20°, and assuming no structural repetition, the overall thickness of the Triassic succession in the Bukken Fiord area is estimated to be between 3000 and 4000 m. During fieldwork this entire succession was examined and sampled.

The Triassic succession north of Bukken Fiord is shale-dominated, with interbedded units of siltstone and fine-grained sandstone becoming more common higher in the succession. Lithologies and depositional style are similar throughout the succession, with the exception of one prominent limestone unit (Gore Point Member of the Roche Point Formation) and it is commonly difficult to distinguish between the component formations of the Blaa Mountain Group.

The Blind Fiord Formation was encountered in the north of the study area, and its thickness estimated to be ∼250 m. The formation was dominated by shale, with one prominent ∼20 m thick siltstone unit (Fig. 4.7). Exposure was poor or inaccessible, making it difficult to establish a depositional environment and thus

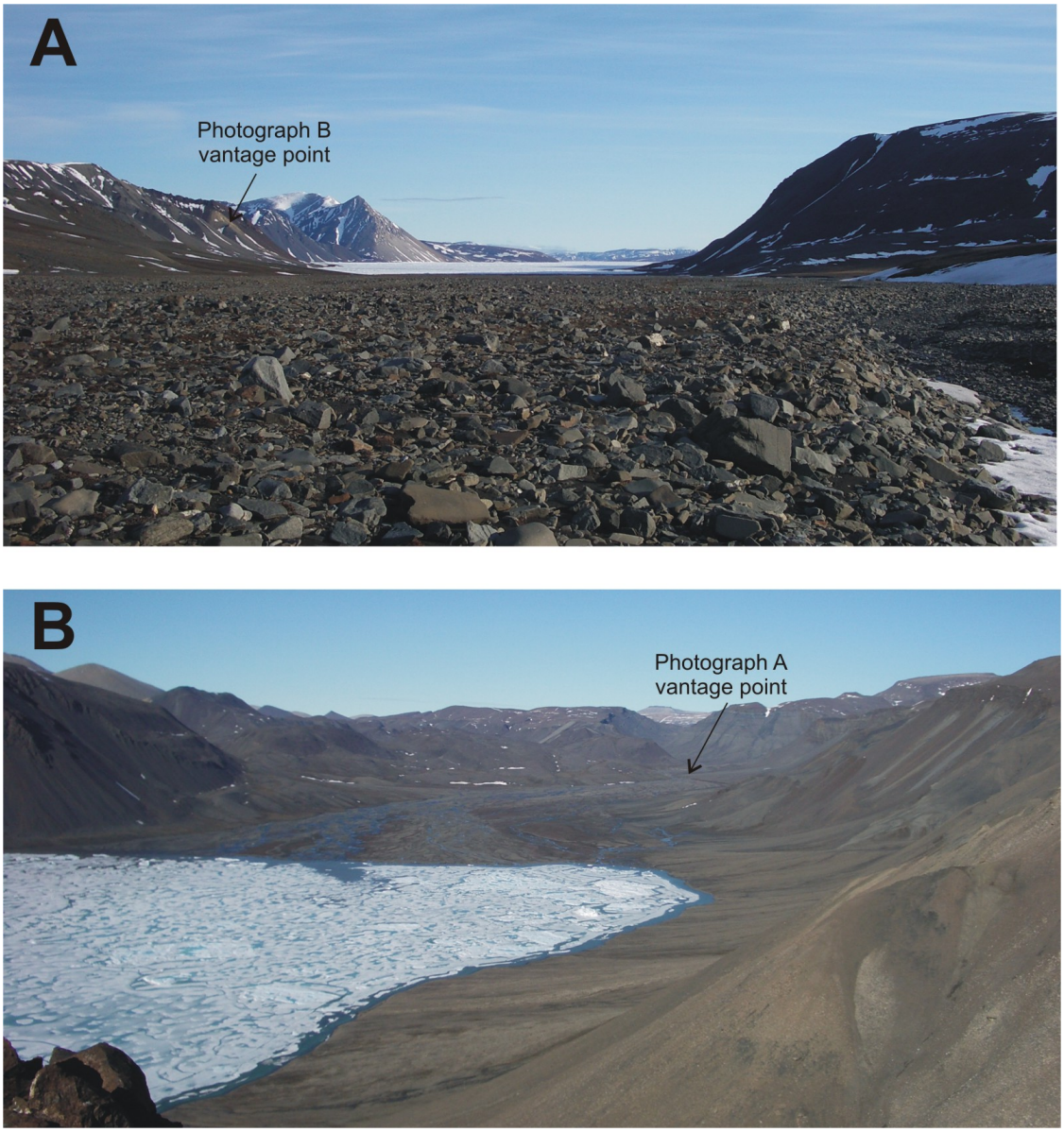

Figure 4.5: Views of the Bukken Fiord region. (A) View to southwest from base camp. The hillslope on the left exposes Triassic strata (Murray Harbour to Heiberg Formation) and the Cretaceous Isachsen Formation. On the right is a fault zone exposing Carboniferous Otto Fiord Formation evaporites, which cross the fiord and passes through the conical mountain seen on the left. This mountain contains pale Permo-Carboniferous limestones on the right and darker Triassic (Heiberg Fm) strata on the left. (B) View northeast showing the Bukken Fiord and Quaternary outwash plain in the foreground. The right hand side shows the Heiberg Formation. The rest of the photo mainly shows the shale-dominated Hoyle Bay Formation, capped by sills. Pale coloured rocks in the distance are Carboniferous-Permian carbonates.

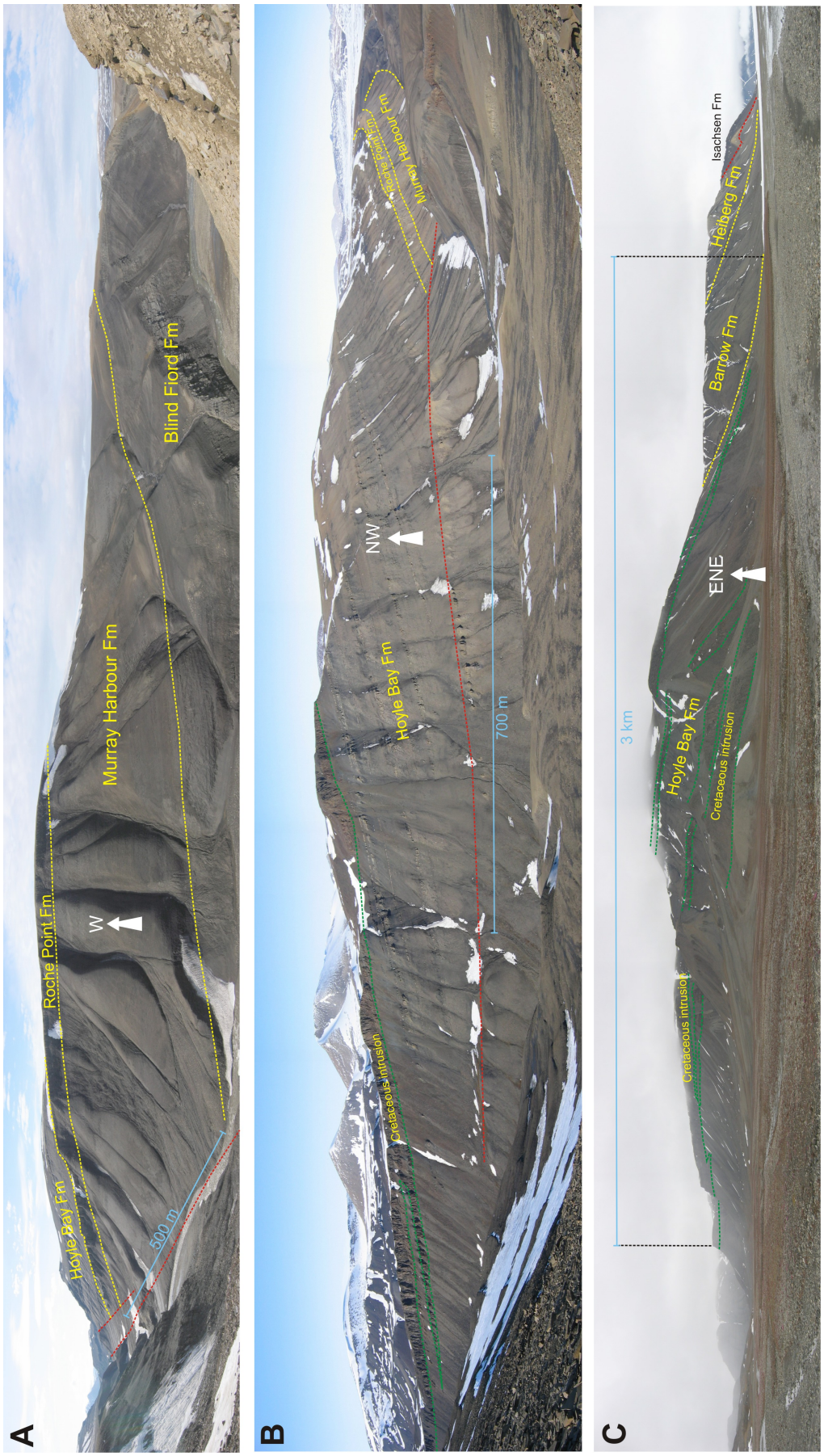

Figure 4.6: Panoramic views of the Bukken Fiord area. Yellow dashed lines are formation boundaries; red dashed lines are faults; green dashed lines are intrusion margins. Section A connects to section B. The photographs were taken and annotated by Robert Scott.

there are no data with which to support or challenge the outer shelf interpretation of Embry (1986). Biostratigraphic data collected from this unit proved inconclusive (Kelly *et al.*, 2008).

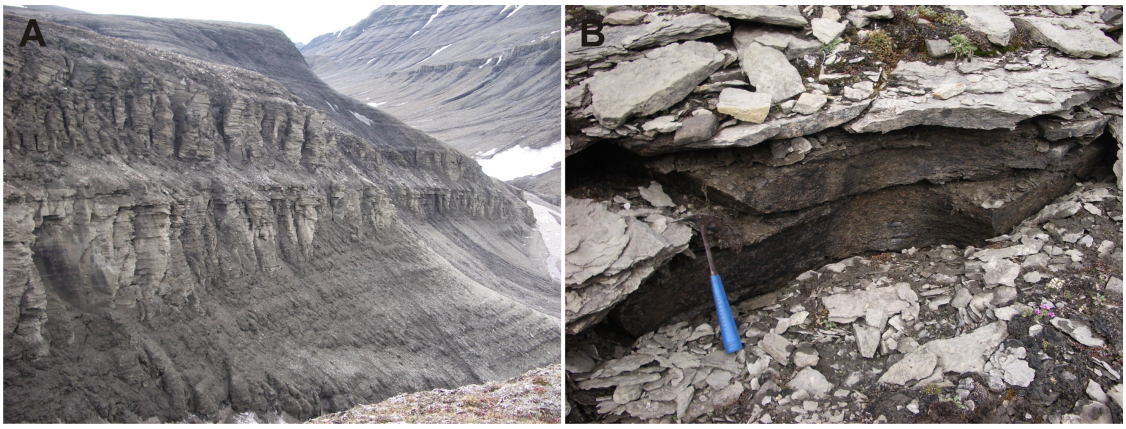

Figure 4.7: Blind Fiord Formation. (A) Basal section of the Blind Fiord Formation, showing abundant siltstone layers. (B) Siltstone exposure, from which sample J1740 was collected.

The Murray Harbour Formation was encountered in the north of the study area and its thickness estimated to be up to 300 m. The unit is dominated by shale with minor siltstone and is well exposed in stream sections (Fig. 4.8). The unit has been interpreted as outer shelf-slope (Embry, 1991a) and the fine-grained nature of the sediment supports this. The Murray Harbour Formation has been assigned a Middle Triassic (Anisian-Ladinian) age on the basis of ammonites and bivalves (Embry, 1984). The presence of bivalve species *Daonella elegans* Mclearn, collected during fieldwork, is consistent with a Ladinian age (Kelly *et al.*, 2008).

The Hoyle Bay Formation crops out over an extensive part of the study area, with an estimated thickness of ∼1000 m. Sandstone units occurring within the Hoyle Bay Formation could be classified as the Pat Bay Formation, but as discrimination between the Hoyle Bay and Pat Bay formations is not clear and the units are interbedded, the entire interbedded shale-sandstone unit is here referred to as the Hoyle Bay Formation. In the study area, the exposure of this formation is good (Figs. 4.6 and 4.9). Laterally continuous sandstones show tabular cross-beds, dipping towards southeast, with occasional symmetrical ripples. Embry (1984) suggested an outer shelf to slope setting for the Hoyle Bay Formation and a nearshore marine environment for the Pat Bay Formation. The presence of tabular cross-bedding and symmetrical ripples in sandstones, coupled with thick shale packages indicate a shallow wave-dominated shelf. The fossil assemblage collected includes

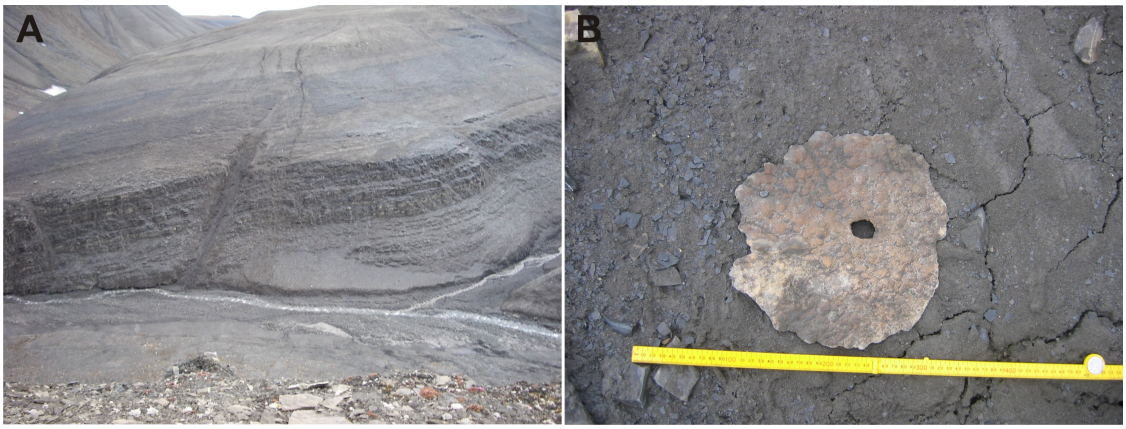

Figure 4.8: Murray Harbour Formation. (A) View of shale-dominated Middle Triassic Murray Harbour Formation showing active erosion by streams. (B) Loose concretion cone-in-cone structure, typical of organic-rich mudstones. Photograph taken by Robert Scott.

bivalves (*Meleagrinella antiqua* Tozer, *Myophoria* spp. and *Oxytoma* sp.) and ammonoids (*Sirenites nanseni* Tozer, *S.* cf. *costatus* Tozer and *Plagiostoma* spp.) which indicate a Carnian age (Kelly *et al.*, 2008). The presence of molluscan fauna suggests a marginal marine setting.

The Barrow Formation was encountered in the southern part of the study area and is estimated to be up to 600 m thick. The Barrow Formation is transitional in character between the underlying Hoyle Bay Formation and overlying Heiberg Formation, making it difficult to define the boundaries of this unit. The Barrow Formation is composed of poorly exposed bioturbated shale and siltstone, with packages of well-bedded brownish sandstone (Fig. 4.10). The sandstone beds display symmetrical wave ripples. A shallow, wave-dominated, marine shelf environment is suggested for this unit in the study area. This is at odds with the published interpretation of prodelta and offshore marine shelf/slope environment (Embry, 1984, 1991a). The bivalve species *Halobia (Zittelihalobia)* aff. *zittelli* is indicative of a Carnian or Norian age (Kelly *et al.*, 2008). Palynological material, *Rhaetopollis germanicus*, *Ricciisporites tuberculatus* and *Kyrtomisporis* spp., is indicative of an age no older than Early-Late Norian (Kelly *et al.*, 2008).

The lower Heiberg Formation (Romulus Member) was encountered in the southern part of the study area with an estimated thickness of at least 800 m. The upper part of the formation is faulted out against Cretaceous strata in the study area (Mayr *et al.*, 2002) (Fig. 4.4). This contact was not directly viewed in the field. The Heiberg Formation in this area is composed of a coarsening-upwards succes-

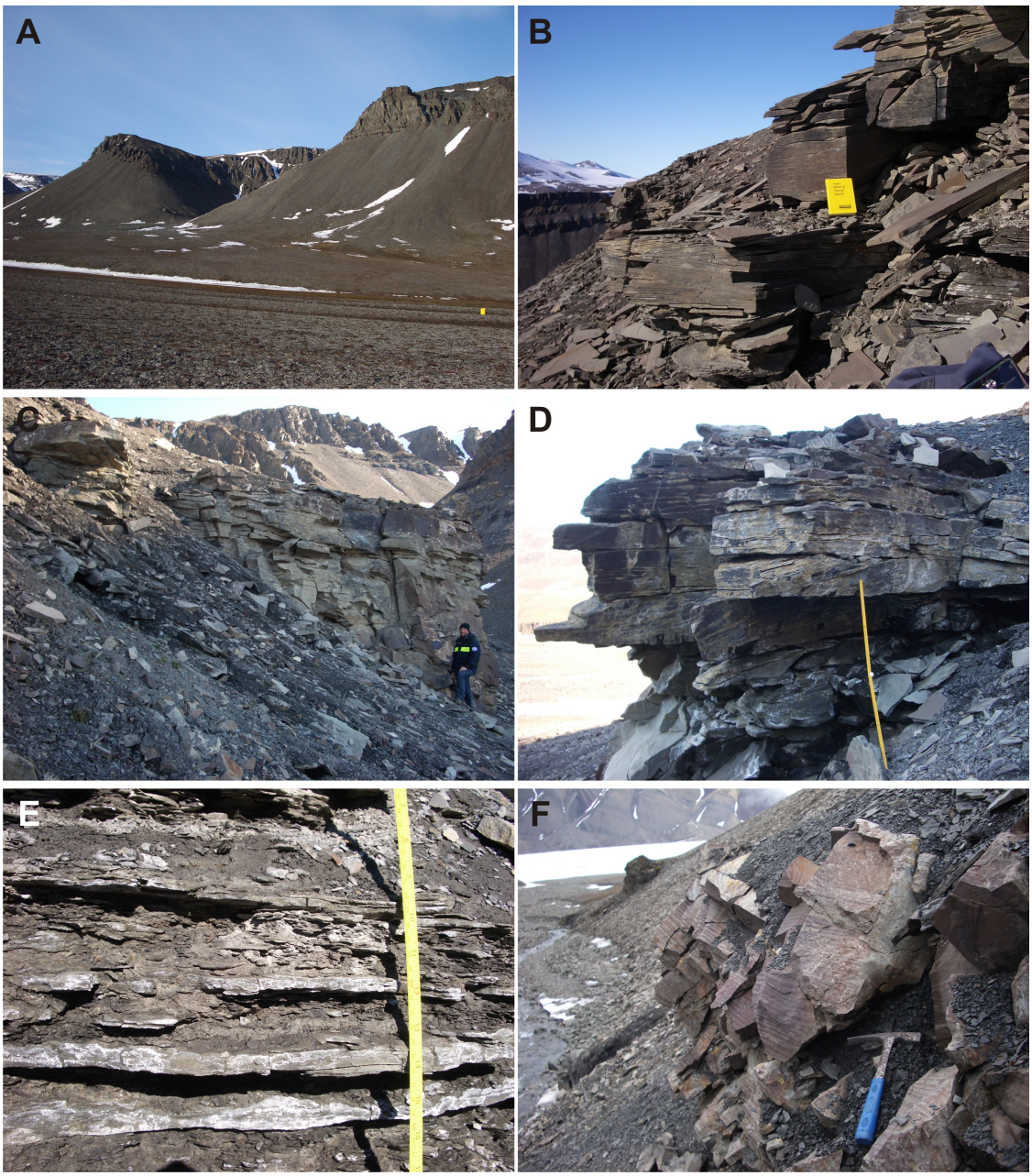

Figure 4.9: Hoyle Bay Formation. (A) View from basecamp of Hoyle Bay Formation strata capped by Cretaceous sills. (B) Siltstone, at base of the Hoyle Bay Formation in the Bukken Fiord region. (C) View looking east showing ∼4 m thick exposure of cross-bedded sandstone. Foresets dip to southeast. Cretaceous sills are visible in the background. (D) View northwest of fine-grained sandstone, with tabular cross-bedding and foresets dipping towards southeast. Rule is 1 m. Sample J1715 was collected here. (E) Interbedding of shale and siltstone. (F) Red and white-striped Hoyle Bay Formation exposure. Bukken Fiord is visible in the background. Samples J1730-1 were collected here.

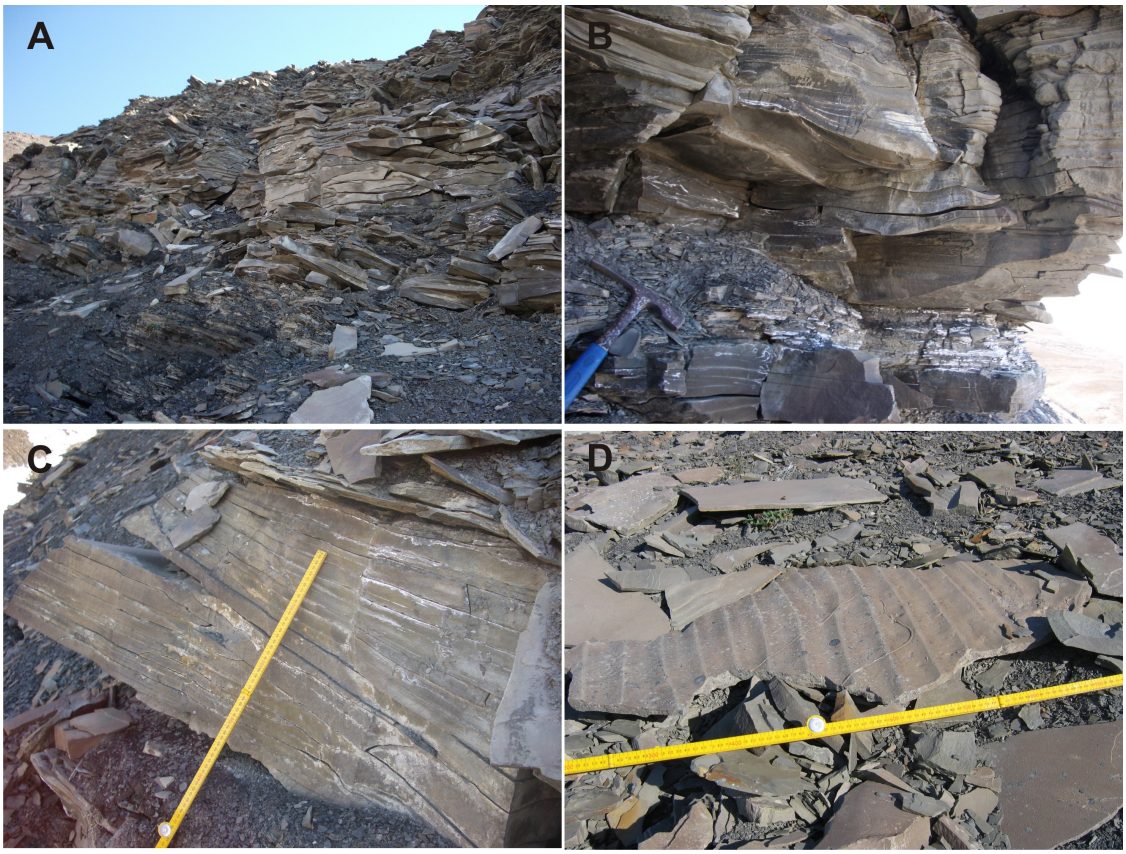

Figure 4.10: Barrow Formation. (A-B) View of Barrow Formation exposures showing interbedding of sandstone and shale. Sample J1726 was collected from this exposure. (C) Fine-grained sandstone showing planar cross bedding. (D) Loose block of fine-grained brown sandstone showing symmetrical ripples and a feeding trail. Photograph taken by Robert Scott.

sion of interbedded sandstone and minor shale (Fig. 4.11). Sandstone units contain abundant plant debris, symmetrical ripples and extensive bioturbation. A wave-dominated shallow marine to delta front environment with periodic emergence is interpreted. The presence of bivalve species *Meleagrinella antiqua* Tozer suggests a Carnian-Norian age (Kelly *et al.*, 2008). However, the presence of palynological species *Chasmatosporites* spp., *Limbosporites* cf. *lundbladii* and *Ricciisporites tuberculatus* spp. indicate a late Rhaetian-early Hettangian age.

Cretaceous succession

Cretaceous sedimentary and associated volcanic rocks were examined in the south of the study area where they are mapped as the Isachsen, Christopher, Hassel and Strand Fiord formations (Mayr *et al.*, 2002) (Fig. 4.4). This succession is faulted

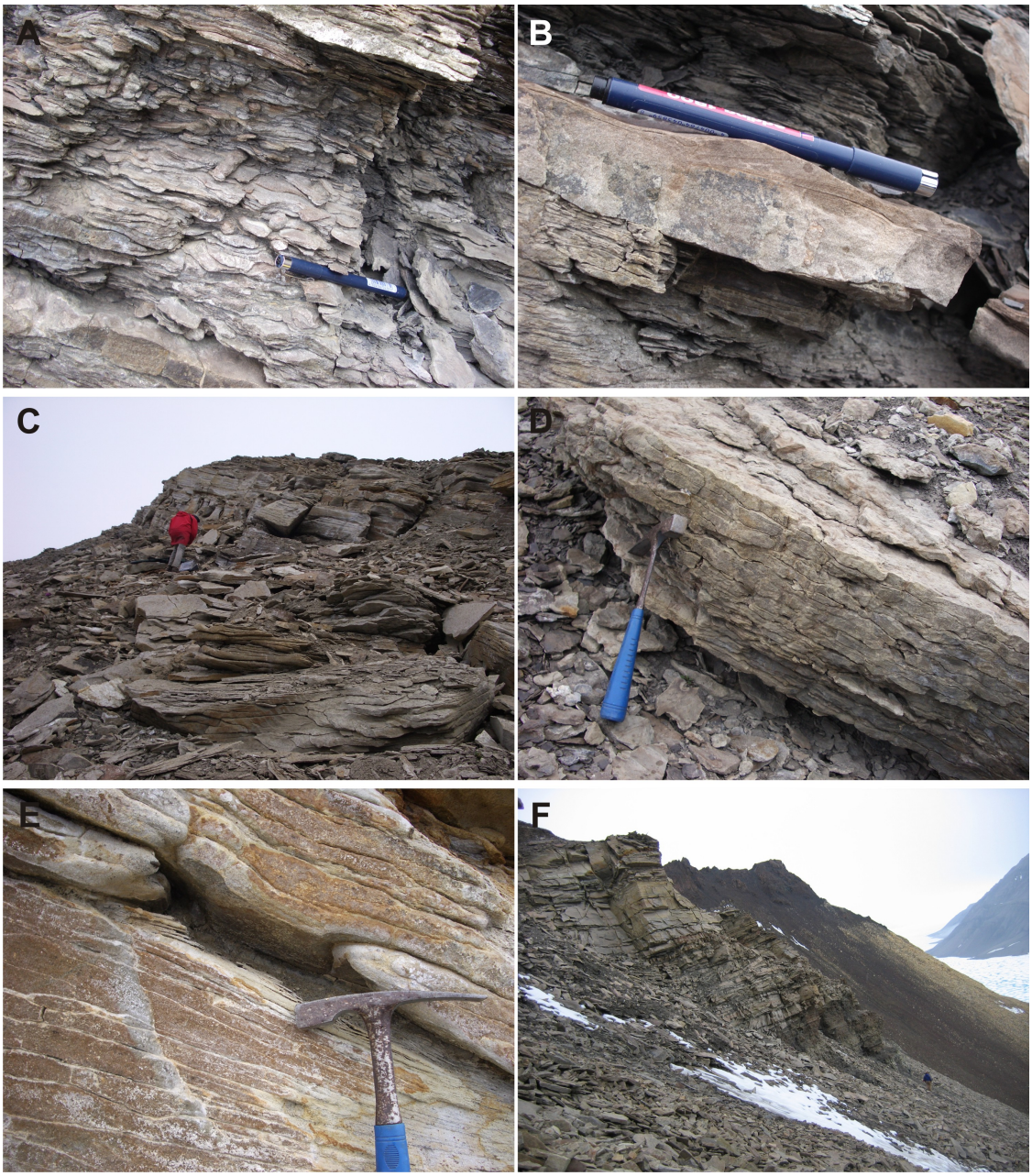

Figure 4.11: Heiberg Formation. (A-B) Burrows and ripples in the lower portion of the succession. Sample J1734 was collected here. (C-D) More thickly bedded sandstones. Sample J1735 was collected here. (E) White sandstone showing iron-rich nodules. (F) View south of coarsening-upward sandstone package within the Heiberg Formation. Sample J1737 was collected here. Photograph taken by Robert Scott. Note the author for scale.

against the Triassic Heiberg Formation.

The Isachsen Formation is comprised of medium to coarse-grained sandstones with channelized conglomerate layers containing well-rounded quartz pebbles and coal seams (Fig 4.12). The sandstones are 1-2 m thick and interbedded with palagonitized (shallow water) basalt flows also 1-2 m thick. Embry (1982) suggested a deltaic depositional setting.

The Christopher Formation is poorly exposed in the study area (Fig. 4.13). Lenticular bodies of fine-grained sandstones in an area of scree may represent the Christopher Formation. However, no fossils were recovered and the poor exposure did not allow the depositional environment of this formation to be established.

The Strand Fiord Formation was encountered in the southernmost part of the field area, on the coast of the Bukken Fiord (Fig. 4.13). Basalt flows, pyroclastic rocks and lapilli tuffs were encountered. Interbedded conglomerate lenses were sampled. The interpreted depositional environment of mainly subaerial eruption and sedimentation proposed by Ricketts *et al.* (1984) is accepted for this unit.

4.5 Petrography results

Figures 4.14-4.18 illustrate point counting results for 28 Axel Heiberg samples (Table 4.1). Photomicrographs of the analysed samples are shown in figures 4.19-4.27. The complete dataset is included in the accompanying CD.

The Early Triassic Blind Fiord Formation samples J1740 and C4030730 were studied for petrography. Sample J1740 was collected north of Bukken Fiord during 2007 fieldwork. Sample C403730 was collected by Ashton Embry further north on Axel Heiberg Island (Fig. 4.2). Sample J1740 is moderately sorted, silt-sized, quartz arenitic wacke (Fig. 4.14). The sample is dominated by monocrystalline quartz (91% non-undulose and 6% undulose) (Fig. 4.15). Sample C403730 is a pebbly sandstone with well-rounded chert pebbles (up to 1.5 cm in diameter) embedded in a very fine-grained arenitic matrix (Fig. 4.14). This is unusually coarse for the Blind Fiord Formation. The pebbles are presumably derived from underlying Permian strata. The point counting data record the chert pebbles present in this sample and 69% of the recorded quartz is chert (Fig. 4.15). Most of the remainder is non-undulose monocrystalline quartz (28%). Disregarding the chert pebbles present in sample C403730, the sedimentary characteristics of the two Blind Fiord Formation samples are similar. The predominance of monocrystalline quartz suggests derivation from a plutonic source. On a QtFL plot, the samples plot within the 'craton interior' field. On a QmFLt plot, the samples plot within the 'craton

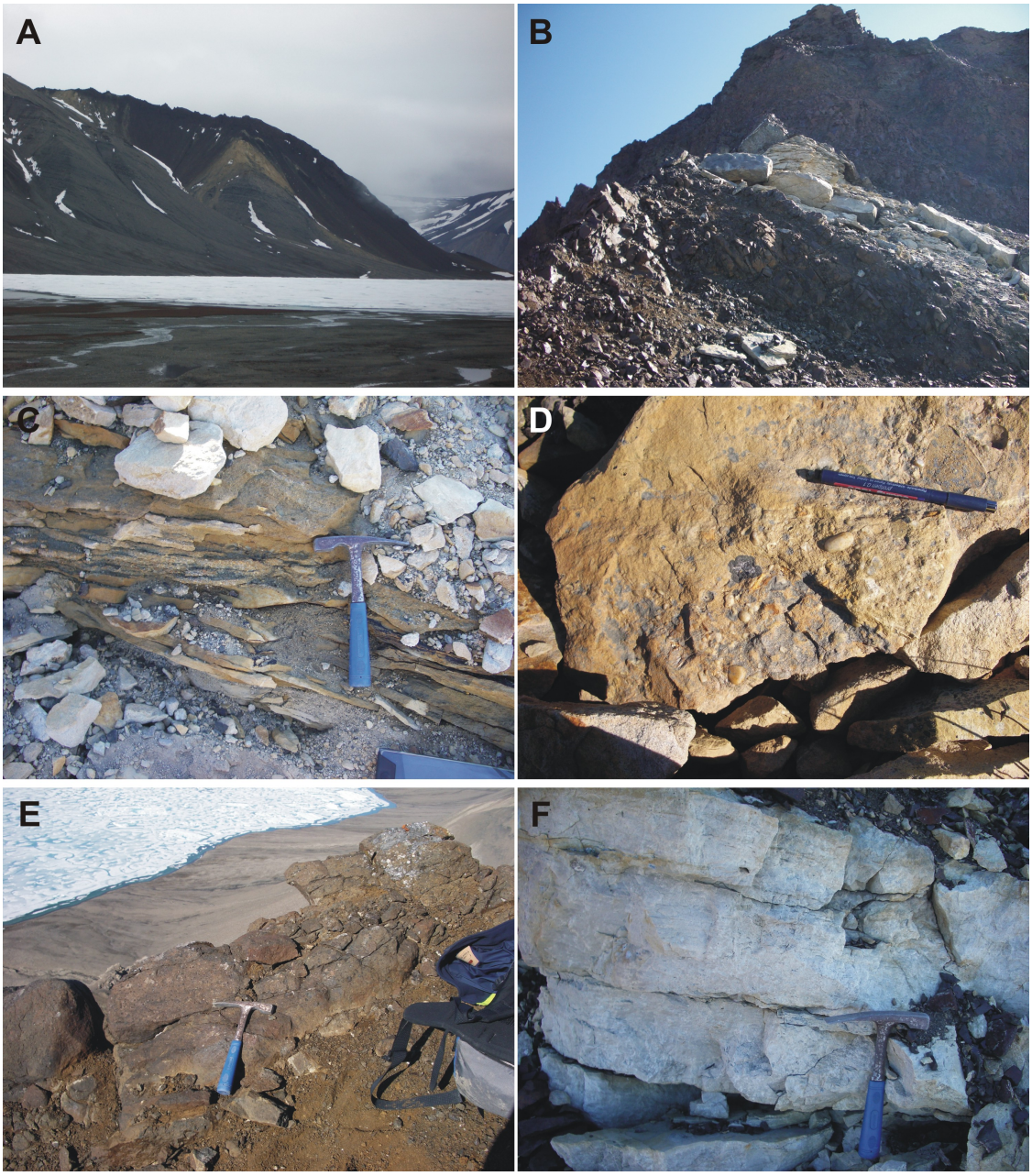

Figure 4.12: Isachsen Formation. (A) View southeast showing scree of the Late Triassic Heiberg Formation (grey coloured sediment) overlain by the Early Cretaceous Isachsen Formation (yellow coloured sediment) and Strand Fiord Formation (red coloured volcanics. The Heiberg and Isachsen formations are separated by a fault. The Bukken Fiord is in the foreground. (B) View south of basalt flows and interbedded sandstone units. (C) Conglomerate layers (left of hammer) cutting into medium to coarse-grained sandstone beds. On the right, dark staining is caused by the presence of coal. (D) Loose block showing rounded quartz pebbles in a medium to coarse-grained sandstone. (E) View north of shallow marine basaltic units with the Bukken Fiord in the background. (F) White sand of the Isachsen Formation.

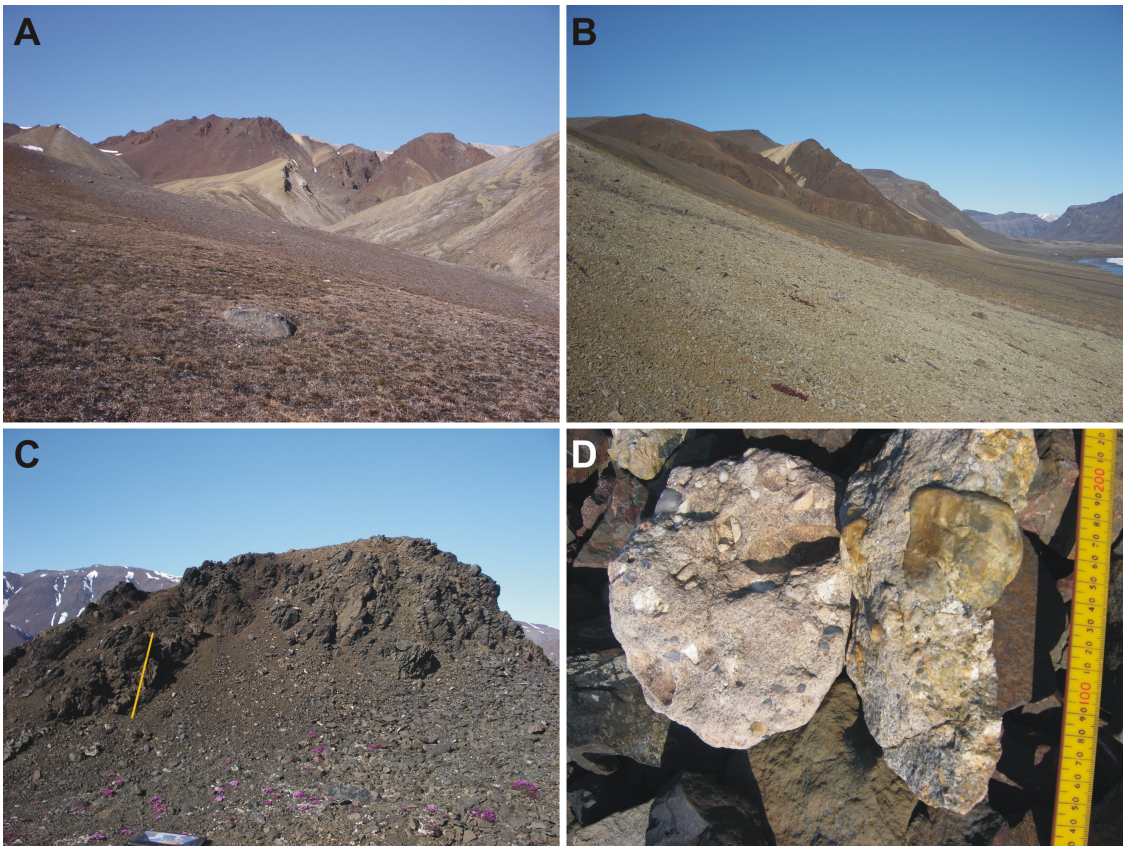

Figure 4.13: Strand Fiord and Christopher formations. (A-B) General views north of Strand Fiord volcanics and associated strata. The pale foreground scree in both photographs is the Christopher Formation. (C) View towards west of Strand Fiord volcanics. (D) Loose blocks of polymictic conglomerates derived from lenses within the Strand Fiord Formation. Polymictic matrix- and clast-supported conglomerates are present and clasts are angular to rounded.

interior' (J1740) and 'recycled orogen' (C403730) fields (Fig. 4.17). The 'recycled orogen' classification for sample C403730 on the QmFLt plot reflects the presence of the chert clasts in this sample.

In total, seven Hoyle Bay Formation samples were studied for petrography. Sample J1703 was collected at the base of the formation and is similar to the underlying Blind Fiord Formation: silt-sized quartz arenitic wacke dominated by non-undulose monocrystalline quartz (93%) (Figs. 4.14 and 4.15). Samples J1715, J1717 and J1721 were collected higher in the succession (Fig. 4.4). These samples are fine-grained, moderately sorted sublitharenites (Fig. 4.14). Quartz grains are dominated by monocrystalline quartz (60-75% non-undulose and 4-6% undulose) that show abundant fluid inclusions, characteristic of plutonic quartz (Fig. 4.15). The samples also show 10-32% polycrystalline quartz with four or more sub-

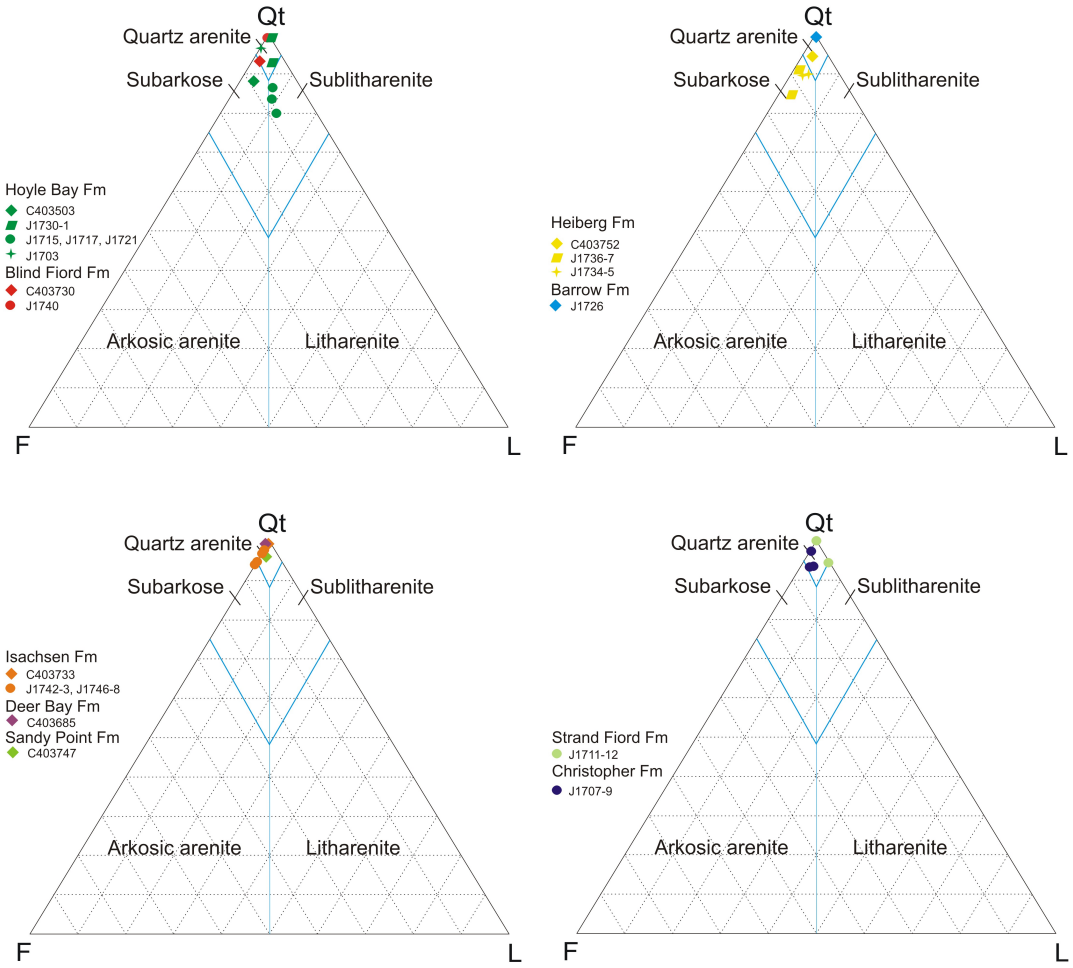

Figure 4.14: Sediment classification of Axel Heiberg samples. QtFL sandstone classification plot, modified after Pettijohn *et al.* (1987).

grains. These quartz grains show elongate, sutured subgrains, typical of metamorphic sources. There is 1-7% chert present. Lithic clasts constitute between 8-12% of grains in these samples and are mainly mica schist: polycrystalline quartz and mica showing schistose fabric. Feldspar constitutes 6-8% of the samples, and both plagioclase and alkali feldspar are present (Fig. 4.16). On QtFL and QmFLt plots, the samples plot within the 'recycled orogen' fields (Fig. 4.17).

Samples J1730 and J1731 were collected close to the top of the Hoyle Bay Formation in the Bukken Fiord field area (Fig. 4.4). These samples are moderately well to well-sorted, very fine to fine-grained quartz arenites (Fig. 4.14). Quartz types are dominated by non-undulose monocrystalline quartz (87-95%) with abundant fluid inclusions, characteristic of a plutonic source (Fig. 4.15). On a QtFL plot, the samples plot within the 'recycled orogen' field. On a QmFLt plot, the

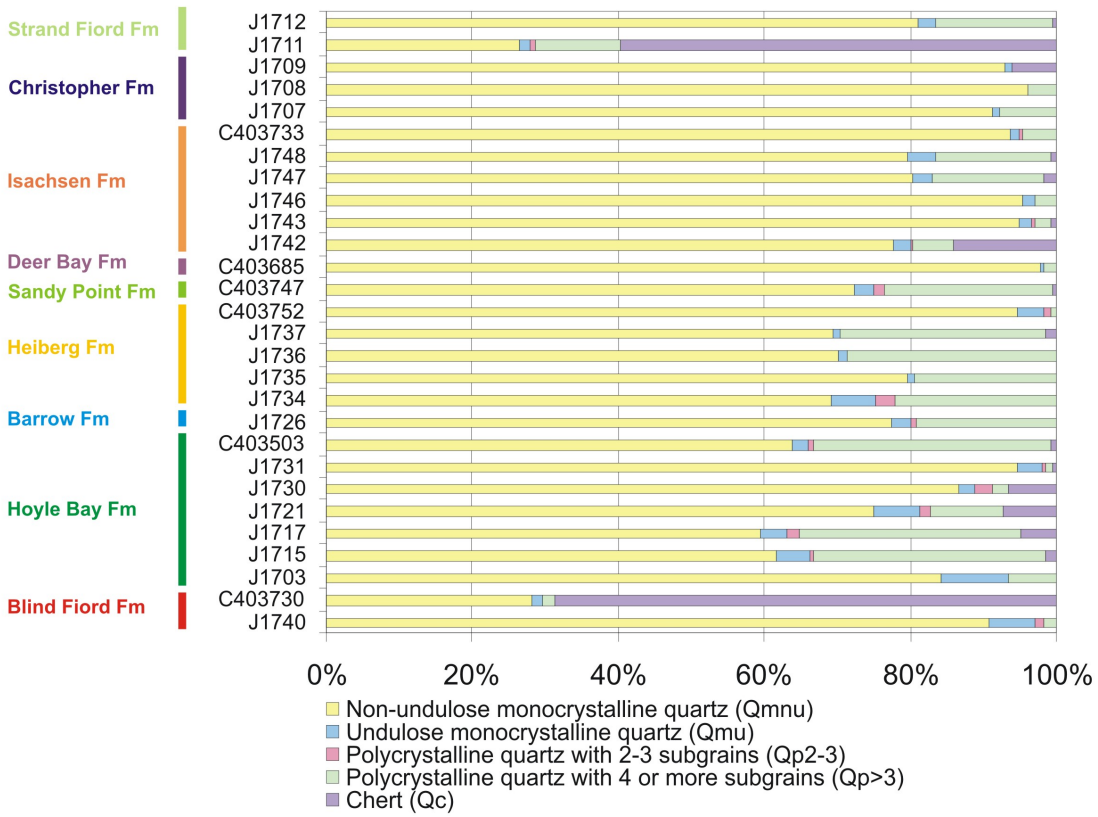

Figure 4.15: Quartz types identified by point counting, plotted as percentage of Total Quartz and Chert (Chapter 3). Most samples are dominated by monocrystalline quartz, with the exception of C403733 and J1711, which are conglomerates showing predominantly chert clasts.

samples plot within the 'craton interior' and 'recycled orogen' fields (Fig. 4.17).

Sample C403503 is a moderately sorted, fine-grained, subarkose (Fig. 4.14) and shows a mixture of quartz types: 64% non-undulose monocrystalline quartz and 32% polycrystalline quartz with four or more subgrains, evidence of a mixed source for the sediment (Fig. 4.15). The sample shows a mixture of plagioclase and alkali feldspar (Fig. 4.16). Anorthite compositions for the plagioclase grains are estimated at 30%, suggesting derivation from a metamorphic source. On QtFL and QmFLt plots, the samples plot within the 'recycled orogen' fields (Fig. 4.17).

Barrow Formation sample J1726 is a well-sorted, very fine-grained quartz arenite (Fig. 4.14) and shows a mixture of quartz types, dominated by non-undulose monocrystalline quartz (77%) and polycrystalline quartz with four or more subgrains (19%), evidence of a mixed source for the sediment (Fig. 4.15). There is more plagioclase than alkali feldspar in this sample (Fig. 4.16). On a QtFL plot, the samples plot within the 'craton interior' field. On a QmFLt plot, the sample

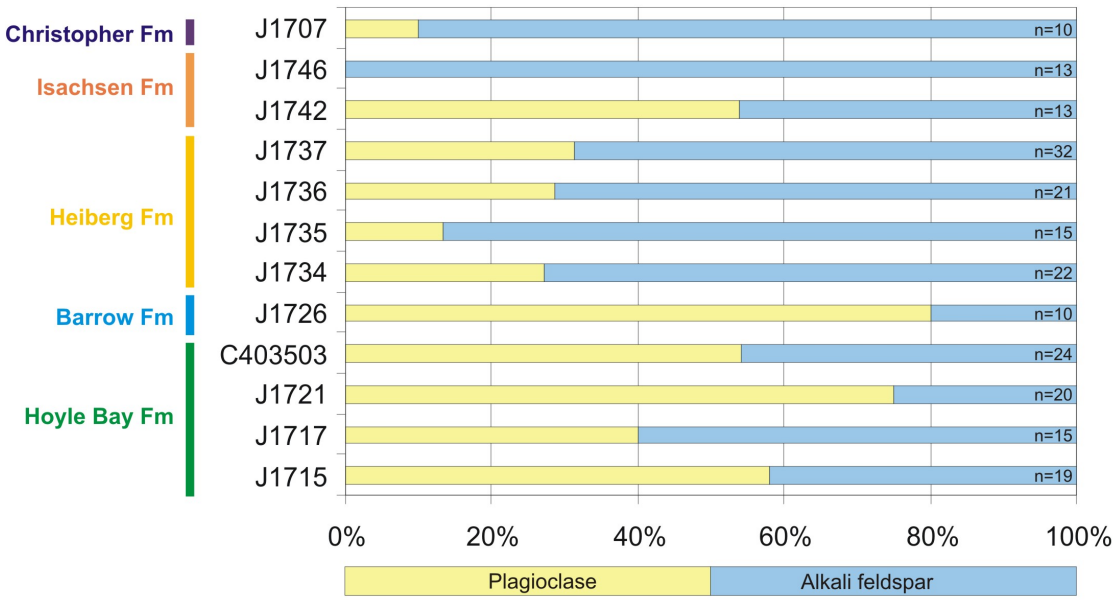

Figure 4.16: Feldspar compositions of the Axel Heiberg samples. Relative abundance of alkali feldspar and plagioclase.

plots within the 'recycled orogen' field (Fig. 4.17).

Heiberg Formation samples J1734-7 and C403752 were studied for petrography. Lower Heiberg Formation (Romulus Member) samples J1734-7 are moderately sorted, very fine to fine-grained subarkoses (Fig. 4.14) and show a mixture of quartz types, with 69-80% non-undulose monocrystalline quartz and 19-29% polycrystalline quartz with four or more subgrains, evidence of a mixed source for the sediment (Fig. 4.15). There is a mixture of plagioclase and alkali feldspar in these samples (Fig. 4.16). Anorthite compositions for the plagioclase grains are estimated to be 30%, suggesting derivation from a metamorphic source. On a QtFL plot, the samples plot within the 'craton interior' field. On a QmFLt plot, the samples plot within the 'recycled orogen' field (Fig. 4.17). Upper Heiberg Formation (Remus Member) sample C403752 was collected by Ashton Embry southeast of Bukken Fiord (Fig. 4.2). The sample is different to the Romulus Member samples discussed above. The sample is a moderately sorted, medium-grained quartz arenite (Fig. 4.14). The quartz type in the sample is almost exclusively non-undulose monocrystalline quartz (95%), with lesser amounts of undulose crystalline quartz (4%), showing evidence of a plutonic source for the sediment (Fig. 4.15). On QtFL and QmFLt plots, the samples plot within the 'craton interior' fields (Fig. 4.17).

Sandy Point Formation sample C403747 was studied for petrography. This

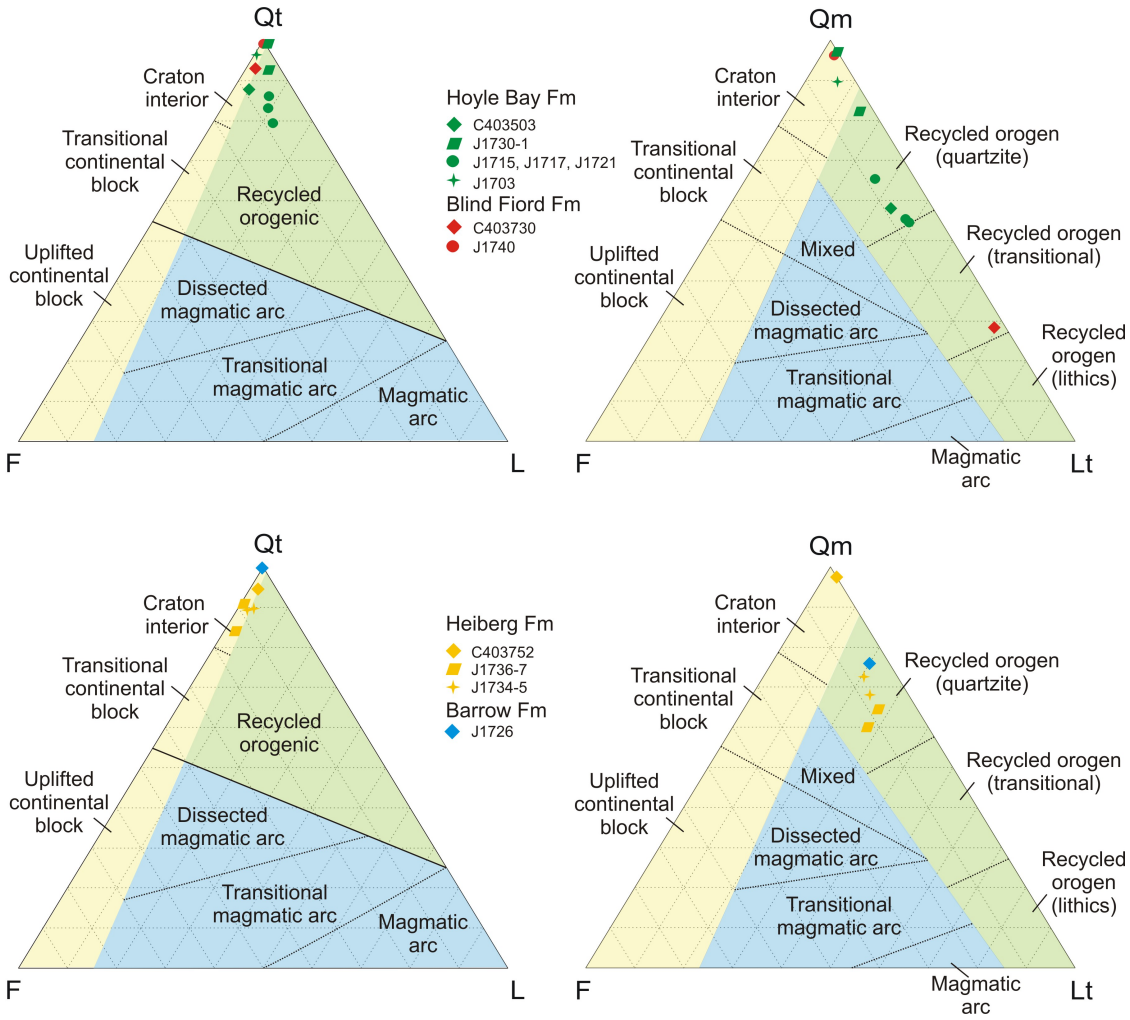

Figure 4.17: Sediment petrography results for the Sverdrup samples. QtFL and QmFLt provenance discrimination diagrams are modified after Dickinson & Suczek (1979).

sample was collected by Ashton Embry northwest of Bukken Fiord (Fig. 4.2). The sample is a moderately sorted, fine-grained quartz arenite (Fig. 4.14) and shows a mixture of non-undulose monocrystalline quartz (72%) and polycrystalline quartz (23%) with four or more subgrains, evidence of a mixed source for the sediment (Fig. 4.15). On QtFL and QmFLt plots, the sample plots within the 'recycled orogen' fields (Fig. 4.18).

Deer Bay Formation sample C403685 was studied for petrography. This sample was collected by Ashton Embry southwest of Bukken Fiord (Fig. 4.2). Sample C403685 is a moderately sorted, fine-grained quartz arenite (Fig. 4.14) and contains almost exclusively non-undulose monocrystalline quartz (98%) suggesting derivation from a plutonic source (Fig. 4.15). On QtFL and QmFLt plots, the sample plots within the 'craton interior' fields (Fig. 4.18).

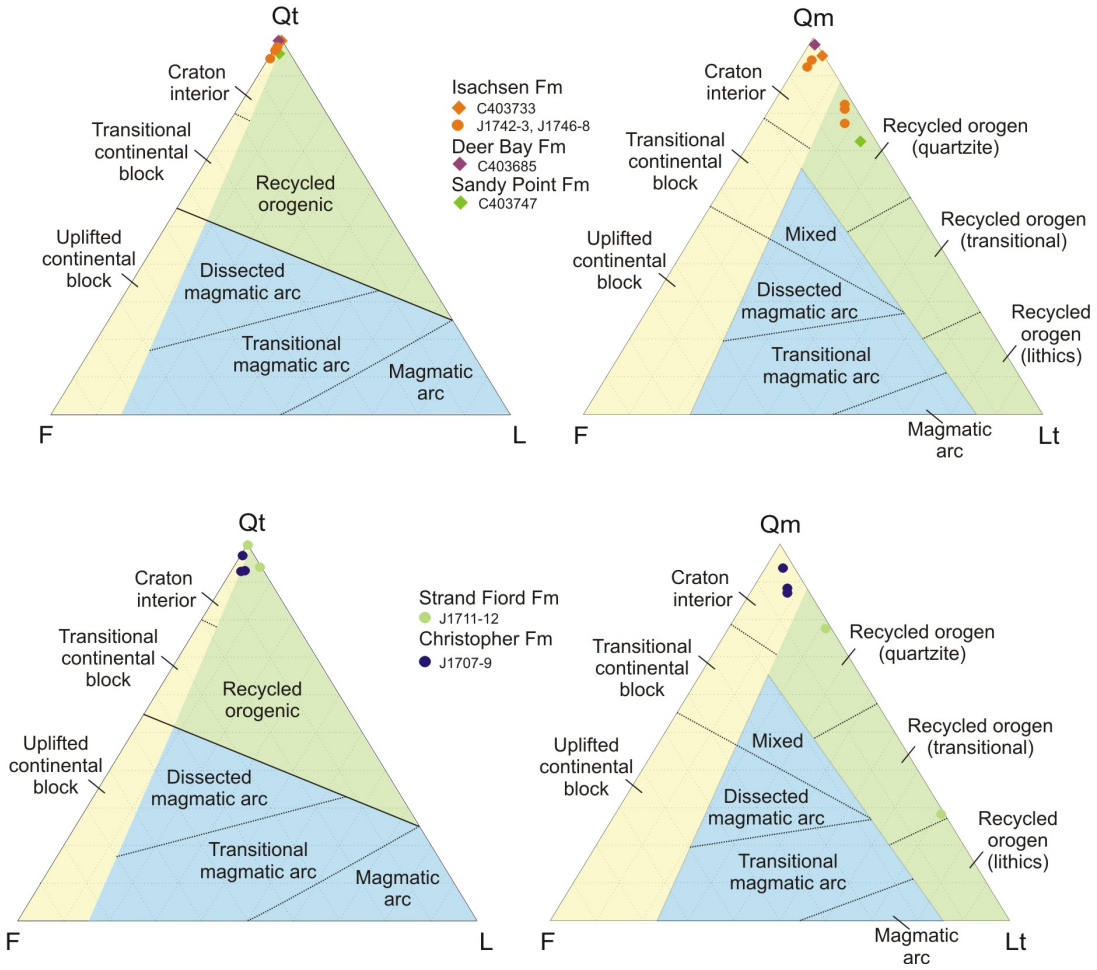

Figure 4.18: Sediment petrography results for the Sverdrup samples. QtFL and QmFLt provenance discrimination diagrams are modified after Dickinson & Suczek (1979).

Isachsen Formation samples J1742-3, J1746-8 and C403733 were studied for petrography. J-samples are poorly sorted, medium to coarse-grained quartz arenites (Fig. 4.14) and are dominated by non-undulose, monocrystalline quartz (78-96%) with some polycrystalline quartz (2-16%) and chert (0-14%) (Fig. 4.15). The samples show a mixture of plagioclase and alkali feldspar (Fig. 4.16). On a QtFL plot, the samples plot within the 'craton interior' field. On a QmFLt plot, the samples plot within the 'craton interior' and 'recycled orogen' fields (Fig. 4.18). Isachsen Formation sample C403733 was collected by Ashton Embry south of Bukken Fiord (Fig. 4.2). This sample is a moderately sorted, coarse-grained quartz arenite (Fig. 4.14). The quartz types are dominated by non-undulose monocrystalline quartz (94%) with some polycrystalline quartz with four or more subgrains (5%) (Fig. 4.15). On QtFL and QmFLt plots, the sample plots within the 'craton interior'

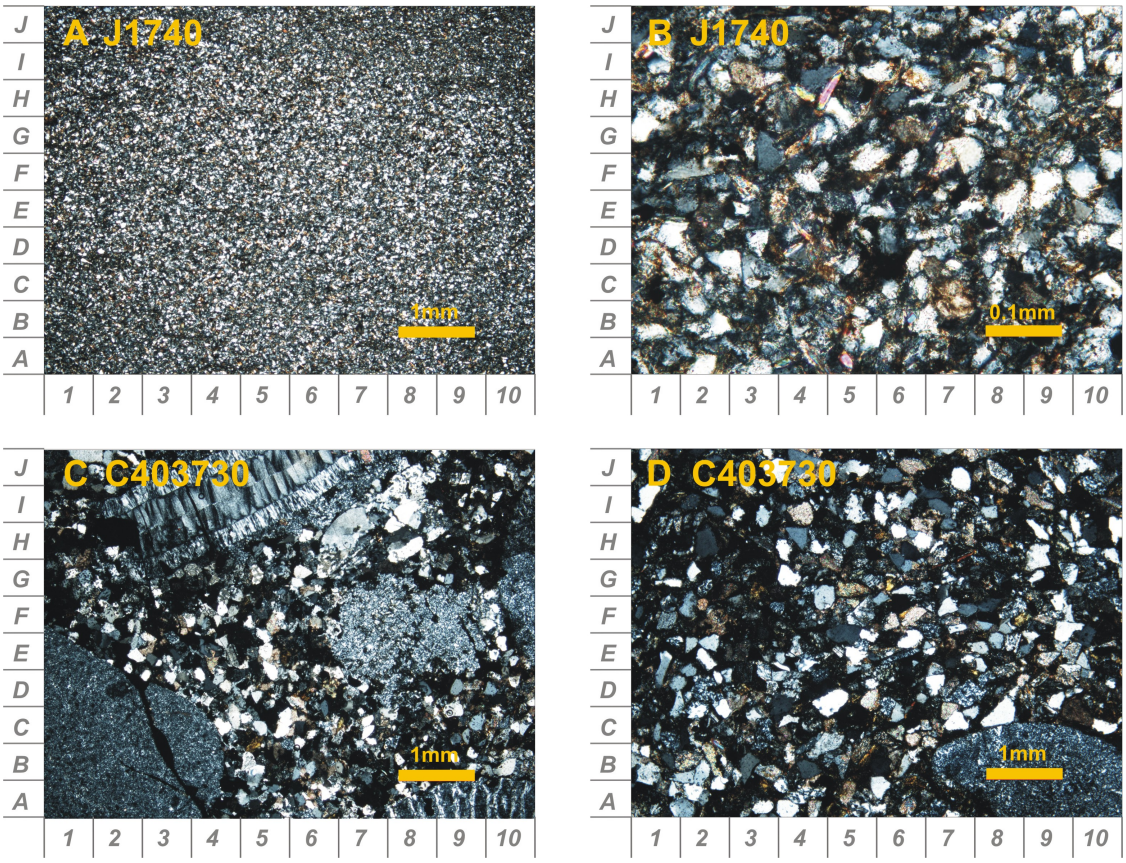

Figure 4.19: Photomicrographs of the Blind Fiord Formation. (A) General view of the moderately sorted, silt-sized, quartz arenite wacke. (B) Angular grains, mainly quartz, are shown in a matrix of mud, mica grains and calcite cement. (C-D) Views of the matrix-supported conglomerate showing biogenic chert clasts in moderately well sorted fine-grained quartz arenite sand matrix. Photograph C shows a silicified coral (B9). Other biogenic clasts, not visible, include foraminifera and sponges. Alkali feldspar is stained yellow.

fields (Fig. 4.18).

Christopher Formation samples J1707-9 were studied for petrography. The samples are moderately-well sorted, very fine to fine-grained quartz arenites (Fig. 4.14). The samples are dominated by non-undulose monocrystalline quartz (91-96%) with some polycrystalline quartz with four or more subgrains (0-8%) (Fig. 4.15). On QtFL and QmFLt plots, the sample plots within the 'craton interior' fields (Fig. 4.18).

Strand Fiord Formation conglomerates J1711-2 were analysed for sediment petrography. The samples are moderately to poorly sorted, very fine and medium-grained quartz arenites (Fig. 4.14). The two samples are different, showing variable non-undulose monocrystalline quartz (27 and 81%), polycrystalline quartz

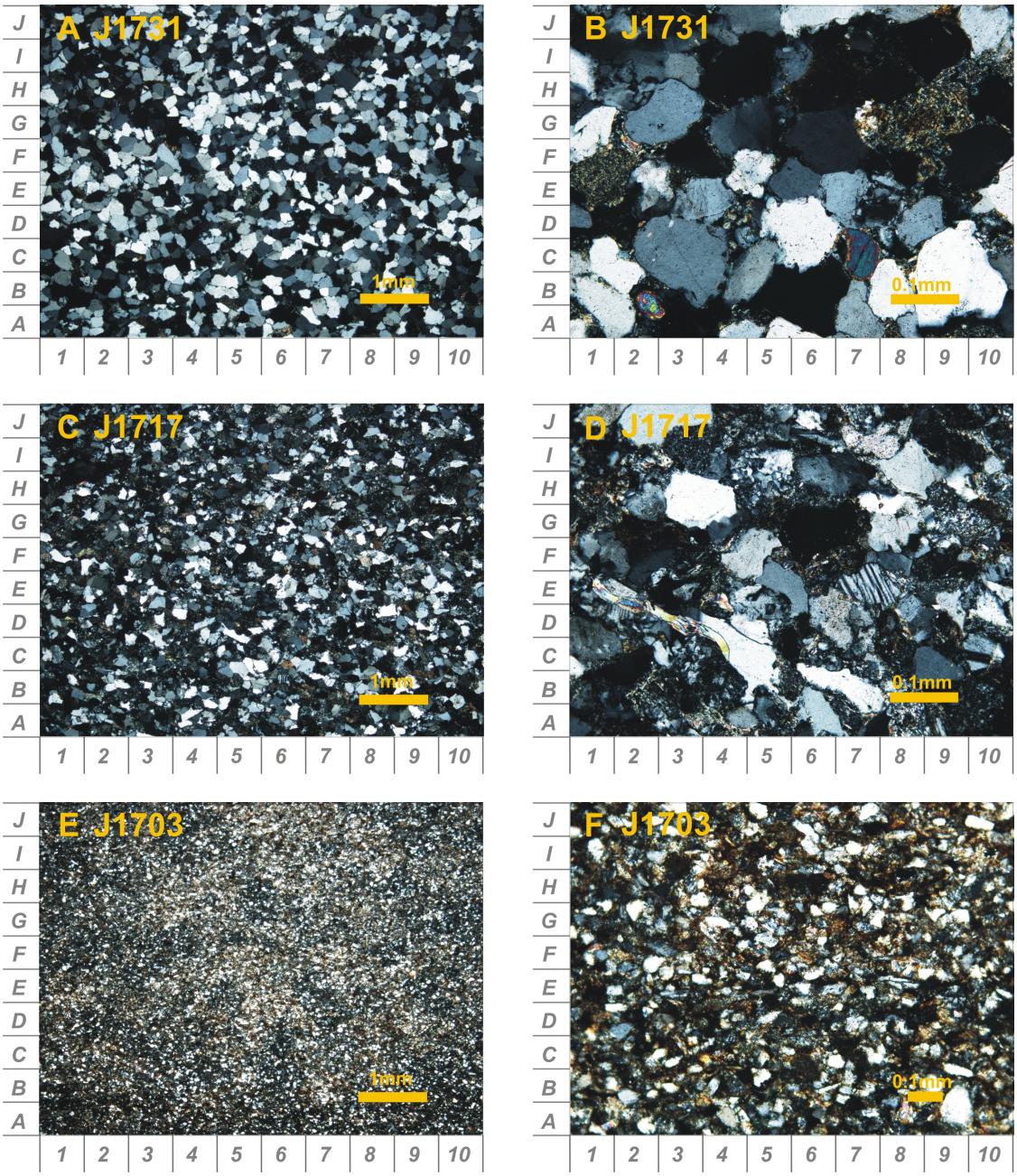

Figure 4.20: Photomicrographs of the Hoyle Bay Formation showing samples from the upper (J1731), middle (J1717) and lower (J1703) Hoyle Bay Formation. (A) General view of the well-sorted, fine-grained quartz arenite. (B) Sutured and concavo-convex grain boundaries and lack of cement suggest that the sample was strongly compacted or deformed, possibly the effect of intrusions. Most quartz grains are monocrystalline and non-undulose and show fluid inclusion trails, characteristic of plutonic quartz. Zircon (A2) and tourmaline (C7) are visible. (C) General view of the moderately sorted, fine-grained sublitharenite. (D) A mixture of mono- and polycrystalline quartz is visible as well as plagioclase and mica. (E) General view of moderately well-sorted, silt-sized quartz arenite-wacke. (F) The angular-subangular nature of the grains is visible. Alkali feldspar is stained yellow.

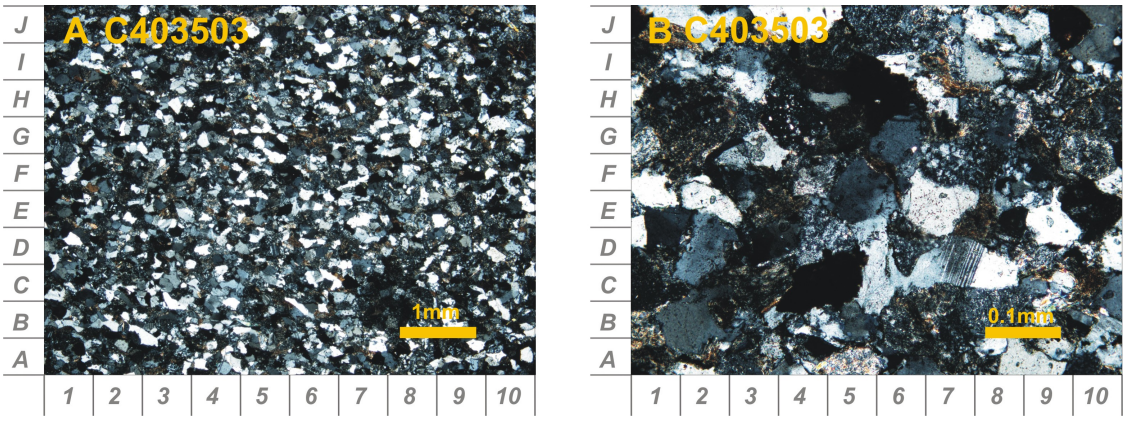

Figure 4.21: Photomicrographs of the Hoyle Bay Formation. (A) General view of the moderately sorted, fine-grained subarkose. (B) The well-compacted nature of the sediment is visible. Alkali feldspar is stained yellow.

with four or more subgrains (12 and 16%) and chert (0 and 60%). This reflects chert clasts dominating one conglomerate. On a QtFL plot, the samples plot within the 'recycled orogen' field. On a QmFLt plot, the samples plot within the 'quartzite recycled orogen' and 'transitional recycled orogen' fields (Fig. 4.18).

4.6 Heavy mineral results

A subset of 18 samples were suitable for heavy mineral analysis (Table 4.1). Figures 4.28-4.29 illustrate the heavy mineral results. The complete dataset is included in the accompanying CD. There are two main heavy mineral assemblages present in these samples: apatite- and garnet-dominated assemblages (Fig. 4.28). Two samples show ultrastable zircon-dominated assemblages.

Heavy mineral species

The Blind Fiord Formation samples did not contain sufficient heavy minerals for full analysis and it was only possible to carry out a rudimentary heavy mineral analysis of sample C403730. Based on a count of only 70 grains, the sample contains an ultrastable detrital heavy mineral population, dominated by zircon (78%), with some tourmaline (13%), apatite (9%) and rutile (3%) (Fig. 4.28). The zircon and tourmaline grains show a mixed assemblage of well-rounded and euhedral morphologies suggesting at least two sources for this sediment, one proximal and one recycled. The apatite grains are well-rounded.

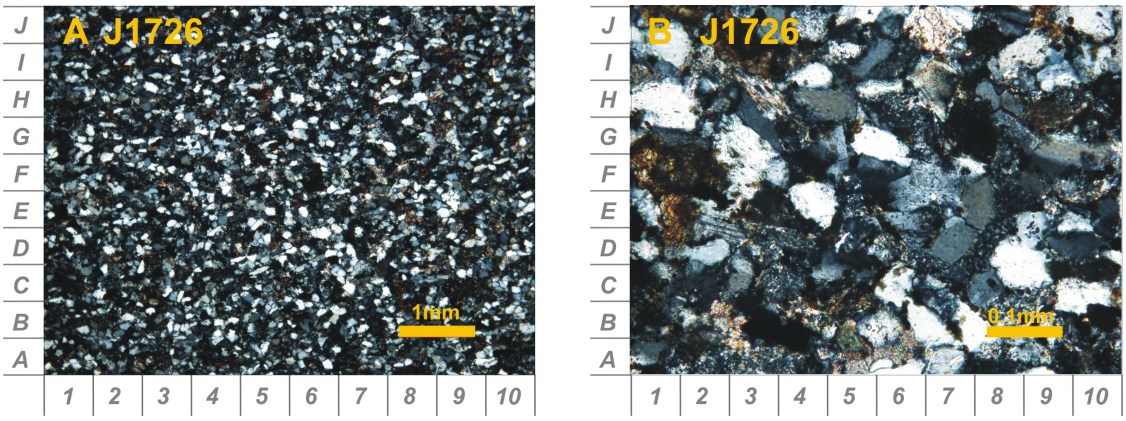

Figure 4.22: Photomicrographs of the Barrow Formation. (A) General view of the well-sorted, very fine-grained quartz arenite. (B) The well-compacted nature of the sediment is seen. Alkali feldspar is stained yellow.

The Hoyle Bay Formation, Barrow Formation, Romulus Member Heiberg Formation and Sandy Point Formation samples contain similar detrital heavy mineral assemblages, named sand type 1. The assemblage is dominated by apatite (37-75%) with lesser amounts of zircon (10-30%), tourmaline (7-26%) and chloritoid (0-16%), minor rutile (1-6%), garnet (0-2%) and chrome spinel (1-2%) (Fig. 4.28). The apatite grains show a mixture of rounded, euhedral and broken morphologies. The tourmaline grains show a mixture of colours and both rounded and euhedral morphologies. The presence of chrome spinel in all samples is noteworthy and indicates derivation from a mafic or ultramafic source. The zircon grains in the samples show varying morphology. The Hoyle Bay Formation samples show mostly euhedral but some rounded zircon grains. The Barrow Formation sample shows a mixed assemblage of euhedral and rounded zircon grains. The Romulus Member Heiberg Formation samples show mainly rounded zircon grains. The overlying Sandy Point Formation sample shows mainly euhedral zircon grains.

Heiberg Formation sample C403752 shows an ultrastable heavy mineral assemblage, named sand type 2, dominated by zircon (73%) with lesser tourmaline (23%) and minor rutile, sphene and apatite (all 1%) (Fig. 4.28). Acidic weathering may have altered the heavy mineral assemblage, preferentially removing apatite. Zircon and tourmaline grains in this sample show rounded morphology.

The Deer Bay, Isachsen, Christopher and Strand Fiord Formation samples contain a different detrital heavy mineral assemblage, sand type 3, dominated by garnet (47-84%) with lesser amounts of zircon (4-31%), tourmaline (2-33%), rutile (1-11%), apatite (0-11%) and chloritoid (0-5%) (Fig. 4.28). The garnet grains in

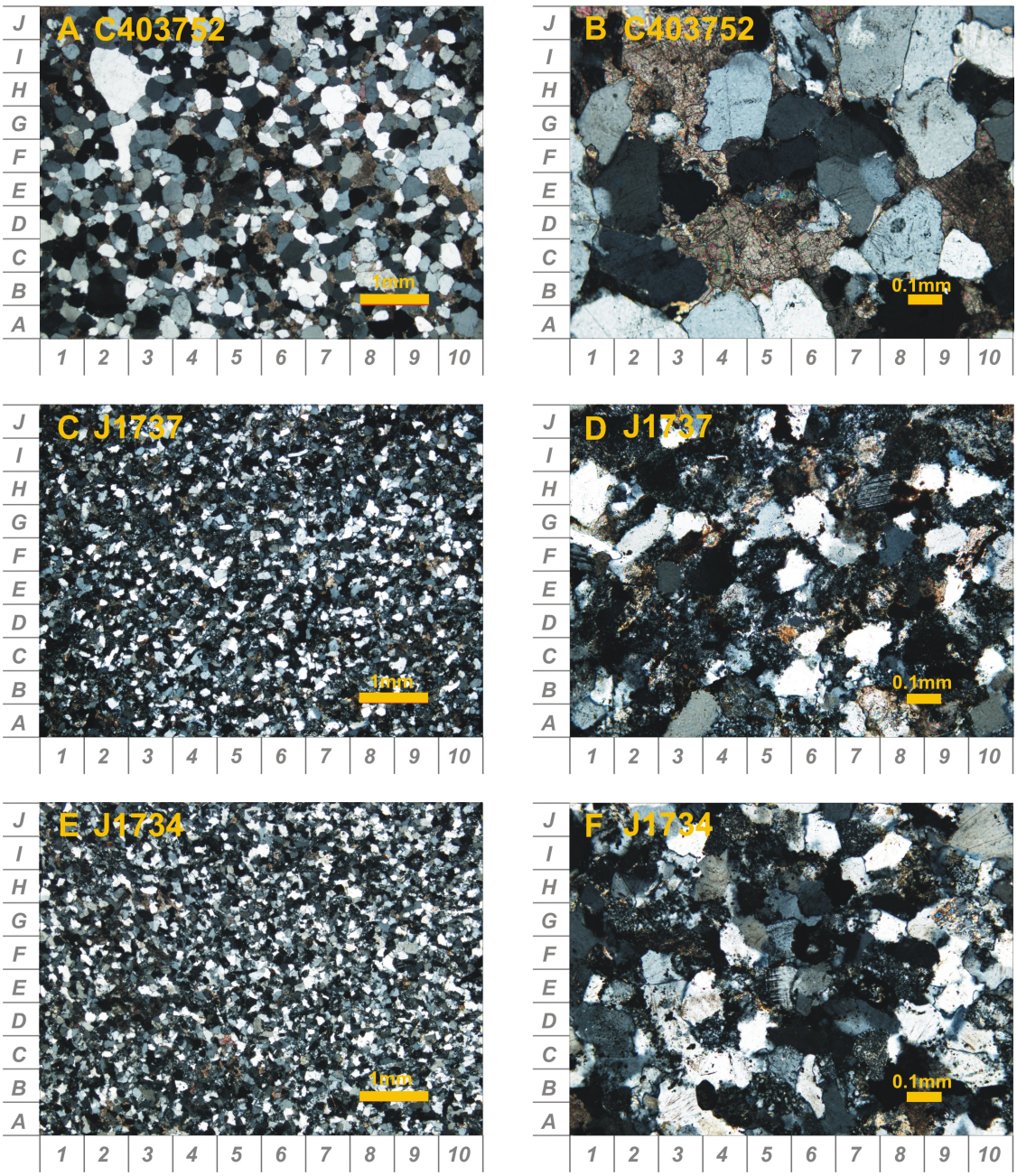

Figure 4.23: Photomicrographs of the Heiberg Formation. (A) Remus Member. General view of the moderately sorted, medium-grained quartz arenite. (B) Most quartz grains are monocrystalline and contain fluid inclusions, typical of plutonic origin. Some polycrystalline grains are visible (I6). The sample contains abundant of calcite cement and a large amount of compaction. (C) Romulus Member. General view of the moderately sorted, very fine-grained subarkose. (D) A variety of clasts is seen and a lot of matrix. (E) Romulus Member. General view of the moderately sorted, very fine-grained subarkose. (F) A variety of quartz grains and a microcline grain (E5) are shown. Alkali feldspar is stained yellow.

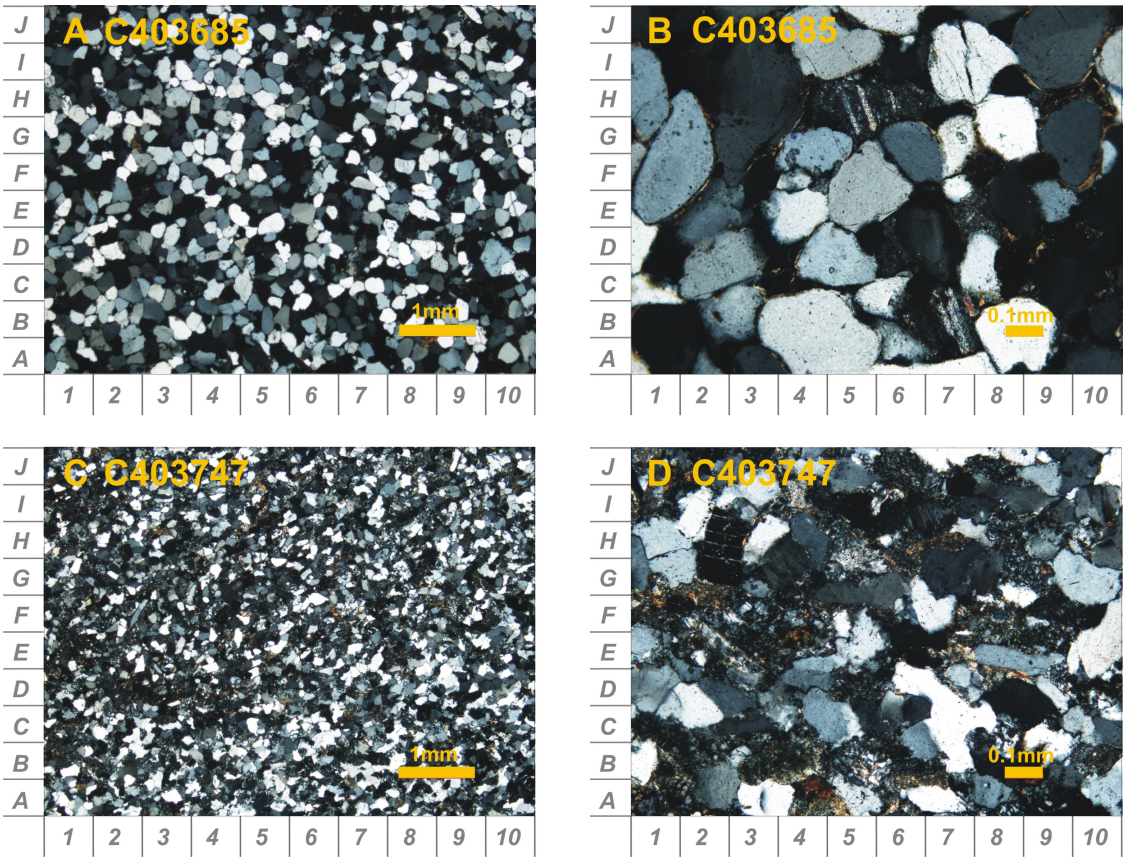

Figure 4.24: Photomicrographs of the Sandy Point and Deer Bay formations. (A) General view of the moderately sorted, medium-grained quartz arenite. (B) Quartz grains are mainly monocrystalline and rounded. (C) General view of the moderately sorted, fine grained quartz arenite. (D) View of a variety of grain types and quartz cement. Alkali feldspar is stained yellow.

these samples are unetched, with the exception of sample C403685 which contains moderately etched garnet grains. The zircon grains are mostly rounded.

Heavy mineral ratios

Ratios of stable heavy mineral species of similar specific gravity may be used to distinguish different provenance groups, as outlined in Chapter 3. The heavy mineral indices are calculated as: GZi=(garnet/(garnet+zircon))×100 (Fig. 4.29).

In this sample set, three main provenance groups (sand types) can be distinguished. The Late Triassic through Middle Jurassic (Hoyle Bay through Sandy Point Formation) samples show low GZi, high CZi and high ATi values (sand type 1). There was insufficient material to study Blind Fiord Formation sample C403730 for heavy mineral ratios, although the mineral species present suggest it fits within

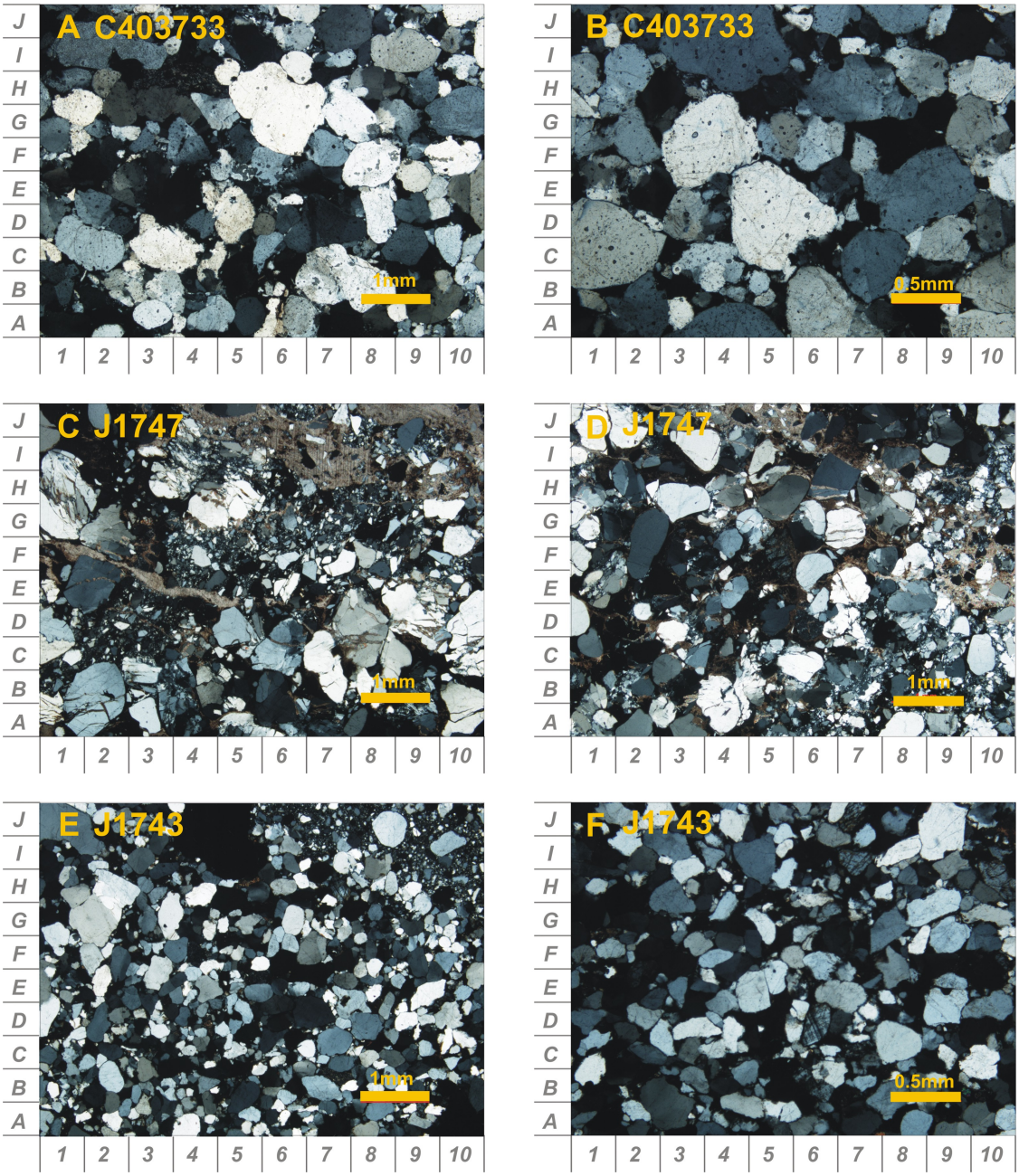

Figure 4.25: Photomicrographs of the Isachsen Formation. (A) General view of the moderately sorted, coarse-grained quartz arenite. (B) The plutonic nature of the quartz grains is shown by the fluid inclusions in the grains. Quartz overgrowths are visible. (C) General view of the poorly sorted, coarse-grained quartz arenite. This rock was fractured and cemented by calcite cement. (D) Well fractured nature of the sample is visible. (E) General view of the poorly sorted, medium-grained quartz arenite. (F) A rounded microcline grain is visible (D6). Alkali feldspar is stained yellow.

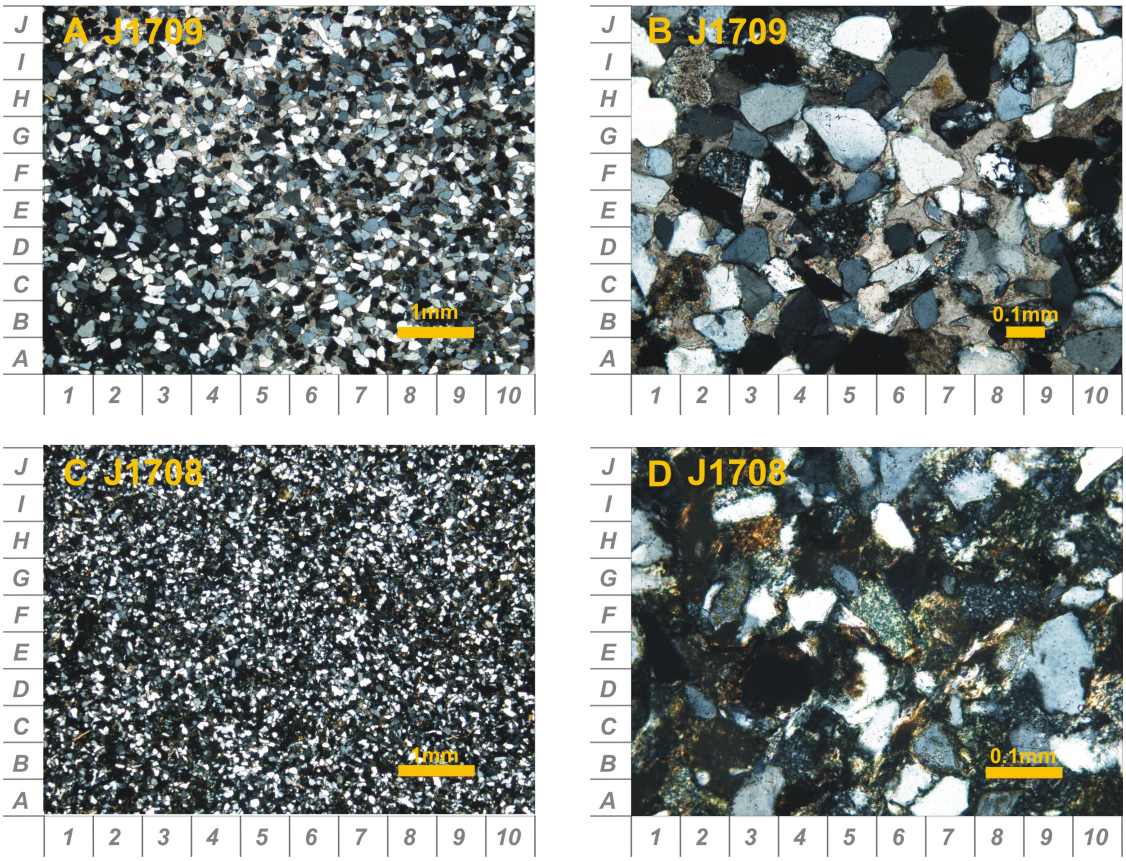

Figure 4.26: Photomicrographs of the Christopher Formation. (A) General view of the moderately well-sorted, fine-grained quartz arenite. (B) This sample shows abundant poikolitic calcite cement. (C) General view of the moderately sorted, fine grained quartz arenite. (D) This sample shows abundant matrix. Alkali feldspar is stained yellow.

sand type 1. Garnet may have been dissolved from this succession during burial diagenesis. However, the ATi and CZi values also confirm this sand type as distinct from the other sand types.

The Early Jurassic Heiberg Formation (Remus Member) sample C403752 contains an ultrastable heavy mineral assemblage, dominated by zircon and tourmaline. Abundant mineral dissolution is suspected. The sample shows low GZi, CZi and ATi and is named sand type 2. The Late Jurassic through Late Cretaceous (Deer Bay through Strand Fiord Formation) samples show high GZi, low CZi and low ATi (sand type 3). Moderate CZi and ATi values in some of the Cretaceous samples suggests a component of sand type 1 in strata mainly composed of sand type 3. Sample C403733 is not included in Figure 4.29 as only GZi could be determined. GZi shows this sample to belong to sand type 3.

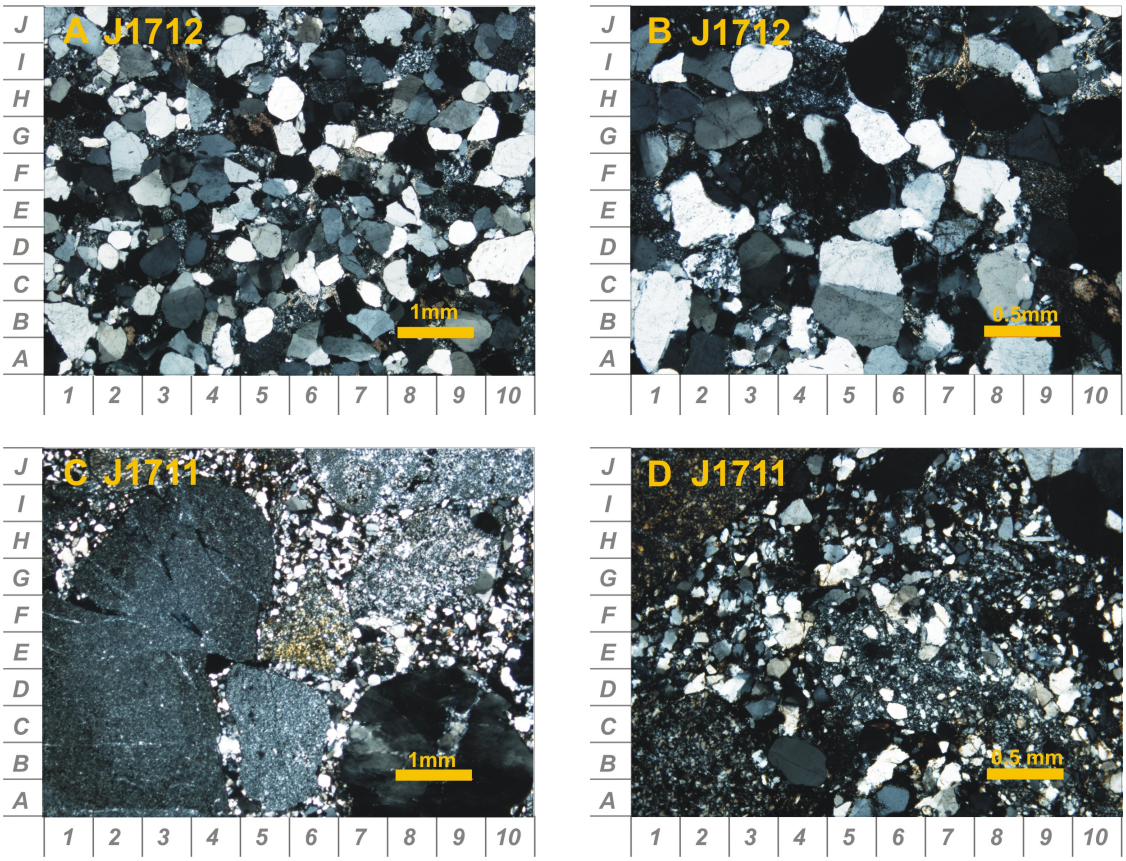

Figure 4.27: Photomicrographs of the Strand Fiord Formation. (A) General view of moderately sorted, medium-grained quartz arenite. (B) Metamorphic quartz (D2), microcline (I7) and a mica schist clast (F9) are visible. (C) General view of the clast-supported conglomerate showing clasts of biogenic chert, mono- and polycrystalline quartz in a poorly sorted, very fine-grained quartz arenite matrix. (D)Biogenic chert clasts are visible. Alkali feldspar is stained yellow.

4.7 Garnet chemistry results

A subset of four samples were analysed for garnet chemistry (J1708, J1743, C403733 and C403685) (Table 4.1). The data are presented in Figure 4.30. The full dataset is included in the accompanying CD. Garnet chemistry for all samples shows predominance of almandine (Fe-rich garnet) in relation to spessartine (Mn-rich garnet) and in total 83% of analyses contain 0-5% Mn in relation to Fe. The garnet grains are unetched, with the exception of moderate etching in sample C403685, such that the garnet assemblage should be taken as representative of the original assemblage.

Garnets of the Deer Bay Formation sample (C403685) plot as type A, Bi and Bii (Fig. 4.30). Type A garnets are sourced from high-grade granulite facies metasedimentary rocks and charnokites or from intermediate-acidic igneous rocks

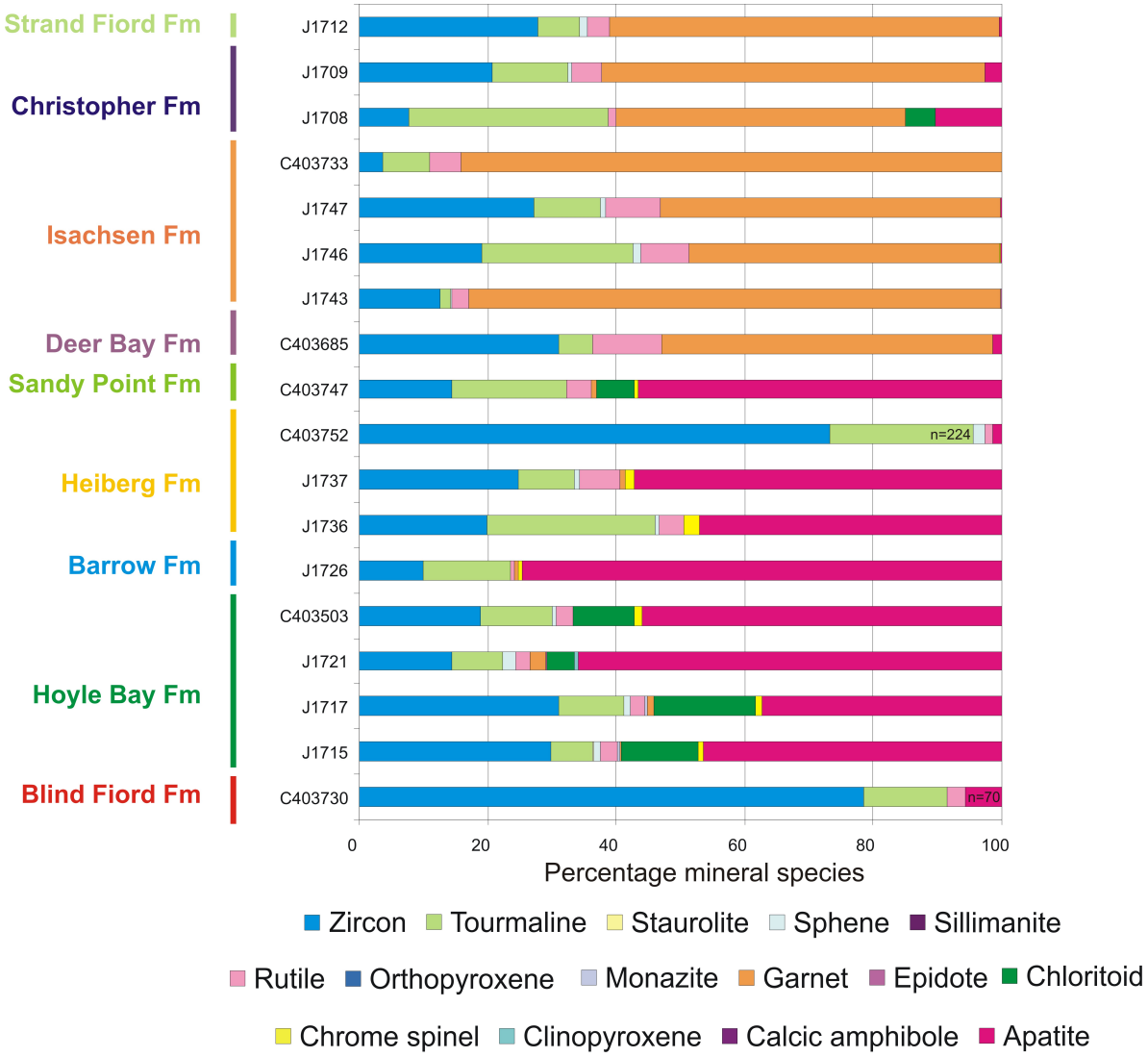

Figure 4.28: Axel Heiberg samples heavy mineral assemblages, showing the relative importance of various heavy mineral species. The data are based on counts of minimum 300 heavy minerals unless otherwise shown.

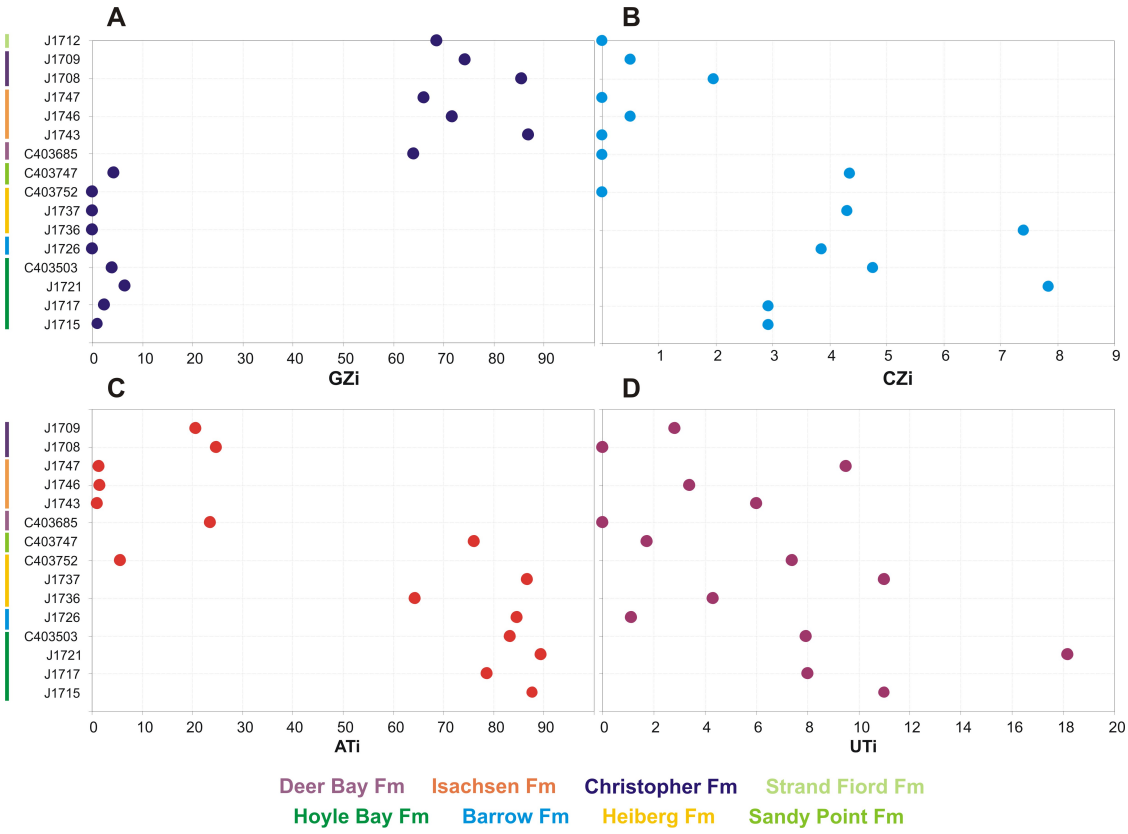

Figure 4.29: Axel Heiberg samples heavy mineral ratios. Indices are calculated as: GZi=(garnet/(garnet+zircon))×100. (A) GZi (garnet-zircon index), showing two clusters. Late Triassic through Early Jurassic (Hoyle Bay through Sandy Point Formation) samples show low GZi values. Late Jurassic through Late Cretaceous (Deer Bay through Strand Fiord Formation) samples show high GZi values. (B) CZi (chrome spinel-zircon index), showing two clusters. The Hoyle Bay through Sandy Point Formation samples show high CZi, with the exception of Heiberg Formation sample C403752, which shows an ultrastable (presumably altered) heavy mineral assemblage. The Deer Bay through Strand Fiord Formation samples show low CZi although importantly there is still chrome spinel present. (C) ATi (apatite-tourmaline index), showing two clusters. Hoyle Bay through Sandy Point Formation samples show high ATi, with the exception of Heiberg Formation sample C403752, which shows an ultrastable (presumably altered) heavy mineral assemblage. The Deer Bay through Strand Fiord Formation samples show low ATi. (D) UTi (unstable minerals-tourmaline index), showing no obvious trends. Unstable minerals are amphibole, epidote and sphene.

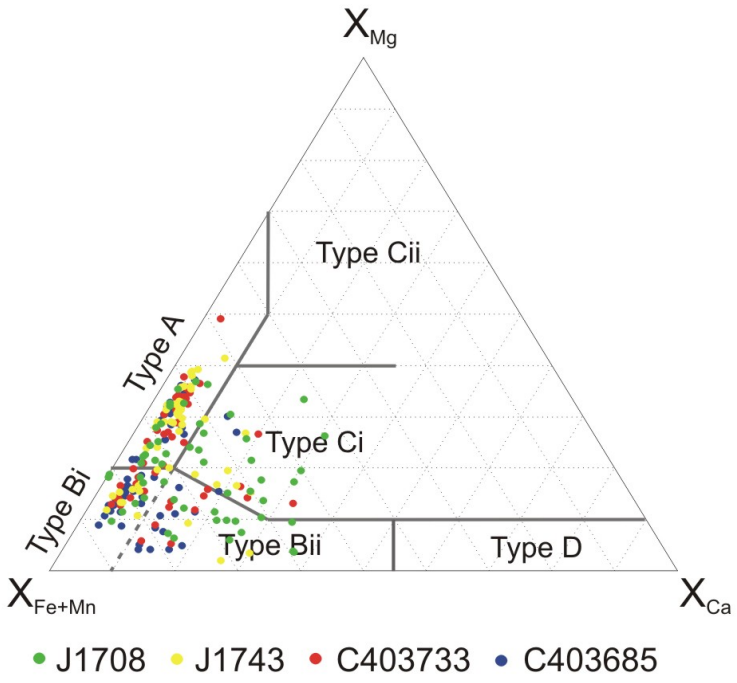

Figure 4.30: Garnet compositions in Axel Heiberg samples, shown on the garnet classification diagram of Morton *et al.* (2004). X_{Mg}, X_{Fe}, X_{Mn}, X_{Ca} = molecular proportions of Mg, Fe, Mn and Ca, with all Fe calculated as Fe^{2+}. The samples show similar chemistry and mainly plot as type A and Bi garnets, with some Bii and Ci garnets. Garnet chemistry shows predominance of almandine (Fe-rich garnet) in relation to spessartine (Mn-rich garnet).

from deep crustal magmas (Morton *et al.*, 2004). Type B garnets are sourced from amphibolite facies metasedimentary rocks and gneisses (Bi and Bii) or intermediate-acidic igneous rocks (Bi, although associated with high-Mn chemistries) (Morton *et al.*, 2004).

Similarly, garnets of the Isachsen Formation samples (J1743 and C403733) plot as type A, Bi and Bii, with a smaller amount of Ci (Fig. 4.30). Ci garnets are sourced from high-grade mafic gneisses (Morton *et al.*, 2004). Garnets of the Christopher Formation sample (J1708) show a wider spread of garnet chemistries and plot evenly across fields A, Bi, Bii and Ci (Fig. 4.30). Due to low-Mn values, a metasedimentary origin is preferred for the type B garnets seen in these four samples. The presence of Ci garnets and chrome spinel in the Christopher Formation reinforces that a component of mafic-ultramafic rocks is a source for the Christopher Formation and for Blind Fiord through Sandy Point Formation sand type 1 samples.

4.8 Tourmaline chemistry results

A subset of thirteen samples were analysed for tourmaline chemistry (Table 4.1). The data are presented in Figures 4.31-4.32. The complete dataset is included in the accompanying CD.

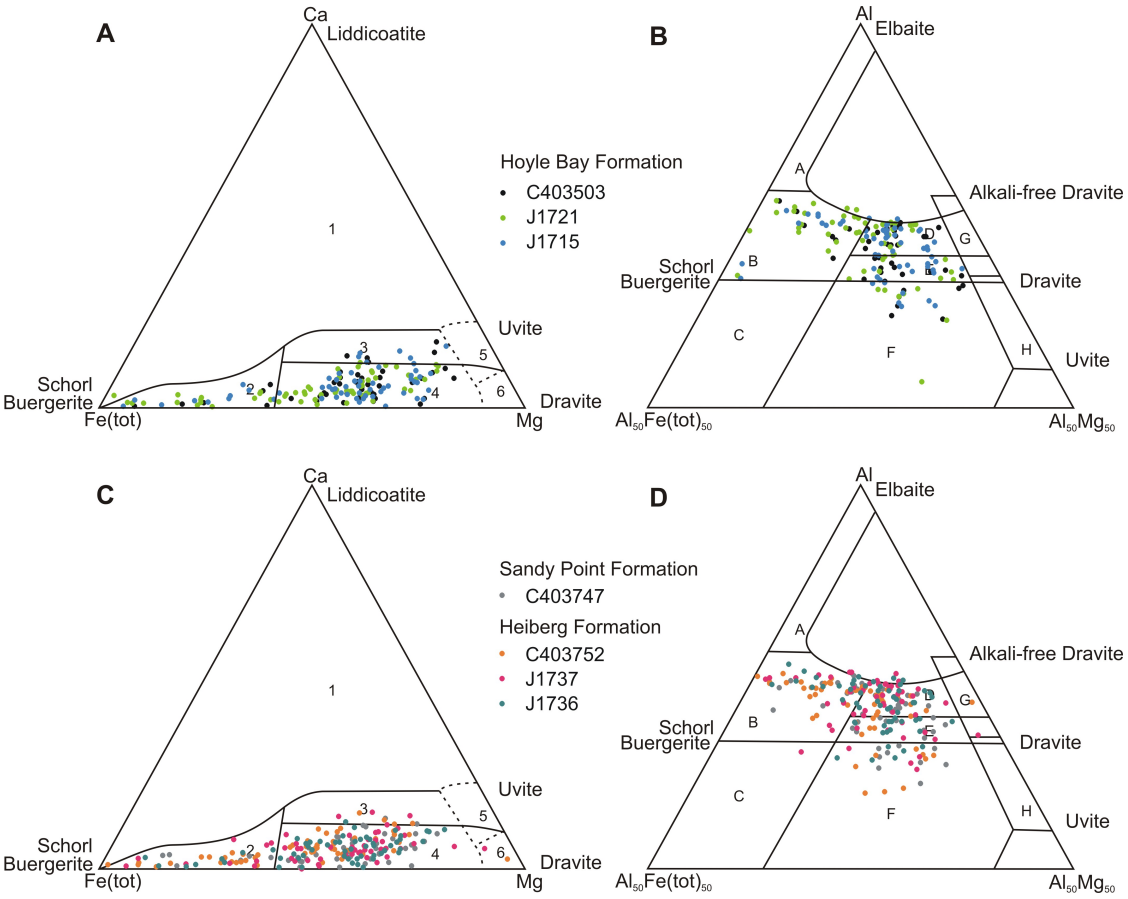

Figure 4.31: Tourmalines of the Hoyle Bay, Heiberg and Sandy Point formations plotted on discrimination diagrams of Henry & Guidotti (1985). Field 2, Li-poor granitoids, pegmatites and aplites. Field 3, Ca-rich metapelites, metapsammites and calcsilicates. Field 4, Ca-poor metapelites, metapsammites and quartz tourmaline rocks. Field B, Li-poor granitoids, pegmatites and aplites. Field D, Aluminous metapelites and metapsammites. Field E, Al-poor metapelites and metapsammites. Field F, Fe^{3+}-rich quartz-tourmaline rocks, calc-silicates and metapelites.

The Hoyle Bay, Heiberg and Sandy Point Formation samples show similar tourmaline chemistry and will be discussed together (Fig. 4.31). On a Ca-Fe-Mg diagram, the samples plot mainly in field 4, representing Ca-poor metapelites, metapsammites and quartz tourmaline rocks. Some grains also plot in fields 3 (Ca-rich metapelites, metapsammites and quartz tourmaline rocks) and 2 (Li-poor

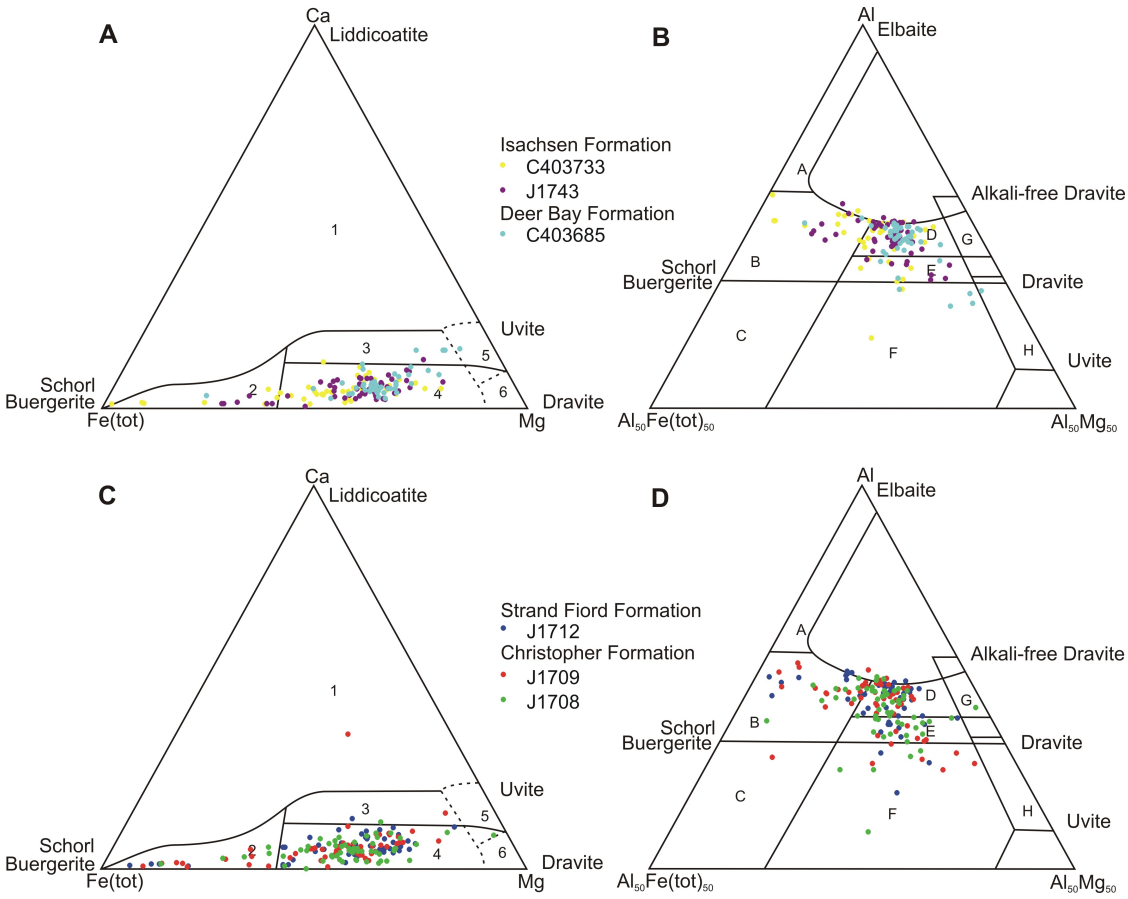

Figure 4.32: Tourmalines of the Late Jurassic-Cretaceous samples plotted on discrimination diagrams of Henry & Guidotti (1985). Field 2, Li-poor granitoids, pegmatites and aplites. Field 3, Ca-rich metapelites, metapsammites and calcsilicates. Field 4, Ca-poor metapelites, metapsammites and quartz tourmaline rocks. Field B, Li-poor granitoids, pegmatites and aplites. Field D, Aluminous metapelites and metapsammites. Field E, Al-poor metapelites and metapsammites. Field F, Fe^{3+}-rich quartz-tourmaline rocks, calc-silicates and metapelites.

granitoids, pegmatites and aplites) (Henry & Guidotti, 1985). On an Al-$Al_{50}Fe_{50}$-$Al_{50}Mg_{50}$ diagram the grains plot mainly in fields D and E, reflecting aluminous (field D) and Al-poor (field E) metapelites and metapsammites (Henry & Guidotti, 1985). Some grains plot in field F (Fe^{3+}-rich quartz-tourmaline rocks, calc-silicates and metapelites) and field B (Li-poor granitoids, pegmatites and aplites).

The Deer Bay Formation and Isachsen Formation samples, C403865, J1743 and C403733, show more restricted tourmaline chemistry than the underlying formations (Fig. 4.32). On a Ca-Fe-Mg diagram, the grains plot almost exclusively in field 4, representing Ca-poor metapelites, metapsammites and quartz tourmaline rocks. Isachsen Formation samples (J1743 and C403685) show some grains in field 2 (Li-poor granitoids, pegmatites and aplites) (Henry & Guidotti, 1985). On an Al-$Al_{50}Fe_{50}$-$Al_{50}Mg_{50}$ diagram the grains plot almost exclusively in field D (and E), reflecting aluminous metapelites and metapsammites. Samples J1743 and C403685 also show some grains in field B (Li-poor granitoids, pegmatites and aplites) (Henry & Guidotti, 1985).

The Christopher and Strand Fiord Formation samples, J1708, J1709 and J1712, show similar tourmaline chemistry to the underlying Isachsen Formation (Fig. 4.32). On a Ca-Fe-Mg diagram, the grains plot almost exclusively in field 4, representing Ca-poor metapelites, metapsammites and quartz tourmaline rocks. Christopher Formation samples (J1708 and J1709) show some grains in field 2 (Li-poor granitoids, pegmatites and aplites) (Henry & Guidotti, 1985). On an Al-$Al_{50}Fe_{50}$-$Al_{50}Mg_{50}$ diagram the grains plot mainly in fields D and E, reflecting aluminous (field D) and Al-poor (field E) metapelites and metapsammites. Some grains plot in field B (Li-poor granitoids, pegmatites and aplites) (Henry & Guidotti, 1985).

4.9 Zircon geochronology results

Detrital zircons from five samples were dated using SIMS (Table 4.1). The data are presented in figures 4.33-4.35. The complete dataset is included in the accompanying CD. U-Pb ages discussed here are within 10% of concordance unless otherwise stated. $^{206}Pb/^{238}U$ ages are quoted for ages younger than 1200 Ma; $^{207}Pb/^{206}Pb$ ages are quoted for ages older than 1200 Ma.

The Early Triassic Blind Fiord Formation sample C403730 contains zircon ages that fall into two modes: a robust, tight Permian peak and a broad range of Mesoproterozoic ages (Fig. 4.33). The Permian grains (19 grains) range in age from 290

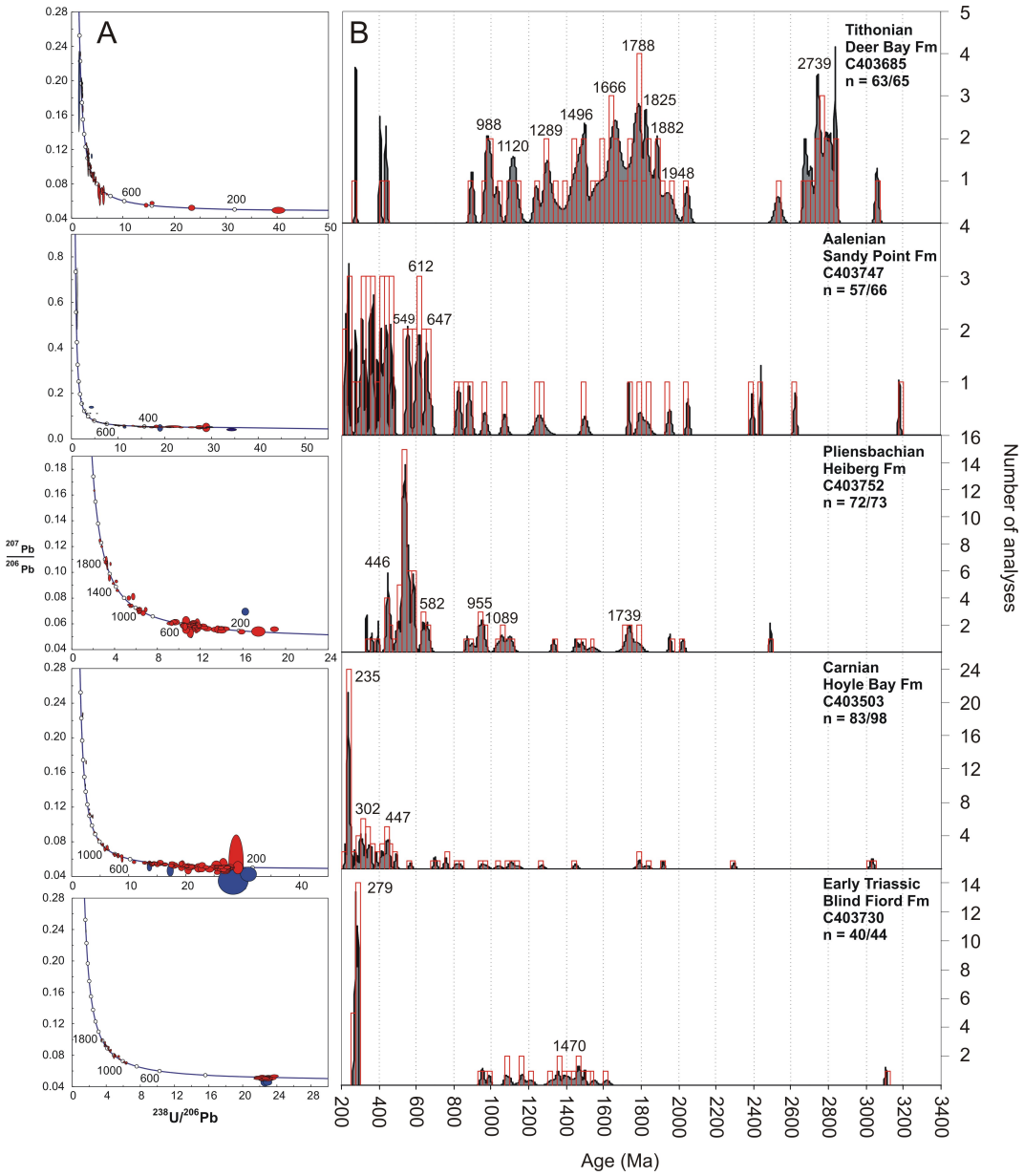

Figure 4.33: Concordia and cumulative frequency diagrams for Axel Heiberg samples. (A) Tera-Wasserberg concordia diagram for Sverdrup samples. The data have been common lead corrected. Data point ellipses are 2σ. The red error ellipses represent analyses with a discordance less than 10%. The blue ellipses represent analyses with a discordance more than 10%. (B) Cumulative frequency diagrams, with histograms, of U-Pb detrital zircon ages from northwest Axel Heiberg Island. N denotes the number of analyses with 90-110% concordancy relative to all analyses.

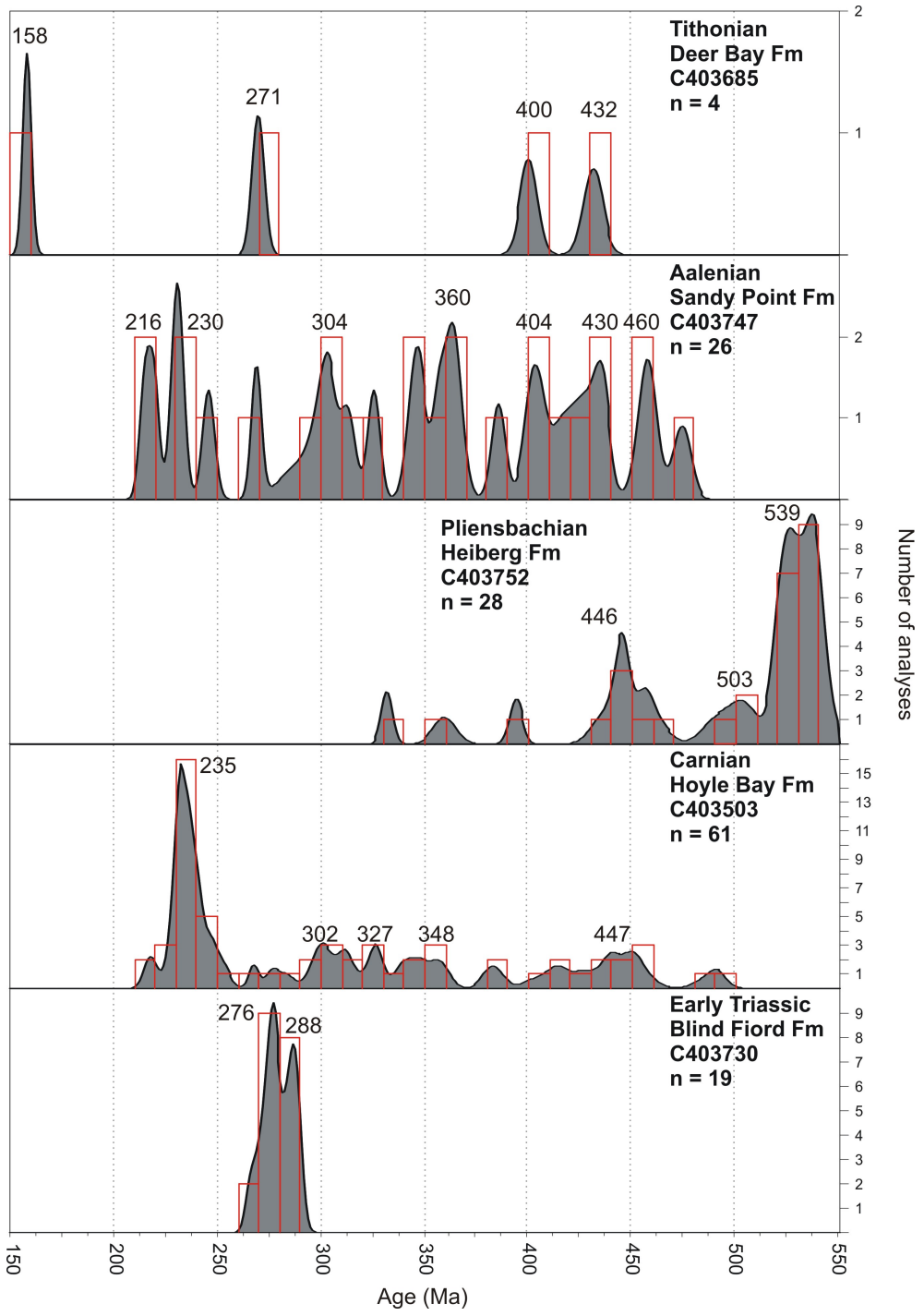

Figure 4.34: Cumulative frequency diagrams, with histograms, of Phanerozoic U-Pb detrital zircon ages from northwest Axel Heiberg Island. N denotes the number of analyses with 90-110% concordancy relative to all analyses.

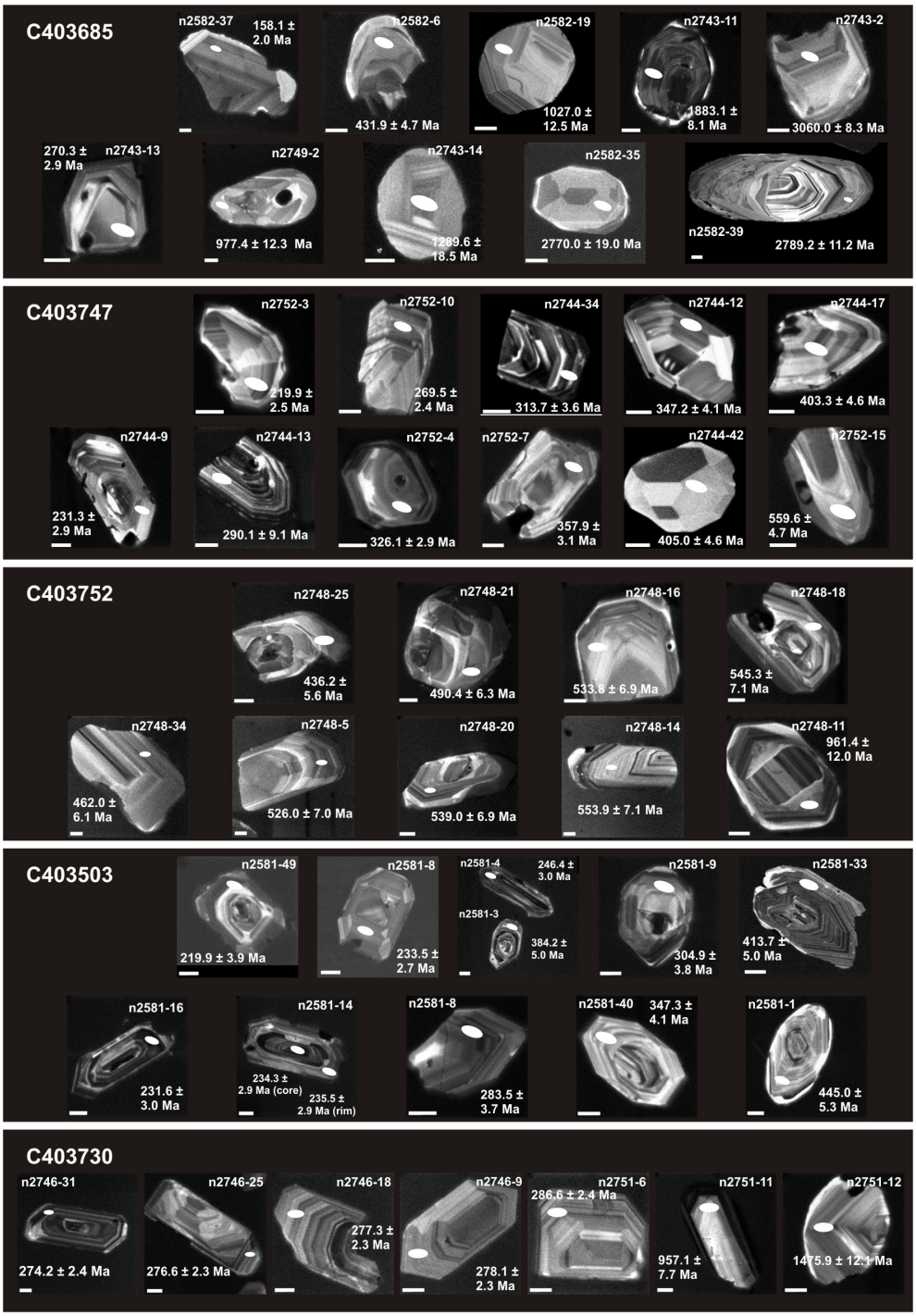

Figure 4.35: Cathodoluminescence images of Axel Heiberg samples showing morphology and internal structure of representative zircon grains. U-Pb age, with 1σ uncertainty, is shown for each analysis. Ages younger than 1200 Ma are $^{206}Pb/^{238}U$ ages. Ages older than 1200 Ma are $^{207}Pb/^{206}Pb$ ages. Analytical spots are indicated by ellipses. The scale bars equal 20 μm.

to 265 Ma, with a major peak at 279 Ma (Fig. 4.34) and are euhedral, doubly vergent, oscillatory zoned magmatic grains (Fig. 4.35). Their euhedral shape suggests that the grains have a proximal source. The Mesoproterozoic zircon populations are represented by rounded, recycled grains with two broad age clusters: 1206-959 Ma (eight grains) and 1497-1356 Ma (12 grains), centred at 1470 Ma. There is one Archean grain (∼3100 Ma).

The Carnian Hoyle Bay Formation sample C403503 has a broad range of zircon ages (Fig. 4.33), but is dominated by Phanerozoic grains with a robust Middle Triassic peak (235 Ma; 27 grains) (Fig. 4.34). Zircons of the 235 Ma peak are euhedral, doubly vergent and magmatic in origin (Fig. 4.35) and range in age from ∼254 to 218 Ma. This peak is contemporaneous with the Carnian deposition of the Hoyle Bay Formation. The remaining zircons define a spread of latest Cambrian to Permian ages (∼493-268 Ma; 34 grains), with peaks at 302, 327, 348 and 447 Ma. The sample also contains 21 grains of Precambrian age, with no robust peaks present.

The Pliensbachian Heiberg Formation sample C403752 contains ages of several groups. The youngest dominant peaks are represented by 660-330 Ma zircons (44 grains) (Fig. 4.34). The most dominant peak (24 grains) is 539 Ma and represented by grains of ∼559-522 Ma. There are three grains at 393-330 Ma, 5 grains centred around 446 Ma, three grains centred around 503 Ma, six grains centred around 582 Ma and five grains at ∼623-668 Ma. The second group of zircons is represented by two peaks at 955 and 1089 Ma (11 grains), with the range ∼1092-867 Ma. There are four grains clustered around 1400 Ma and six grains clustered around 1739 Ma. There is one grain at ∼2490 Ma.

The Aalenian Sandy Point Formation sample C403747 has a wider distribution of zircon ages than seen in the older samples, with ages from Mesoarchean to Late Triassic. It has a higher proportion of Precambrian grains compared with previous samples (18 grains). The younger grains can be divided into two main groups: Ordovician to Late Triassic grains (474-215 Ma; 26 grains) and Late Neoproterozoic to earliest Cambrian grains (681-545 Ma; 13 grains) (Fig. 4.34). The Ordovician to Late Triassic grains have peaks at ∼216, 230, 304, 360, 404, 430 and 460 Ma. The Neoproterozoic-Cambrian grains show three peaks: ∼549, 612 and 647 Ma. The older zircon ages in this sample show few robust peaks. The sample contains two Archean zircons.

The Tithonian Deer Bay Formation sample C403685 detrital zircon ages are very different to the previous samples, with a dominant older component. Phanerozoic zircon ages are represented by four grains are ∼158, 271, 400 and 432 Ma (Fig.

4.34). Precambrian zircons divide into Proterozoic ages (2044-895 Ma; 44 grains) and Archean ages (3060-2530 Ma; 15 grains). There is one Neoproterozoic peak at 988 Ma, three Mesoproterozoic peaks at 1120, 1289 and 1496 Ma and five Paleoproterozoic peaks at 1666, 1788, 1825, 1882 and 1948 Ma. The Archean ages form a significant peak centred at 2739 Ma, represented by grains of age ∼2837-2674 Ma.

4.10 Summary of results

During 2007 fieldwork in the Bukken Fiord area the Triassic and Cretaceous successions were examined. The Triassic succession is characterized by deep to shallow marine shale-dominated strata. The Cretaceous succession is characterized by shallow marine to continental sandstones and conglomerates interbedded with basaltic lava flows.

All samples studied plot in the 'craton interior' and 'recycled orogen' fields on QtFL and QmFLt diagrams. Blind Fiord, Hoyle Bay, Sandy Point and Strand Fiord Formation samples plot only in the 'recycled orogen' fields, whereas Heiberg and Isachsen Formation samples plot in both the 'recycled orogen' and 'craton interior' fields. Christopher Formation samples plot only in the 'craton interior' field.

Most samples studied are characterized as quartz arenites, with the exemption of four Hoyle Bay Formation sublitharenites and subarkoses and four Heiberg Formation subarkoses. All samples are dominated by non-undulose monocrystalline quartz, suggesting a mainly plutonic or very low-grade metamorphic source for the succession. Upper Hoyle Bay, Barrow, lower Heiberg, Sandy Point, some Isachsen, Christopher and Strand Fiord Formation samples include a significant proportion of polycrystalline quartz with four or more subgrains, indicative of an additional metamorphic source.

The detrital heavy mineral results can be divided into three assemblages: apatite-dominated (sand type 1), Heiberg Formation zircon-dominated (sand type 2) and garnet-dominated (sand type 3). The Triassic through Middle Jurassic (Blind Fiord, Hoyle Bay, Barrow, Heiberg and Sandy Point Formation) samples show apatite-dominated assemblages, also containing chrome spinel. Upper Heiberg Formation sample C403752 contains an ultrastable zircon-dominated heavy mineral assemblage. The Late Jurassic through Late Cretaceous (Deer Bay, Isachsen, Christopher and Strand Fiord Formation) samples show garnet-dominated assemblages. This third group also contains some apatite, chrome spinel and chloritoid,

suggesting some mixing of sand type 1 with sand type 3 in these formations. The presence of chrome spinel suggests derivation from mafic-ultramafic rocks.

Garnet chemistry for the Deer Bay, Isachsen and Christopher formations plot mainly as types A and Bi garnets, with some grains plotting as types Bii and Ci. Source lithologies for these garnet chemistries include granulite-facies metasedimentary rocks and charnokites or intermediate-acidic deep crustal magmas (type A), amphibolite-facies metasedimentary rocks and gneisses (type B) and high-grade mafic gneisses (type Ci) (Morton *et al.*, 2004). Christopher Formation sample J1708 shows relatively high CZi and the highest proportion of Ci type garnet, strengthening the link between the presence of chrome spinel and derivation from a mafic-ultramafic source and suggests that the Blind Fiord through Sandy Point Formation samples, showing high CZi, were also sourced in part from a mafic-ultramafic source. Metamorphic source terranes are considered the most likely for these sediments.

Tourmaline chemistry for the studied samples show the source lithologies for the entire Triassic through Cretaceous succession to be mainly Ca-poor, aluminous metapelites and a lesser Li-poor granitoids, pegmatites and aplites. The granitic source becomes less important in Deer Bay Formation and younger samples, reinforcing a metamorphic source for these formations as suggested by the garnet data.

Zircon data for the five studied samples show three different assemblages. The Blind Fiord, Hoyle Bay and Sandy Point Formation samples are dominated by young (Permo-Triassic), euhedral zircons (sand type 1). The Heiberg Formation Remus Member sample is dominated by Neoproterozoic zircons (sand type 2). The Deer Bay Formation sample is dominated by Proterozoic and Archean zircons (sand type 3).

4.11 Discussion

The zircon and heavy mineral data show three distinct sediment sources (sand types 1, 2, 3) (Fig. 4.36). The interpreted sediment sources to northwestern Axel Heiberg Island during the Mesozoic are summarised in Fig. 4.37.

Blind Fiord Formation - Sand type 1

The zircon age spectrum acquired from sample C403730 is dominated by a Permian age (∼280 Ma) peak and contains a spread of Meso- to Neoproterozoic ages

(between 1500 and 960 Ma). The Permian age peak is a robust and isolated occurrence of magmatic zircons (Fig. 4.34). The euhedral morphology of the Permian zircons and the isolated nature of the age peak indicates that the source was proximal. There is evidence of magmatic activity on Axel Heiberg Island during Early Permian time (Davies & Nassichuk, 1991), which may considered to be a possible source for these zircon grains. However, this magmatic activity is basaltic in nature so would not generally be considered a likely candidate for zircon grains. The Taimyr Peninsula, a northern continuation of the Permo-Carboniferous Uralian Orogen, is another likely source for Permian zircons. Vernikovsky *et al.* (1995) and Pease (2001) reported granites of the same age (early to mid Permian) from Northern Taimyr. The Uralian Orogen further south than Taimyr is also a possible source (Pease, 2001; Scarrow *et al.*, 2002; Vernikovsky *et al.*, 1995).

The rounded nature of the Meso- to Neoproterozoic zircon grains (∼1500-960 Ma) suggests that this sediment has been recycled. One likely source for this sediment is the Grenvillian Orogen of Canada and Greenland, an event which took place between ∼1190 and 980 Ma (Rivers, 1997). Crustal rocks of age ∼1500 to 1200 have been incorporated in this orogen (Rivers, 1997 and references therein) although a larger range of zircon ages that seen in sample C403730 would be expected from a Grenvillian source. Another possible source for these zircons may be from a northern source area eroding Grenville-age crust. The Taimyr Peninsula records granites of with a young Grenvillian age (∼1000 to 885 Ma) and should also be considered as a possible source (Pease, 2001). Due to similarities with the heavy mineral assemblages of Hoyle Bay and Sandy Point Formation samples, the Blind Fiord Formation is tentatively classified as sand type 1.

Hoyle Bay Formation - Sand type 1

There was a major influx of northerly derived sediment into the Sverdrup Basin during Carnian time (Embry, 1991a). Sample C403503 is similar to the Blind Fiord Formation sample C403730, being characterized by a prominent peak of young magmatic zircon ages, penecontemporaneous with the deposition of the sediment. However, in contrast to the Permian zircons in the Blind Fiord Formation, the Hoyle Bay Formation preserves a Middle Triassic (∼235 Ma) peak. There is no magmatic activity of Triassic age known from the Canadian-Greenland Shield region (Hoffman, 1989) but Triassic zircon ages have been reported from other Arctic regions: Permo-Triassic boundary age (∼252 Ma) from gabbros on the New Siberian Islands (Kuzmichev & Pease, 2007) and Early Triassic age (∼249-241 Ma)

from granites on the Taimyr Peninsula (Vernikovsky *et al.*, 2003). This area is considered to be a likely source for the Triassic zircons. It is important to note the presence of chrome spinel in this sample. This strengthens of Taimyr as a a source for Triassic zircons, given the wide extent of mafic-ultramafic igneous rocks associated with the Siberian Traps (Reichow *et al.*, 2009). Permo-Triassic zircon ages of 265-235 Ma are reported in detrital samples from Chukotka, Wrangel Island and the Lisburne Hills of Alaska (Miller *et al.*, 2006). The similarities in detrital zircon ages preserved between the northern Sverdrup Basin and the Alaska-Chukotka microplate (Chukotka, Wrangel Island and Lisburne Hills of Western Alaska) suggest that these sediments may have been derived from the same Triassic source.

This sample also contains zircons with latest Cambrian to Permian ages (∼493-268 Ma). These ages are known from the Taimyr Peninsula (∼300-265 Ma granites; Pease, 2001; Vernikovsky *et al.*, 2003), Severnaya Zemlya (∼343 Ma granites; Lorenz *et al.*, 2007), Baltica Caledonides (Late Cambrian to Early Devonian age; Roberts, 2003 and references therein) and from the Uralian Orogen (Scarrow *et al.*, 2002 and references therein).

Heiberg Formation - Sand type 2

Facies relationships in the Sverdrup Basin show that the deltaic sediment comprising the Heiberg Formation was shed into the basin from the east and south (Greenland/Svalbard and Canadian Shield). Studies here show that the lower Heiberg Formation (Romulus Member) has similarities with the northerly derived Hoyle Bay Formation, whereas the upper Heiberg Formation (Remus Member) has a different, less proximal provenance. The Remus Member sediment contains well-rounded grains and an ultrastable heavy mineral assemblage.

Sample C403752 shows a broad spread in zircon ages and is dominated by a peak of late Neoproterozoic-early Cambrian age (∼670-520 Ma, centred at ∼540 Ma). Late Neoproterozoic-early Cambrian magmatism is present in the Arctic region within the Timanian Orogen, northwestern Russia (Gee & Pease, 2004 and references therein) suggesting ultimate sediment derivation from the Barents Shelf, presumably from northern regions such as Severnaya Zemlya or Taimyr (Pease & Scott, 2009). The Barents Shelf would have been much closer to Axel Heiberg Island prior to the opening of the Eurasia Basin in Cenozoic time. Based on seismic mapping and well studies, Lundshein *et al.* (2008) described the progradation of large scale deltaic clinoforms across the Barents Shelf during Triassic time, from the east and southeast to the west, providing a potential transport mechanism

for sediment from the Timanian Orogen toward the Sverdrup Basin in the Early Jurassic.

The sample also contains zircons of Silurian-Devonian-Carboniferous age, possibly representing the Caledonian and Uralian orogenies of northern Baltica and Taimyr (Roberts, 2003; Scarrow *et al.*, 2002). The final age cluster in this sample, represented by peaks at 1090 and 960 Ma, can be correlated to the Grenville Orogen (Rivers, 1997).

Sandy Point Formation - Sand type 1

Sample C403747 shows a large spread of zircon ages. The heavy mineral population is similar to the Carnian Hoyle Bay Formation sample (C403503) and is dominated by apatite, with lesser amounts of zircon, tourmaline, rutile and importantly, chrome spinel. Chrome spinel is a mineral that indicates an ultramafic sediment source. There are two Triassic zircon peaks in this sample (230 and 216 Ma), in addition to Permo-Carboniferous, Devonian, Silurian and Ordovician peaks. Older ages preserved in this sample are of Grenvillian age (Rivers, 1997). It should be noted that the ∼1740 Ma age, very obvious here, represents a time of ubiquitous crustal formation in the North Atlantic region. Older ages show few robust peaks.

The two Triassic zircon peaks in this sample (230 and 216 Ma) may indicate derivation from the Taimyr Peninsula, as suggested for the Hoyle Bay sample. Permo-Carboniferous, Devonian, Silurian and Ordovician peaks may also suggest a Taimyr or northern Baltica derivation. The Carboniferous-Ordovician peaks are of Caledonian and Uralian age and similar to the ages presented by Miller *et al.* (2006) for samples from far eastern Russia and Western Alaska. The sample contains Neoproterozoic to early Cambrian age zircons (∼680-545 Ma) suggesting a component of Timanide zircons, again suggesting a northern Baltica-Taimyr derivation.

Deer Bay Formation - Sand type 3

Sample C403685 is different from the other four zircon samples, in both mineralogy and zircon ages. It contains an abundance of garnet and contains mainly older zircon grains. Seventy per cent of the zircons are Proterozoic age and 24% are Archean age. The zircon ages of this sample are consistent with the derivation from the south and east (Greenland-Canada Shield). Archean zircons could be derived from the Slave, Superior, Rae and Hearne terranes of the Canadian Shield or the

Nain terrane of Greenland Shield (Hoffman, 1989). Proterozoic ages present in this sample are reflect from the ages of crustal formation found in the Greenland-Canada Shield (e.g. Kirkland *et al.*, 2009; Rainbird *et al.*, 1992) although late Paleoproterozoic time (1700-1600 Ma) and Early Mesoproterozoic time (1600-1300 Ma) zircons are rare in the Greenland-Canada Shield.

The zircon ages reported for sample C403685 are virtually identical to those reported by Miller *et al.* (2006) from the Bjorne Formation, an Early Triassic sandstone sample deposited on the southern margin of the Sverdrup Basin and believed to be southerly derived. However, the zircon ages in this sample are more consistent with derivation from the Baltic Shield, with zircon ages possibly representing Baltic Archean craton formation (3100-2500 Ma), the Svecofennian Orogeny (2000-1860 Ma), the Transscandinavian Igneous Belt (1850-1550 Ma) and the Sveconorwegian Orogeny (1760-900 Ma) (e.g. McNicoll *et al.*, 1995).

The succession could be derived from the south and east of the Sverdrup Basin during Jurassic-Cretaceous time, from the Devonian clastic wedge that may have ultimate Baltica provenance (McNicoll *et al.*, 1995), or directly from the north of the Sverdrup Basin.

4.12 Conclusions

The zircon data from five samples show considerable variability although there are some important similarities visible. Young, magmatic zircon ages dominate the two Triassic samples. The Early Triassic Blind Fiord Formation sample shows a Permian age peak and the Late Triassic Hoyle Bay Formation sample shows a Triassic age peak. The Aalenian Sandy Point Formation also contains zircons of Triassic age. All samples except the Blind Fiord Formation sample show zircon ages of Silurian-Carboniferous age (Ellesmerian-Caledonian-Uralian age). Zircon grains of Neoproterozoic (Grenvillian) age are found in all samples. Young Grenvillian ages (∼960 Ma), in particular, are common in north Greenland/Svalbard. On the basis of the zircon evidence and heavy mineral characteristics, samples of the Blind Fiord, Hoyle Bay and Sandy Point formations are interpreted to be northerly derived from the Taimyr Peninsula. The Early Jurassic Heiberg Formation sample shows derivation from the Timanian and Caledonian orogenies on the Barents Shelf. Provenance of the Tithonian Deer Bay Formation sample may be derived from the Canada-Greenland Shield, the northerly derived Devonian clastic wedge or directly from another Proterozoic-Archean terrane in the Arctic region (most likely Baltica).

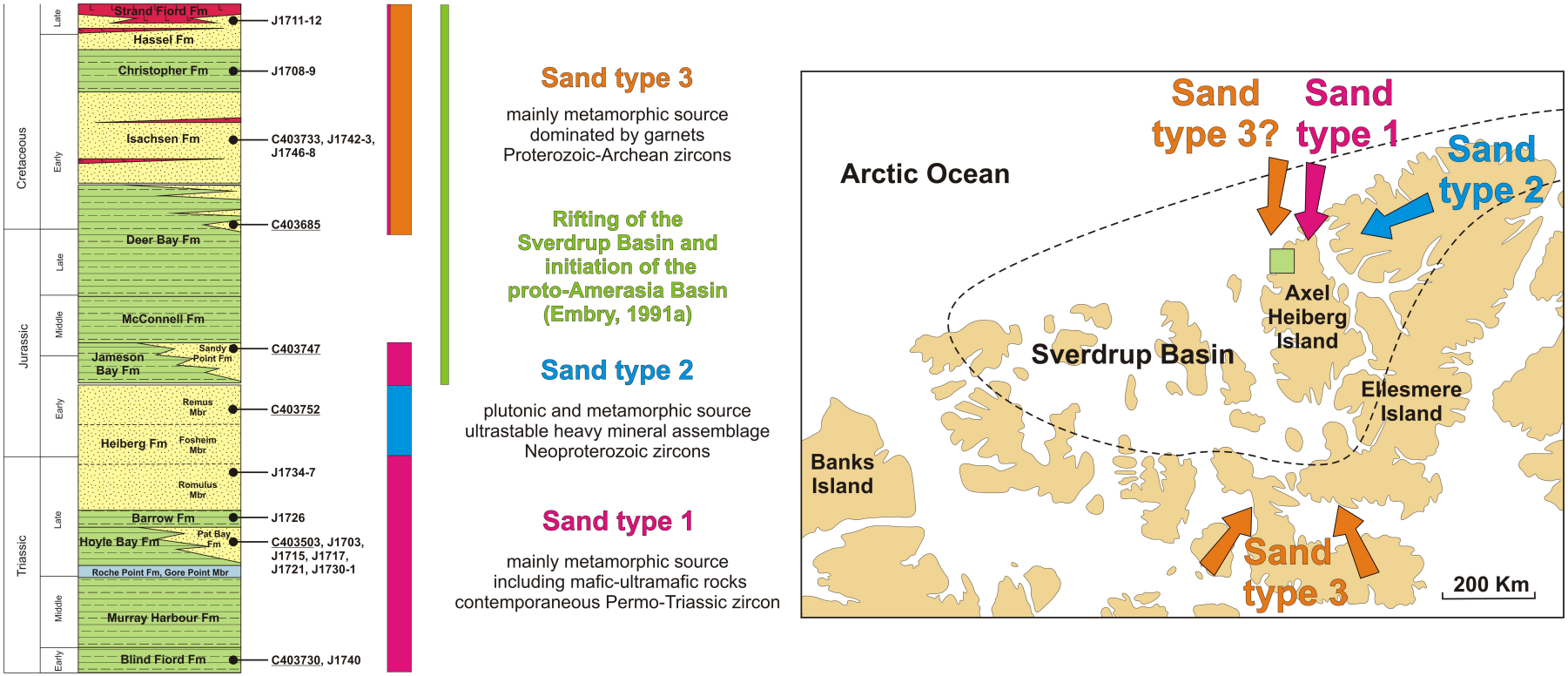

Figure 4.36: Sediment provenance pathways to the northern Sverdrup Basin during Mesozoic time, showing three distinctive sediment sources. Sand type 1: Blind Fiord, Hoyle Bay, Barrow, lower Heiberg (Romulus Member) and Sandy Bay formations. Sand type 2: upper Heiberg Formation (Remus Member). Sand type 3: Deer Bay, Isachsen, Christopher and Strand Fiord formations. Samples studied for detrital zircon ages are underlined.

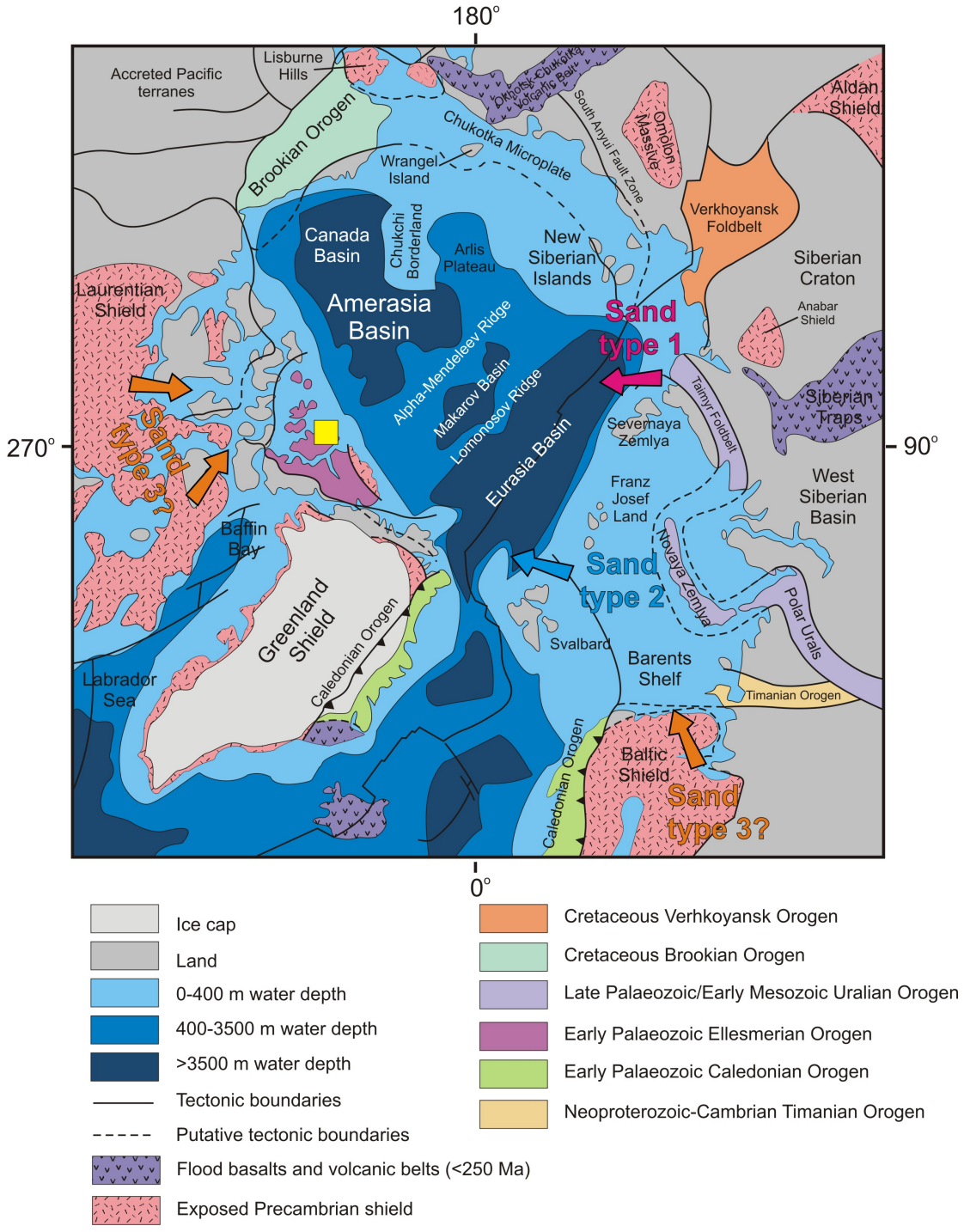

Figure 4.37: Tectonic map of the Arctic region. Bathymetry and topography are modified after the IBCAO Arctic Bathymetry database (Jakobsson *et al.*, 2008). Plate boundaries and geological features are modified after Harrison (2005). Neoproterozoic and younger orogenic belts outcrops on land are shown with different shadings. Interpreted provenance of sand types 1, 2, 3 is shown.

Chapter 5

Composition and provenance of Mesozoic sandstones of Svalbard and the southwestern Barents Shelf

In this chapter, 21 Mesozoic samples from Svalbard and the southwestern Barents Shelf are studied to evaluate the sediment characteristics, sediment dispersal patterns and source areas to the Barents Shelf during Mesozoic time. Two distinctive provenance types are identified (sand types 1 and 3). Triassic samples from Svalbard and the southwestern Barents Shelf show heavy mineral assemblages dominated by apatite in association with late Silurian through mid Carboniferous zircon grains (sand type 1). These sediments are inferred to be derived from the Uralian Orogen. Late Triassic through Early Cretaceous samples from Svalbard and the Barents Shelf show ultrastable heavy mineral assemblages dominated by zircon in association with Proterozoic zircon grains (sand type 3). These sediments are inferred to be derived from Baltica (Eurasian Plate). From Early Jurassic time on the Barents Shelf and Early Cretaceous time on Svalbard, sand type 3 occurs mixed with sand type 1. This indicates either renewed influx from the Urals/Siberian Traps or recycling of previously deposited sediment from those areas. The naming of the sand types reflects similarities with sand types from other areas and will be discussed later.

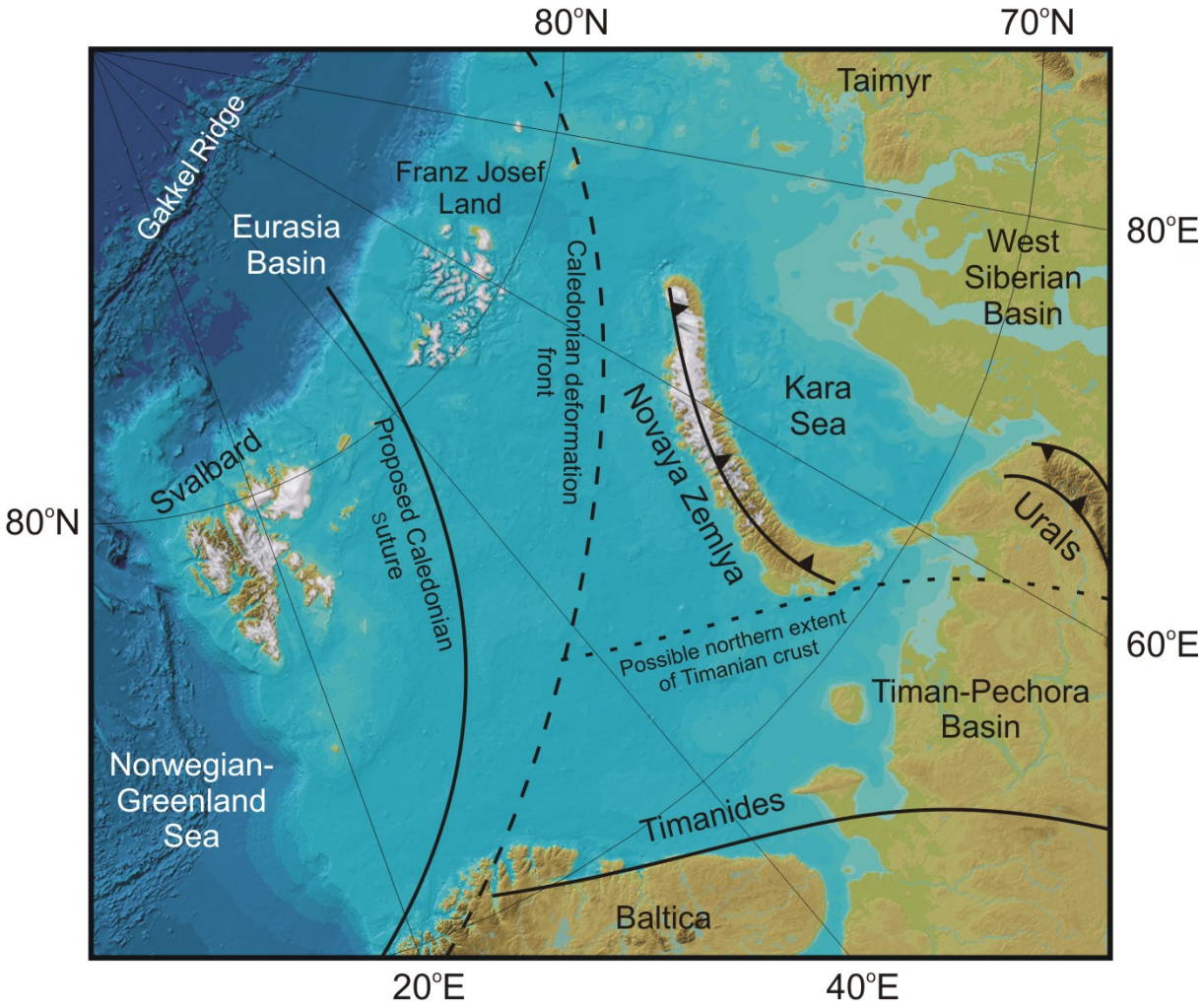

Figure 5.1: Regional setting of the Barents Shelf, including the Svalbard archipelago, on a base map modified after the IBCAO Arctic Bathymetry database (Jakobsson *et al.*, 2008). The Barents Shelf lies at the northern margin of the Eurasian Plate/Baltica. The Caledonian suture crosses the Barents Shelf, presumably between Svalbard and Franz Josef Land (e.g. Grantz *et al.*, 2009). The Svalbard Archipelago is a fragment of Laurentia.

5.1 Introduction

The Barents Shelf lies at the northwestern margin of the European continent (Eurasian Plate) and is bounded by Norway and Russia to the south, Novaya Zemlya to the east, the Arctic Ocean to the north and the Norwegian-Greenland Sea to the west (Fig. 5.1). Most of the shelf is covered by shallow water (less than 500 m), with the Svalbard and Franz Josef Land archipelagoes emergent in the north. The crust underlying the Barents Shelf was amalgamated and deformed during Late Neoproterozoic through Late Paleozoic time by the Timanian, Caledonian and Uralian orogenies.

This chapter presents sediment provenance results from Triassic through Cretaceous samples from Svalbard and the southwestern Barents Shelf (Fig. 5.2). The results show the importance of Siberian Trap magmatism at the Permo-Triassic boundary for Mesozoic sedimentation patterns across the Barents Shelf.

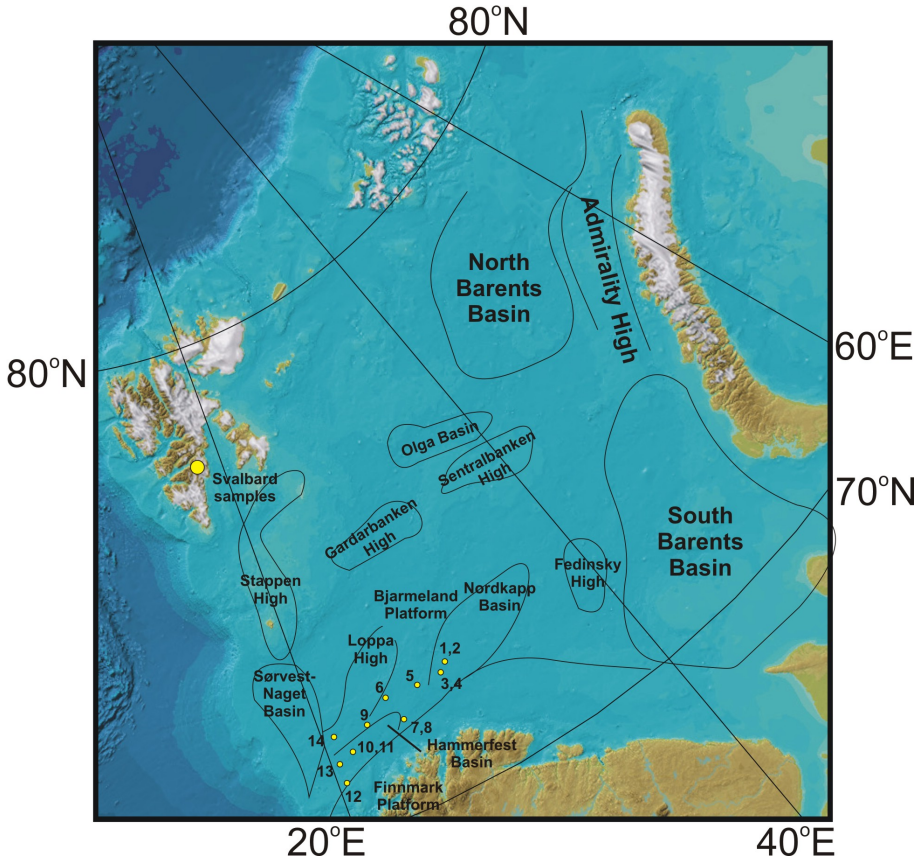

Figure 5.2: Location of Barents Shelf and Svalbard samples on a base map modified after the IBCAO Arctic Bathymetry database (Jakobsson *et al.*, 2008). The Barents Shelf samples, numbered, are prefixed by JO NPD.

5.2 Geological setting

During the Late Neoproterozoic-Cambrian Timanian Orogeny (600-575 Ma), crust of unknown affinity and island arc material was accreted to the northern margin of Baltica (Siedlecka *et al.*, 2004). During late Early Silurian to late Early Devonian time, the western margin of Baltica collided with the eastern margin of Laurentia in the Scandian phase of the Caledonian Orogeny (Lawver *et al.*, 2002). During Carboniferous time, closure of the Uralian Ocean between Baltica and Siberia affected the eastern margin of the Barents Shelf (Hamilton, 1970; Zonenshain *et al.*, 1984). In Novaya Zemlya and the Taimyr Peninsula, Uralian deformation continued into early Mesozoic time (Inger *et al.*, 1999). At the Permo-Triassic boundary (252 Ma), the Siberian flood basalts were erupted, extruding a several kilometre thick succession of volcanic rocks in less than two million years (Reichow *et al.*, 2009). Mafic extrusive and intrusive rocks related to this event are found on the Siberian Platform, the Western Siberian lowlands and the Taimyr Peninsula (Kamo *et al.*, 2003).

Crust of the Timanide Orogen crops out in the Timan Range of northwestern Russia, sections of the Urals mountain chain, Novaya Zemlya, coastal regions of Russia and Norway and underlies the Timan-Pechora Basin and parts of the Barents Shelf (Gee & Pease, 2004). The extent and nature of the Timanian Orogen beneath the Barents Shelf is poorly known: it possibly extends from the poorly known Early Paleozoic Caledonian suture (Baltica-Laurentia boundary) in the west, to the Late Paleozoic Uralian Orogen (Baltica-Siberia boundary) in the east and the edge of the Barents Shelf with the Eurasia Basin to the north. Similarly, the possible geographical continuation of the Caledonian and Uralian orogenies north of the Barents Shelf is poorly understood and merits further study. Crust affected by the Timanian, Caledonian and Uralian orogenies may underlie putative continental crust of the Central Arctic region and possibly beyond.

While the eastern Barents Shelf was affected by Uralian orogenesis, Permo-Carboniferous time on the western Barents Shelf was initially characterized by extensional tectonism with deposition of locally derived continental clastic sediments in elongate grabens. During Late Carboniferous time tectonism waned and a stable carbonate platform developed. The slow subsidence of this stable platform lasted until Late Permian time, when an extensive hiatus of regional character developed. After the Late Permian hiatus, clastic deposition resumed (Mørk *et al.*, 1999). During Early Cretaceous time, magmatic activity associated with the Early Cretaceous High Arctic Large Igneous Province (HALIP) and the opening of the Arctic Ocean affected Svalbard and the Barents Shelf, leading to uplift and erosion

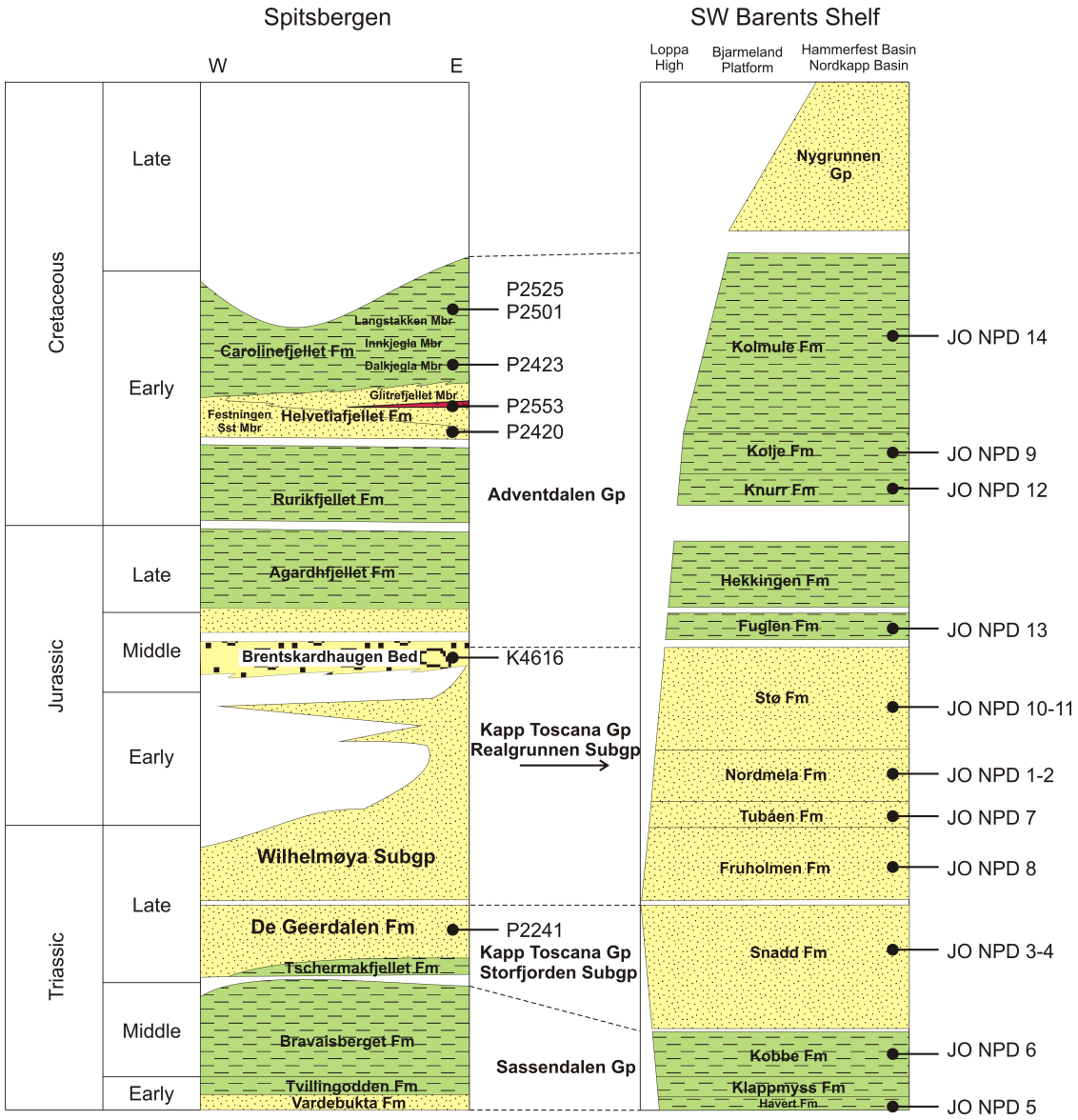

Figure 5.3: Stratigraphic columns for Svalbard and southwestern Barents Shelf, modified after Mørk *et al.* (1999), showing a simplified stratigraphy. Stratigraphic position of the samples are shown. For this study, the nomenclature of Mørk *et al.* (1999) will be used throughout. In this scheme, the lithostratigraphic succession of the Barents Shelf (including Svalbard) is subdivided into three lithostratigraphic groups: the Sassendalen Group, Kapp Toscana Group and Adventdalen Group.

on the northern Barents Shelf (Maher, 2001). During Cenozoic time, the Eurasia Basin formed to the north of the present-day shelf and the Norwegian-Greenland Sea formed to the west of the present-day shelf.

Barents Shelf Mesozoic succession

Above an extensive late Permian unconformity, Triassic to Cretaceous clastic rocks were deposited on the Barents Shelf (Mørk *et al.*, 1999). Basins formed on the shelf, separated by shallow shelf or platforms areas including local highs (Fig. 5.2). Potential source areas for the Mesozoic succession of the Barents Shelf and Svalbard lay to the west of Svalbard (northeastern Greenland), to the north or northeast of the Barents Shelf and to the south (Eurasian Plate/Baltica) (present-day coordinates).

The Early to Middle Triassic Sassendalen Group comprises shale, siltstone and subordinate sandstone. Coastal and deltaic sediments exposed on western Spitsbergen grade into shelf mudstones eastwards and southwards. In the Hammerfest Basin, on the southern margin of the Barents Shelf, a southerly derived marine coastal clastic succession is preserved, reaching a thickness of 1000 m (Mørk *et al.*, 1999). On the southern Barents Shelf, the Sassendalen Group is divided into three formations: the Havert, Klappmyss and Kobbe formations (Fig. 5.3). The Havert and Klappmyss formations preserve shallow marine to marginal marine siltstones and sandstones. The Kobbe Formation preserves a phosphatic, organic-rich shale and subordinate sandstone succession.

The deposition of the late Middle Triassic to Middle Jurassic Kapp Toscana Group follows a major Middle Triassic unconformity. The Kapp Toscana Group represents a major change in depositional regime to an environment of presumed northeasterly derived shallow marine and deltaic deposition across the entire shelf (Mørk *et al.*, 1999).

The late Middle Triassic to Late Triassic Storfjorden Subgroup comprises the immature lower part of the Kapp Toscana Group and preserves shallow marine, prodelta and delta top depositional environments. The basal section of the subgroup is represented by shales of the Tschermakfjellet Formation (on Svalbard) and lower Snadd Formation (on the Barents Shelf). Overlying this is the sandstone-dominated succession of the De Geerdalen Formation (on Svalbard) and upper Snadd Formation (on the Barents Shelf) (Mørk *et al.*, 1999). The base of this subgroup is diachronous: Ladinian on the Barents Shelf and early Carnian on Svalbard.

The upper Kapp Toscana Group is subdivided into the Wilhelmøya Subgroup on Svalbard and the Realgrunnen Subgroup on the Barents Shelf. The Wilhelmøya Subgroup is a condensed equivalent of the Realgrunnen Subgroup (Mørk *et al.*, 1999) (Fig. 5.3). Correlation between the two subgroups is made difficult by poor biostratigraphic control and numerous hiati (Mørk *et al.*, 1999). The Wilhelmøya Subgroup contains texturally mature coastal plain, deltaic and shallow marine sandstones (Mørk *et al.*, 1999). This unit thins towards the west and northwest and hiati become more abundant. Phosphatic nodular beds are common (e.g. the Brentskardhaugen Bed). There is discussion as to whether the Brentskardhaugen Bed belongs to the underlying Kapp Toscana Group or the overlying Adventdalen Group. The stratigraphic scheme of Mørk *et al.* (1999), used here, places the unit at the top of the Kapp Toscana Group.

The Realgrunnen Subgroup is defined on the Barents Shelf and is dominated by sandstone with minor shale and coal. The subgroup is divided into the Fruholmen, Tubåen, Nordmela and Stø formations (Fig. 5.3). The Fruholmen Formation consists of sandstones and shales inferred to be derived from the south (Mørk *et al.*, 1999). The Tubåen Formation consists of shale, sandstone and coal deposited in a marginal marine environment, with inferred source areas to the south (Mørk *et al.*, 1999). The Nordmela Formation is composed of siltstone, sandstone, shale and minor coal and is deposited in a southwestward or westward-thickening wedge, deposited in tidal-flat to flood-plain environments. The Stø Formation is composed of mineralogically mature sandstone, with minor shale and siltstone deposited in prograding coastal marine environments (Mørk *et al.*, 1999).

The latest Middle Jurassic to Early Cretaceous Adventdalen Group is composed of shales and sandstones deposited across Svalbard and the Barents Shelf (Fig. 5.3). During Late Jurassic time, organic-rich shales were deposited in shelf environments across the region. This deposition was disturbed by a hiatus at the Jurassic-Cretaceous boundary above which renewed shale deposition occurred in the basins, with calcareous deposition on platform areas (Mørk *et al.*, 1999). During Early Cretaceous time, regional uplift occurred on the northern margin of the Barents Shelf (Mørk *et al.*, 1999).

The base of the Adventdalen Group defines an unconformity with the underlying Kapp Toscana Group (Mørk *et al.*, 1999). Overlying the unconformity in the Hammerfest Basin is the Fuglen Formation, composed of pyritic mudstones with limestone interbeds. Sand bodies occur in the south. Above this, the organic-rich claystones of the Hekkingen Formation occur over large areas of the Barents Shelf (Mørk *et al.*, 1999). On Svalbard, shale, siltstone and sandstone of the Agardhfjellet

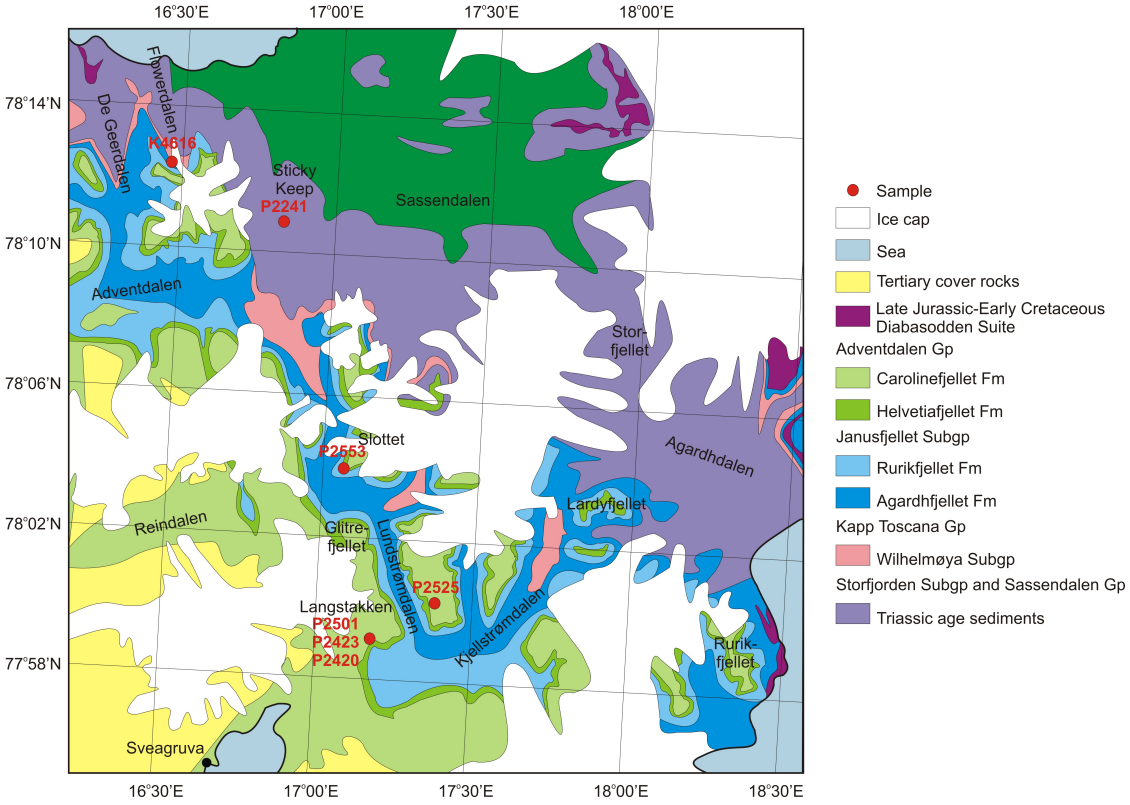

Figure 5.4: Location of Spitsbergen samples on a simplified geological map modified after Mørk *et al.* (1999).

Formation were deposited in an open marine shelf environment with intermittent restricted environment (Mørk *et al.*, 1999). Above a major unconformity at the Jurassic-Cretaceous boundary, the Knurr Formation was deposited as claystones in the Hammerfest Basin and limestones on platform areas. Subsequently, basinal conditions returned and shales of the Kolje Formation were deposited. On Svalbard, shales, siltstone and sandstone of the Rurikfjellet Formation were deposited in an open marine environment.

Above an unconformity on Svalbard, the Barremian age Helvetiafjellet Formation was deposited, including coarse-grained sandstone, shale, coal and conglomerate. The Lower Helvetiafjellet Formation, the Festningen Sandstone Member, contains interbedded sandstones, shales and coal. The Upper Helvetiafjellet Formation, the Glitrefjellet Member, contains coarse-grained, ripple-laminated sandstone with interbedded coal deposited in fluvio-deltaic environments. Material of volcanic origin is present. This is attributed to the Barremian age magmatism seen in many localities in the Arctic (High Arctic Large Igneous Province) (Maher, 2001). On Kong Karls Land, basaltic lava flows and pyroclastic rocks are

interbedded with sandstones (Mørk *et al.*, 1999).

The Carolinefjellet Formation on Svalbard and Kolmule Formation on the Barents Shelf are equivalent. Shale, siltstone and sandstone of the Carolinefjellet Formation were deposited in fluvio-deltaic and later distal marine conditions. Shale, siltstone and glauconitic sandstones of the Kolmule Formation were deposited in open marine environments (Mørk *et al.*, 1999).

5.3 Samples and methods

Two sample sets were used for this study: outcrop samples from Svalbard and well core samples from the southwestern Barents Shelf. The stratigraphic positions of the samples are shown in Figure 5.3. Locations of the Barents and Svalbard samples, on a regional map, are shown in Figure 5.2. Locations of the Svalbard samples, on a geological map, are shown in Figure 5.4.

The southwestern Barents Shelf samples were collected from petroleum exploration wells stored in the Norwegian Petroleum Directorate core store in Stavanger, Norway. The samples are from the Nordkapp Basin, Bjarmeland Platform, Hammerfest Basin and Loppa High areas of the southwestern Barents Shelf (Fig. 5.2). Stratigraphic logs, including well names and sample depths, can be found in Appendix A.

The Svalbard samples were collected on Spitsbergen by John Parker in 1963 and 1964 (P-samples) and Simon Kelly in 1985 (K-sample) (Figs. 5.2-5.4).

The Late Triassic De Geerdalen Formation sample P2241 was collected from the Sticky Keep area, from a unit described as flaggy fine-grained current-bedded brown sandstone (Parker, 1966). The Middle Jurassic Brentskardhaugen Bed sample K4616 was collected from Flowerdalen, from a phosphatic conglomerate (Kelly, pers. comm.). The Early Cretaceous Helvetiafjellet Formation Festningen Member sample P2420 was collected from the Langstakken area. The sample was collected from a unit of coarse-grained grey-white sandstone with conglomerate bands (Parker, 1966). The Early Cretaceous Helvetiafjellet Formation Glitrefjellet Member sample P2553 was collected from the Slottet area. The sample was collected from a unit of grey carbonaceous sandstones, interbedded with thin coal seams and black carbonaceous shales (Parker, 1966). The Early Cretaceous Carolinefjellet Formation Langstakken Member samples P2501 and P2525 were collected from the Langstakken area. The samples were collected from a unit of fine-grained thinly bedded flaggy grey sandstones with shaley interbeds. The Early Cretaceous

Carolinefjellet Formation Dalkjegla Member sample P2423 was collected the Lundstrømdalen area from a unit described as flaggy grey sandstone interbedded with red siltstone (Parker, 1966).

The samples were analysed for petrography, heavy mineral analysis, garnet and tourmaline chemistry and SIMS zircon analysis (Table 5.1) following analytical methods outlined in Chapter 3.

5.4 Petrography results

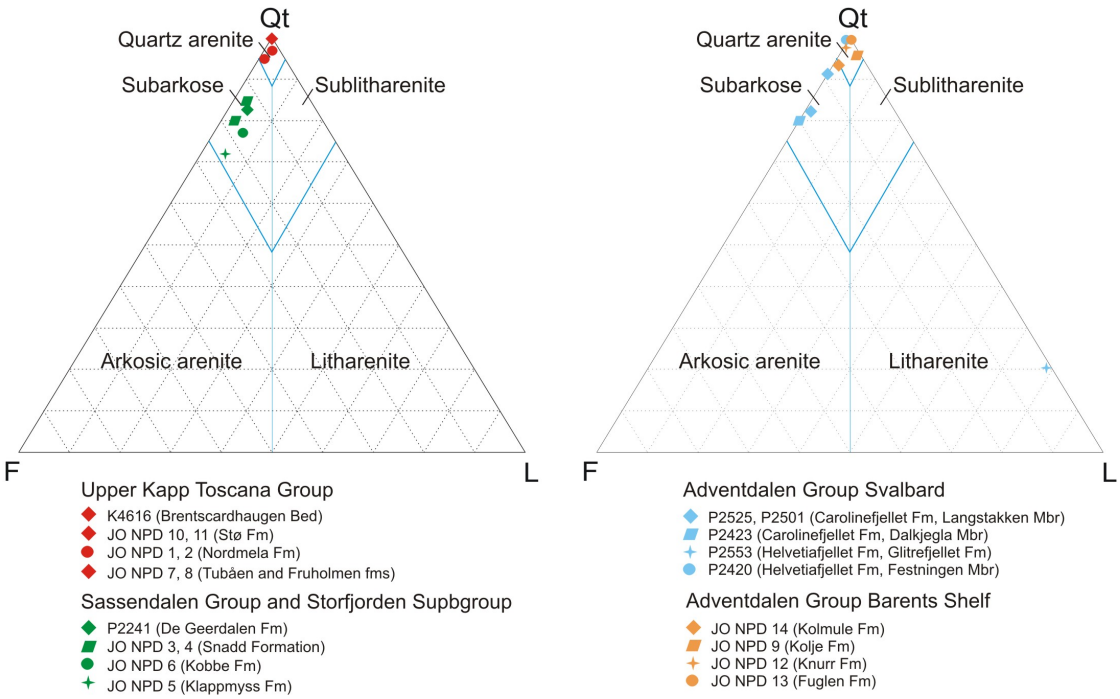

Figure 5.5: Sediment classification of Barents Shelf samples. QtFL sandstone classification plot, modified after Pettijohn *et al.* (1987). Some samples have the same symbols (e.g. Upper Kapp Toscana Group samples) as they plot in the same place on the ternary diagrams.

Figures 5.5-5.7 illustrate point counting results for seven Svalbard samples and fourteen Barents Shelf samples (Table 5.1). The complete dataset is included in the accompanying CD. Photomicrographs of the analysed samples are shown in Figures 5.8-5.12.

Early to Late Triassic Sassendalen Group and Storfjorden Subgroup samples from Svalbard and the Barents Shelf were analysed for sediment petrography. The samples are moderately well-sorted, silt-sized to medium-grained subarkoses (Fig.

Svalbard

Sample	Formation	Age	Petro-graphy	HM analysis	Garnet chemistry	Tourmaline chemistry	Zircon dating
P2525	Carolinefjellet Langstakken Mbr	K1	y	y	y	y	
P2501	Carolinefjellet Langstakken Mbr	K1	y	y			
P2423	Carolinefjellet Dalkjegla Mbr	K1	y	y			
P2553	Helvetiafjellet Glitrefjellet Mbr	K1	y				
P2420	Helvetiafjellet Festningen Mbr	K1	y	y		y	y
K4616	Brentskard -haugen Bed	J2	y	y		y	y
P2241	De Geerdalen	T3	y	y		y	

SW Barents

Sample	Formation	Age	Petro-graphy	HM analysis	Garnet chemistry	Tourmaline chemistry	Zircon dating
JO NPD 14	Kolmule	K1	y	y	y	y	
JO NPD 9	Kolje	K1	y	y		y	
JO NPD 12	Knurr	K1	y	y	y	y	
JO NPD 13	Fuglen	J2	y	y		y	
JO NPD 10	Stø	J1-2	y	y		y	
JO NPD 11	Stø	J1-2	y	y			
JO NPD 1	Nordmela	J1	y	y	y	y	
JO NPD 2	Nordmela	J1	y	y	y	y	
JO NPD 7	Tubåen	J1	y	y		y	
JO NPD 8	Fruholmen	T3	y	y	y	y	y
JO NPD 3	Snadd	T2-3	y	y	y	y	y
JO NPD 4	Snadd	T2-3	y	y		y	
JO NPD 6	Kobbe	T1-2	y	y		y	
JO NPD 5	Havert	T1	y	y	y	y	

Table 5.1: Overview of analyses performed on the Barents Shelf samples. Y=sample analysis done. The samples are listed in stratigraphic order, with the youngest samples at the top. P-samples were collected by John Parker in 1963 and 1964. The K-sample was collected by Simon Kelly in 1985. HM = Heavy mineral.

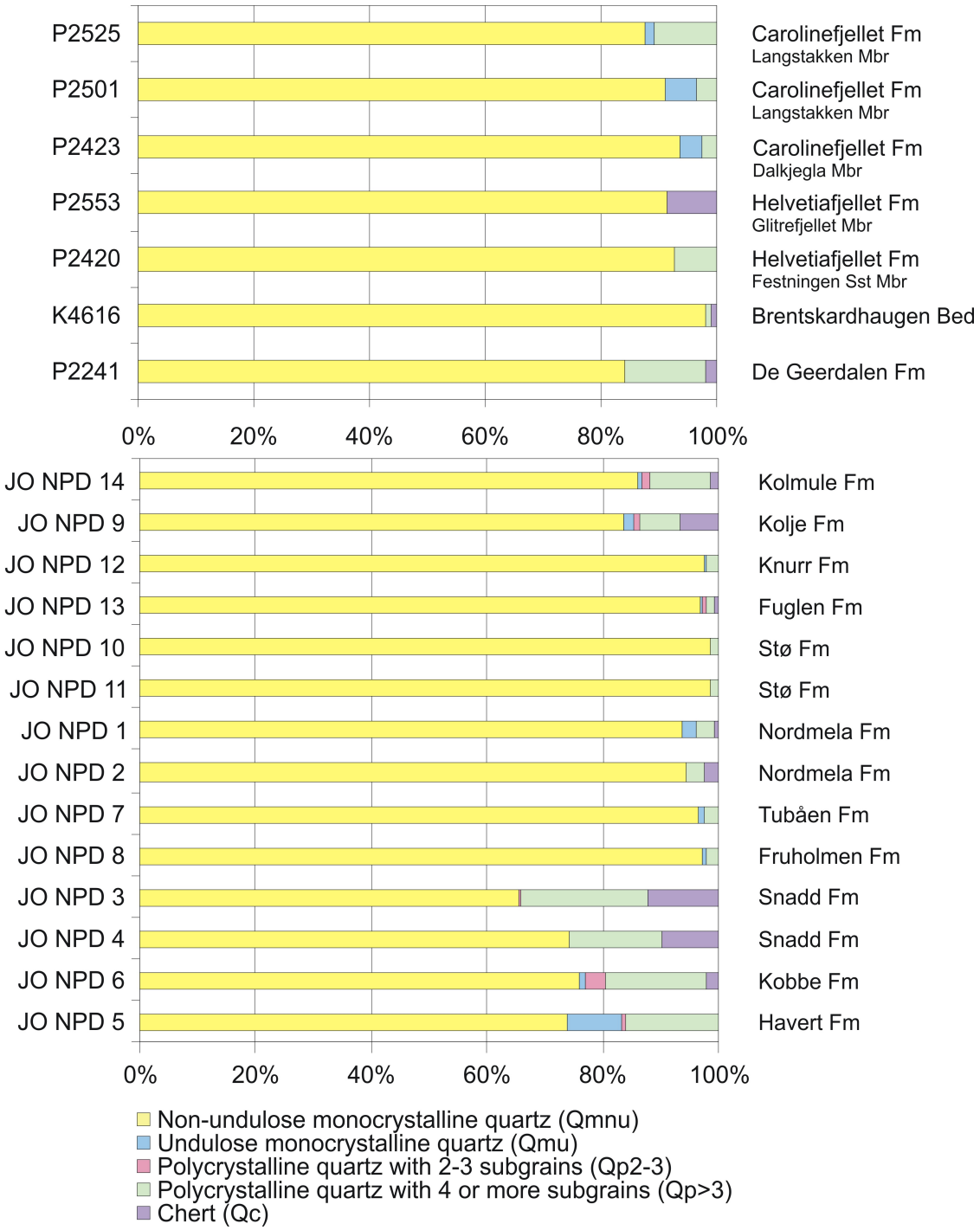

Figure 5.6: Quartz types identified by point counting, plotted as percentage of Total Quartz and Chert (Chapter 3). Most samples are heavily dominated by monocrystalline quartz.

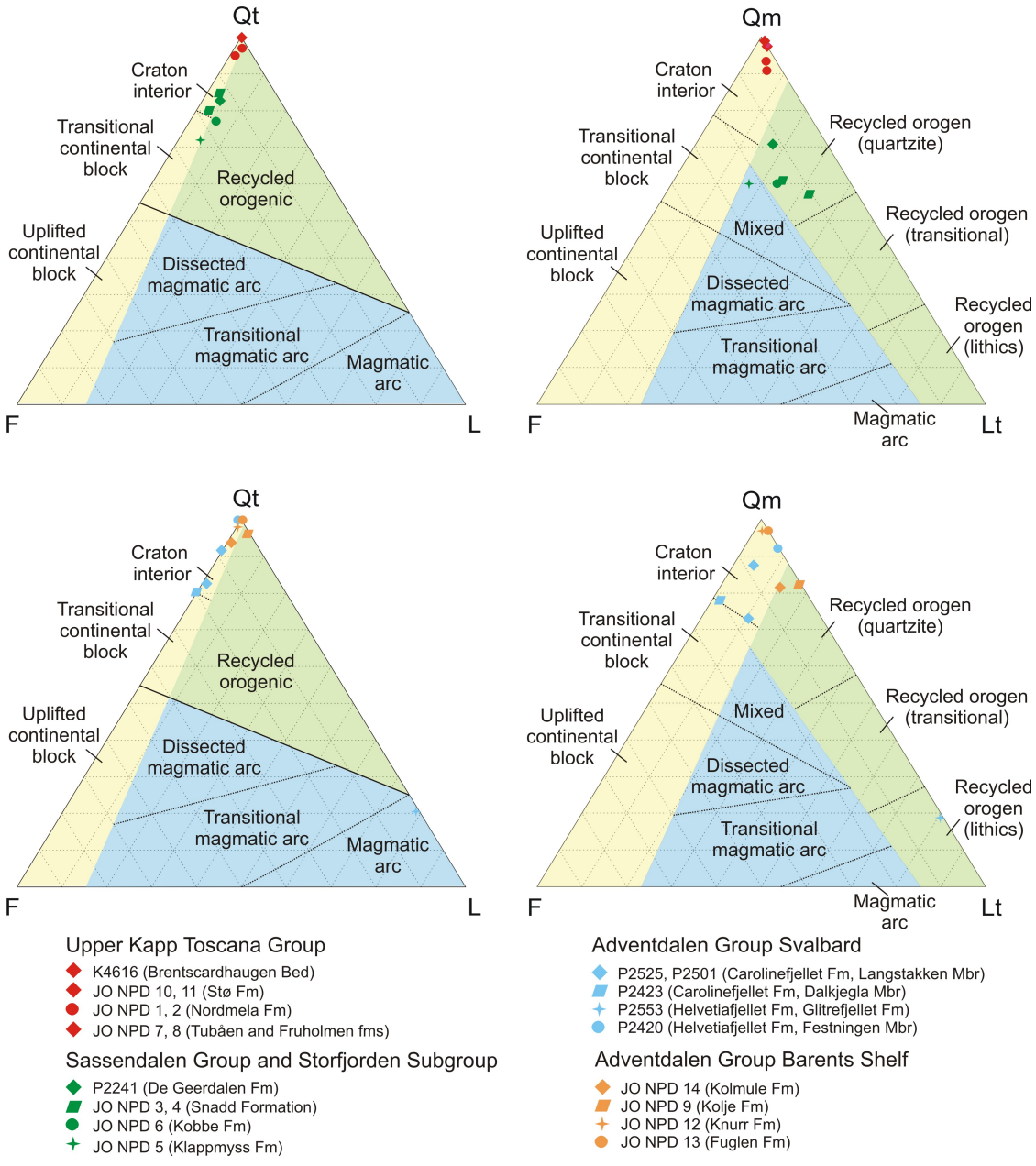

Figure 5.7: Sediment petrography results for the Svalbard samples. QtFL and QmFLt provenance discrimination diagrams are modified after Dickinson & Suczek (1979). Some samples have the same symbols (e.g. Upper Kapp Toscana Group samples) as they plot in the same place on the ternary diagrams.

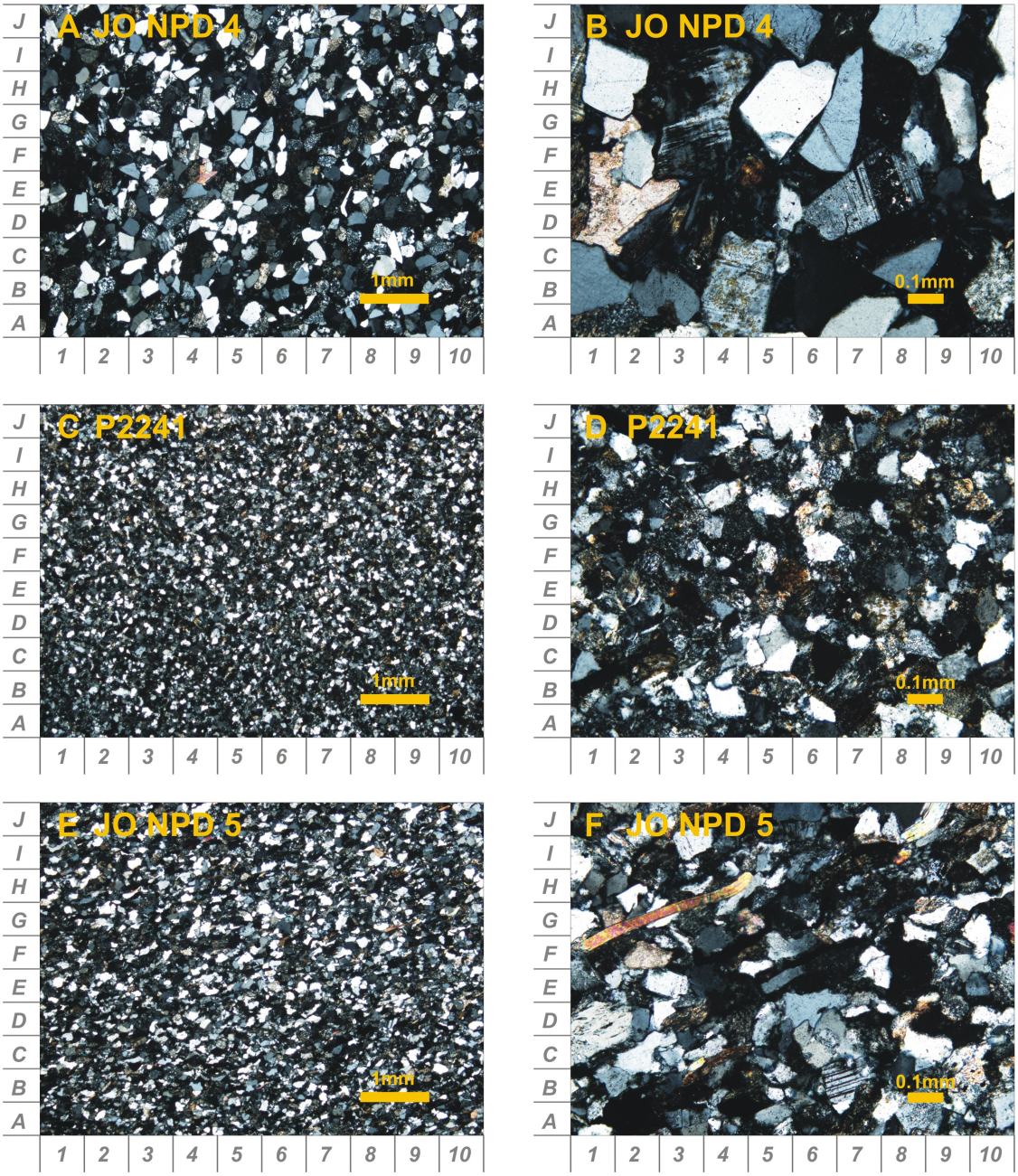

Figure 5.8: Photomicrographs of the Sassendalen Group and Storfjorden Subgroup samples. (A) Snadd Formation. General view of the moderately well sorted, fine-grained subarkose. (B) The sample contains plagioclase (E7), microcline (G3) and calcite cement (E2). (C) De Geerdalen Formation. General view of the moderately sorted, subarkosic siltstone. (D) The immature nature of the sediment is visible. An alkali feldspar grain is shown (D8). (E) Kobbe Formation. General view of the moderately well sorted, fine-grained subarkose. (F) The sediment contains abundant plagioclase (B7) and muscovite (G3).

5.5). The quartz species in the samples are dominated by non-undulose monocrystalline quartz (66-84%) with lesser amounts of polycrystalline quartz with four or more subgrains (14-22%), chert (2-12%) and undulose monocrystalline quartz (0-9%) (Fig. 5.6). The samples show a mixture of plagioclase and alkali feldspar (67-85% plagioclase and 2-33% alkali feldspar). On QtFL and QmFLt plots, the samples plot mainly within the 'craton interior' and 'recycled orogen' fields (Fig. 5.7).

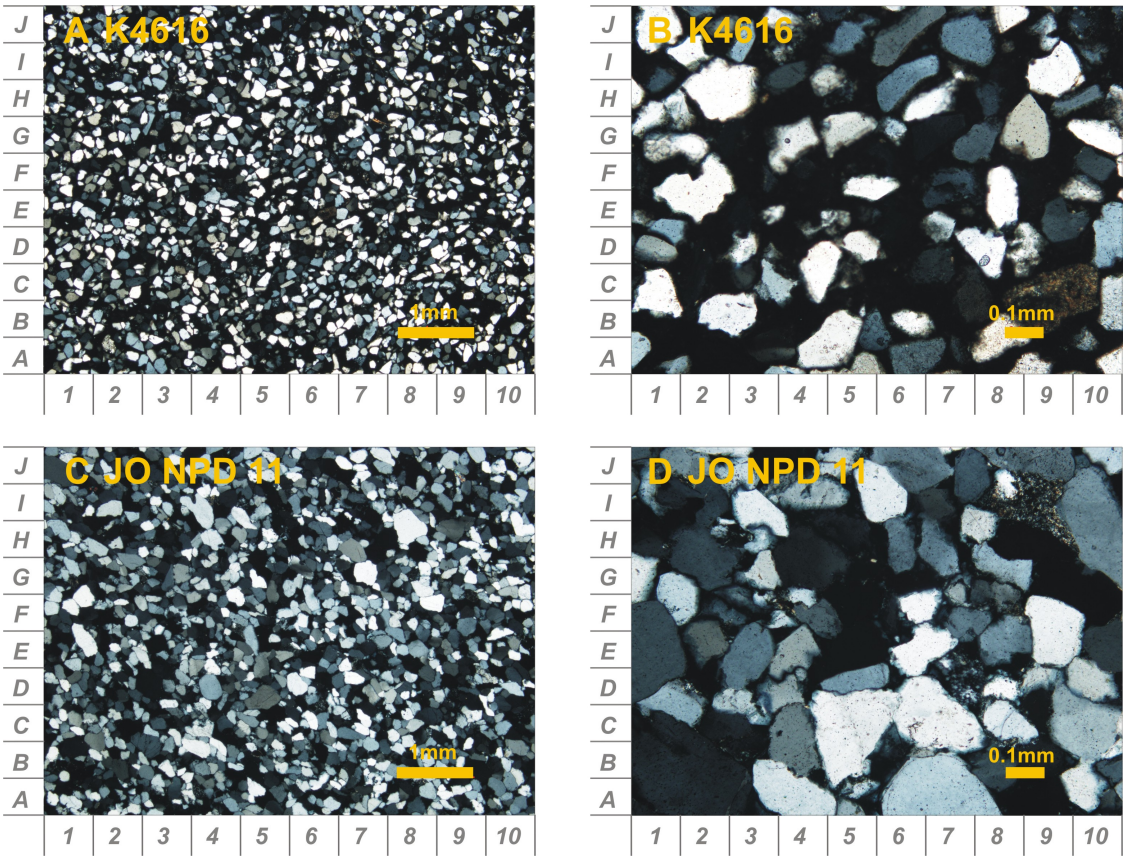

Figure 5.9: Photomicrographs of the upper Kapp Toscana Group samples. (A) Brentskardhaugen Bed. General view of the moderately sorted, fine-grained quartz arenite. (B) The grains are cemented by phosphatic isopacheous cement. (C) Stø Formation. General view of the moderately sorted, fine-grained quartz arenite. (D) The sediment is mostly composed of monocrystalline non-undulose quartz, with some monocrystalline quartz (E7).

Samples from the Late Triassic to Middle Jurassic upper Kapp Toscana Group and the Early Cretaceous Helvetiafjellet (Festningen Sandstone Member, sample P2420) were analysed for sediment petrography. The samples are poorly to moderately well-sorted, fine- to medium-grained quartz arenites (Fig. 5.5). The quartz

species in the samples are heavily dominated by non-undulose monocrystalline quartz (93-99%) (Fig. 5.6). The predominance of monocrystalline quartz suggests derivation from a plutonic source. On QtFL and QmFLt plots, the samples plot within the 'craton interior' fields (Fig. 5.7).

The Early Cretaceous Helvetia Formation, Glitrefjellet Member sample P2553 was analysed for sediment petrography. Sample P2553 is a moderately sorted, medium-grained litharenite (Fig. 5.5). The sample is dominated by rounded volcanic lithic clasts (80% of grains counted) with lesser quartz (19%) surrounded by poikolitic calcite cement. The quartz is dominated by non-undulose monocrystalline quartz (91%) with lesser chert (9%) (Fig. 5.6). On a QtFL plot the sample plots in the 'magmatic arc' field. On a QmFLt plot, the sample plots within the 'recycled orogen, lithics' field (Fig. 5.7).

The Early Cretaceous Carolinefjellet Formation samples were analysed for sediment petrography. The samples are moderately well sorted, silt-sized to very fine-grained subarkoses (Fig. 5.5). The samples are dominated by non-undulose monocrystalline quartz (88-94%) with minor undulose monocrystalline quartz (1-5%) and polycrystalline quartz with four or more subgrains (3-11%) (Fig. 5.6). The predominance of monocrystalline quartz suggests derivation from a plutonic source. The sample shows a mixture of plagioclase and alkali feldspar (70% plagioclase, 30% alkali feldspar). On QtFL and QmFLt plots, the samples plot within the 'craton interior' fields (Fig. 5.7).

The Late Jurassic-Early Cretaceous Adventdalen Group samples of the Barents Shelf were analysed for petrography. The samples are poorly to moderately well sorted, fine to medium-grained quartz arenites (Fig. 5.5). The samples are dominated by non-undulose monocrystalline quartz (84-98%) with minor undulose monocrystalline quartz (0-2%) and polycrystalline quartz with four or more subgrains (1-10%). The predominance of monocrystalline quartz suggests derivation from a plutonic source. On QtFL and QmFLt plots, the samples plot within the 'craton interior' and 'recycled orogen' fields (Fig. 5.7).

5.5 Heavy mineral results

The Early Cretaceous Glitrefjellet Member sample, a litharenite, did not contain sufficient heavy minerals for study, so heavy mineral analysis was carried out on 20 remaining samples (Table 5.1). Figures 5.13-5.14 illustrate the heavy mineral results. The complete dataset is included in the accompanying CD. There are two

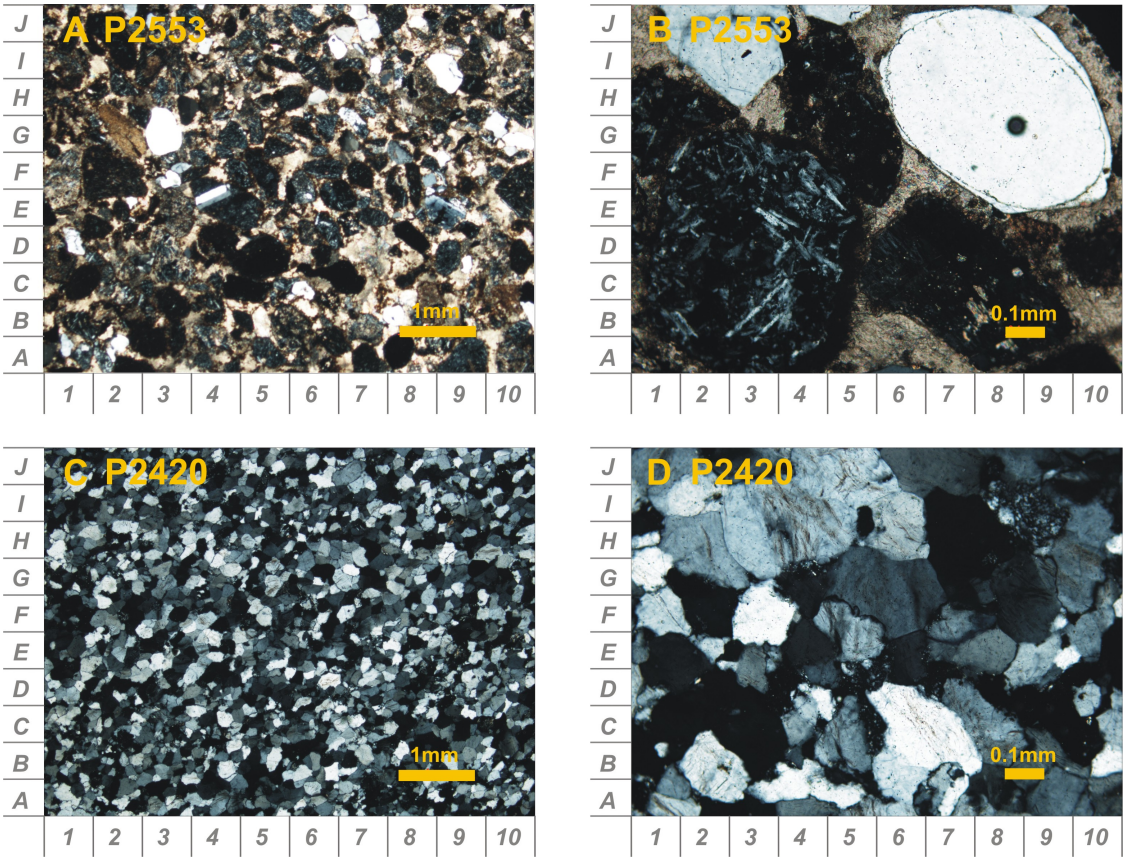

Figure 5.10: Photomicrographs of the Helvetia Formation samples. (A) Glitrefjellet Member. General view of the moderately well sorted, medium-grained litharenite. The sample shows clasts of mainly plagioclase-rich volcanic clasts in a poikolitic carbonate cement. Note large feldspar crystal within volcanic clast (E4). (B) A volcanic fragment on left of image and monocrystalline, non-undulose quartz fragment on the right, showing quartz overgrowth. (C) Festningen Sandstone Member. General view of the moderately well sorted, fine-grained quartz arenite. (D) The grains show a well-compacted or altered nature. Grains show quartz overgrowths (I3). One polycrystalline quartz grain, with four or more subgrains, is shown (H9).

main heavy mineral assemblages present in these samples: apatite- and zircon-dominated assemblages (Fig. 5.13).

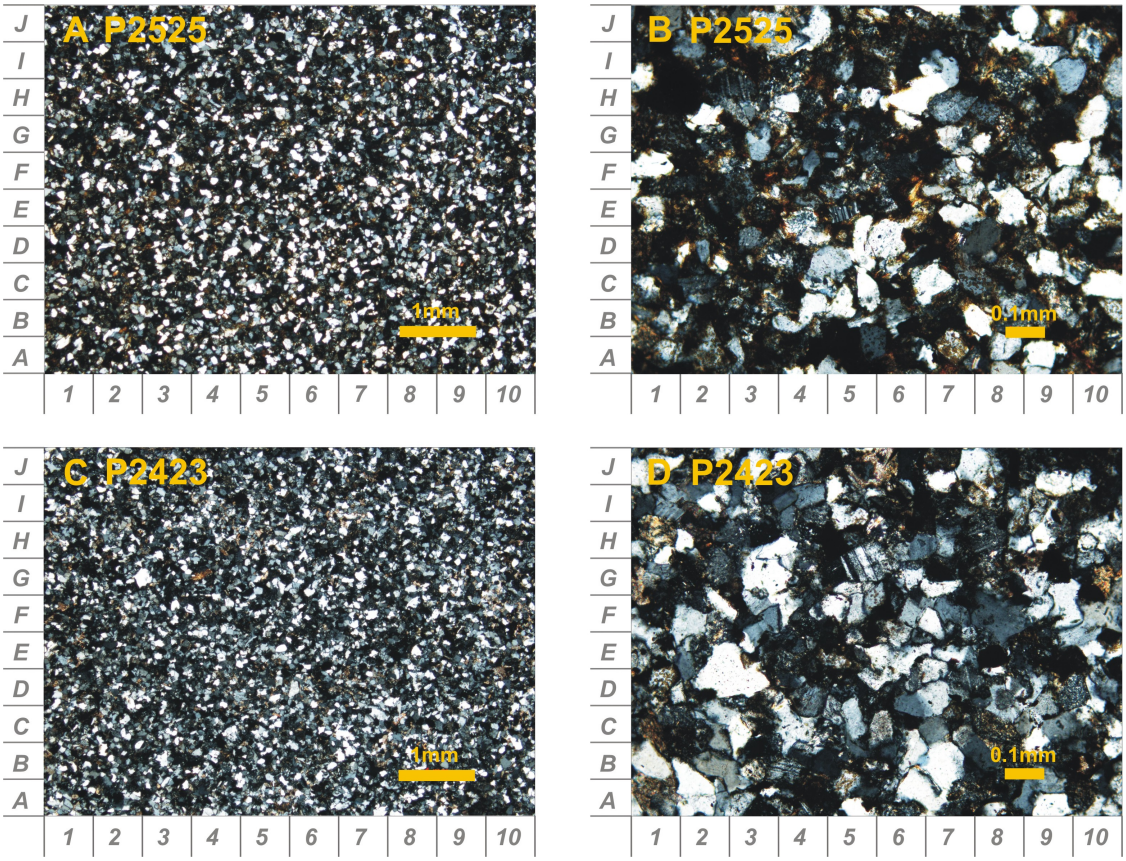

Figure 5.11: Photomicrographs of the Caroline Formation samples. (A) Langstakken Member. General view of the moderately well sorted, very fine-grained subarkose. (B) Plagioclase grains (E5 and H3) and angular nature of grains shows the immature nature of the sediment. (C) Dalkjegla Member. General view of the moderately well sorted, subarkosic siltstone. (D) The image shows the angular nature of the grains

Heavy mineral species

The Early to Late Triassic Barents Shelf Sassendalen Group and Storfjorden Subgroup samples (JO NPD 5, 6, 3, 4) show unstable heavy mineral assemblages containing chloritoid (23-39%), apatite (16-41%), zircon (12-21%), garnet (1-20%), epidote (0-25%) and lesser tourmaline (1-6%), rutile (1-5 %), chrome spinel (1-3%), sphene (0-2%) and amphibole (0-1%) (Fig. 5.13). The samples show euhedral apatite grains, evidence of a proximal sediment source. The dominance of apatite and presence of chrome spinel suggests that a component of the source is of mafic-ultramafic igneous origin. The presence of chloritoid and epidote suggests that

a significant component of the source comprises medium-grade metamorphosed metapelite. The zircon grains in these samples are mostly euhedral. This assemblage is classified as sand type 1.

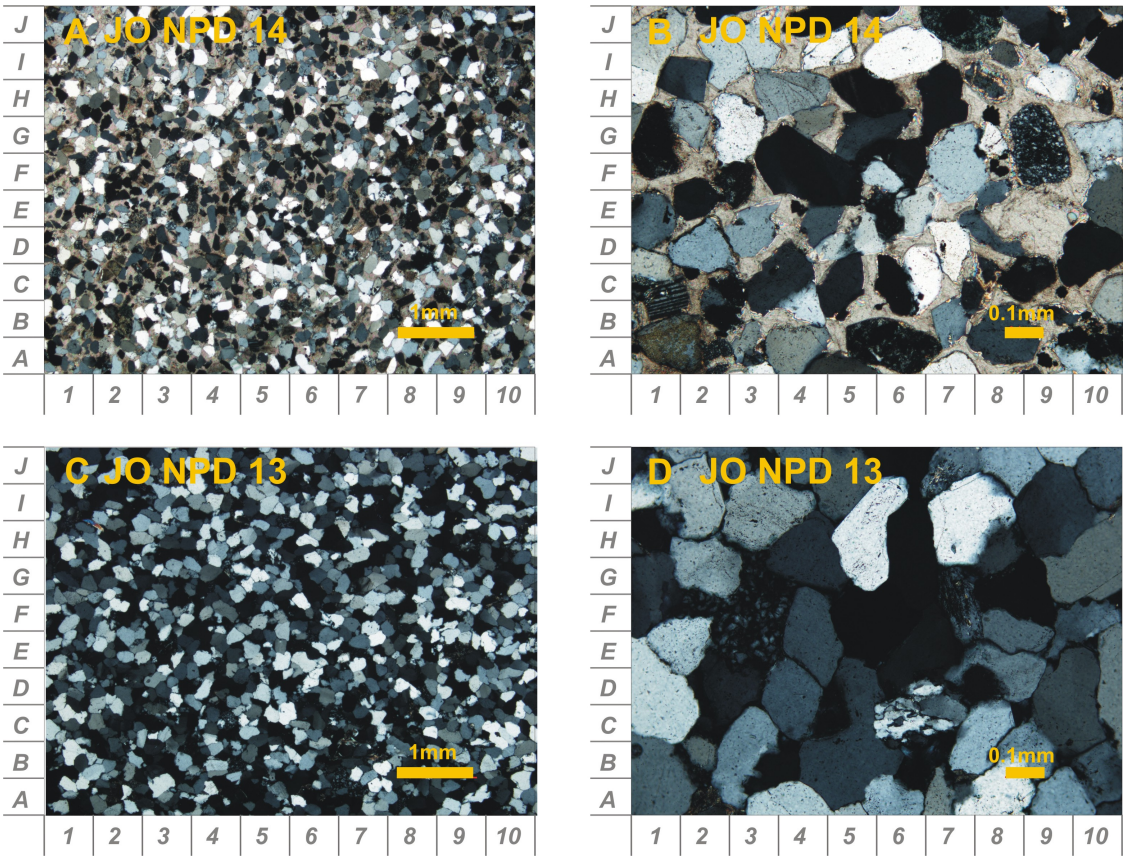

Figure 5.12: Photomicrographs of the Barents Shelf Adventdalen Group samples. (A) Kolmule Formation. General view of the moderately well sorted, fine-grained quartz arenite. (B) Grains are surrounded by a poikolitic calcite cement. Plagioclase (B1), alkali feldspar (A1) and polycrystalline (G9) grains are visible. (C) Fuglen Fm. General view of the moderately well sorted, fine-grained quartz arenite. (D) The sediment is dominated by monocrystalline quartz. Some polycrystalline quartz is visible (D6). Quartz overgrowths are common (I2).

The Late Triassic De Geerdalen Formation sample (P2241) is also classified as sand type 1. It shows an unstable heavy mineral assemblage dominated by apatite (62%) and chloritoid (30%), with lesser tourmaline (3%), zircon (3%), rutile (1%) and garnet (1%) and trace chrome spinel (Fig. 5.13).

There is a major change in heavy mineral assemblage above the Storfjorden Subgroup. The Late Triassic-Early Jurassic Fruholmen and Tubåen Formation samples (JO NPD 8, 7) show an ultrastable heavy mineral assemblage, dominated

by zircon (57-78%), with lesser rutile (17-22%), tourmaline (5-10%), garnet (1-11%) and sphene (1%). This assemblage is classified as sand type 3. The Nordmela Formation samples (JO NPD 1, 2) have a similar heavy mineral assemblage but are dominated by garnet (49-72%), in addition to zircon (10-18%), tourmaline (3-25%), rutile (7-14%) and sphene (1%). Most zircon grains in these samples show a rounded morphology. This assemblage is also classified as sand type 3 as garnet cannot be used as a provenance-diagnostic mineral in these samples due to likely garnet dissolution during burial.

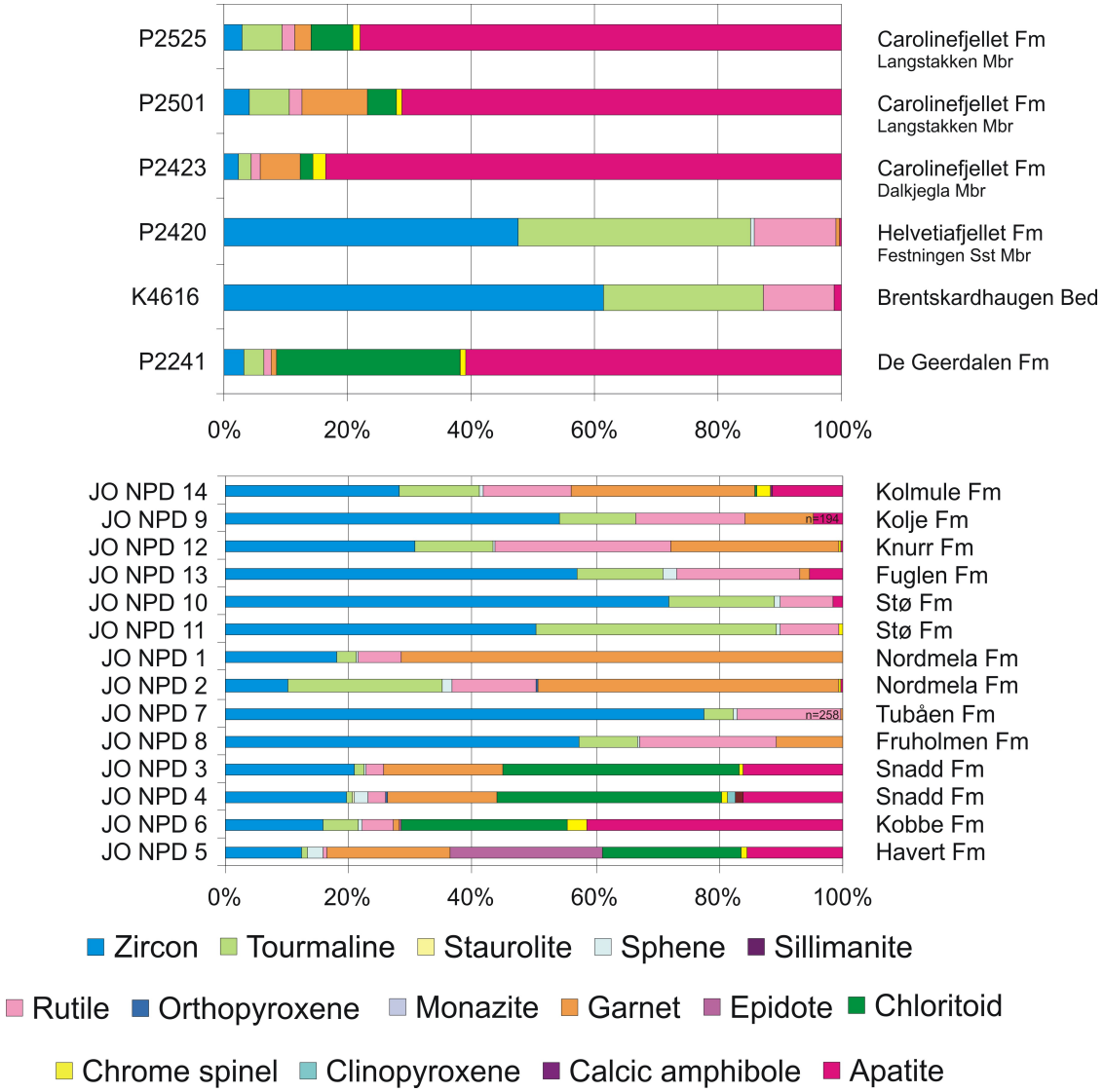

Figure 5.13: Svalbard and Barents Shelf heavy mineral assemblages, showing the relative importance of detrital heavy mineral species. The data are based on counts of minimum 300 heavy minerals unless otherwise stated.

The shift from sand type 1 to sand type 3 is also seen in the Svalbard samples.

The Middle Jurassic Brentskardhaugen Bed and Early Cretaceous Helvetiafjellet Formation samples (K4616 and P2420) show ultrastable heavy mineral assemblages dominated by zircon (48-61%), with significant tourmaline (26-38%) and rutile (12-14%) and minor apatite (1%) (Fig. 5.13). The samples show mostly rounded zircon grains, evidence of a recycled, far-traveled source for the sediment. The tourmaline grains are a mixture of rounded and euhedral grains. This assemblage is classified as sand type 3.

The remaining Barents Shelf samples (Early Jurassic-Early Cretaceous Stø, Knurr, Kolje and Kolmule formations, JO NPD 10, 11, 13, 12, 9, 14) show heavy mineral assemblages consistent with sand type 3 (Fig. 5.13). However, the presence of apatite (0-5%), chrome spinel (0-2%) and chloritoid (0-1%), increasing with stratigraphic height, suggests that there is some addition of sand type 1.

The Early Cretaceous Carolinefjellet Formation samples (P2423, P2501 and P2525) show heavy mineral assemblages dominated by apatite (62-84%), with lesser chloritoid (2-30%), garnet (1-11%), tourmaline (2-7%), zircon (2-4%) and rutile (1-2%) (Fig. 5.13), consistent with sand type 1. All samples show euhedral apatite grains, evidence of a proximal source of the sediment. The Carolinefjellet Formation sample shows unetched garnets; the other samples show etched garnets. The dominance of apatite and presence of chrome spinel suggests that a component of the source is of mafic-ultramafic igneous origin. The presence of chloritoid suggests that a component of the source is a medium grade metamorphosed metapelites.

Heavy mineral ratios

Ratios of stable heavy mineral species of similar specific gravity may be used to distinguish different provenance groups, as outlined in Chapter 3. The heavy mineral indices are calculated as: GZi=(garnet/(garnet+zircon))×100 (Fig. 5.14).

The Svalbard samples show clear variations in GZi, CZi and ATi and two sand types may be distinguished. RuZi does not show clear trends. Late Triassic De Geerdalen Formation sample P2241 and Early Cretaceous Carolinefjellet Formation samples P2423, P2501 and P2525 show moderate to high GZi, high CZi and high ATi (sand type 1). The Middle Jurassic Brentskardhaugen Bed sample K4616 and Early Cretaceous Helvetiafjellet Formation, Festningen Sandstone Member sample P2420 show zero GZi and CZi and low ATi (sand type 3).

The Barents Shelf samples do not show clear trends in heavy mineral ratios although there are some similarities with the Svalbard samples. GZi shows no clear trend, possibly due to garnet dissolution during burial. Several samples show garnet grains with etched surfaces, evidence of garnet dissolution. CZi values are highest

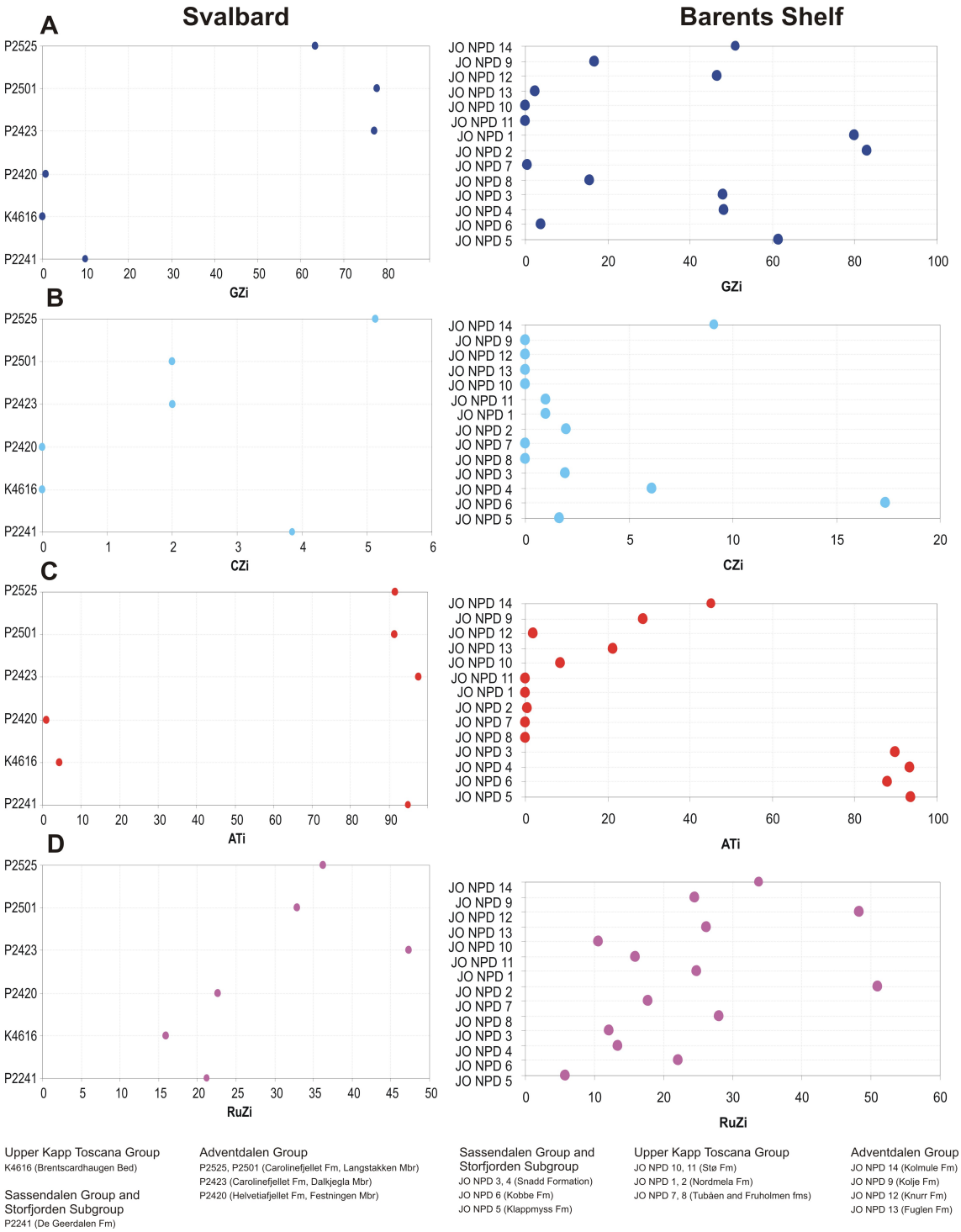

Figure 5.14: Svalbard and Barents Shelf heavy mineral ratios. Indices are calculated as: GZi=(garnet/(garnet+zircon))×100. (A) GZi (garnet-zircon index), showing clear variation in Svalbard samples but no clear trend in the Barents Shelf samples. (B) CZi (chrome spinel-zircon index), showing clear variation in the Svalbard samples and some variation in the Barents Shelf samples. (C) ATi (apatite-tourmaline index), showing clear variation in the Svalbard and Barents Shelf samples. (D) RuZi (rutile-zircon index), showing wide variability, but with overall increasing trend.

in the Triassic Sassendalen Group, Storfjorden Subgroup and Early Cretaceous Kolmule Formation samples (JO NPD 5, 6, 3, 4, 14). CZi values are zero in the Late Triassic-Early Jurassic Fruholmen and Tubåen Formation samples (JO NPD 7, 8) and in the Middle Jurassic-Early Cretaceous Fuglen, Knurr and Kolje Formation samples (JO NPD 10, 13, 12, 9). CZi values are low in the Early Jurassic Stø and Nordmela Formation samples (JO NPD 11, 1, 2). ATi shows clear variation within the Barents Shelf sample set, with high values in the Sassendalen and Storfjorden Subgroup samples (sand type 1), zero in the Fruholmen to Stø Formation samples (sand type 3) and increasing in the Stø Formation through Kolmule Formation samples, possibly indicating a mixing of sand types 1 and 3.

5.6 Garnet chemistry results

A subset of eight samples were analysed for garnet chemistry (Table 5.1). The data are presented in Figure 5.15. The complete dataset is included in the accompanying CD. Seven of eight samples were collected from southwestern Barents Shelf wells and it is possible that the samples have been affected by burial dissolution of garnet (Morton *et al.*, 2004). Several samples show garnet grains with an etched morphology: evidence of garnet dissolution.

The Early to Late Triassic Snadd Formation and Havert Formation samples plot mainly in fields Bi and Bii, with some grains plotting in Ci. Garnets of the overlying Late Triassic Fruholmen Formation and Early Jurassic Nordmela Formation (sample JO NPD 2 only) also plot in these fields (Fig. 5.15). The Adventdalen Group samples (Carolinefjellet Formation, Kolmule Formation and Knurr Formation) and Early Jurassic Nordmela Formation sample JO NPD 1 show more restricted garnet chemistry, plotting mainly in fields A and Bi.

It is unclear whether the differences seen in the samples are due to a difference in provenance or garnet dissolution in some or all of the samples. Garnet dissolution would result in a preferential reduction in Ca-rich garnet grains, which may account for some grains plotting in fields Bii and Ci and other not plotting in these fields. However, it is noted that the garnets with more restricted chemistries occur in the younger four samples in the sample set (Fig. 5.15).

Type B garnets are sourced from amphibolite facies metasedimentary rocks and gneisses (Bi and Bii) or intermediate-acidic igneous rocks (Bi, associated with high-Mn chemistries) (Morton *et al.*, 2004). Type A garnets are sourced from high-grade granulite facies metasedimentary rocks and charnokites or from intermediate-acidic

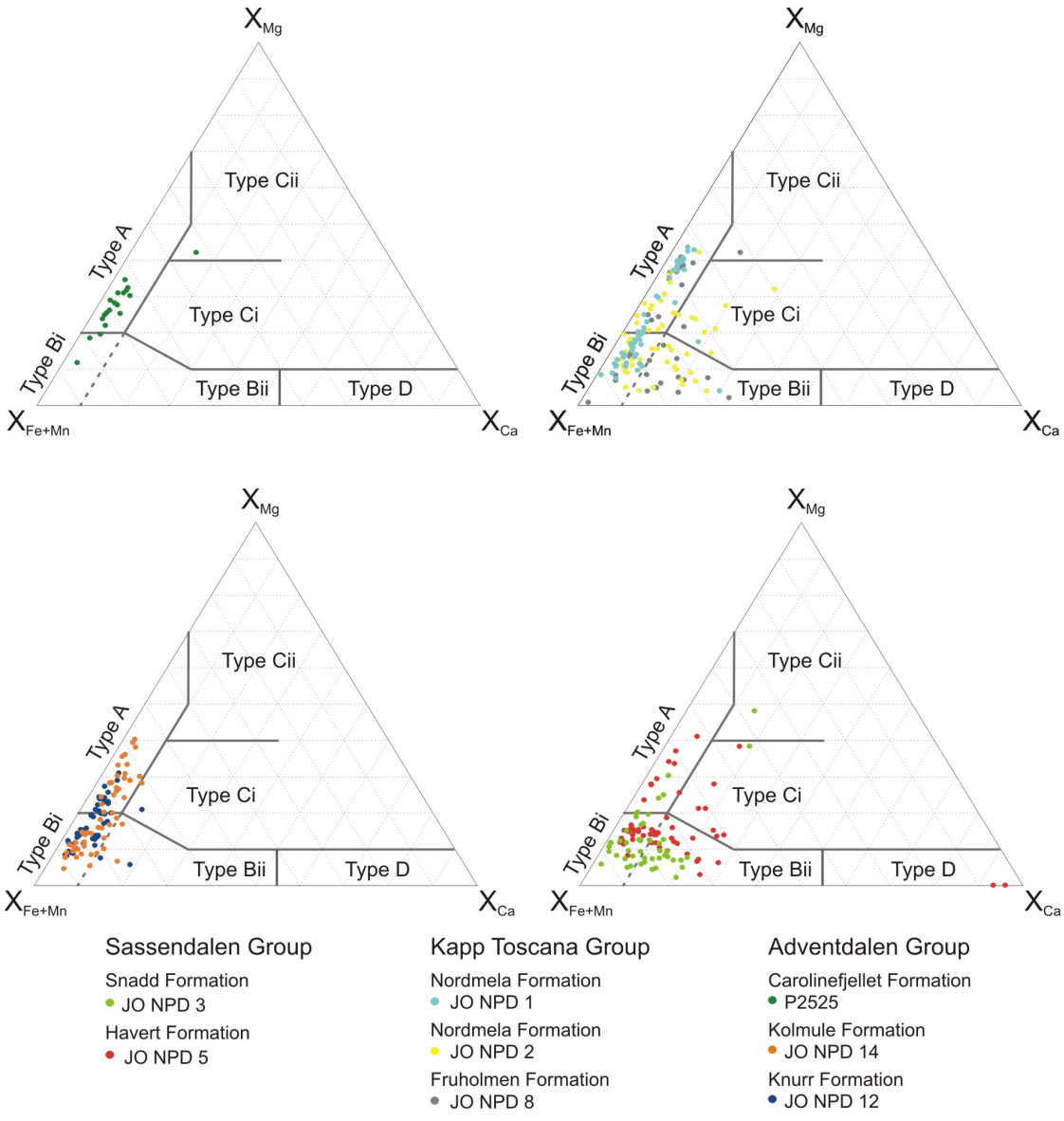

Figure 5.15: Garnet compositions of Svalbard and Barents Shelf samples, shown on the garnet classification diagram of Morton *et al.* (2004). X_{Mg}, X_{Fe}, X_{Mn}, X_{Ca} = molecular proportions of Mg, Fe, Mn and Ca, with all Fe calculated as Fe^{2+}.

igneous rocks from deep crustal magmas. Type Ci garnets are sourced from high-grade mafic gneisses. The data suggest that the Svalbard and southwestern Barents Shelf samples are sourced from a mixture of medium-grade metamorphic rocks and intermediate-acidic igneous rocks.

5.7 Tourmaline chemistry results

A subset of 17 samples were analysed for tourmaline chemistry (Table 5.1). The data are presented in Figures 5.16-5.20. The complete dataset is included in the accompanying CD. The tourmaline chemistry data show no clear variations with stratigraphic age, although two main tourmaline chemistry populations are visible in the data (Figs. 5.16-5.20). The significance of these populations for the provenance of the Barents Shelf region is presently unclear.

The Triassic Sassendalen Group and Storfjorden Subgroup samples of the Barents Shelf (Havert, Kobbe and Snadd formations), the Early Jurassic Realgrunnen Subgroup samples (Tubåen and Nordmela formations) and the Early Cretaceous Adventdalen Group samples of the Barents Shelf (Knurr and Kolje formations) show similar tourmaline chemistry. On a Ca-Fe-Mg diagram, the samples plot almost exclusively in field 4, reflecting a source of Ca-poor metapelites, metapsammites and quartz tourmaline rocks (Henry & Guidotti, 1985). On an Al-$Al_{50}Fe_{50}$-$Al_{50}Mg_{50}$ diagram the samples plot mainly in fields D and E, reflecting a source of aluminous (field D) and Al-poor (field E) metapelites and metapsammites (Henry & Guidotti, 1985).

The Late Triassic De Geerdalen Formation, the Late Triassic Fruholmen Formation, the Early to Middle Jurassic Stø Formation and Fuglen formations and the Early Cretaceous Kolmule Formation samples show similar chemistries. On a Ca-Fe-Mg diagram, the samples plot mainly in field 4, reflecting a source of Ca-poor metapelites, metapsammites and quartz tourmaline rocks and also in field 2, reflecting an additional source of Li-poor granitoids, pegmatites and aplites (Henry & Guidotti, 1985). On an Al-$Al_{50}Fe_{50}$-$Al_{50}Mg_{50}$ diagram the samples plot in fields D and E, reflecting a source of aluminous (field D) and Al-poor (field E) metapelites and metapsammites (Henry & Guidotti, 1985) but also in field F, reflecting an additional source of Fe^{3+}-rich quartz-tourmaline rocks, calc-silicates and metapelites.

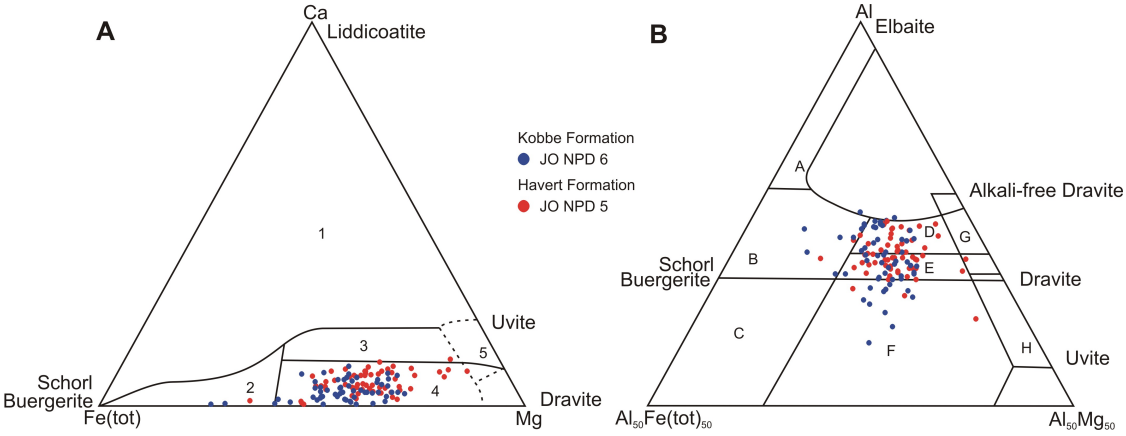

Figure 5.16: Tourmaline compositions of the Sassendalen Group plotted on discrimination diagrams of Henry & Guidotti (1985). (A) Field 2, Li-poor granitoids, pegmatites and aplites. Field 4, Ca-poor metapelites, metapsammites and quartz tourmaline rocks. (B) Field B, Li-poor granitoids, pegmatites and aplites. Field D, Aluminous metapelites and metapsammites. Field E, Al-poor metapelites and metapsammites. Field F, Fe^{3+}-rich quartz-tourmaline rocks, calc-silicates and metapelites.

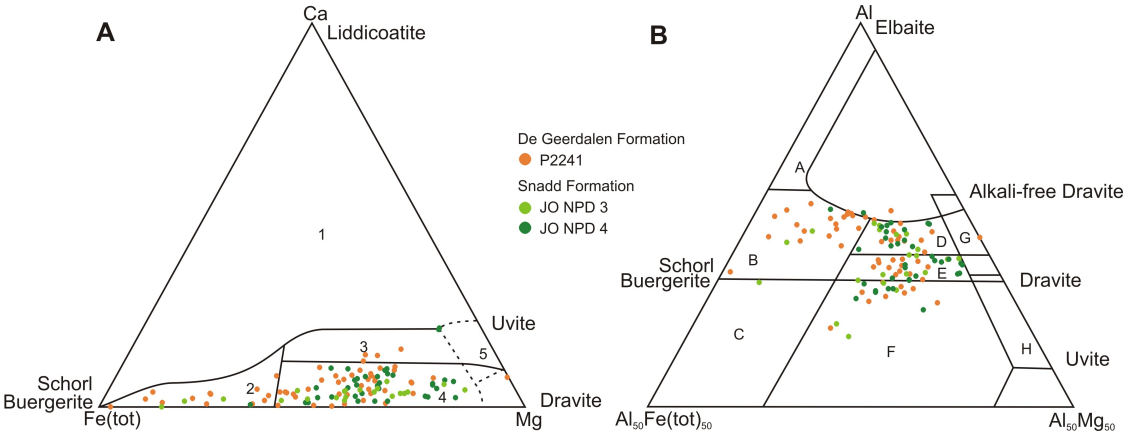

Figure 5.17: Tourmaline compositions of the Storfjorden Subgroup plotted on discrimination diagrams of Henry & Guidotti (1985). (A) Field 2, Li-poor granitoids, pegmatites and aplites. Field 3, Ca-rich metapelites, metapsammites and calcsilicates. Field 4, Ca-poor metapelites, metapsammites and quartz tourmaline rocks. (B) Field B, Li-poor granitoids, pegmatites and aplites. Field D, Aluminous metapelites and metapsammites. Field E, Al-poor metapelites and metapsammites. Field F, Fe^{3+}-rich quartz-tourmaline rocks, calc-silicates and metapelites.

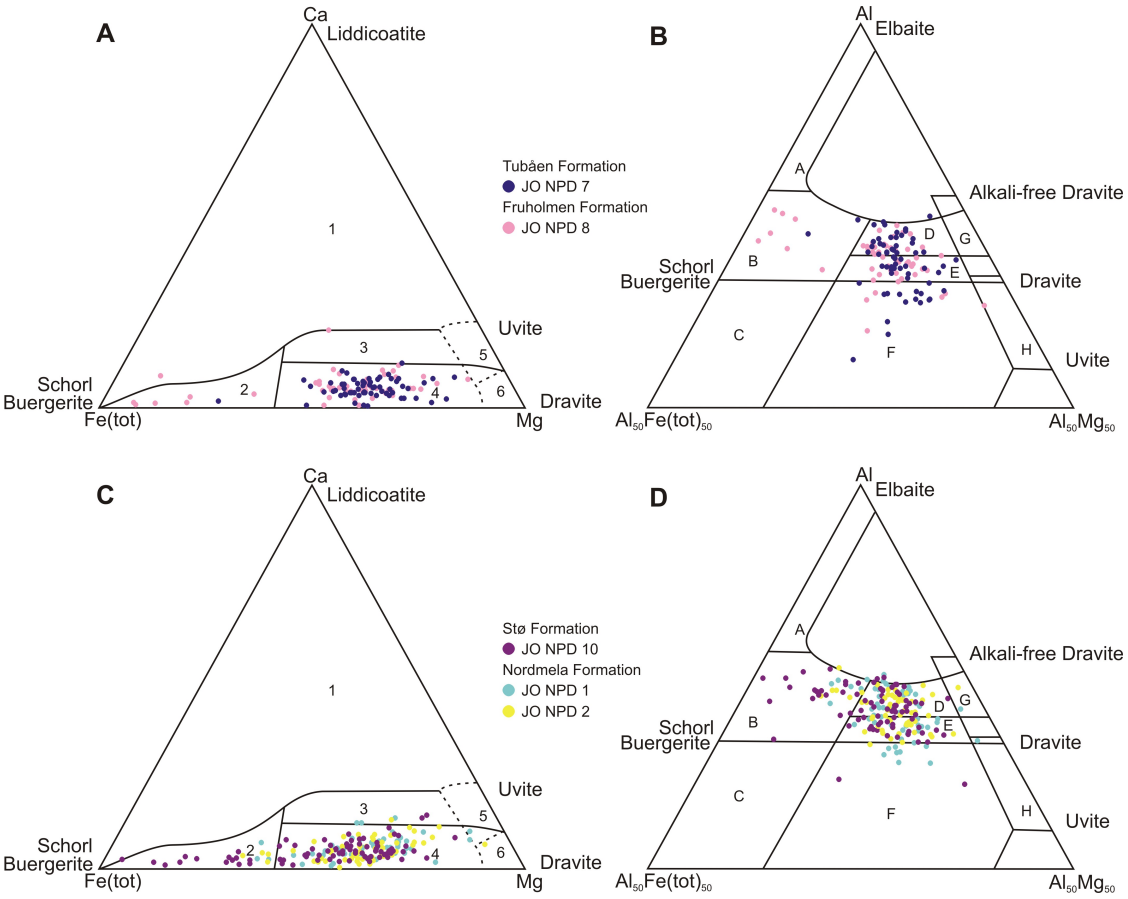

Figure 5.18: Tourmaline compositions of the Realgrunnen Subgroup plotted on discrimination diagrams of Henry & Guidotti (1985). (A) Fruholmen and Tubåen formations. Field 2, Li-poor granitoids, pegmatites and aplites. Field 3, Ca-rich metapelites, metapsammites and calcsilicates. Field 4, Ca-poor metapelites, metapsammites and quartz tourmaline rocks. (B) Field B, Li-poor granitoids, pegmatites and aplites. Field D, Aluminous metapelites and metapsammites. Field E, Al-poor metapelites and metapsammites. Field F, Fe^{3+}-rich quartz-tourmaline rocks, calc-silicates and metapelites. (C) Nordmela and Stø formations. Field 2, Li-poor granitoids, pegmatites and aplites. Field 3, Ca-rich metapelites, metapsammites and calcsilicates. Field 4, Ca-poor metapelites, metapsammites and quartz tourmaline rocks. (D) Field B, Li-poor granitoids, pegmatites and aplites. Field D, Aluminous metapelites and metapsammites. Field E, Al-poor metapelites and metapsammites. Field F, Fe^{3+}-rich quartz-tourmaline rocks, calc-silicates and metapelites.

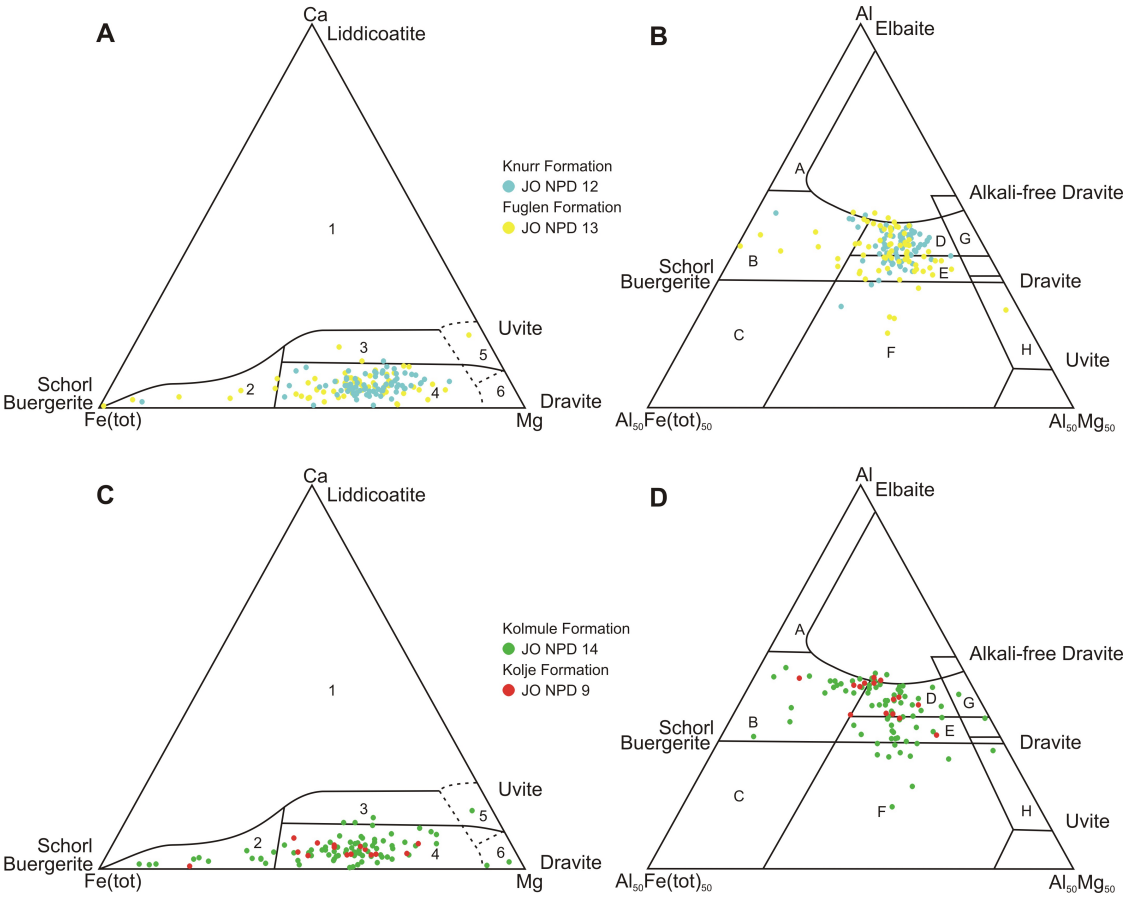

Figure 5.19: Tourmaline compositions of the Barents Shelf Adventdalen Group samples plotted on discrimination diagrams of Henry & Guidotti (1985). (A) Fuglen and Knurr formations. Field 2, Li-poor granitoids, pegmatites and aplites. Field 4, Ca-poor metapelites, metapsammites and quartz tourmaline rocks. (B) Field B, Li-poor granitoids, pegmatites and aplites. Field D, Aluminous metapelites and metapsammites. Field E, Al-poor metapelites and metapsammites. Field F, Fe^{3+}-rich quartz-tourmaline rocks, calc-silicates and metapelites. (C) Kolje and Kolmule formations. Field 2, Li-poor granitoids, pegmatites and aplites. Field 4, Ca-poor metapelites, metapsammites and quartz tourmaline rocks. Field 6, Metapyroxenites. (D) Field B, Li-poor granitoids, pegmatites and aplites. Field D, Aluminous metapelites and metapsammites. Field E, Al-poor metapelites and metapsammites. Field F, Fe^{3+}-rich quartz-tourmaline rocks, calc-silicates and metapelites. Field G, Low-Ca ultramafics.

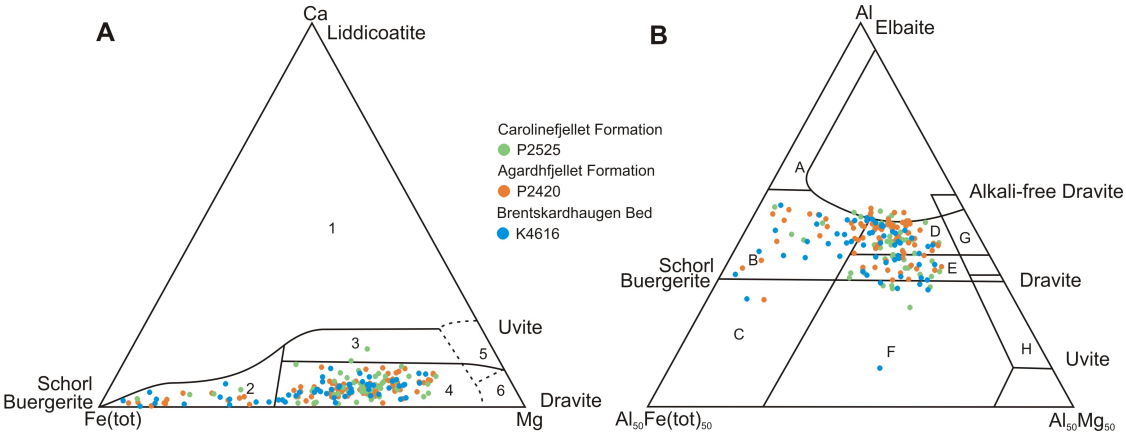

Figure 5.20: Tourmaline compositions of the Svalbard Adventdalen Group and Brentskardhaugen Bed samples plotted on discrimination diagrams of Henry & Guidotti (1985). (A) Field 2, Li-poor granitoids, pegmatites and aplites. Field 4, Ca-poor metapelites, metapsammites and quartz tourmaline rocks. (B) Field B, Li-poor granitoids, pegmatites and aplites. Field D, Aluminous metapelites and metapsammites. Field E, Al-poor metapelites and metapsammites.

5.8 Zircon geochronology results

Detrital zircons from four samples were dated using SIMS (Table 5.1). The data are presented in Figures 5.21-5.27. The complete dataset is included in the accompanying CD. U-Pb ages discussed here are within 10% of concordance unless otherwise stated. $^{206}Pb/^{238}U$ ages are quoted for ages younger than 1200 Ma; $^{207}Pb/^{206}Pb$ ages are quoted for ages older than 1200 Ma.

The Middle-Late Triassic Snadd Formation sample JO NPD 3 is dominated by Paleozoic ages (31 grains) and also contains a spread of 14 Proterozoic grains (Fig. 5.22). Most zircon grains show euhedral, magmatic morphology, suggesting that much of the sediment is first cycle and the source is proximal (Fig. 5.24). The sample contains one isolated Permo-Triassic boundary grain (250 Ma) and one isolated early Permian grain (275 Ma). The sample is dominated by a spread of late Silurian to mid Carboniferous age (19 grains, 419-300 Ma, forming major peaks at 419, 365, 339 and 300 Ma) (Fig. 5.23). The sample contains eight isolated mid Neoproterozoic through Ordovician ages (674-474 Ma), with one peak at 520 Ma. A spread of 11 Neoarchean to early Neoproterozoic grains is seen, with no robust peaks.

The Late Triassic Fruholmen Formation sample JO NPD 8 is dominated by a spread of Paleoproterozoic to Mesoproterozoic ages (53 grains), with a prominent Late Paleoproterozoic peak at 1630 Ma. The sample also contains some late Meso-

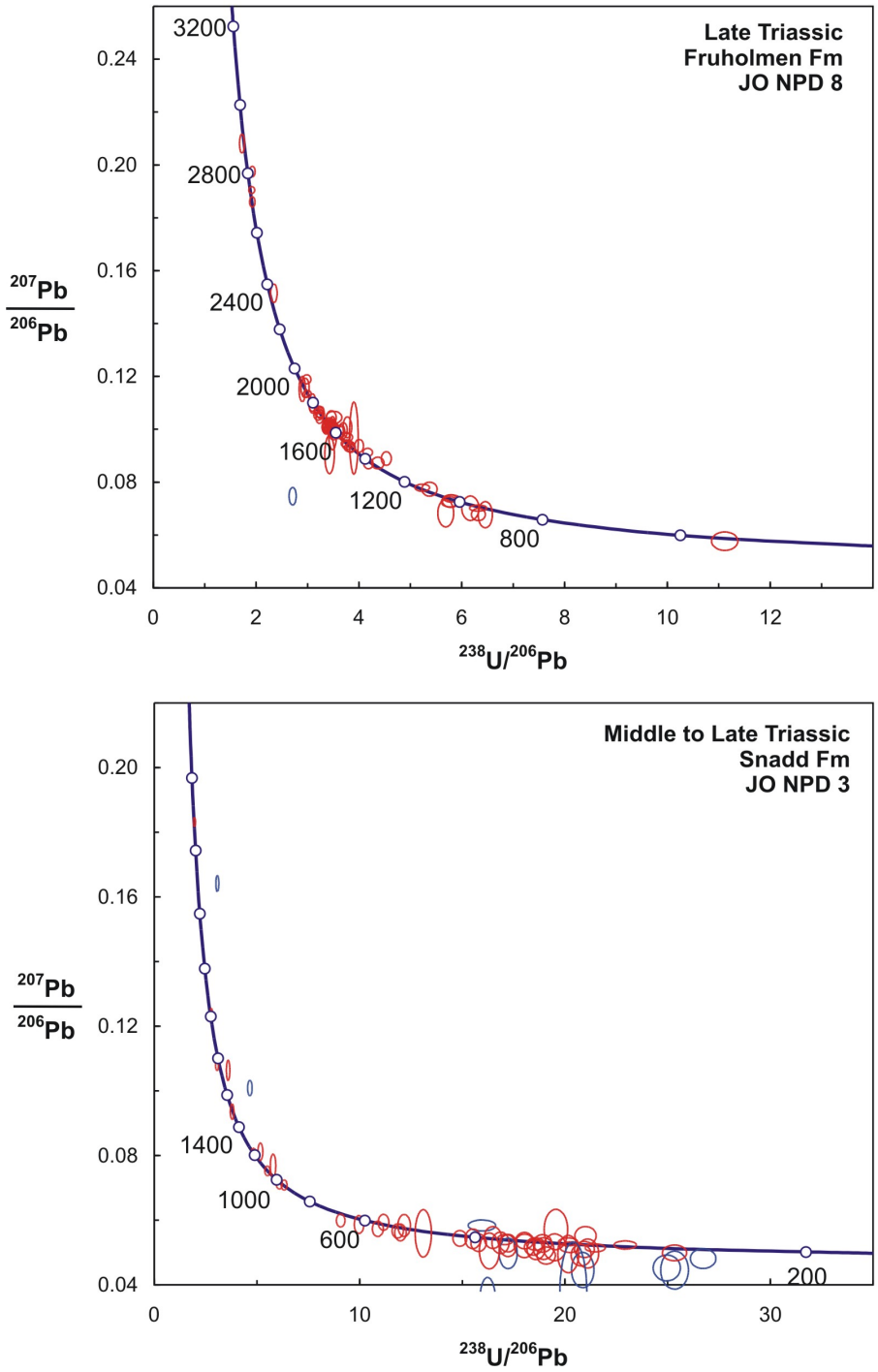

Figure 5.21: Tera-Wasserberg concordia diagram for Barents Shelf samples. The data have been common lead corrected. Data point ellipses are 2σ.

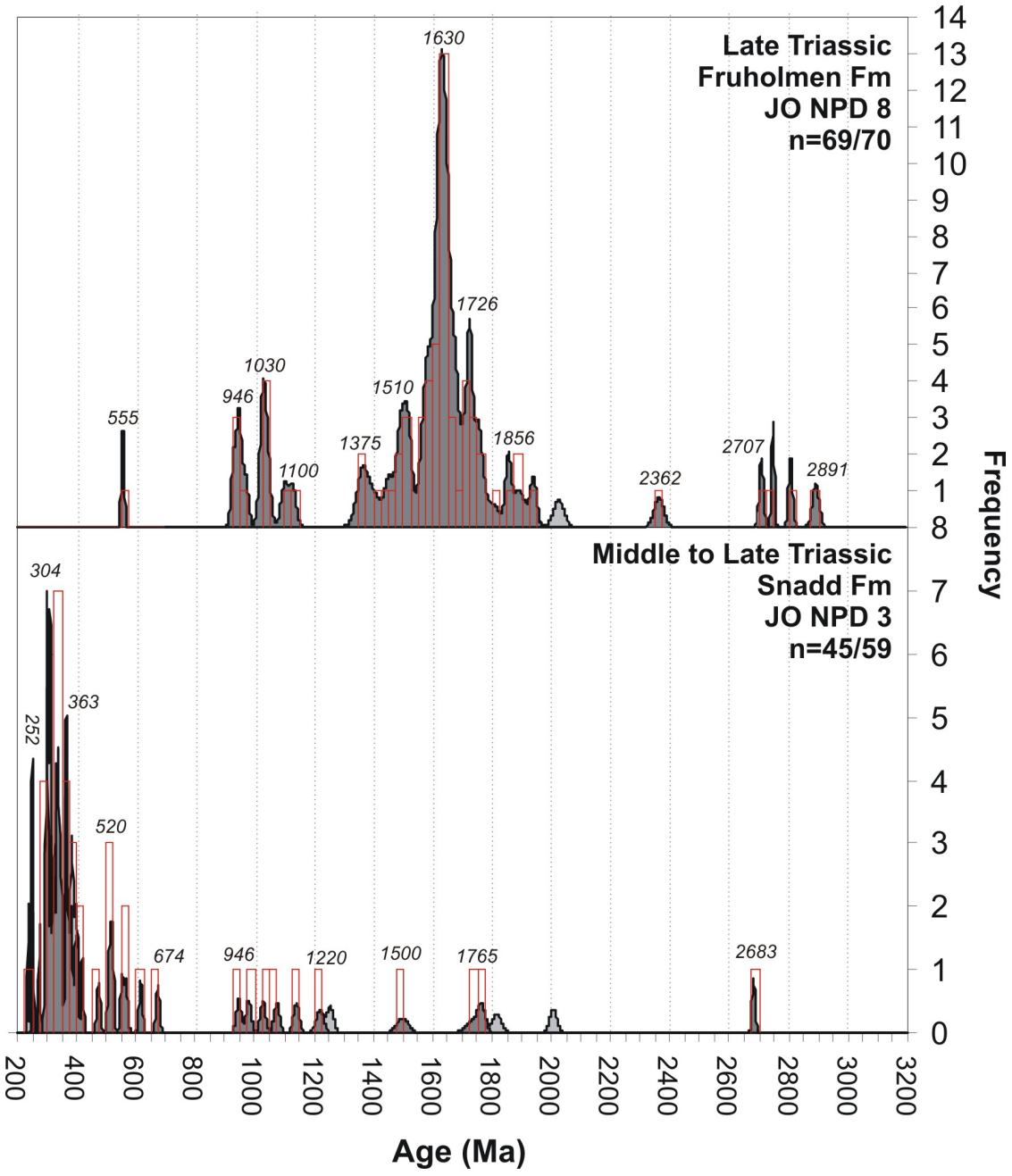

Figure 5.22: Cumulative frequency diagrams, with histograms, of U-Pb detrital zircon ages from the Barents Shelf. U-Pb age, with 1σ uncertainty, is shown. Ages younger than 1200 Ma are $^{206}Pb/^{238}U$ ages. Ages older than 1200 Ma are $^{207}Pb/^{206}Pb$ ages. Ages with 90-110% concordancy are shown by histograms and dark grey cumulative frequency curves. More discordant data are shown by pale grey cumulative frequency curves. N denotes the number of analyses with 90-110% concordancy relative to all analyses.

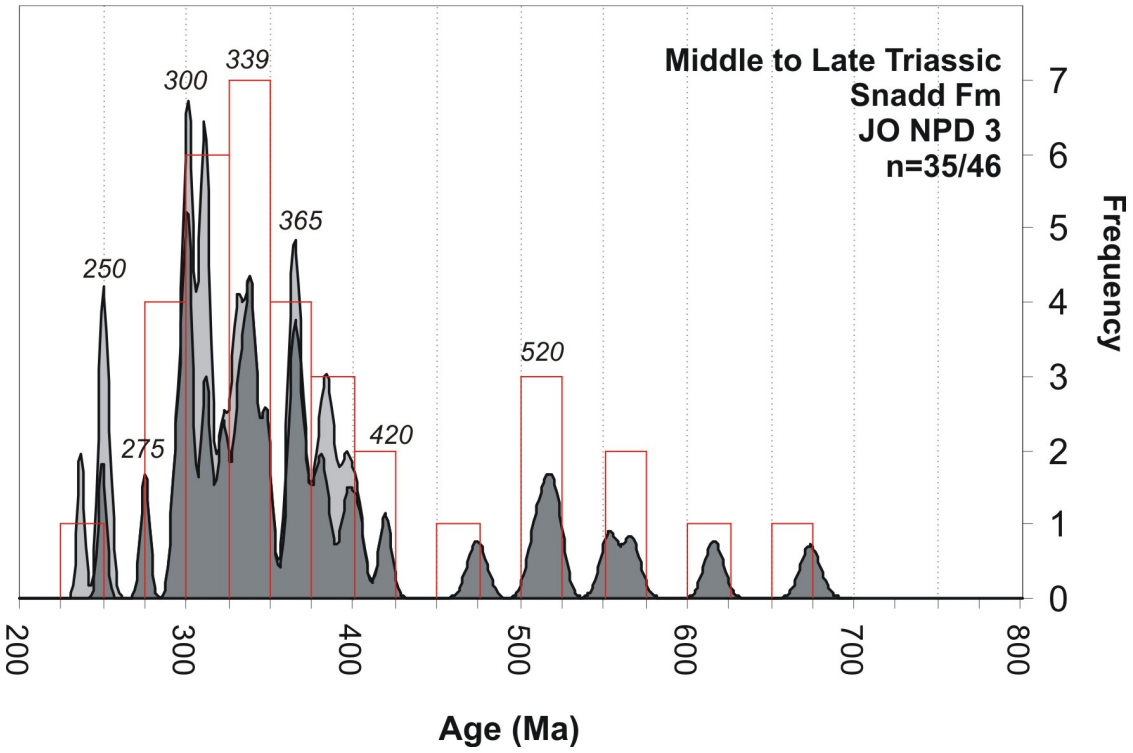

Figure 5.23: Phanerozoic-Neoproterozoic cumulative frequency diagrams, with histograms, of U-Pb detrital zircon ages from the Barents Shelf. U-Pb age, with 1σ uncertainty, is shown. Ages are $^{206}Pb/^{238}U$ ages. Ages with 90-110% concordancy are shown by histograms and dark grey cumulative frequency curves. More discordant data are shown by pale grey cumulative frequency curves. N denotes the number of analyses with 90-110% concordancy relative to all analyses.

proterozoic to late Neoproterozoic ages and some Archean ages (Fig. 5.22). Most grains show rounded morphology, indicative of a recycled sediment source (Fig. 5.24). The sample contains one isolated latest Neoproterozoic age grain (555 Ma). A cluster 10 grains of late Mesoproterozoic to early Neoproterozoic ages form three peaks at 1100, 1030 and 946 Ma. A total of 53 grains define a spread of mid Paleoproterozoic to mid Mesoproterozoic ages. A mid Mesoproterozoic peak, centred at 1375 Ma is composed of two grains. An early Mesoproterozoic peak is visible (8 grains, 1520-1403 Ma, centred at 1510 Ma). The dominant late Paleoproterozoic to early Mesoproterozoic age peak is composed of 29 grains, 1679-1561 Ma, centred at 1630 Ma. A smaller peak, (nine grains, 1765-1702 Ma, centred at 1726 Ma) is also seen. Five mid Paleoproterozoic ages, 1940-1801 Ma, are present. The sample contains five isolated Mesoarchean to early Paleoproterozoic grains, 2891-2362 Ma.

The Middle Jurassic Brentskardhaugen Bed sample K4616 is dominated by a wide spread of Paleoproterozoic to Mesoproterozoic ages (47 grains) and also con-

tains six Paleozoic to early Neoproterozoic grains and four Archean grains (Fig. 5.26). The grains show largely rounded morphology, suggesting that much of the sediment is recycled (Fig. 5.27). The sample contains six isolated Paleozoic-Neoproterozoic ages: one early Permian grain (273 Ma), two early Silurian grains (433 Ma), one late Neoproterozoic grain (582 Ma) and two early Neoproterozoic ages (941 and 976 Ma). The dominant population in the sample is a latest Mesoproterozoic peak, composed of 13 grains ranging in age from 1101 to 1005 Ma, with peaks at 1010 and 1070 Ma. There is mid Mesoproterozoic peak, composed of nine grains ranging in age from 1369 Ma to 1244 Ma, with peaks at 1256, 1325 and 1363 Ma. A latest Paleoproterozoic-early Mesoproterozoic peak is present, composed of nine grains ranging in age from 1649 to 1544 Ma, with peaks at 1550 and 1623 Ma. A mid to late Paleoproterozoic peak is present, composed of 12 grains ranging in age from 1869 to 1701 Ma, with peaks at 1745, 1790 and 1865 Ma. There are three mid Paleoproterozoic grains at 2031, 1993 and 1941 Ma. The sample contains one Neoarchean peak, composed of three grains ranging in age from 2789 to 2756 Ma, with a peak at 2788 Ma. There is one Mesoarchean grain (3095 Ma).

The Early Cretaceous Helvetiafjellet Formation sample P2420 shows a very similar zircon age spectrum to sample K4616. The zircon spectrum for sample P2420 is dominated by a wide spread of earliest Neoproterozoic to Paleoproterozoic ages (59 grains) and contains two Silurian grains, one mid Neoproterozoic grain and five Archean grains (Fig. 5.26). The grains show largely rounded morphology, indicative that much of the sediment is recycled (Fig. 5.27). The sample shows two early Silurian grains (435 Ma) and one mid Neoproterozoic peak at 663 Ma. The earliest Neoproterozoic to Paleoproterozoic spread of ages can be roughly subdivided. A late Mesoproterozoic to earliest Neoproterozoic peak is present, composed of 22 grains ranging in age from 1187 to 973 Ma, with peaks at 1170, 1093, 1037 and 981 Ma. A mid Mesoproterozoic peak, composed of three grains, is centred at 1240 Ma. An early Mesoproterozoic spread of ages is present, composed of 12 grains, ranging in age from 1503 to 1335, with peaks at 1499, 1429 and 1345 Ma. A mid Paleoproterozoic to earliest Mesoproterozoic spread of 19 grains, ranging in age from 1898 to 1592, show robust peaks at 1898, 1772 and 1646 Ma. The sample contains three mid Paleoproterozoic grains at 2006, 1973 and 1957 Ma. A Neoarchean peak is visible, containing four grains, ranging in age from 2748 to 2651 Ma, with a peak at 2745 Ma. A single Mesoarchean grain is present, at 2984 Ma.

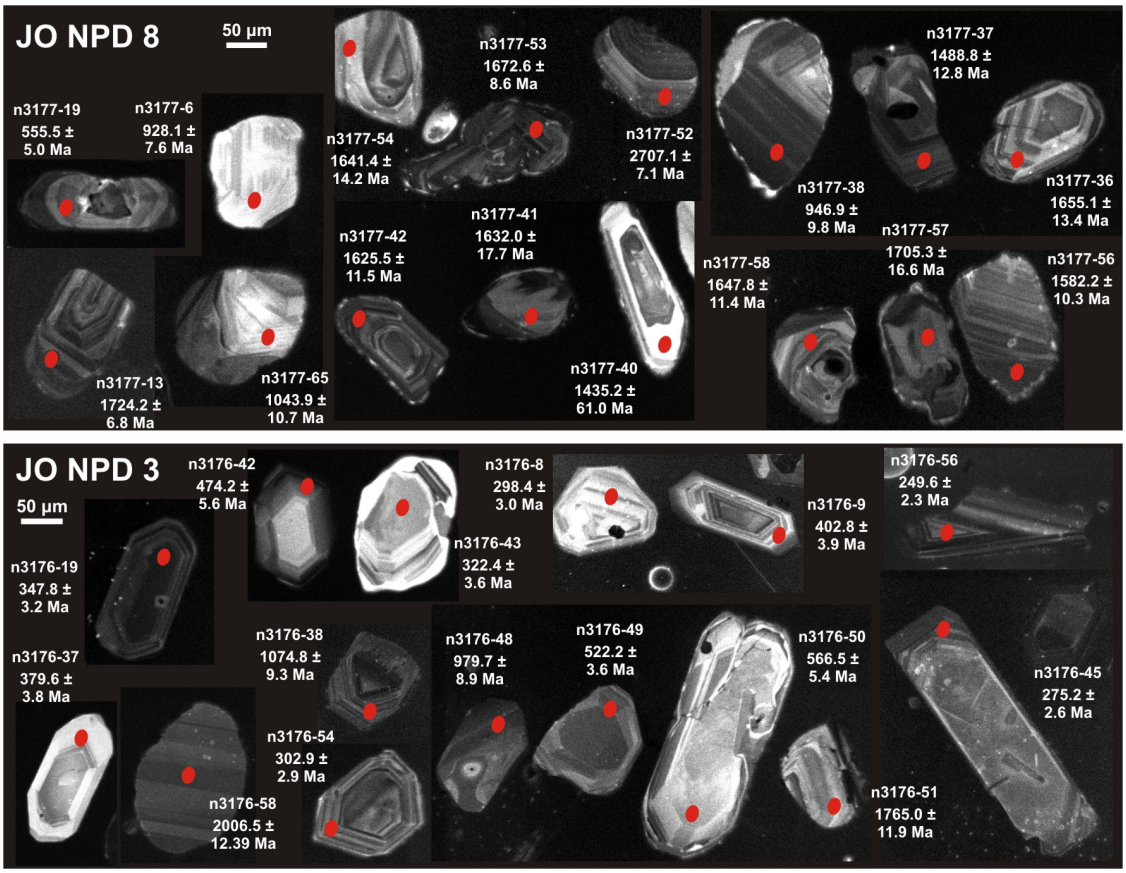

Figure 5.24: Cathodoluminescence images of Barents Shelf samples showing morphology and internal structure of representative zircon grains. U-Pb age, with 1σ uncertainty, is shown for each analysis. Ages younger than 1200 Ma are $^{206}Pb/^{238}U$ ages. Ages older than 1200 Ma are $^{207}Pb/^{206}Pb$ ages. Analytical spots are indicated by ellipses.

5.9 Summary of results

The Early-Middle Triassic Sassendalen Group, Middle-Late Triassic Storfjorden Subgroup and Early Cretaceous Carolinefjellet Formation samples are classified as sand type 1. The samples have a subarkosic composition and plot in the 'recycled orogen' and 'craton interior' fields on QtFL and QmFLt diagrams. The heavy mineral assemblages of the samples are dominated by apatite and chloritoid, with trace amounts of chrome spinel, evidence of mafic to ultramafic material in the source (apatite and chrome spinel) and of a medium-grade metamorphic component (chloritoid and epidote). Many heavy mineral grains are euhedral, evidence of a proximal source. The Late Triassic Snadd Formation sample (JO NPD 3) is dominated by Devonian-Permian age zircon grains.

The Late Triassic to Middle Jurassic Fruholmen Formation, Tubåen Formation

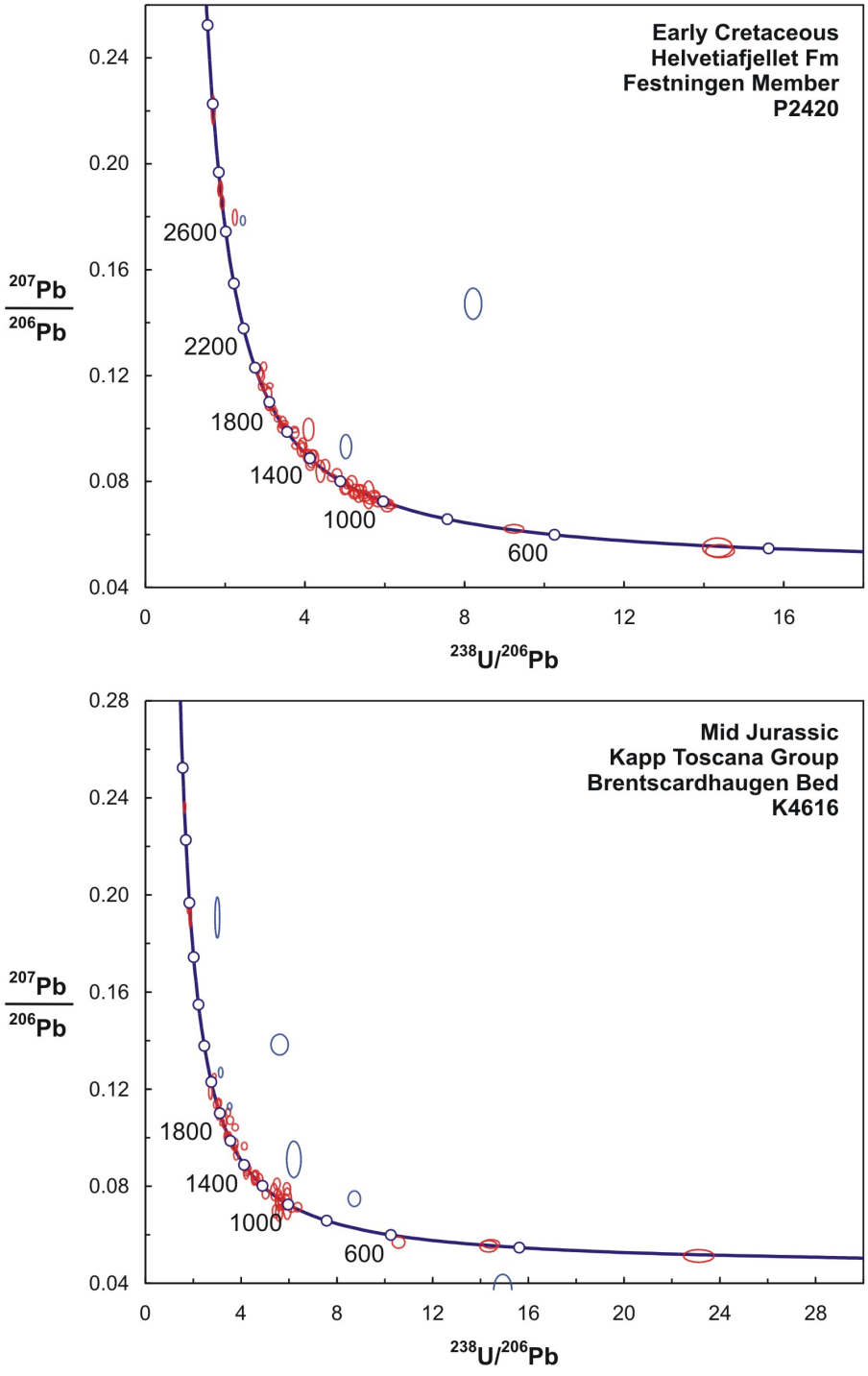

Figure 5.25: Tera-Wasserberg concordia diagram for Svalbard samples. The data have been common lead corrected. Data point ellipses are 2σ.

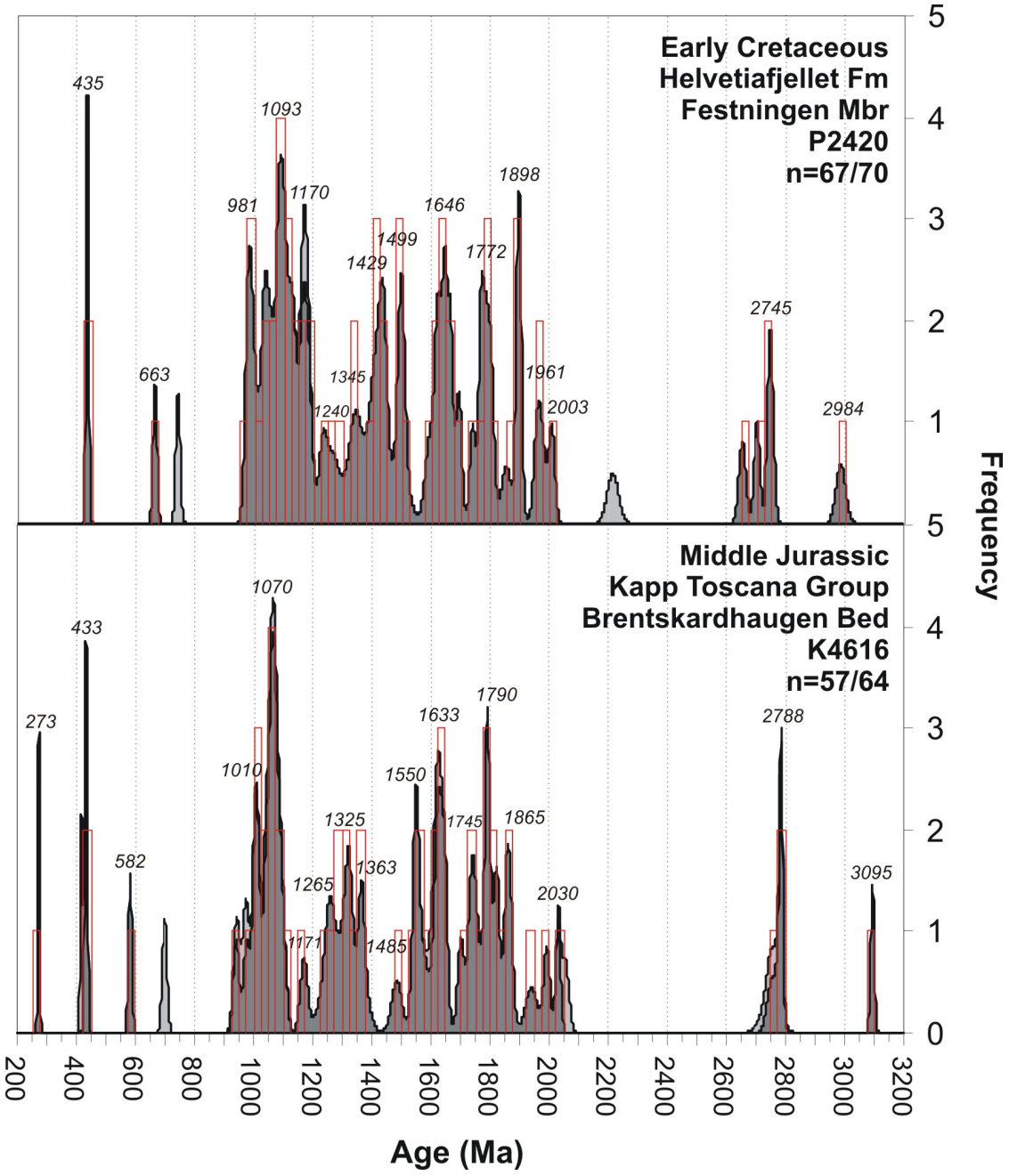

Figure 5.26: Cumulative frequency diagrams, with histograms, of U-Pb detrital zircon ages from Svalbard. U-Pb age, with 1σ uncertainty, is shown. Ages younger than 1200 Ma are $^{206}Pb/^{238}U$ ages. Ages older than 1200 Ma are $^{207}Pb/^{206}Pb$ ages. Ages with 90-110% concordancy are shown by histograms and dark grey cumulative frequency curves. More discordant data are shown by pale grey cumulative frequency curves. N denotes the number of analyses with 90-110% concordancy relative to all analyses.

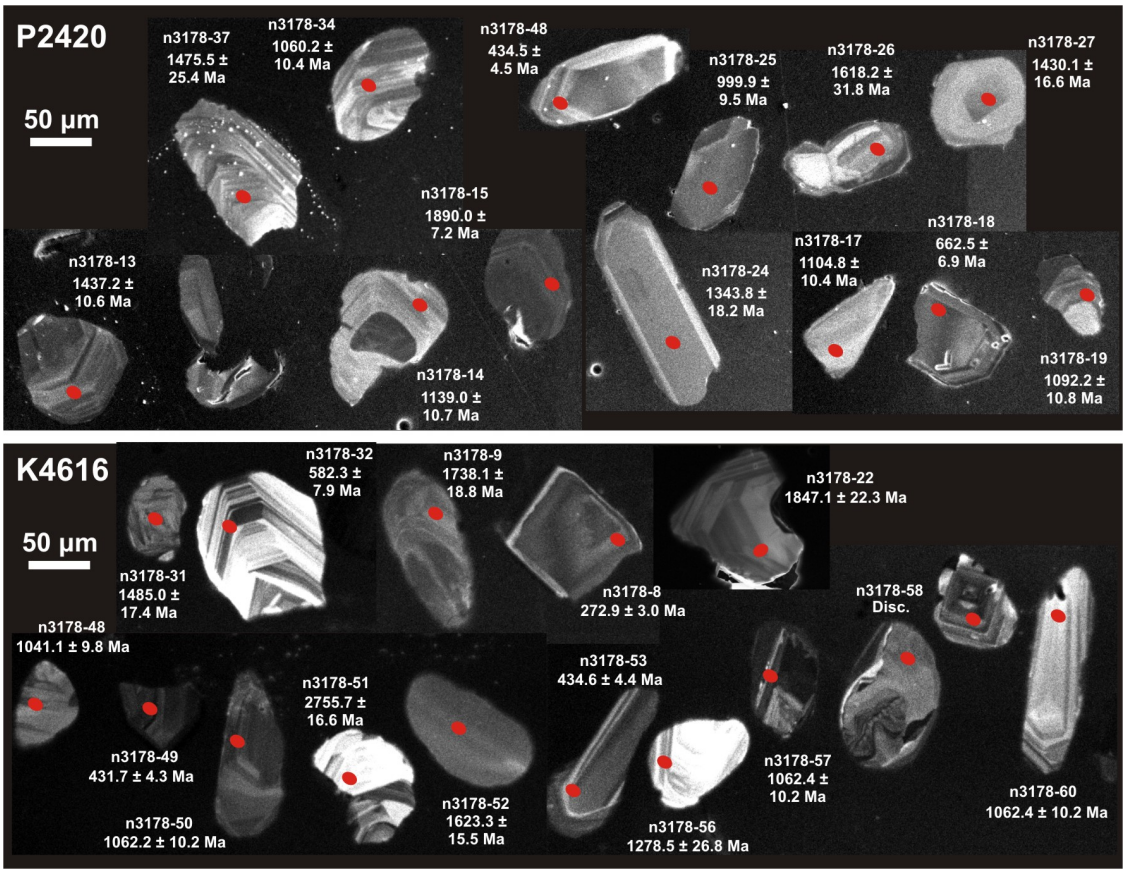

Figure 5.27: Cathodoluminescence images of Svalbard samples showing morphology and internal structure of representative zircon grains. U-Pb age, with 1σ uncertainty, is shown for each analysis. Ages younger than 1200 Ma are $^{206}Pb/^{238}U$ ages. Ages older than 1200 Ma are $^{207}Pb/^{206}Pb$ ages. Analytical spots are indicated by ellipses.

and Nordmela Formations of the Barents Shelf (upper Kapp Toscana Group, Realgrunnen Subgroup) and the Middle Jurassic Brentskardhaugen Bed and Early Cretaceous Helvetiafjellet Formation (Glitrefjellet Member) of Svalbard are classified as sand type 3. The samples are quartz arenites and plot in the 'craton interior' field on QtFL and QmFLt diagrams. The heavy mineral assemblages are ultrastable and zircon-dominated. Some samples contain significant garnet populations (e.g. Nordmela Formation samples). However, this is not considered provenance-diagnostic due to the likelihood of garnet dissolution in many samples. Most grains are rounded, evidence of a recycled source. The Brentskardhaugen Bed, Helvetiafjellet Formation and Fruholmen Formation samples are dominated by Proterozoic zircon grains.

The Early Jurassic-Early Cretaceous Stø Formation through Kolmule Formation samples are composed of sand type 3, with lesser amount of sand type 1. The

proportion of sand type 1 increases with stratigraphic height. The samples are quartz arenites. The Stø through Knurr Formation samples plot in the 'craton interior' fields on QtFL and QmFLt diagrams. The Kolje Formation and Kolmule Formation samples plot in the 'recycled orogen' fields on QtFL and QmFLt diagrams. The samples are all zircon-dominated, with varying amounts of apatite, generally increasing with stratigraphic height.

5.10 Discussion

The petrological, heavy mineral and zircon data allow two sand types to be distinguished (sand types 1 and 3). The stratigraphic distribution of sand types 1 and 3 in the Mesozoic succession of Svalbard and the Barents Shelf can be seen in Figure 5.28.

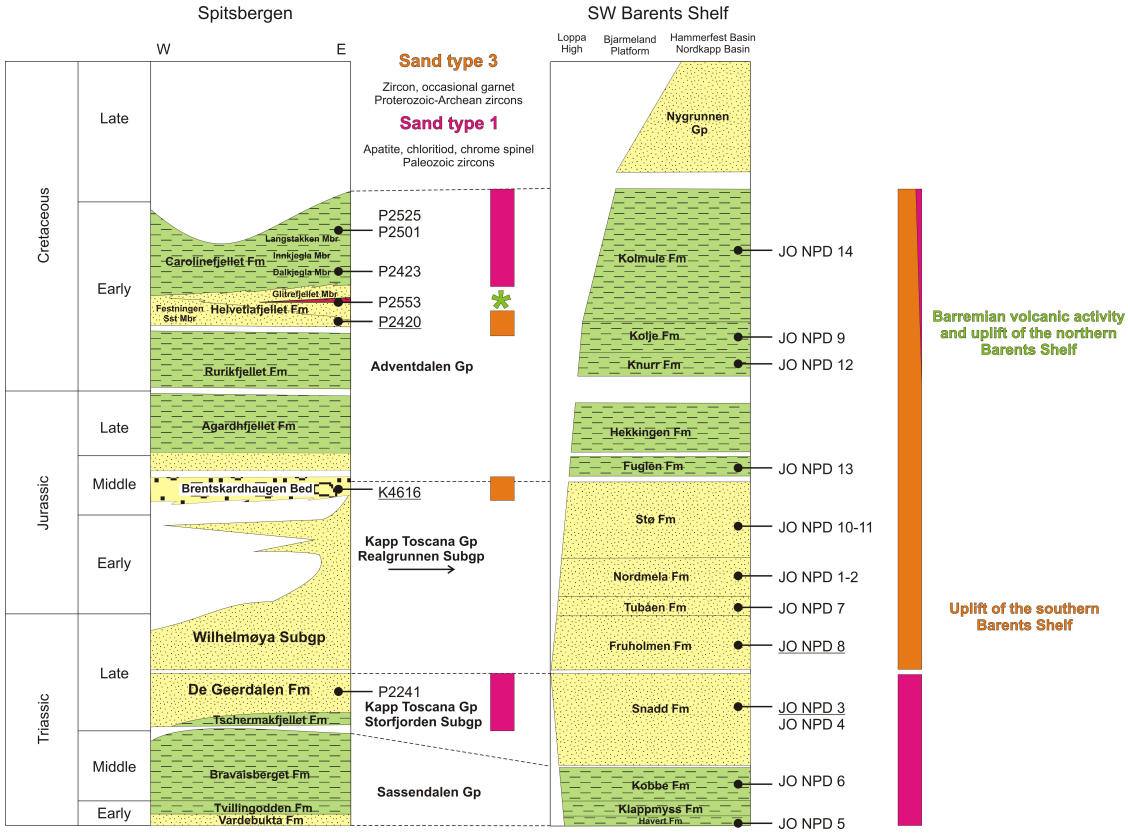

Figure 5.28: Barents Shelf stratigraphy showing the presence of sand types 1 and 3. Samples studied for detrital zircon ages are underlined.

Sand type 1

The sandstones classified as sand type 1 are texturally and compositionally immature, showing euhedral, angular grains and subarkosic composition. They show an unstable heavy mineral assemblage, dominated by apatite, chloritoid and epidote, in association with chrome spinel.

The Early-Late Triassic Sassendalen Group and Storfjorden Subgroup samples of the Barents Shelf are classified as sand type 1 (Fig. 5.28). These samples were deposited on the southwestern Barents Shelf, east of the Hammerfest Basin. The Snadd Formation sample (JO NPD 3) shows zircon ages dominated by a spread of late Silurian to mid Carboniferous ages (419-300 Ma) (Fig. 5.22). There is also an Early Cambrian peak (520 Ma) and a spread of Precambrian ages, with no robust peaks.

These zircon ages are consistent with derivation from the Urals (Scarrow *et al.*, 2002). The Early Cambrian and older ages represent Timanian and older crust recycled in the Uralian Orogen (Scarrow *et al.*, 2002) (Fig. 5.30). The textural and compositional characteristics and heavy mineral assemblages of the Sassendalen Group and Storfjorden Subgroup samples are also consistent with sediment derivation from a proximal orogenic source, providing euhedral zircon grains and exposing metamorphic terranes. The presence of chrome spinel shows that mafic-ultramafic igneous rocks composed some of the source material.

The Late Triassic De Geerdalen Formation sample (from Svalbard) shares the same mineral characteristics of the Barents Shelf Sassendalen Group and Storfjorden Subgroup samples and is interpreted to be derived from the Uralian Orogen. The presence of Uralian material on Svalbard suggests that the Urals shed a large amount of sediment. The Late Triassic Vasilyev Formation and Thegetthoff Formation of Franz Josef Land share sedimentary characteristics with these samples (V. Pease, pers. comm.) and supports the idea that the Uralian Orogen provided sediment to a large area during Triassic time.

Sand type 3

The sandstones classified as sand type 3 are texturally and compositionally mature, with rounded grains and quartz arenitic composition. They show an ultrastable heavy mineral assemblage, dominated by zircon, tourmaline and rutile, with occasional garnet.

Sandstones with these characteristics unconformably overly the Storfjorden Subgroup on the Barents Shelf (Fig. 5.28). The unconformity reflects the up-

lift of the southern Barents Shelf during Late Triassic time (Nøttvedt *et al.*, 1992). Following the unconformity, the Uralian source was replaced with a more mature, recycled sediment source. The Late Triassic-Early Cretaceous succession of the southwestern Barents Shelf (Realgrunnen Subgroup and Adventdalen Group) is classified as sand type 3. Samples from the Middle Jurassic Brentskardhaugen Bed and Early Cretaceous Helvetiafjellet Formation (Festningen Sandstone Member) are also classified as sand type 3. The classification of the Wilhelmøya Subgroup, Agardhfjellet Formation and Rurikfjellet Formation of Svalbard is uncertain, but they are tentatively assigned to sand type 3 (Fig. 5.28).

From this succession (sand type 3), three samples were U-Pb dated: the Late Triassic Fruholmen Formation, Middle Jurassic Brentskardhaugen Bed and Early Cretaceous Helvetiafjellet Formation (JO NPD 8, P2420 and K4616). The samples show remarkably similar zircon ages, dominated by a spread of Paleoproterozoic to Mesoproterozoic ages (Fig. 5.29). The similarities between the samples argue strongly for the same source for the samples. The zircon ages seen in the samples are consistent with derivation from the Baltic Shield. The zircon ages represent Baltic Archean craton formation (3100-2500 Ma), the Svecofennian Orogeny (2000-1860 Ma), the Transscandinavian Igneous Belt (1850-1550 Ma) and the Sveconorwegian Orogeny (1760-900 Ma) (e.g. McNicoll *et al.*, 1995).

There is facies and stratigraphic evidence to suggest that sediment deposited on Svalbard during Jurassic-Early Cretaceous time was westerly, northerly and northwesterly derived (Mørk *et al.*, 1999 and references therein) and not southerly derived. However, the zircon data collected from the Middle Jurassic Brentskardhaugen Bed and Early Cretaceous Helvetiafjellet Formation samples argue strongly for a Baltica source for this sediment. The Wilhelmsøya Subgroup was not sampled and could have a different provenance to the samples discussed here, being possibly northerly derived. However, another explanation is that the samples described here may be northerly derived but that the northern source area (presumably putative crust flooring the central Arctic Ocean) may have a Baltic Shield affinity or be covered by sediment of Baltica Shield affinity (possibly shed off Baltica in response to the Caledonian orogeny).

Early Cretaceous Glitrefjellet Member

The next change in sediment characteristics observed in the Svalbard-Barents Shelf dataset occurs in the Early Cretaceous (Barremian) Helvetiafjellet Formation Glitrefjellet Member sample. The sample is a litharenite and is dominated by

mafic volcanogenic clasts. This volcanic material is likely related to the Diabaseodden Suite: dolerite sills and dikes intruding older rocks on Svalbard and present as volcanic flows on Kong Karls Land, east of Spitsbergen (Mørk *et al.*, 1999). This is related to volcanism of the same age (Barremian) in other areas of the Arctic, known as the High Arctic Large Igneous Project (HALIP) and subsequent uplift north of the Barents Shelf (Maher, 2001).

5.11 Conclusions

Examination of 21 Mesozoic age southwestern Barents Shelf and Svalbard sandstone samples show two main sediment sources to the Barents Shelf during Mesozoic time. Triassic samples are compositionally immature and show mainly late Silurian to mid Carboniferous zircon grains, evidence of provenance from the Urals Orogen (sand type 1). Jurassic-Cretaceous sediments are compositionally mature and show mainly Proterozoic and Archean zircon grains, evidence of provenance from the Baltic Shield or areas containing Baltic Shield crustal signatures (sand type 3). Early Cretaceous (Albian) magmatism and subsequent uplift north of Svalbard led to a reemergence of sand type 1 in Svalbard, where it replaced sand type 3. On the southwestern Barents Shelf, there was a mixing of sand types 1 and 3 after the initiation of volcanic activity.

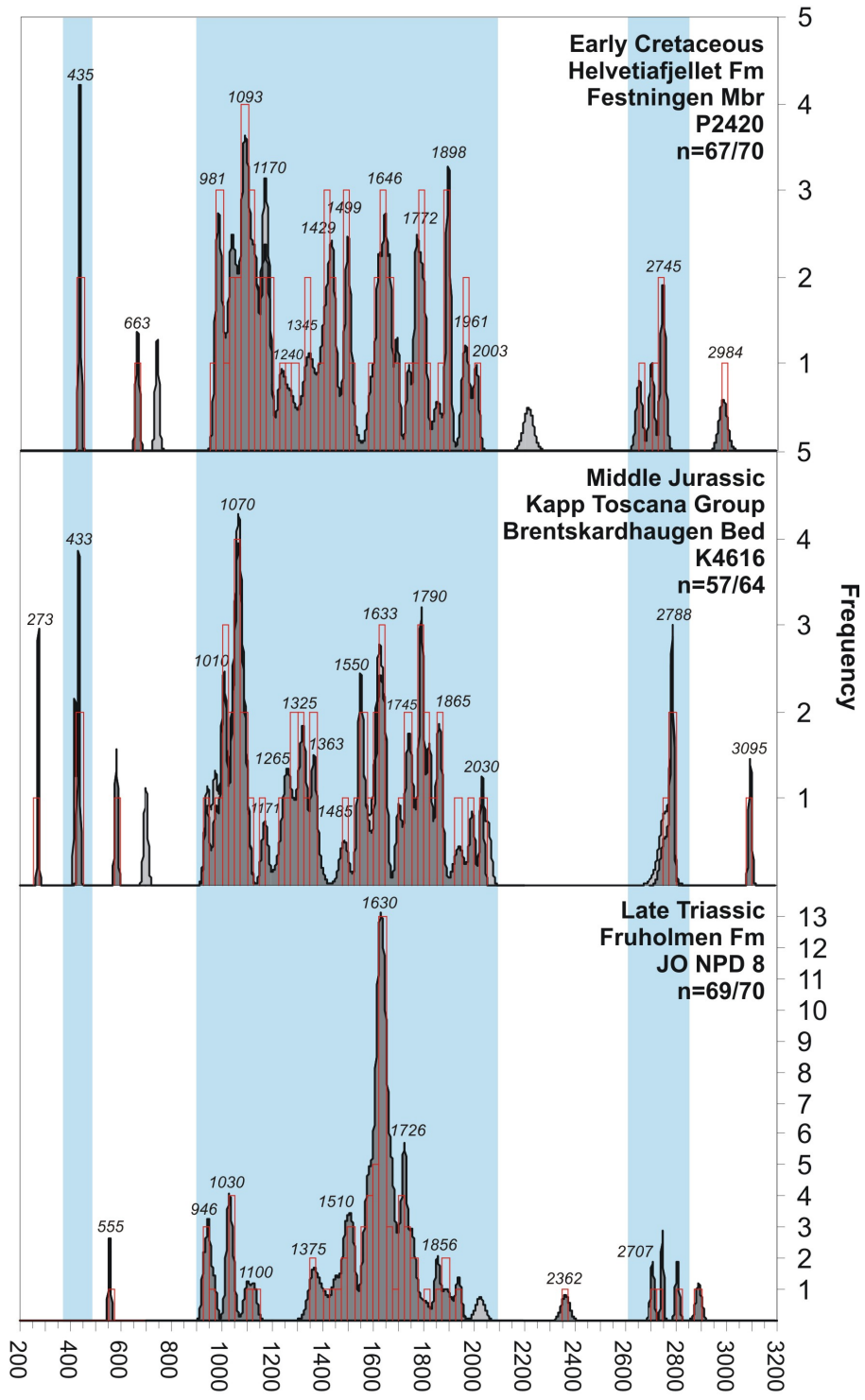

Figure 5.29: Sand type 3 cumulative frequency diagrams, with histograms, of U-Pb detrital zircon ages showing sand type 3. The similarities between the three samples is clear. U-Pb age, with 1σ uncertainty, is shown. Ages younger than 1200 Ma are $^{206}Pb/^{238}U$ ages. Ages older than 1200 Ma are $^{207}Pb/^{206}Pb$ ages. Ages with 90-110% concordancy are shown by histograms and dark grey cumulative frequency curves. More discordant data are shown by pale grey cumulative frequency curves. N denotes the number of analyses with 90-110% concordancy relative to all analyses.

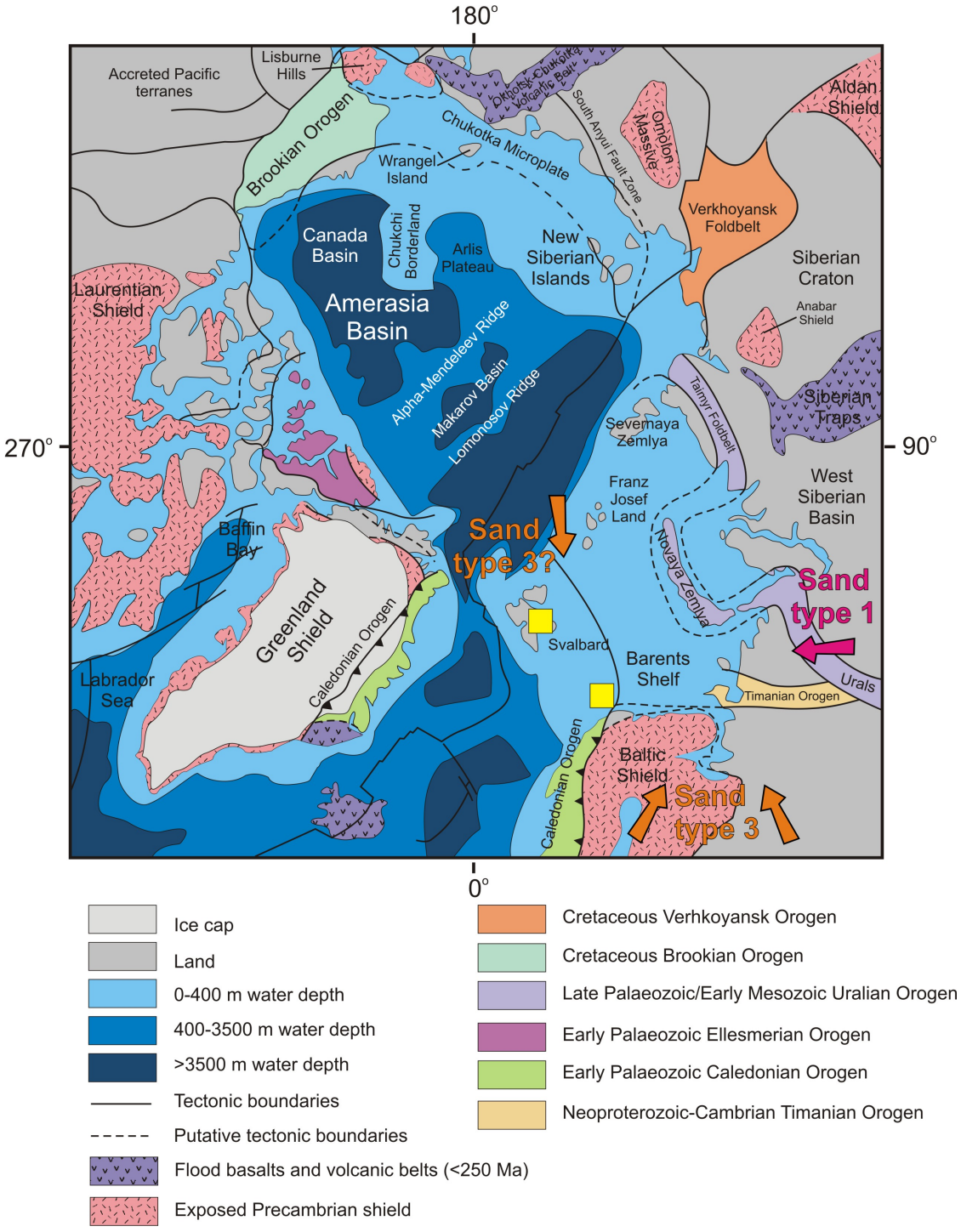

Figure 5.30: Tectonic map of the Arctic region. Bathymetry and topography are modified after the IBCAO Arctic Bathymetry database (Jakobsson *et al.*, 2008). Plate boundaries and geological features are modified after Harrison (2005). Neoproterozoic and younger orogenic belts outcrops on land are shown with different shadings. Interpreted provenance of Barents Shelf sand types 1 and 3 is shown.

Chapter 6

Composition and provenance of Late Paleozoic-Mesozoic sandstones from the Taimyr Peninsula, Arctic Russia

The sedimentary and provenance characteristics of six Permo-Carboniferous and two Early Cretaceous samples from the Taimyr Peninsula were studied. The Permo-Carboniferous samples have a mixed provenance of recycled and first cycle sediment, sourced from metamorphic and igneous terranes. Zircon data show a mixture of Precambrian-Paleozoic ages and euhedral, penecontemporaneous Permian grains suggesting derivation from the Uralian and Timanian orogens, with additional Caledonian material presumably from Baltica. The Early Cretaceous samples also have a mixed provenance of metamorphic and igneous source rocks, of mainly first cycle detritus and an unstable heavy mineral assemblage dominated by staurolite, suggesting local derivation. Detrital zircon ages fall almost exclusively into one Late Permian-Early Triassic cluster, suggesting that the Taimyr area was an important source of zircons of Siberian Trap age.

6.1 Introduction

The Taimyr Peninsula lies on the northern margin of the Eurasian landmass, bounded by the Laptev Sea to the east and the Kara Sea to the north and west (Fig. 6.1). Taimyr consists of two NE-SW trending allochthonous terranes (Northern and Central Taimyr) accreted to the passive margin of Siberia (Southern Taimyr). Central Taimyr became attached to Siberia during Late Precambrian

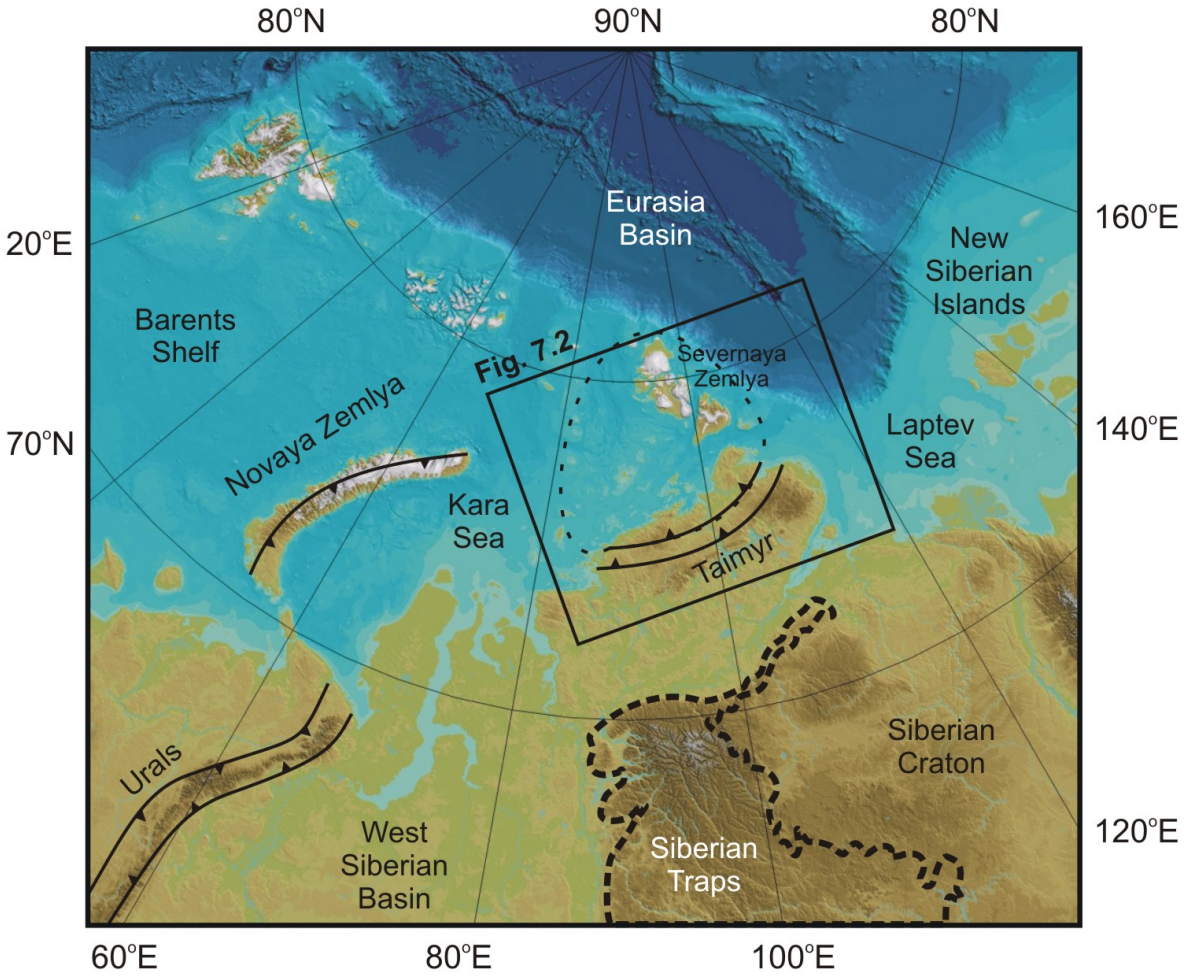

Figure 6.1: Regional setting of the Taimyr Peninsula. Taimyr lies north of the Siberian craton and West Siberian Basin and is bounded by the Laptev Sea to the east and the Kara Sea to the north and west. Taimyr is interpreted to be a continuation of the Urals Orogen, through Novaya Zemlya (Vernikovsky *et al.*, 1995). The thin dashed line outlines the presumed extent of the Kara Block (Bezzubtsev *et al.*, 1986). The thick dashed line outlines the surface extent of the Siberian Traps. Bathymetry and topography are from the IBCAO Arctic Bathymetry database (Jakobsson *et al.*, 2008).

time (Vernikovsky *et al.*, 1995). Northern Taimyr became attached to the accreted margin (South/Central Taimyr) during Late Paleozoic time, as part of the Uralian Orogeny (Vernikovsky *et al.*, 1995). Recent data suggest that Northern Taimyr has a Baltica affinity (Pease & Scott, 2009).

This chapter presents sediment provenance results of Permo-Carboniferous and Early Cretaceous samples from Taimyr. The Permo-Carboniferous samples provide information about the contemporaneous Uralian Orogen from which they are sourced. The Early Cretaceous samples may provide information about the geological setting of Taimyr in the Early Cretaceous - the period of Amerasia Basin formation.

6.2 Geological setting

The Taimyr Peninsula can be divided into three NE-SW trending structural zones, separated by south-verging thrust faults (Uflyand *et al.*, 1991) (Fig. 6.2).

Southern Taimyr exposes unmetamorphosed Ordovician to mid Carboniferous carbonate-dominated platform strata of the Siberian craton. This passive margin succession is overlain by Late Carboniferous-Permian shallow marine to continental clastic sediments, derived from the north and west, assumed to be shed off the developing Uralian collisional belt. The clastic rocks are interbedded with Permo-Triassic intrusive and extrusive rocks (Inger *et al.*, 1999; Walderhaug *et al.*, 2005). Reichow *et al.* (2009) showed that these igneous rocks formed concurrently with ∼252 Ma Siberian trap magmatism, the largest igneous province in the world, extending over 5 million km^2 and extruded in less than one million years. Minor A-type granites and syenites, related to the trap basalts, subsequently intruded the Paleozoic succession on the northern coast of southwestern Taimyr during Early Triassic time (249-241 Ma) (Vernikovsky *et al.*, 2003).

During Late Triassic to earliest Jurassic time, the autochthonous succession of Southern Taimyr was folded and thrust southward in a dextrally transpressive event (Inger *et al.*, 1999; Torsvik & Andersen, 2002; Walderhaug *et al.*, 2005). Deformed Paleozoic sediments and Permo-Triassic igneous rocks are unconformably overlain by undeformed Early Jurassic clastic sediments, providing an upper age limit on the cessation of folding (Walderhaug *et al.*, 2005).

Central Taimyr is a structurally and lithologically complex accretionary terrane (Uflyand *et al.*, 1991; Zonenshain & Natapov, 1989). Neoproterozoic (and possibly older) sedimentary, volcanogenic and intrusive complexes are interpreted as ophiolites, island-arc and back-arc complexes and continental fragments. Widespread,

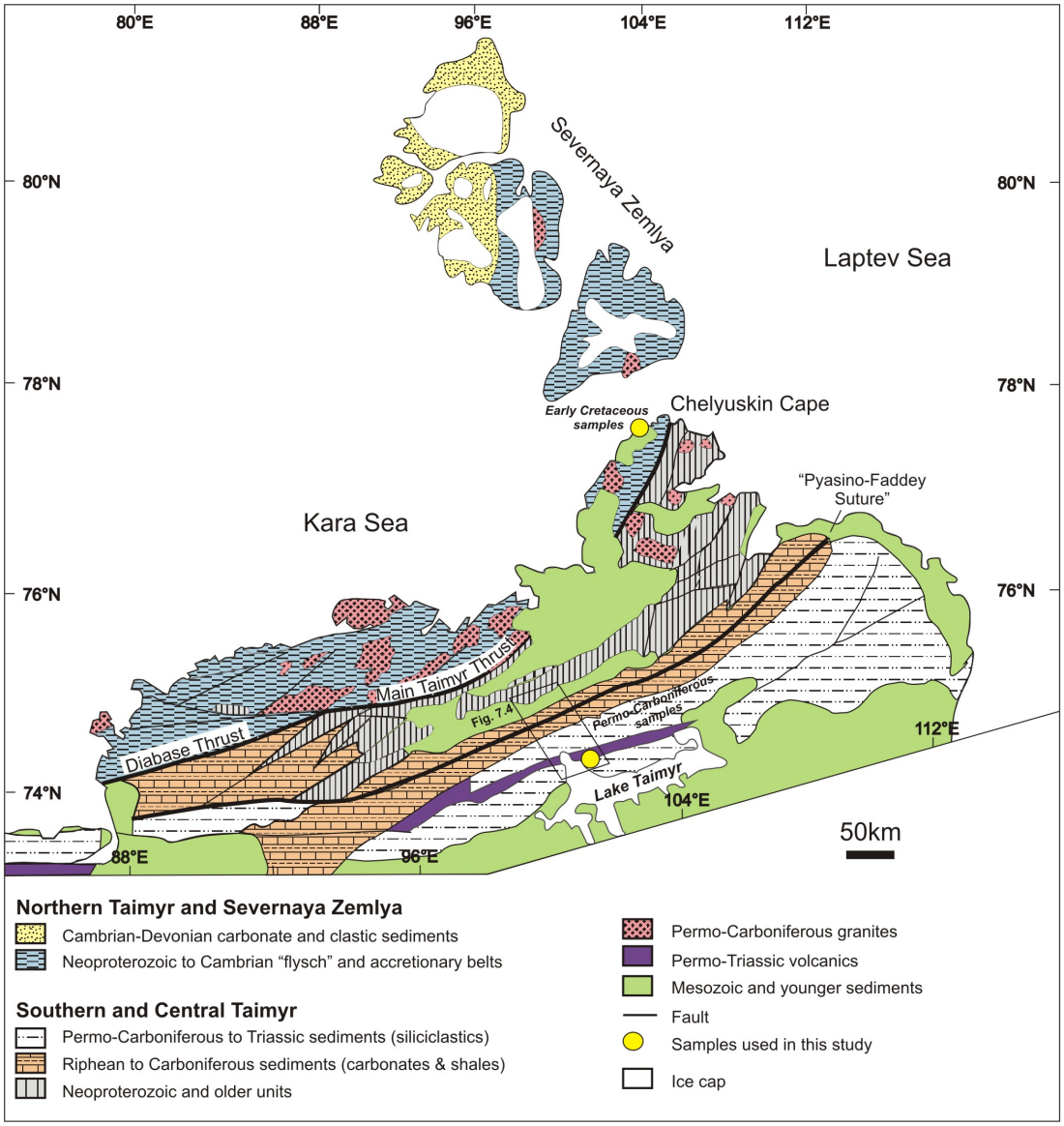

Figure 6.2: Geological map of the Taimyr Peninsula, after Bezzubtsev *et al.* (1983); Inger *et al.* (1999). Taimyr is generally divided into two allochthonous terranes, Northern Taimyr and Central Taimyr, separated by the Diabase and Main Taimyr Thrusts, and one autochthonous terrane, Southern Taimyr, south of the Pyasino-Faddey Suture. Yellow circles indicate sample localities.

high-grade metamorphism occurred in Central Taimyr around 600 Ma (Late Neoproterozoic), probably recording the collision of Central Taimyr with the margin of Siberia (Vernikovsky *et al.*, 1995). Overlying the accretionary basement is an unmetamorphosed Vendian to Early Carboniferous siliciclastic and carbonate continental margin succession. This succession is inferred to be the deeper-water equivalent of Siberian continental margin sediments found in Southern Taimyr (Inger *et al.*, 1999). These sediments, together with Permo-Carboniferous syn- and post-tectonic Uralian granites, were deformed by Mesozoic transpression (Inger *et al.*, 1999; Pease, 2001; Vernikovsky *et al.*, 1995).

Northern Taimyr and Severnaya Zemlya are often depicted as a separate continental block, commonly referred to as the Kara block (Bezzubtsev *et al.*, 1986). This block may have been attached to Baltica during Neoproterozoic Timanian collision and has Baltica affinities from at least earliest Paleozoic time (Pease & Scott, 2009). Northern Taimyr and southeastern Severnaya Zemlya are dominated by interbedded Neoproterozoic-Cambrian sandstones, siltstones and mudstones, interpreted as turbidites formed on the continental slope of the Kara block (Bezzubtsev *et al.*, 1986). Late Paleozoic (Uralian) deformation resulted in regional greenschist and amphibolite facies metamorphism of the Kara block, including intensive deformation, migmatisation, and granite intrusion, marking the collision of the Kara block with the rest of Taimyr (Vernikovsky *et al.*, 1995). The deformed Neoproterozoic sediments are overlain by unmetamorphosed, subhorizontal Jurassic and Cretaceous marginal marine clastic sediments (Bezzubtsev *et al.*, 1983).

6.3 Samples and methods

The samples discussed in this chapter were collected from two areas: Southern Taimyr, in the vicinity of Lake Taimyr, and Northern Taimyr, close to the northern coast at Chelyuskin Cape (Fig. 6.2). The stratigraphic positions of the samples are shown in Figure 6.3.

The Permo-Carboniferous samples were collected by CASP during a 1998 field season. The succession from which they were obtained is composed of coarsening-up cycles, on a scale of 100 m, of shale, siltstone and very fine- to fine-grained sandstones (Inger & Scott, 1999). Figure 6.4 shows the position of the samples on a geological map. Figure 6.5 shows a typical appearance of the Permo-Carboniferous succession. The depositional environments of the Permo-Carboniferous strata of Southern Taimyr have been interpreted as fluvial in the west to shallow marine in the east, with palaeocurrents towards the southeast. In the Lake Taimyr region

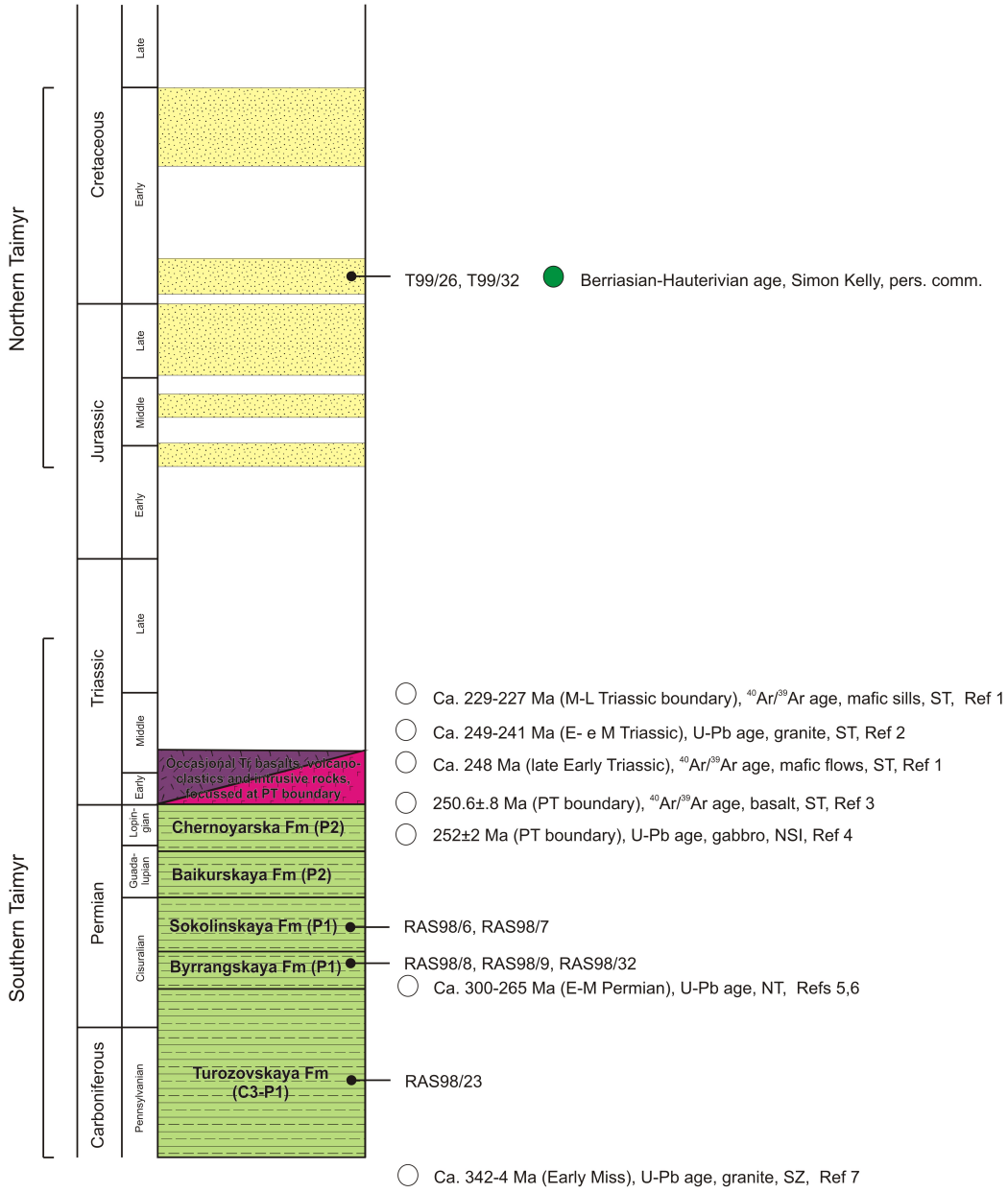

Figure 6.3: Composite stratigraphic column for Taimyr. Late Paleozoic stratigraphy, Southern Taimyr, is modified after Bezzubtsev *et al.* (1983) and Inger *et al.* (1999). Ages for these formations are poorly known. Mesozoic stratigraphy, Northern Taimyr, is modified after Natapov *et al.* (1997). The stratigraphic positions of the samples discussed in this text are shown. The Early Cretaceous samples were dated by Simon Kelly (green circle). White circles show selected published age data for Taimyr and adjacent regions. Ref. 1: Walderhaug *et al.* (2005); Ref. 2: Vernikovsky *et al.* (2003); Ref. 3: Reichow *et al.* (2009); Ref. 4: Kuzmichev & Pease (2007); Ref. 5: Vernikovsky *et al.* (1995); Ref. 6: Pease (2001); Ref. 7: Lorenz *et al.* (2007). ST = South Taimyr, CT = Central Taimyr, NT = North Taimyr, SZ = Severnaya Zemlya, NSI = New Siberian Islands. The Walderhaug *et al.* (2005) data have been challenged by Reichow *et al.* (2009).

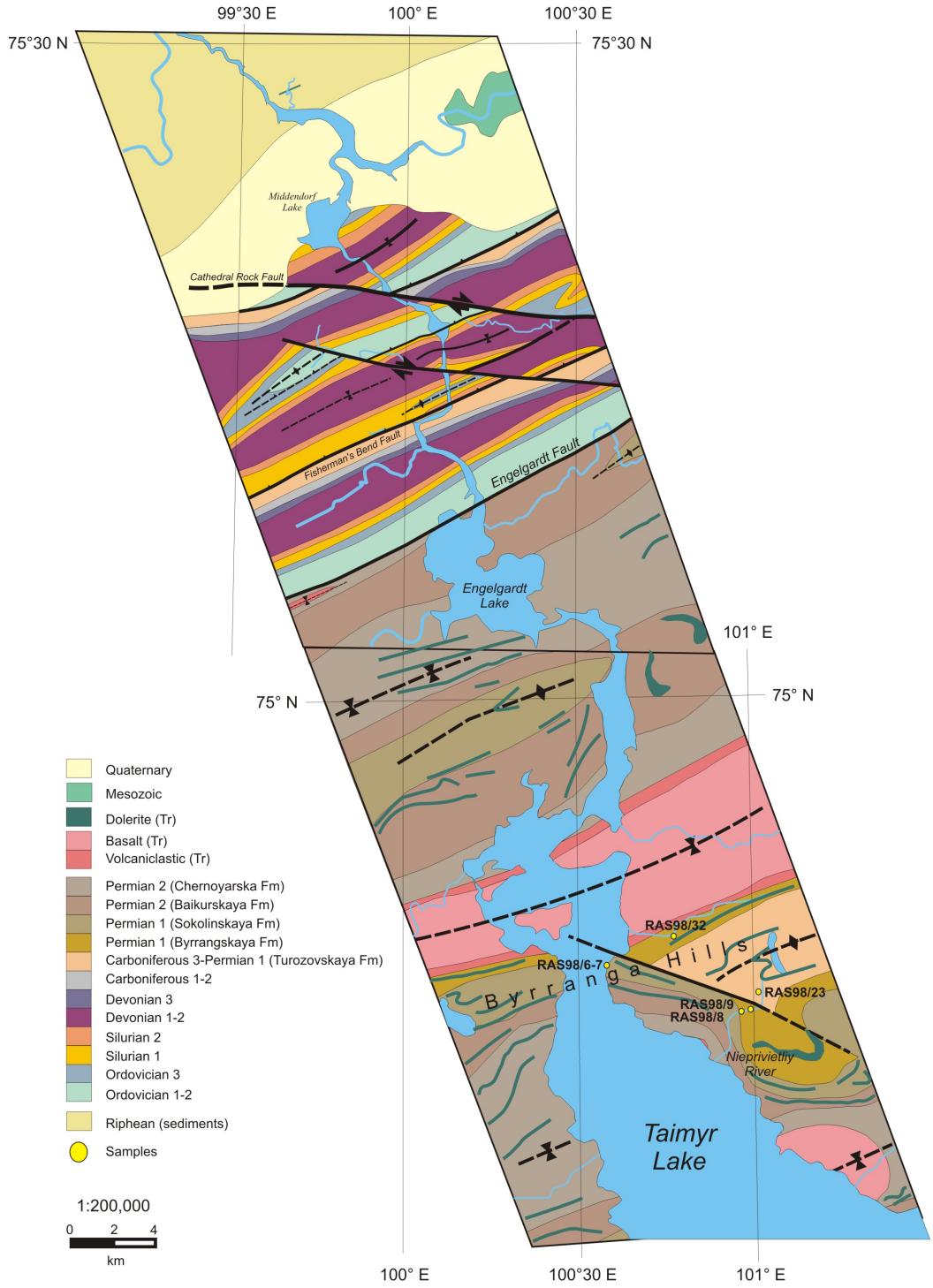

Figure 6.4: Geological map showing Paleozoic sample locations, modified after Bezzubtsev *et al.* (1983) and largely unchanged from Inger & Scott (1999).

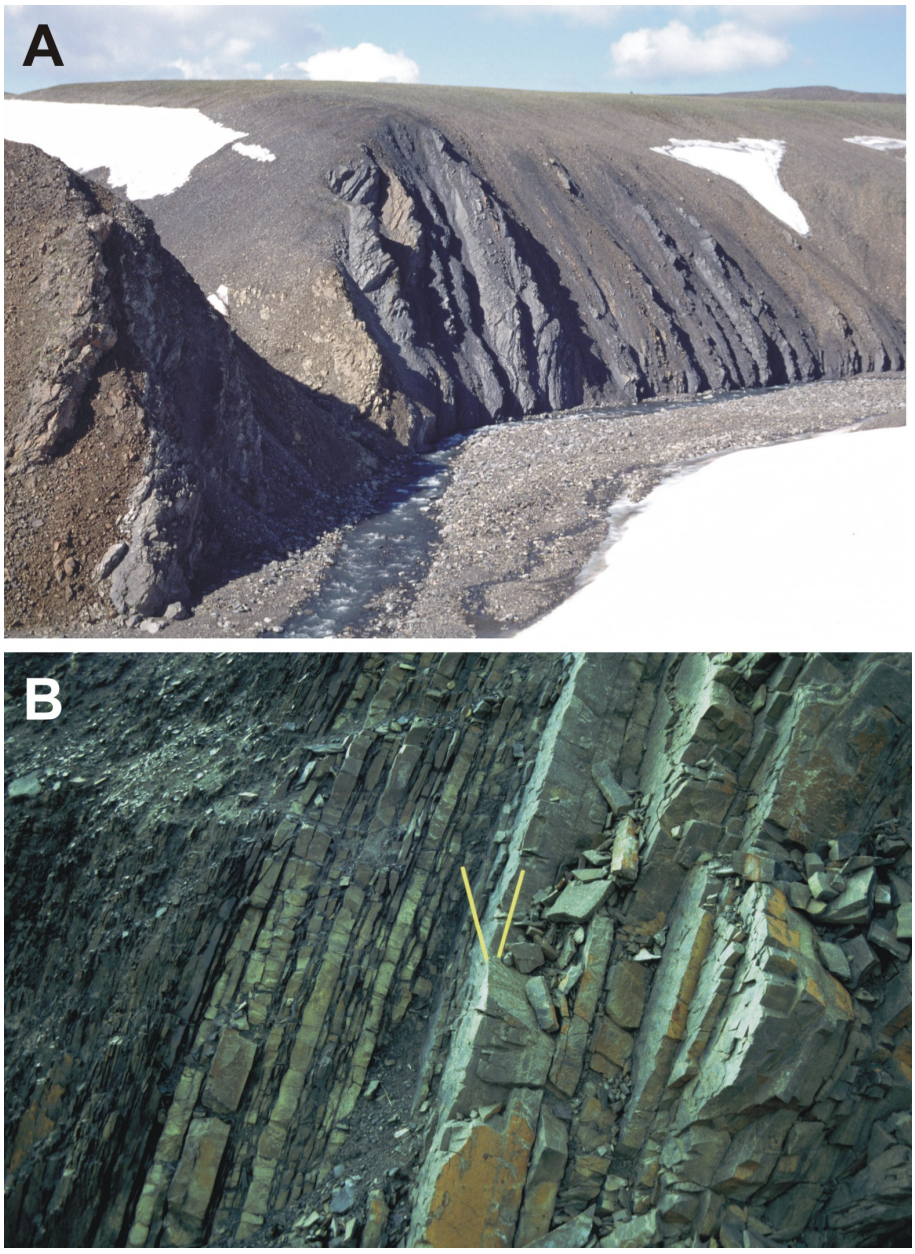

Figure 6.5: Photographs of Nieprivietlivy River sediments, taken by Robert Scott. (A) Late Carboniferous-Early Permian clastic sediments exposed along the Nieprivietlivy River. Turozovskaya Formation sandstones and siltstones form coarsening-up cycles averaging 150 m thickness. Cliff height is 40 m. (B) Cycle-top sandstone (right) change to dark silty mudstones of the overlying cycle (left) in the marine/deltaic succession of the Turuzovskaya Formation. Yellow rules are 50 cm.

Sample	Formation	Age	Petro-graphy	HM ratios	Garnet chemistry	Tourmaline chemistry	Zircon dating
T99/32	Unnamed	K1	y	y	y	y	
T99/26	Unnamed	K1	y	y	y	y	y
RAS98/7	Sokolinskaya	P2	y				
RAS98/6	Sokolinskaya	P2	y	y		y	y
RAS98/32	Byrrangskaya	P1	y				
RAS98/9	Byrrangskaya	P1	y	y			
RAS98/8	Byrrangskaya	P1	y	y		y	y
RAS98/23	Turozovskaya	C3-P1	y	y		y	

Table 6.1: Overview of analyses performed on the Taimyr samples. HM = Heavy mineral. The formations are listed in stratigraphic order, with the youngest at the top. Y indicates that sample analysis was carried out.

Figure 6.6: Photograph of Chelyuskin Cape sediments, taken by Per Möller. The photograph shows the horizontally stratified nature of the Jurassic-Cretaceous sediment. The Early Cretaceous samples discussed in this chapter were collected from this exposure.

they are interpreted as delta plain deposits (Inger & Scott, 1999). The strata are not dated to stage level and are mapped as Permo-Carboniferous in age (Bezzubtsev *et al.*, 1983) (Fig. 6.3).

The Cretaceous samples were collected during a 1999 field season by Per Möller, Lund University, on behalf of CASP. The Jurassic-Cretaceous marginal marine strata are unconsolidated and flat-lying, unconformably overlying deformed Paleozoic and Early Triassic units (Fig. 6.6). The sediments were dated with a variety of macrofossils (Natapov *et al.*, 1997 and references therein). The samples discussed here are Early Cretaceous (Berriasian-Hauterivian) age (Simon Kelly, pers. comm.) on the basis of a pectinid bivalve species: Camptonectes (Mclearnia) cinctus (J. Sowerby).

The samples were analysed for sediment petrography, heavy mineral analysis, garnet and tourmaline chemistry and U-Pb LA-ICP-MS zircon analysis (Table 6.1), following analytical methods outlined in Chapter 3.

6.4 Petrography results

The petrography of eight samples was examined (Table 6.1). Figures 6.7-6.9 illustrate point counting results for these samples. The complete dataset is included in the accompanying CD. Photomicrographs of the analysed samples are shown in figures 6.10-6.13.

The Permo-Carboniferous Turozovskaya Formation and Byrrangskaya Formation samples are classified as sublitharenites (Fig. 6.7). The samples are dominated by monocrystalline quartz (65-82%), showing variable degrees of undulosity. This mineral texture is typical for plutonic rocks (e.g. Smyth *et al.*, 2008). There is also a moderate amount of polycrystalline quartz with four or more subgrains (11-28%), typical for low-grade metamorphic rocks (e.g. Smyth *et al.*, 2008). The samples show a mixture of feldspar compositions (Fig. 6.8). Plagioclase comprises 84% of the feldspar seen the Turozovskaya Formation sample; in the Byrrangskaya Formation samples it is lower (50-58%). Some alkali feldspars are microcline, evidence of a slowly cooled plutonic source. On a QtFL plot, the samples plot within the 'recycled orogenic' field. On a QmFLt plot, the samples plot within the 'quartzite and transitional recycled orogen' fields (Fig. 6.9).

The Permian Sokolinskaya Formation samples are classified as arkosic arenites (Fig. 6.7), suggesting an influx of compositionally less mature, feldspar-rich detritus. A change is also seen in quartz compositions, with a lesser amount of monocrystalline quartz than underlying formations (38-40%). There is a significant

increase in polycrystalline quartz with more than four subgrains (55-59%), suggesting that the change in sediment provenance may reflect more detritus sourced from a metamorphic terrane. The samples contain 68-85% plagioclase (relative to all feldspar). Anorthite compositions for the plagioclase grains was estimated to be 30%, suggesting derivation from a metamorphic source. Some alkali feldspars are microcline, evidence of a slowly cooled plutonic source. On a QtFL plot, the samples plot within the 'uplifted continental block' field. On a QmFLt plot, the samples plot within the 'transitional magmatic arc' field (Fig. 6.9). Sample RAS98/6 was collected from close to a dolerite sill and showed an altered appearance (reddish colouration) (Robert Scott, pers. comm).

The Early Cretaceous samples show markedly different characteristics to the unconformably underlying Paleozoic samples (Figs. 6.10-6.13). The Mesozoic samples are very coarse-grained and unconsolidated, whereas the Paleozoic samples are very fine- to fine-grained and strongly compacted and lithified. The Mesozoic samples are classified as subarkoses (Fig. 6.7). The quartz grains are almost exclusively monocrystalline, non-undulose quartz (80-82%), indicative of a plutonic source. The feldspar compositions for these samples is almost exclusively alkali feldspar (98-99%), often microcline. On QtFL and QmFLt diagrams, the samples plot within the 'transitional continental block' and 'craton interior' fields (Fig. 6.9).

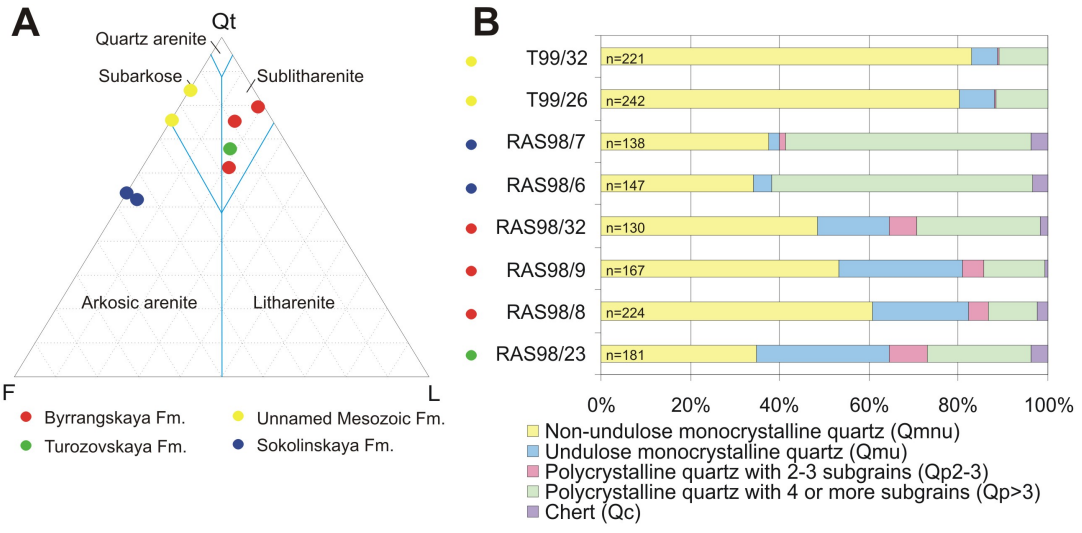

Figure 6.7: Sediment classification of Taimyr samples. (A) QtFL sandstone classification plot, modified after Pettijohn *et al.* (1987). (B) Quartz type identified by point counting, plotted as percentage of Total Quartz and Chert. Most samples are dominated by monocrystalline quartz, with the exception of the Sokolinskaya Formation samples, which are dominated by polycrystalline quartz.

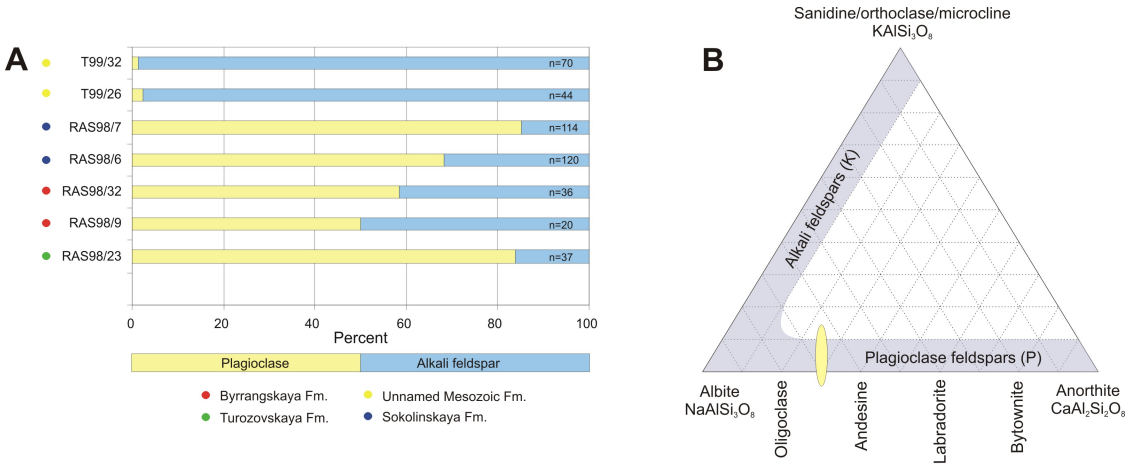

Figure 6.8: Feldspar compositions of the Taimyr samples. (A) Relative abundance of alkali feldspar and plagioclase. (B) Anorthite content of plagioclase grains, on the basis of albite twin angles for samples from the three Paleozoic formations. All plagioclase compositions were similar, approximately 30% anorthite, shown by the yellow ellipse. Plagioclase angles were determined using the petrographic microscope and averaged from ten measurements.

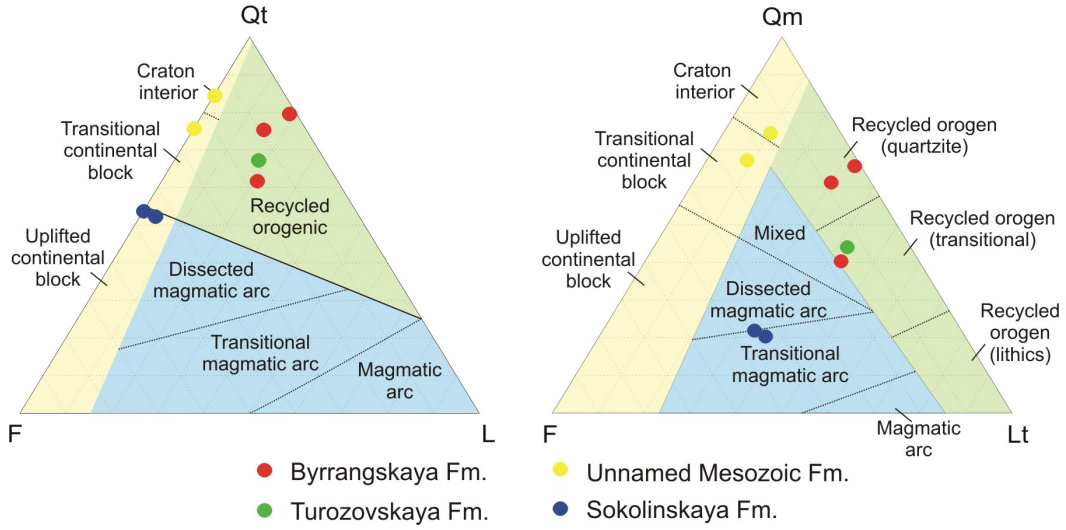

Figure 6.9: Sediment petrography results for the Taimyr samples. QtFL and QmFLt provenance discrimination diagrams are modified after Dickinson & Suczek (1979).

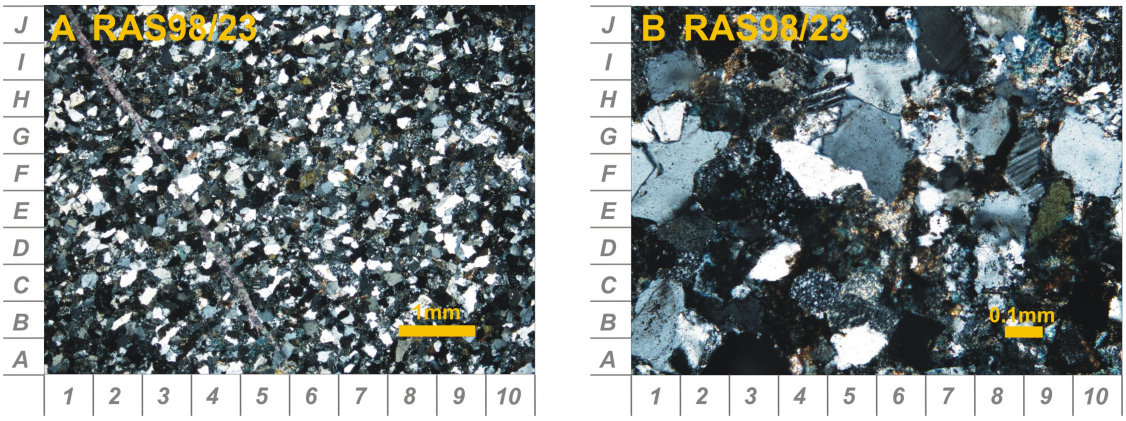

Figure 6.10: Photomicrographs of the Turozovskaya Formation. (A) General view of the moderately sorted, fine-grained, sublitharenite. A calcite vein crosscuts the field of view (A5 to J1). (B) Most grains display concavo-convex contacts, suggesting considerable deformation or alteration by proximity to magmatic intrusions. Overgrowths are visible around quartz grains (C1).

6.5 Heavy mineral results

A subset of six samples showed sufficient heavy mineral recovery for heavy mineral analysis to be performed (Table 6.1). Figures 6.14-6.15 illustrate heavy mineral results. The complete dataset is included in the accompanying CD.

Heavy mineral species

The Turozovskaya Formation sample, RAS98/23, contains an ultrastable heavy mineral assemblage, dominated by apatite (44%), zircon (30%) and tourmaline (13%) (Fig. 6.14). Apatite grains are broken and rounded, suggesting sedimentary recycling and long-range transport. The zircon population is mixed, showing mostly rounded, recycled grains and some perfectly euhedral, doubly vergent magmatic grains. Tourmaline grains also show two populations, with a mixture of broken, rounded brown grains and euhedral green grains. The heavy mineral assemblage contains minor amounts of less stable minerals, including calcic amphibole and sphene. Importantly, the sample also contains minor chrome spinel (2%), a mineral indicating sediment derivation from an ultramafic source.

The Byrrangskaya Formation samples, RAS98/8-9, contain ultrastable heavy mineral assemblages, dominated by apatite (9-46%), zircon (8-42%) and tourmaline (34-40%). In sample RAS98/8, which contains 9% apatite, the morphology is rounded and broken, as seen in sample RAS98/23. In sample RAS98/9, which contains 46% apatite, the morphology is euhedral, suggesting an additional, more prox-

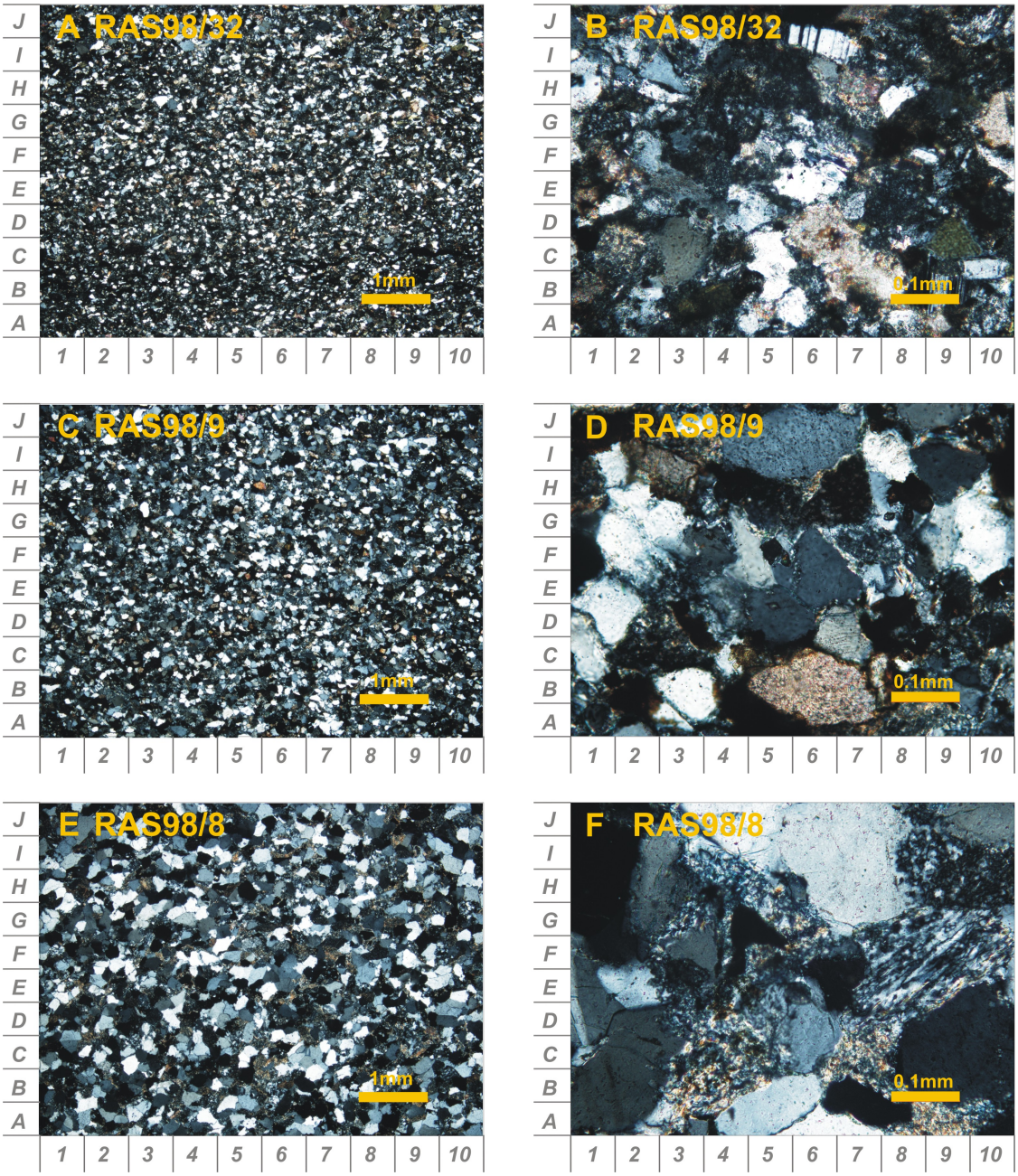

Figure 6.11: Photomicrographs of the Byrrangskaya Formation. (A) General view of the moderately sorted, very fine-grained, sublitharenite. (B) Calcite cement (C7) is shown between concavo-convex grains. Plagioclase (I6) and alkali feldspar (C9) grains are visible. (C) General view of the moderately sorted, very fine-grained sublitharenite. (D) Ferrous cement (B2) is seen between concavo-convex grains. One carbonate grain is visible (B6). (E) General view of the moderately to well sorted, fine-grained, sublitharenite. Numerous sedimentary lithic clasts are visible. (F) A sheared metamorphic quartz grain (F8) and a sedimentary lithic grain composed of quartz and mica (C4) are visible.

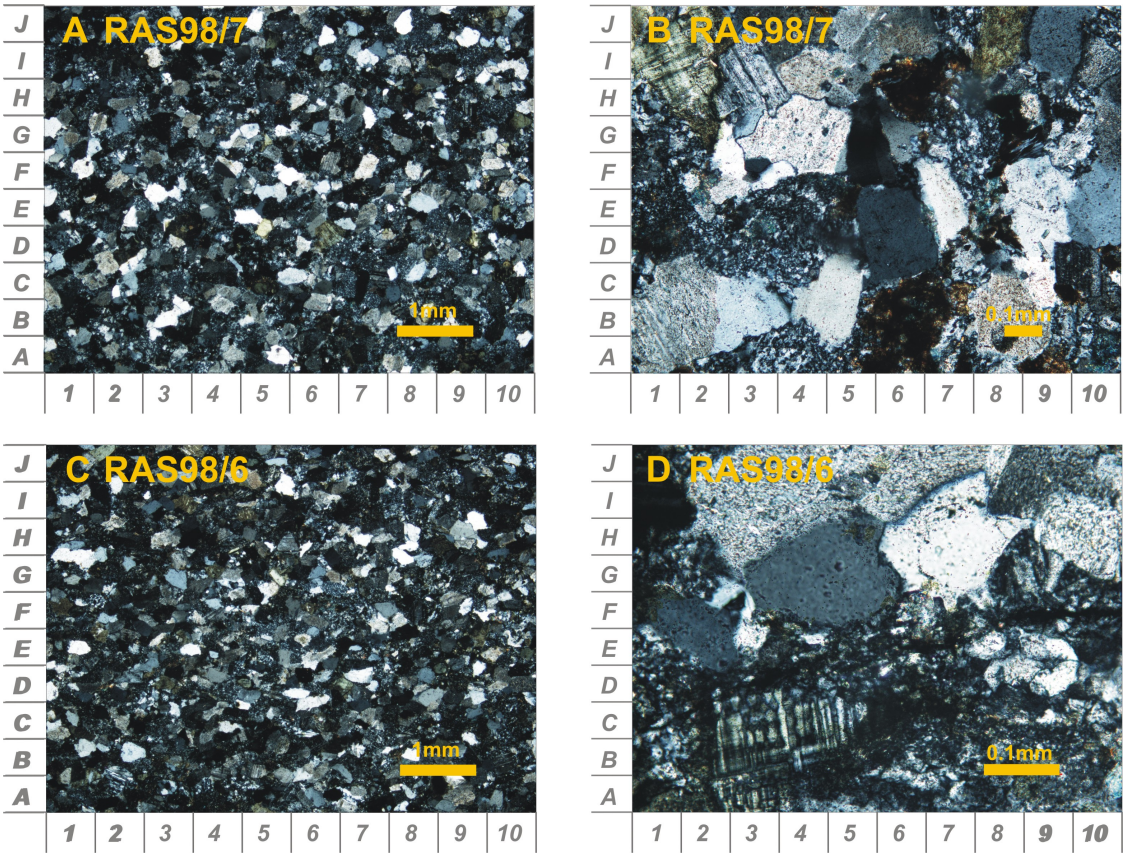

Figure 6.12: Photomicrographs of the Sokolinskaya Formation. (A) General view of the moderately to well sorted, fine-grained, arkosic arenite. Numerous plagioclase and alkali feldspar grains are visible. (B) Strong deformation is shown by suturing grains (G4). Ferrous (A6) and fibrous quartz (F9) cements seen. A microcline grain is visible (I1) (C) General view of the moderately to well sorted, fine-grained, arkosic arenite. (D) A microcline grain (C3) is visible amongst deformed grains.

imal apatite source. Sample RAS98/8 contains mostly broken, rounded tourmaline grains in a mixture of colours. Sample RAS98/9 contains green and brown, mostly euhedral tourmaline grains. Both samples show a mixture of zircon morphologies, with rounded and euhedral grains. Sample RAS98/8 contains 5% chloritoid and 1% chrome spinel.

The Sokolinskaya Formation sample, RAS98/6, contains an ultrastable heavy mineral assemblage, completely dominated by zircon (54%) and tourmaline (44%). The tourmaline grains are yellow and euhedral. The zircon grains show a mixed assemblage of rounded and euhedral grains, with some grains showing rod-like morphology.

The Early Cretaceous samples, T99/26 and T99/32, show very different heavy mineral assemblages in relation to the Permian samples and are dominated by the

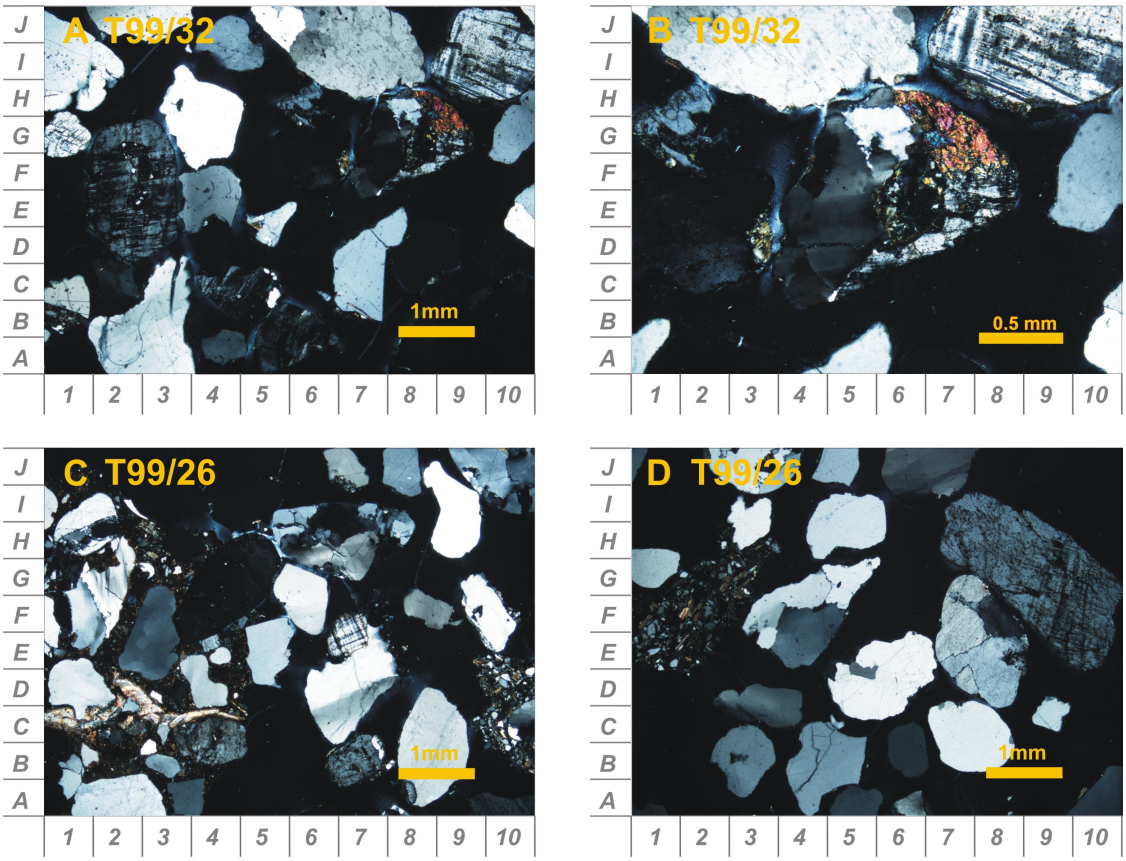

Figure 6.13: Photomicrographs of the Early Cretaceous samples. (A) General view of the poorly sorted, unconsolidated, subarkosic very coarse sand. Rounded microcline (F2) and undulose quartz (B3) grains are visible. (B) A rock fragment of undulose quartz and microcline show the sediment has experienced little weathering. (C) General view of the poorly sorted, unconsolidated, subarkosic very coarse sand. A rock fragment contains rounded grains in a muddy matrix, with some calcite cement (H1-B4). (D) Polycrystalline and undulose quartz grains are visible together with a rounded rock fragment.

unstable mineral staurolite (59-74%) (Fig. 6.14). Staurolite is a characteristic mineral of medium-grade metamorphic pelitic schists (Deer *et al.*, 1992). The samples also contain smaller amounts of zircon (11-15%), garnet (9-10%) and tourmaline (3-8%). Most zircon grains show euhedral, doubly vergent, magmatic, morphologies, although rounded grains are also present. Tourmaline grains are green and euhedral or rounded. Garnet grains in these samples are unetched.

Heavy mineral ratios

Some heavy mineral indices show distinct variation between the samples, whereas other indices seem to show random variation (Fig. 6.15). The seemingly random

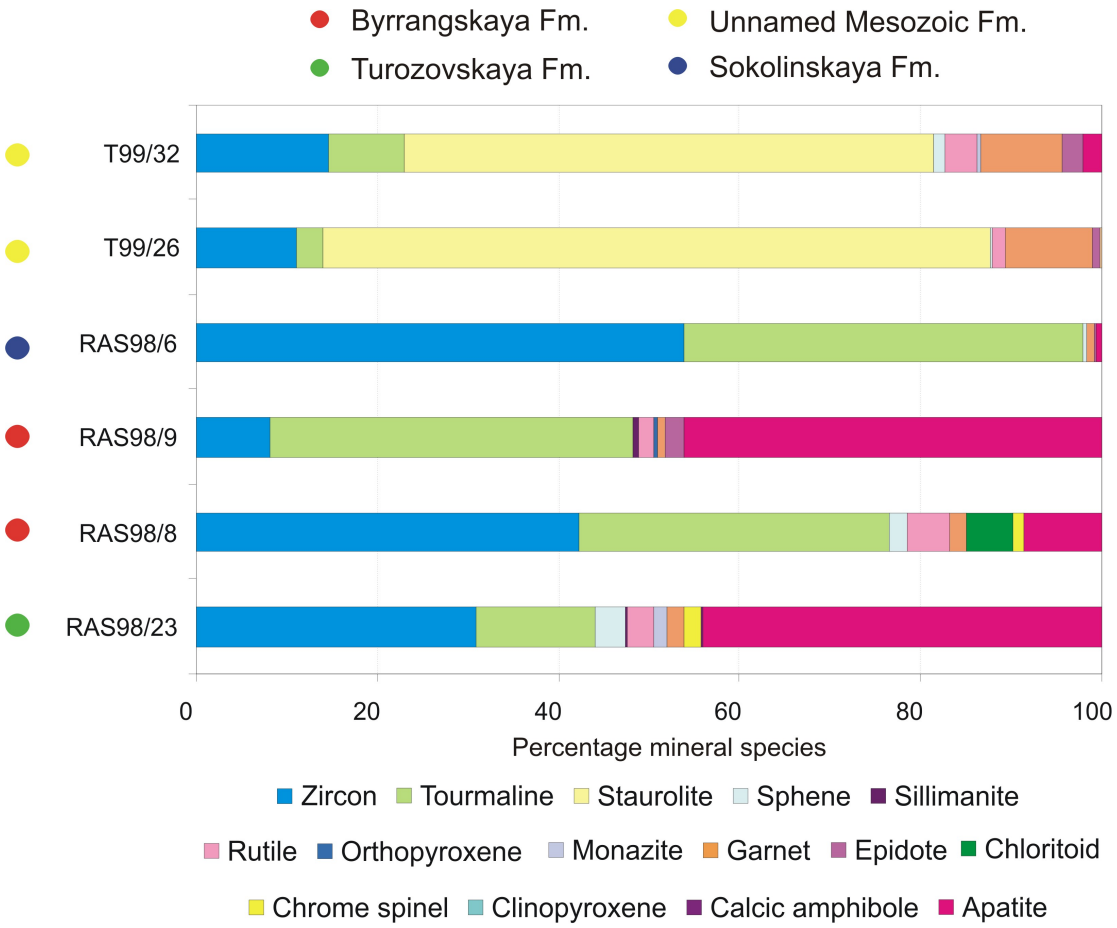

Figure 6.14: Taimyr samples heavy mineral assemblages, showing the relative importance of various heavy mineral species. The data are based on counting a minimum 300 heavy minerals.

variations seen in RuZi and ATi may be related to localized intrastratal dissolution. GZi and SZi show a marked increase from the Permian to the Cretaceous samples. This may represent a true provenance signal, or may indicate that less stable minerals have been dissolved from the Permian samples.

6.6 Garnet chemistry results

Cretaceous samples T99/26 and T99/32 were analysed for garnet chemistry. The results are virtually identical and are plotted together (Fig. 6.16). The complete dataset is included in the accompanying CD. The garnets in these samples are unetched, reducing the possibility that garnet dissolution occurred in these sediments, such that the garnet assemblage should be representative of the original

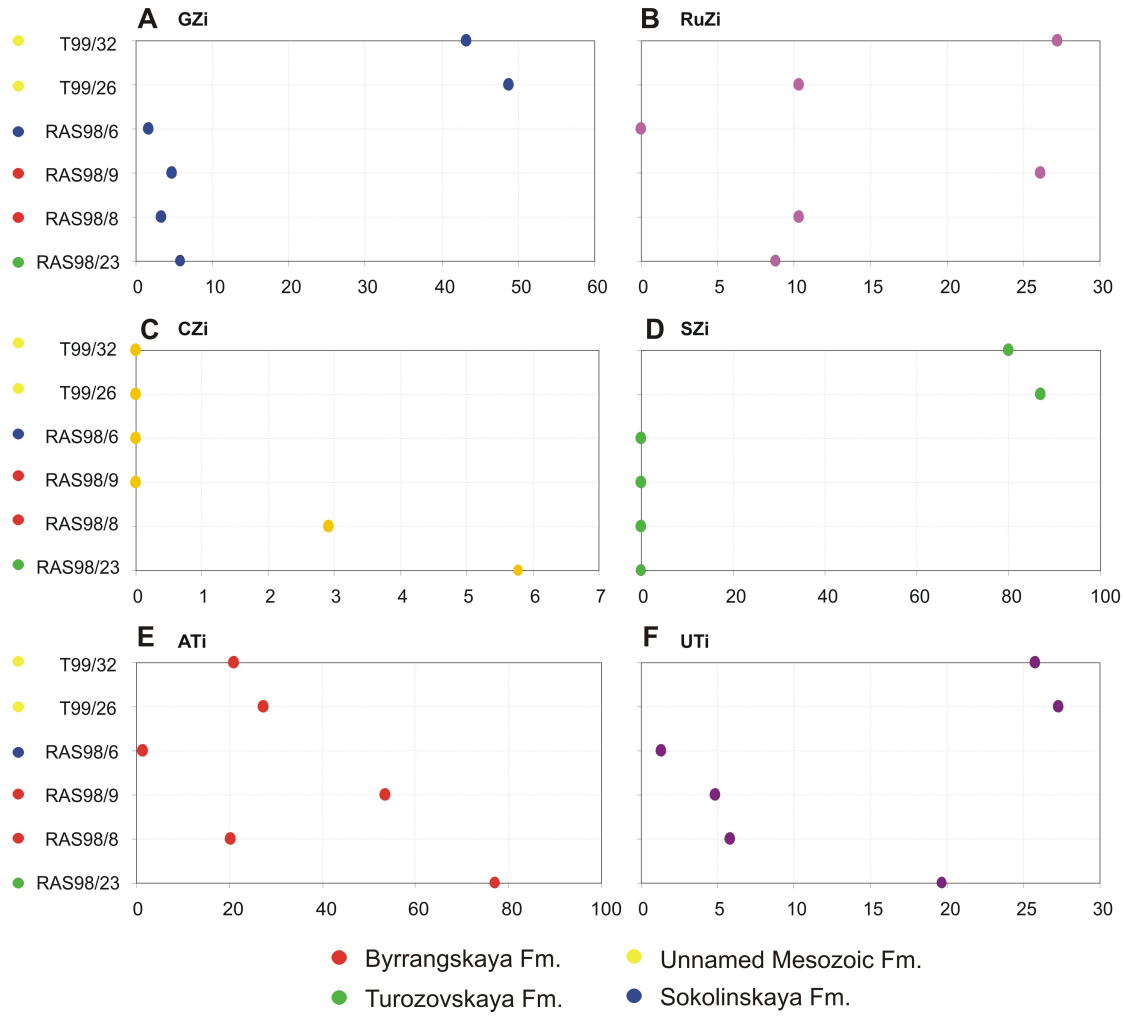

Figure 6.15: Taimyr samples heavy mineral ratios. Indices are calculated as: GZi=(garnet/(garnet+zircon))×100. (A) GZi (garnet-zircon index), showing marked increase in Cretaceous samples. (B) RuZi (rutile-zircon index), showing wide variability. (C) CZi (chrome spinel-zircon index), showing decrease in value with stratigraphic height. (D) SZi (staurolite-zircon index), showing marked increase in Cretaceous samples. (E) ATi (apatite-tourmaline index), showing wide variability. (F) UTi (unstable minerals-tourmaline index), showing marked increase in Cretaceous samples. Unstable minerals are amphibole, epidote and sphene.

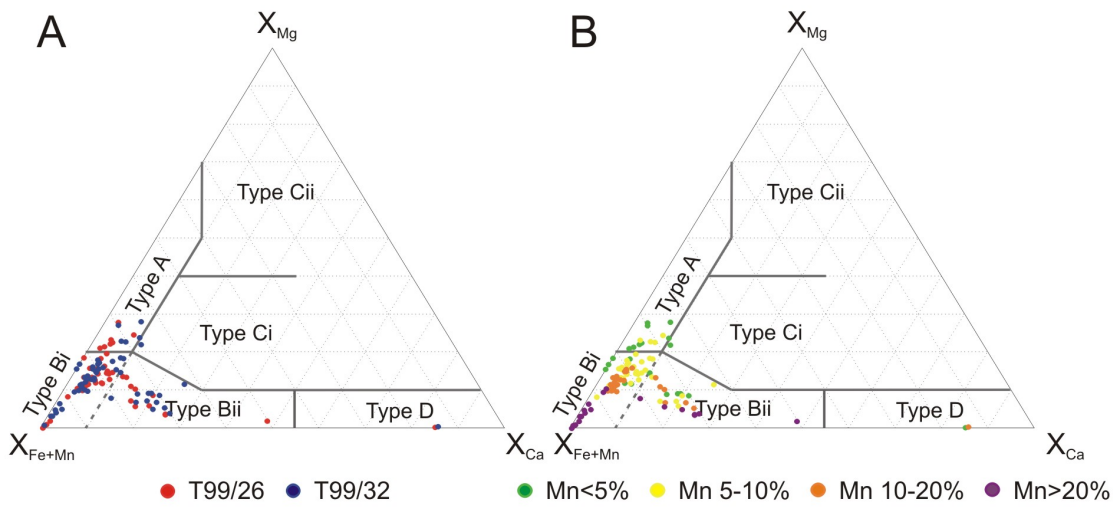

Figure 6.16: Garnet compositions of the Early Cretaceous samples, T99/26 and T99/32, shown on the garnet classification diagram of Morton *et al.* (2004). X_{Mg}, X_{Fe}, X_{Mn}, X_{Ca} = molecular proportions of Mg, Fe, Mn and Ca, with all Fe calculated as Fe^{2+} (A) The samples show very similar chemistry and mainly plot as type Bi and Bii garnets. (B) Garnet chemistry shows both almandine (Fe-rich garnet) and spessartine (Mn-rich garnet).

assemblage. The garnet chemistry is dominated by Fe and Mn, and plot predominantly as type Bi, and to a lesser degree type Bii and A, as defined by Morton *et al.* (2004). Type B garnets are sourced from amphibolite facies metasedimentary rocks (Bi, Bii) or intermediate-acidic igneous rocks (Bi). Type A garnets are sourced from high-grade granulite facies metasedimentary rocks and charnokites or from intermediate-acidic igneous rocks from deep crustal magmas. Two grains show Ca-rich garnet chemistry (type D), possibly sourced from metamorphosed calcareous sediments.

6.7 Tourmaline chemistry results

A subset of five samples were analysed for tourmaline chemistry (Table 6.1). The data are presented in Figures 6.17-6.19. The complete dataset is included in the accompanying CD.

The Turozovskaya and Byrrangskaya Formation samples, RAS98/23 and RAS98/8, show similar tourmaline chemistry and will be discussed together. On a Ca-Fe-Mg diagram, the samples plot in mainly fields 2 and 4, reflecting Li-poor granitoids, pegmatites and aplites (field 2) and metapelites, metapsammites and quartz tour-

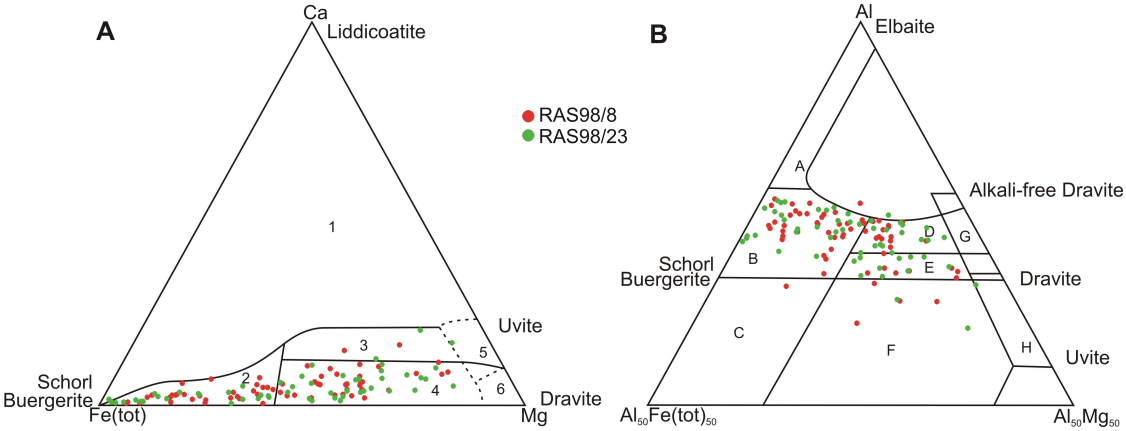

Figure 6.17: Tourmaline compositions of the Turozovskaya and Byrrangskaya formations plotted on discrimination diagrams of Henry & Guidotti (1985). (A) Field 2, Li-poor granitoids, pegmatites and aplites. Field 3, Ca-rich metapelites, metapsammites and calcsilicates. Field 4, Ca-poor metapelites, metapsammites and quartz tourmaline rocks. (B) Field B, Li-poor granitoids, pegmatites and aplites. Field D, Aluminous metapelites and metapsammites. Field E, Al-poor metapelites and metapsammites.

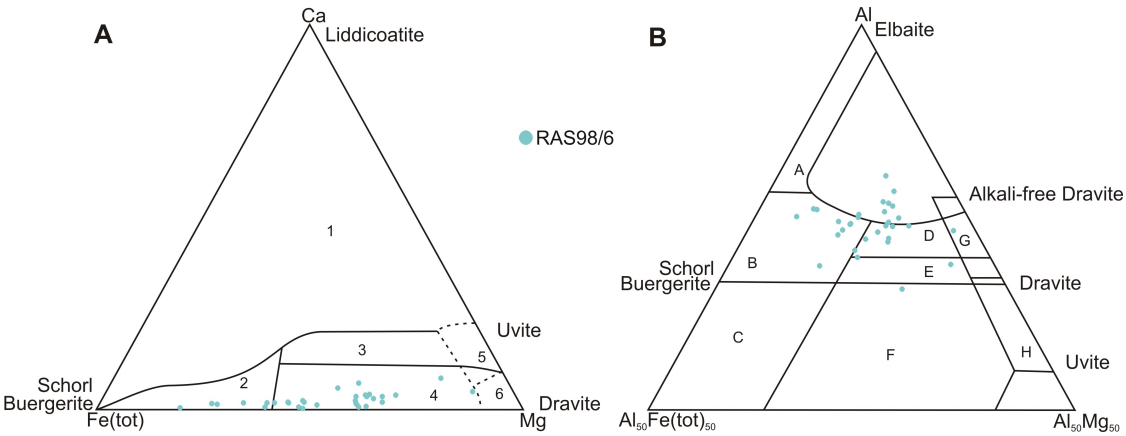

Figure 6.18: Tourmaline compositions of the Sokolinskaya Formation plotted on discrimination diagrams of Henry & Guidotti (1985). (A) Field 2, Li-poor granitoids, pegmatites and aplites. Field 4, Ca-poor metapelites, metapsammites and quartz tourmaline rocks. (B) Field B, Li-poor granitoids, pegmatites and aplites. Field D, Aluminous metapelites and metapsammites.

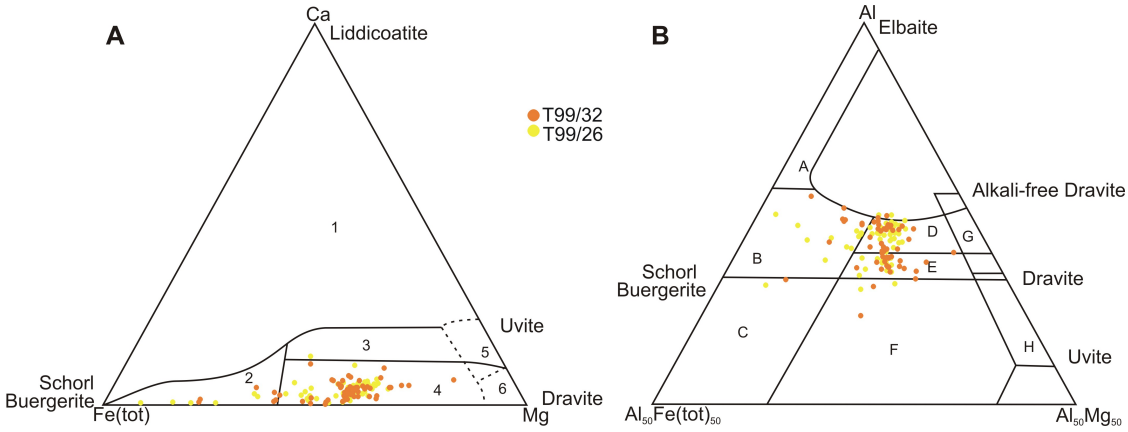

Figure 6.19: Tourmaline compositions of the Early Cretaceous samples plotted on discrimination diagrams of Henry & Guidotti (1985). (A) Field 2, Li-poor granitoids, pegmatites and aplites. Field 4, Ca-poor metapelites, metapsammites and quartz tourmaline rocks. (B) Field D, Aluminous metapelites and metapsammites. Field E, Al-poor metapelites and metapsammites.

maline rocks (field 4). On an Al-$Al_{50}Fe_{50}$-$Al_{50}Mg_{50}$ diagram the samples plot in fields B, D, and E, reflecting Li-poor granitoids, pegmatites and aplites (field B), aluminous (field D) and Al-poor (field E) metapelites and metapsammites (Henry & Guidotti, 1985).

The Sokolinskaya Formation sample, RAS98/6, shows similar tourmaline chemistry to the underlying formations. On a Ca-Fe-Mg diagram, sample RAS98/6 shows less Ca than the underlying formations, plotting in fields 2 and 4: Li-poor granitoids, pegmatites and aplites (field 2) and Ca-poor metapelites, metapsammites and quartz tourmaline rocks (field 4). On an Al-$Al_{50}Fe_{50}$-$Al_{50}Mg_{50}$ diagram, sample RAS98/6 shows more Al than underlying formations, plotting in fields B and D: Li-poor granitoids, pegmatites and aplites (field B), aluminous metapelites and metapsammites (field D) (Henry & Guidotti, 1985). Tourmaline grains in this sample plot outside the natural range of tourmaline chemistries, suggesting some alteration to the tourmaline grains. Sample RAS98/6 was located close to a sill, offering an explanation for this unusual chemistry.

The Early Cretaceous samples, T99/26 and T99/32, show less variation in tourmaline chemistry than underlying formations. On a Ca-Fe-Mg diagram, the samples plot mainly in field 4, Ca-poor metapelites, metapsammites and quartz tourmaline rocks, with some grains plotting in field 2 (Li-poor granitoids, pegmatites and aplites). On an Al-$Al_{50}Fe_{50}$-$Al_{50}Mg_{50}$ diagram, the samples plot in fields D and E, reflecting aluminous (field D) and Al-poor (field E) metapelites and metap-

sammites (Henry & Guidotti, 1985).

6.8 Zircon geochronology results

Detrital zircons from three samples were dated using LA-ICP-MS (Table 6.1). The data are presented in Figures 6.20-6.23. The complete dataset is included in the accompanying CD. U-Pb ages discussed here are within 10% of concordance unless otherwise stated. $^{206}Pb/^{238}U$ ages are quoted for ages younger than 1200 Ma; $^{207}Pb/^{206}Pb$ ages are quoted for ages older than 1200 Ma.

Byrrangskaya Formation sample RAS98/8 was analysed. In total, 130 grains were analysed, of which 103 yielded ages within 10% of concordance (Fig. 6.20). The sample shows a wide spread of zircon ages (Fig. 6.21). There are Paleoproterozoic ages (1904-1631 Ma) and a spread of Mesoproterozoic ages (1531-1404 Ma, 1310 Ma, 1040-989 Ma). A few Neoproterozoic ages are present (13 grains, 750-698 Ma, with a peak at 710 Ma; 20 grains, 688-568 Ma, with a peak at 583 Ma; three grains, 563-543 Ma, with a peak at 546 Ma). There are 27 Cambrian-Silurian grains (525-420 Ma, with peaks at 513, 479, 453 and 421 Ma) and six Devonian grains, with peaks at 395 and 366 Ma. There are two Carboniferous grains (318 Ma) and seven early-mid Permian ages, 294-267 Ma, with a peak at 280 Ma (Fig. 6.22). There are two isolated Triassic grains (239 and 227 Ma). These two analyses are disregarded due to their isolated ages. Thus the youngest age of the sample, determined by zircon ages, is interpreted as mid Permian age.

The morphology and internal structure of representative zircon grains is shown in cathodoluminescence images (Fig. 6.23) and show a range of morphologies, from rounded to euhedral, with many fragments. The youngest grains in the sample are Permian and show euhedral, magmatic morphology. Older zircon grains are rounded and show a mixture of magmatic and metamorphic internal structures.

Sokolinskaya Formation sample RAS98/6 was analysed. In total 120 grains were analysed, but only 37 grains yielded ages within 10% of concordance (Fig. 6.20). This sample yielded fewer Precambrian ages than sample RAS98/8. There are six Paleoproterozoic ages (1730-1631 Ma) and no Mesoproterozoic ages. There are a few isolated Neoproterozoic grains (854 and 793 Ma). There are 108 Paleozoic ages in this sample, of which only 29 are within 10% of concordance. The discordant peaks mirror the ages of the concordant peaks (Fig. 6.21). Within 10% concordance there are seven Ordovician grains (492-449 Ma, forming a peak at 451 Ma) and five Silurian-Devonian grains (429-396 Ma, forming a peak at 397 Ma) (Fig. 6.22). Associated with the Silurian-Devonian peak is a discordant peak of 14 grains,

centred at 392 Ma. The sample shows isolated Carboniferous grains (341, 336 and 302 Ma) that are also associated with discordant ages. There are six Permian ages within 10% concordancy, forming a peak at 285 Ma and 21 discordant ages, forming peaks at 285 and 266 Ma. Three grains within 10% concordancy yield ages around the Permian-Triassic boundary (∼250 Ma). There is a large, slightly younger discordant peak (28 grains, 230 Ma). The sample contains three isolated Triassic-Jurassic grains (221, 202, 145 Ma), along with a discordant peak at 180 Ma. It is difficult to provide a stratigraphic age for this sample based on zircon data due to the isolated nature of the young grains. However, the youngest robust zircon age peak composed of grains within 10% concordancy is centred at the Permo-Triassic boundary and thus sample RAS98/6 is tentatively interpreted to be deposited approximately at the Permo-Triassic boundary. This sample was in close proximity to a Permo-Triassic sill, providing an explanation for the major discordancy of the sample (Robert Scott, pers. comm).

The morphology and internal structure of representative zircon grains is seen in the cathodoluminescence images in Figure 6.23. The concordant zircons in the sample show a variety of external morphologies, throughout the entire age range, included rounded to euhedral grains, and commonly grain fragments. Internal structures are commonly magmatic. The discordant grains in the sample show the same morphology and structure, although a larger proportion of these grains are euhedral and magmatic.

Early Cretaceous sample T99/26 was analysed. In total, 116 grains were analysed, of which 91 yielded ages within 10% of concordance (Fig. 6.20). The sample is dominated by young, Permo-Triassic zircons. There are eight Neoproterozoic-Cambrian grains, (610-508 Ma, forming a peak of seven grains at 584 Ma) (Figs. 6.21 and 6.22). There are five Carboniferous grains (362-328 Ma, forming a peak at 334 Ma). The Permo-Triassic peak consists of 69 grains, 286-237 Ma, forming a peak at 262 Ma. There is a younger Triassic peak of five grains, 230-222 Ma, centred at 229 Ma.

The morphology and internal structure of representative zircon grains is seen in the cathodoluminescence images in Figure 6.23. The Neoproterozoic-Cambrian grains and Carboniferous grains show rounded to near-euhedral morphology, mostly showing complex magmatic zoning. The Permo-Triassic grains show predominantly perfectly euhedral morphology, with complex magmatic zoning. Most grains show doubly vergent grain morphology, typical of high and low temperature plutonic magmas.

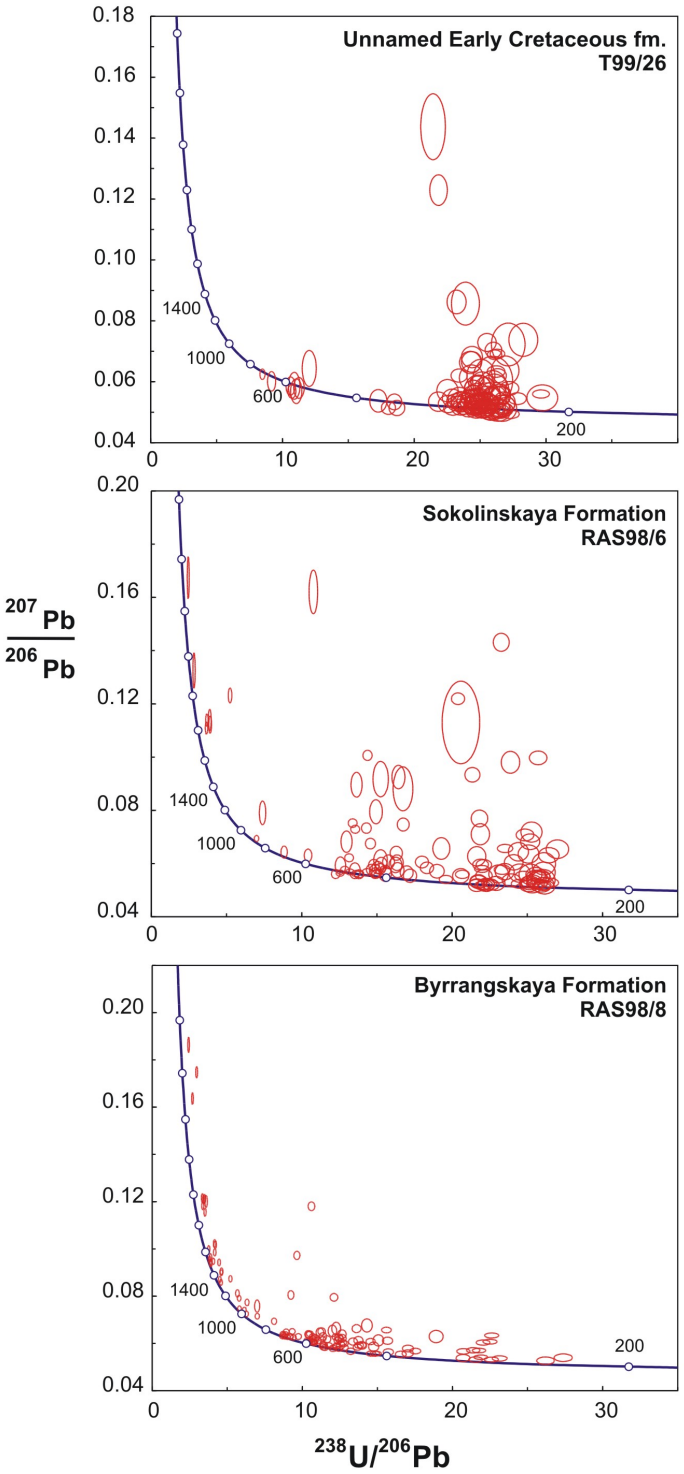

Figure 6.20: Tera-Wasserberg concordia diagram for Taimyr samples. The data have not been common lead corrected. Data point ellipses are 2σ.

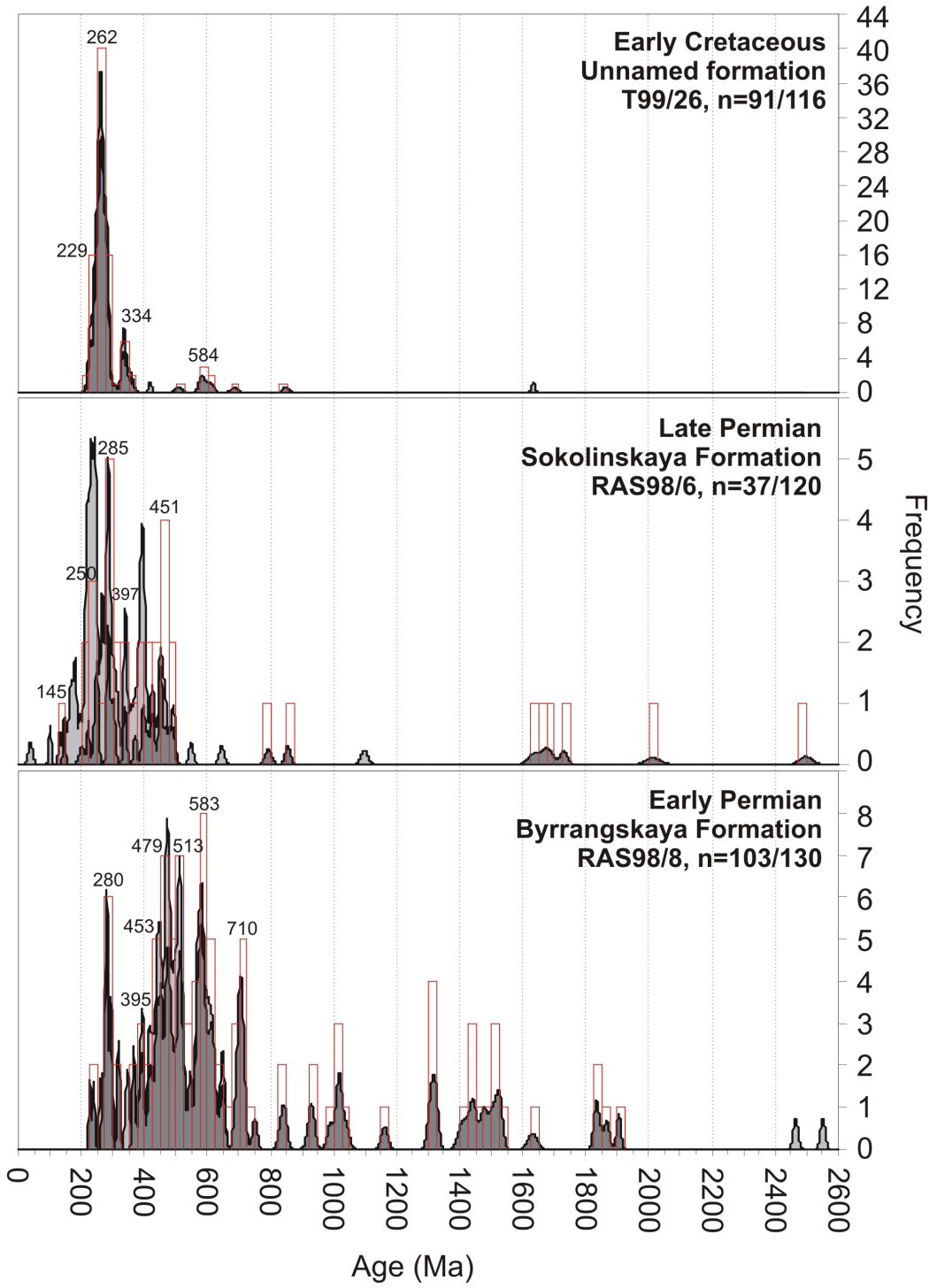

Figure 6.21: Cumulative frequency diagrams with histograms of U-Pb detrital zircon ages from the Taimyr Peninsula. U-Pb age with 1σ uncertainty is shown. Ages younger than 1200 Ma are $^{206}Pb/^{238}U$ ages. Ages older than 1200 Ma are $^{207}Pb/^{206}Pb$ ages. Ages with 90-110% concordancy are shown by histograms and dark grey cumulative frequency curves. More discordant data are shown by pale grey cumulative frequency curves. N denotes the number of analyses with 90-110% concordancy relative to all analyses.

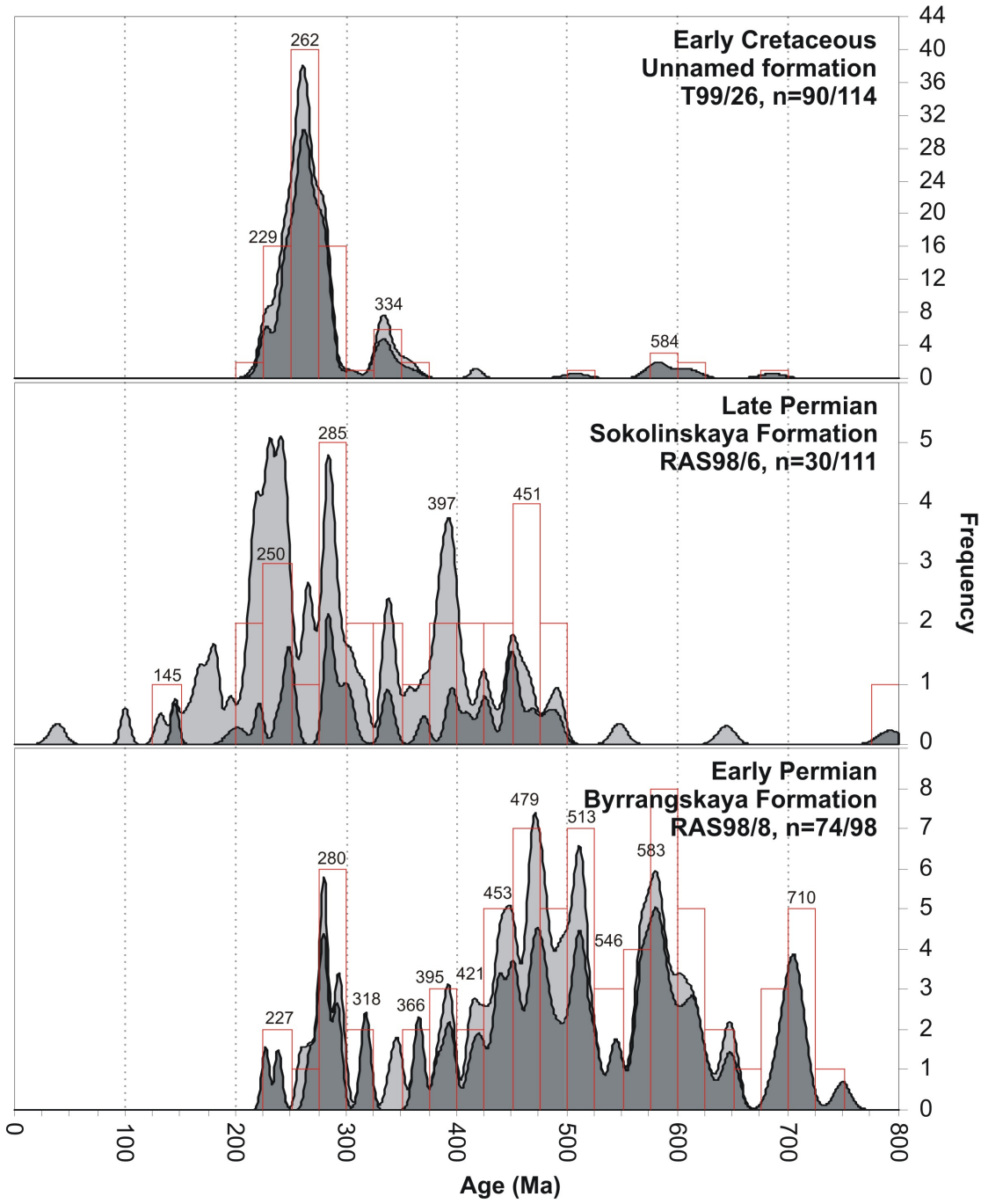

Figure 6.22: Phanerozoic-Neoproterozoic cumulative frequency diagrams with histograms of U-Pb detrital zircon ages from the Taimyr Peninsula. U-Pb age with 1σ uncertainty is shown. Ages are $^{206}Pb/^{238}U$ ages. Ages with 90-110% concordancy are shown by histograms and dark grey cumulative frequency curves. More discordant data are shown by pale grey cumulative frequency curves. N denotes the number of analyses with 90-110% concordancy relative to all analyses.

Figure 6.23: Cathodoluminescence images of Taimyr samples showing morphology and internal structure of representative zircon grains. U-Pb age, with 2σ uncertainty, is shown for each analysis. Ages younger than 1200 Ma represent $^{206}Pb/^{238}U$ ages. Ages older than 1200 Ma represent $^{207}Pb/^{206}Pb$ ages. Analytical spots are indicated by circles.

6.9 Summary of results

Turozovskaya and Byrrangskaya Formations

The Turozovskaya and Byrrangskaya Formation samples are characterized as sublitharenites and plot within the 'recycled orogenic' fields on QtFL and QmFLt diagrams. The samples contain a mixture of monocrystalline quartz (undulose and non-undulose), typical of plutonic rocks, and polycrystalline quartz, with four or more subgrains, typical of low-grade metamorphic rocks. The heavy mineral assemblages of the samples are ultrastable and dominated by mixed populations of apatite, zircon and tourmaline, with some chrome spinel, suggesting input from an ultramafic source. Tourmaline chemistry suggests source areas of granitoids-pegmatites and metasedimentary rocks. Zircon data from the Byrrangskaya Formation are robust and show a spread of ages from Paleoproterozoic though mid Permian time, with the majority of grains of Neoproterozoic and Paleozoic age.

Sokolinskaya Formation

The Sokolinskaya Formation samples are characterized as arkosic arenites and plot within the 'uplifted continental block' and 'transitional magmatic arc' fields on QtFL and QmFLt diagrams. The samples contain mostly polycrystalline quartz grains with four or more subgrains and some non-undulose monocrystalline quartz, suggesting derivation mainly from a low-grade metamorphic source terrane with lesser amounts of plutonic material. The samples contain plagioclase with 30% anorthite, typical of metamorphic terranes and microcline, characteristic of slowly-cooled plutonic rocks. The sample contains an ultrastable heavy mineral assemblage, dominated by zircon and tourmaline. Tourmaline chemistry suggests source areas of granitoids-pegmatites and metasedimentary rocks. Zircon data from the Sokolinskaya Formation are largely discordant, presumably due to proximity of the sample to a Permo-Triassic age dolerite sill. There are grains from Paleoproterozoic through late Permian age, with the majority of grains of Paleozoic age.

Early Cretaceous samples

The Early Cretaceous samples are characterized as subarkoses and plot within the 'continental block' fields on QtFL and QmFLt diagrams. These very coarse-grained samples contain predominantly non-undulose monocrystalline quartz grains, representative of a plutonic quartz source. Feldspar compositions are predominantly alkali feldspar, suggesting a plutonic source. The heavy mineral fraction analysed

is from a different size fraction (fine-grained sand versus very coarse-grained sand) such that the grains may be providing different sediment provenance information. The heavy mineral assemblage of the samples is dominated by staurolite, clearly indicating a low-grade metamorphic source. Zircon and tourmaline grains have a euhedral shape, suggesting local derivation. Zircon grains are mostly doubly vergent magmatic grains. Garnet is present in these samples and the chemistry shows the likely source to be amphibolite-granulite facies metasedimentary rocks, although a component of intermediate-acidic igneous rocks cannot be ruled out. Tourmaline chemistry shows derivation mainly from metasedimentary rocks, with some possibly from acidic igneous rocks. Zircon data from sample T99/26 are robust and are dominated by a Permo-Triassic peak. There are few Precambrian zircons in this sample.

6.10 Discussion

The southern Taimyr Permo-Carboniferous succession was deposited during the late stages of the Uralian Orogeny. Likely source areas for this succession are the Urals Orogen to the north from North Taimyr and Severnaya Zemlya, or from west-southwest areas of the Urals Orogen possibly buried beneath the southern Kara Sea and/or West Siberian Basin. The sedimentological data indicate that the Permo-Carboniferous sediments are derived from a variety of source rocks: microcline-bearing plutonic rocks, low-grade metamorphic rocks and mafic-ultramafic igneous rocks (based on the presence of chrome spinel in some samples).

Zircon data from the Byrrangskaya Formation show a wide spread of ages, with Permian, euhedral, magmatic grains and older, mixed-morphology grains. Some age clusters found in this sample have known sources on the Taimyr Peninsula. The sample preserves Uralian age grains: Carboniferous and early-mid Permian (318, 294-267 Ma, with a peak at 280 Ma). Collisional granites of this age have been sampled on Northern Taimyr (Pease, 2001; Vernikovsky *et al.*, 1995). Paleoproterozoic ages (∼1900-1830 Ma) are recognized from Central Taimyr granite-gneisses (Vernikovskaya, 2001) and may have been recycled during Uralian orogeny in Taimyr. Neoproterozoic ages forming a peak at 710 Ma may correspond to intrusive and extrusive island arc volcanism recorded from North Taimyr (Pease & Persson, 2006), which may also account for the presence of chrome spinel in these samples.

However, the dominant cumulative probability peaks in sample RAS98/8 are Late Neoproterozoic through Silurian age (688-420 Ma), most consistent with local

derivation from Timanide and Caledonian sources of northeastern Baltica (Gee & Pease, 2004 and references therein). The ages presented here are similar to ages reported by Pease & Scott (2009) for Cambro-Ordovician sediments from North Taimyr, which demonstrated that the Kara Block (Severnaya Zemlya and North Taimyr) was a part of Baltica in the early Paleozoic. The Kara Block collided with South and Central Taimyr during Uralian orogeny (Vernikovsky *et al.*, 1995) and it is highly likely that the Kara Block sedimentary succession preserving Timanide and Caledonian-derived sediments were recycled during orogensis and deposited in South Taimyr. Meso-Neoproterozoic grains found in this sample (1040-989 Ma) correspond to the age of the Grenvillian Orogeny (Li *et al.*, 2008; Rivers, 1997), present in northwestern Baltica and provide further evidence for a Baltica derivation for a component of this sediment.

The Sokolinskaya Formation sedimentological characteristics are similar to underlying formations, with evidence of plutonic and low-grade metamorphic sediment sources. However, 70% of zircon grains in sample RAS98/6 yield U-Pb ages more than 10% discordant, probably due to hydrothermal alteration of the sediment by close proximity to thick dolerite sills. Sample RAS98/6 shows a scarcity of Precambrian ages compared to the underlying Byrrangskaya Formation sample. Importantly, Late Neoproterozoic-Cambrian ages sourced from the Timanian Orogen and dominant in Byrrangskaya Formation sample RAS98/6, are largely absent from this sample.

Ordovician-Silurian grains (492-396 Ma) present in this sample may suggest derivation from the Caledonian Orogen although the older grains may alternatively correspond to ∼490 Ma metagranites present in the Polar Urals (Glodny *et al.*, 2004). Permo-Carboniferous ages present are consistent with a Uralian source for this sediment. The Permian peak present in this sample (285 Ma) is similar to sample RAS98/8 and may suggest a North Taimyr collisional granite source for these grains (Pease, 2001; Vernikovsky *et al.*, 1995). However, the lack of Timanide grains in this sample argues for a different Uralide source for this formation. The southern and central terranes of Taimyr Peninsula do not contain basement of Timanide origin and is considered a likely candidate. The sample preserves three zircon grains dated to the Permo-Triassic boundary. Zircons of Permo-Triassic boundary U-Pb age have been reported from gabbros on the New Siberian Islands (Kuzmichev & Pease, 2007) and although relatively scarce in the Siberian Traps, are present in minor amounts, for example in the Norilsk 1 leucogabbro (Kamo *et al.*, 1996).

During Triassic time, the Taimyr Peninsula underwent dextral transpression with associated uplift and erosion. There are no Early Triassic-Pliensbachian sediments preserved on the Taimyr Peninsula and in South Taimyr, North Taimyr and Severnaya Zemlya, Toarcian sediments unconformably overlie deformed Neoproterozoic-Permian strata.

The Early Cretaceous samples are unconsolidated and show an immature heavy mineral assemblage. Staurolite, a low-grade metamorphic index mineral, dominates the sediment. Garnet and tourmaline chemistry also suggest a low-grade metamorphic source for this sediment. However,the zircon population is dominated by euhedral, magmatic zircons and the sediment contains abundant microcline, evidence of a felsic plutonic source. The euhedral and immature character of the mineral assemblage suggests a proximal source for this sediment.

The zircon data are dominated by a robust Permo-Triassic peak, 286-237 Ma with the main peak at 262 Ma. These magmatic, euhedral zircons may reflect Siberian Trap magmatism on Taimyr and nearby islands. Known sources for zircons of this age include gabbros on the New Siberian Islands (Kuzmichev & Pease, 2007), granites in Central and North Taimyr and syenites on islands in the Eastern Barents Sea (Vernikovsky *et al.*, 2003). This sample contains some older zircon grains: Neoproterozoic-Cambrian ages (610-508 Ma), corresponding in age with magmatic events with the Timanian Orogen, and Carboniferous grains (362-328 Ma), likely corresponding to events within the Uralian Orogen. These older grains are consistent with local derivation of these sediments.

The unconsolidated nature of the Early Cretaceous sediments show they have not been buried or deformed since their Early Cretaceous deposition. Apatite fission track analyses, carried out on samples T99/26 and T99/32 by Andrew Carter of University College London, shows that the sediments and their source rocks have not been heated above 50°C since Late Triassic time (ca. 210 Ma) (Fig. 6.24).

6.11 Conclusions

The Permian samples show a mixed provenance of recycled and first cycle sediment, sourced from metamorphic and igneous terranes. Zircon data show a mixture of Precambrian-Paleozoic ages and euhedral, contemporaneous Permian grains. The Byrrangskaya Formation shows local derivation from Taimyr, with a large component of sediment recycled from the Kara Block, showing ultimate Baltica provenance. The Sokolinskaya Formation lacks the Kara Block Timanian-Caledonian signature, but shows Uralian provenance. A minor Siberian Trap signature is also

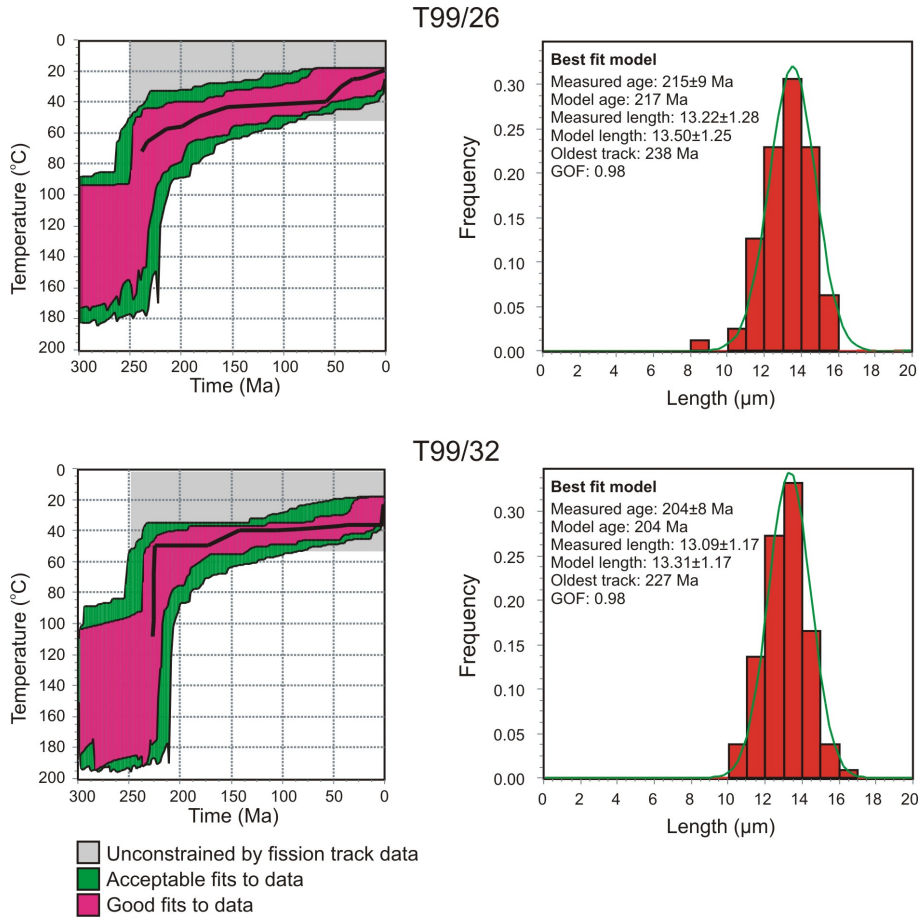

Figure 6.24: Apatite fission track data for Early Cretaceous samples T99/26 and T99/32. The data were generated by Andrew Carter, University College London.

present possibly indicating derivation from the Uralides west of the Taimyr Peninsula. The Early Cretaceous formation shows a mixed, mainly first cycle, metamorphic and igneous provenance and an unstable heavy mineral assemblage dominated by staurolite. The zircon ages are almost exclusively Siberian Trap age. The immature nature suggests local derivation of this sediment, either directly from the Taimyr Peninsula or eastern Urals.

Some conclusions of regional significance should be noted. Pease & Scott (2009) showed that the Kara Block was a part of Baltica from at least early Paleozoic time and probably became attached to the northeastern margin of Baltica during the late Neoproterozoic Timanian Orogeny. This was shown by the presence of Late Neoproterozoic-Cambrian (Timanian age) and Ordovician-Silurian (Caledonian age) zircons in Early Paleozoic sediments of North Taimyr and Novaya Zemlya.

The extent and nature of the Timanian Orogeny has not been extensively stud-

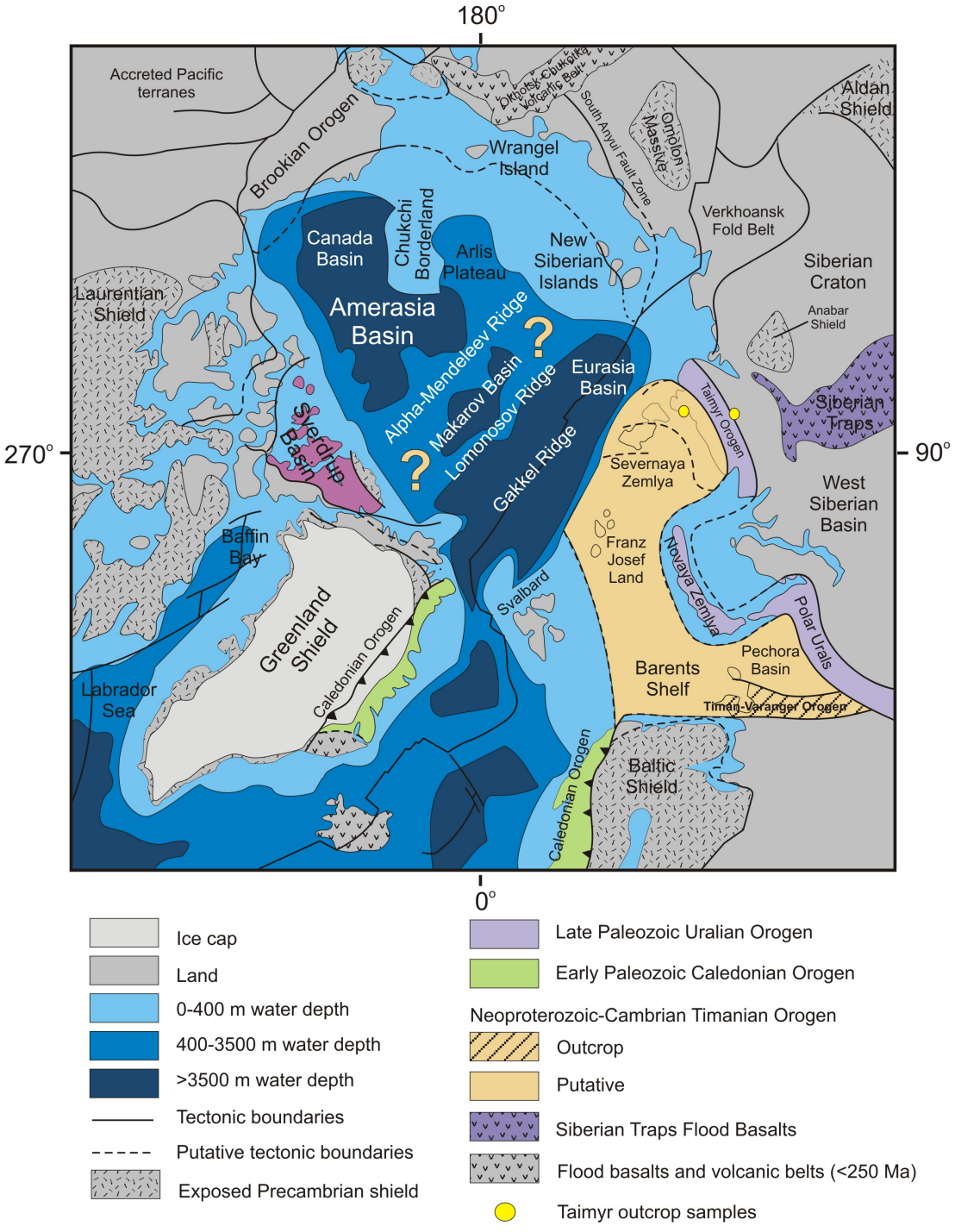

Figure 6.25: Tectonic map of the Arctic region. Bathymetry and topography are modified after the IBCAO Arctic Bathymetry database (Jakobsson *et al.*, 2008). Plate boundaries and geological features are modified after Harrison (2005). Neoproterozoic and younger orogenic belts on land are shown with different shadings. The suggested extent for the Neoproterozoic Timanian Orogeny is illustrated.

ied. It occurs within Uralian thrust sheets in the Ural mountains, along the southern margin of the Pechora Basin, within the Timan mountains of Russia (type section) and along the northern coast of Scandinavia (Fig. 6.25). The extent and nature of the Timanian Orogen beneath the Barents Shelf is poorly known, but Timanian-derived detritus on Novaya Zemlya and Taimyr suggests that the orogen may also be important across the Barents Shelf. Figure 6.25 illustrates the suggested extent of the Timanian Orogen on the Barents Shelf, from the poorly known Early Paleozoic Caledonian suture (Baltica-Laurentia boundary) in the west, to the Late Paleozoic Uralian Orogen (Baltica-Siberia boundary) in the east and the edge of the Barents Shelf to the north. It also suggests that crust affected by the Late Neoproterozoic Timanian Orogeny may underly putative stretched continental crust of the Central Arctic region and possibly beyond. Similarly, the extent of the Caledonian and Uralian orogenies north of the Barents Shelf are poorly understood and merit further study. A better understanding of these events is key for understanding the pre-Cenozoic evolution of the Arctic region.

Detrital zircon ages in the Early Cretaceous sediments fall almost exclusively into one Late Permian-Early Triassic cluster: Siberian Trap age. It is often suggested that zircons of ∼252 Ma would not be sourced from areas associated with the Siberian Large Igneous Province as zircon-bearing source lithologies are typically scarce in a basaltic province. The data presented here from the Early Cretaceous sediments, as well as Permo-Triassic boundary age igneous zircons reported by Vernikovsky *et al.* (2003) and Kuzmichev & Pease (2007) in granites and gabbros suggest that Eurasian Arctic Russian region can be considered as a unique source for zircons of Permo-Triassic age. This area is the only known source of Permo-Triassic boundary age zircons in the Arctic.

Chapter 7

Discussion

Sediment provenance results for Paleozoic and Mesozoic sandstones have been presented from four areas: northern Sverdrup Basin, Svalbard, southwestern Barents Shelf and Taimyr (Fig. 7.1). Two main sand types are recognized (sand types 1 and 3), in addition to a less common sand type (type 2) (Fig. 7.2). The Mesozoic succession of Axel Heiberg Island, northern Sverdrup Basin, shows sand types 1, 2 and 3. The Mesozoic successions of Svalbard and the southwestern Barents Shelf show sand types 1 and 3. Permo-Carboniferous and Cretaceous samples from the Taimyr Peninsula show sand type 1.

In the Sverdrup Basin and on Svalbard and the Barents Shelf, sand type 1 predominated during Triassic time. In the Sverdrup Basin sand type 1 remained dominant throughout Jurassic time, with the exception of the deltaic Heiberg Formation (sand type 2). During Jurassic time, sand type 3 became the dominant sand type in the Sverdrup Basin, on Svalbard and on the southwestern Barents Shelf. During Early Cretaceous time, there was widespread volcanic activity and uplift in the high Arctic and sand type 1 became the dominant sand type again.

Sand type 1

Sand type 1 is characterized by subarkosic composition and an unstable heavy mineral assemblage, dominated by apatite and chloritoid, with lesser chrome spinel. Samples contain principally Paleozoic-Neoproterozoic zircon grains (Fig. 7.3). Based on zircon data, sand type 1 is interpreted to be derived from the Urals and Taimyr Peninsula, with additional material from the Caledonides and Timanides (Fig. 7.1). These areas are the only known major sources in the Arctic for late Neoproterozoic-Cambrian age zircons (Timanian event) or Devonian-Permian age zircons (Uralian event).

Sand type 1 was deposited on the Barents Shelf and Svalbard during Triassic time. This is consistent with uplift and subsequent erosion of the Urals during and after orogenesis and uplift and erosion of areas affected by Siberian Trap magmatism at the Permo-Triassic boundary. The northern Sverdrup Basin was also receiving sediment from the Uralian-Siberian source during Triassic through Middle Jurassic time. Material of presumed sand type 1 composition also composes the Late Triassic succession of Franz Josef Land (Vasilyev Formation and Thegetthoff Formation) (V. Pease, pers. comm.).

Miller *et al.* (2006) reported Triassic samples containing zircons of Late Mesoproterozoic (1300-1000 Ma), Late Neoproterozoic-Silurian (580-420 Ma), Devonian (390-340 Ma), Permo-Carboniferous (320-280 Ma) and Permo-Triassic (265-235 Ma) age, deposited in Chukotka, Wrangel Island and the Lisburne Hills of western Alaska. They interpreted a Uralian-Taimyr sediment source, which suggests that a large amount of sediment was sourced from the Urals-Taimyr area during Triassic time.

Miller *et al.* (2006) also reported on a Triassic sample from the Verkhoyansk Mountain Belt containing Cambro-Silurian (505-410 Ma) and Permo-Carboniferous (320-265 Ma) zircons. This sample was interpreted to be derived from the Baikal Mountain Range (southern Siberian craton). However, it should be noted that the zircon ages of this sample are very similar to other samples interpreted to be derived from the Urals-Taimyr region.

Sand type 2

Sand type 2 is encountered in only one sample: Pliensbachian (Early Jurassic) Heiberg Formation sample C403752 from Axel Heiberg Island, northern Sverdrup Basin. This sample is quartz arenitic in composition and contains an ultrastable heavy mineral assemblage, dominated by zircon, tourmaline and rutile. The Heiberg Formation was deposited from deltas prograding into the Sverdrup Basin from the east and south (Embry, 1982). The sample contains principally Neoproterozoic zircon grains (Fig. 7.3) and is interpreted to be derived from the Timanian Orogen, the only known tectonic event of that age in the Arctic region.

Sand type 3

Sand type 3 is characterized by quartz arenitic composition and a stable heavy mineral assemblage, dominated by zircon, tourmaline and rutile, with occasional

garnet. Samples contain principally Proterozoic and Archean zircon grains (Fig. 7.4).

In this study, sand type 3 is described from Jurassic and Cretaceous sediments in the northern Sverdrup Basin, Svalbard and the southwestern Barents Shelf. The striking similarities in zircon ages between these samples strongly argue for the same source for these samples (Fig. 7.4); a source of predominantly Archean (∼2900-2600) and Proterozoic (∼2100-900) zircon grains, with occasional ∼435 Ma zircon grains. Possible source areas are the Canada-Greenland Shield and Baltic Shield. The zircon ages presented are roughly consistent with derivation from either shield. However, the Baltic Shield provides a better match as late Paleoproterozoic (1700-1600 Ma) and Early Mesoproterozoic (1600-1300 Ma) zircons are rare in the Greenland-Canada Shield. Given a Baltica source, the zircon ages seen in sand type 3 represent Baltic Archean craton formation (3100-2500 Ma), the Svecofennian Orogeny (2000-1860 Ma), the Transscandinavian Igneous Belt (1850-1550 Ma) and the Sveconorwegian Orogeny (1760-900 Ma) (e.g. McNicoll *et al.*, 1995).

The Jurassic-Cretaceous Realgrunnen Subgroup and Adventdalen Group succession of the southwestern Barents Shelf shows a sand type 3 provenance. These samples were deposited on the northern margin of the Baltic Shield, along the Finnmark Platform and in the Hammerfest and Nordkapp basins. They are described to have a southerly provenance. The proximity of these samples to the Baltic Shield clearly argues for a Baltica affinity for these samples.

Mørk *et al.* (1999) and references therein present facies and stratigraphic evidence to suggest that clastic sediment deposited on Svalbard during Jurassic-Early Cretaceous time was westerly, northerly or northwesterly derived: not southerly derived, as implied by a Baltica source. However, the zircon data collected from the Middle Jurassic Brentskardhaugen Bed and Early Cretaceous Helvetiafjellet Formation samples argue strongly for a Baltica source for this sediment. Not all Mesozoic sedimentary units were sampled and it is possible that they show a different provenance (for example the Wilhelmsøya Subgroup). However, an alternative explanation is that the sand type 3 samples described here are indeed northerly derived and that the northern source area (presumably putative crust flooring the Central Arctic Ocean) has a Baltic Shield affinity or is covered by sediment with a Baltica Shield affinity (possibly shed off Baltica in response to the Caledonian Orogeny). Colpron & Nelson (2009) argue for the presence of Baltica affinity crust in the Central Arctic region and suggest that the exotic Pearya Terrane, northern Ellesmere Island, represents one such Baltica fragment.

The provenance of the Late Jurassic to Early Cretaceous sediments from the northern Sverdrup Basin are generally described as being southerly derived (e.g. Embry, 1991a) and thus a Canada-Greenland source is a likely candidate source area for this succession. Zircon ages from these samples are more consistent with Baltica derivation, however. Clastic sediment sourced from the south may be from the Canada-Greenland Shield or the Devonian clastic wedge, shed on to the Laurentian continent from the north following Ellesmerian tectonic events along the northern margin of the Canadian Arctic Islands (northern margin of Laurentia). The source of this clastic wedge is unclear, although McNicoll *et al.* (1995) have suggested that the detrital zircon ages from the clastic wedge sediments prove an excellent fit with Baltica derivation. However, they decided that Greenland was a more likely source area due to its proximity. Alternatively, these sediments could be directly derived from the north of the Sverdrup Basin.

Samples with identical zircon ages (sand type 3) have been described by Røhr *et al.* (2008) (Early Cretaceous sandstone from the Wandel Sea Basin, North Greenland) and by Miller *et al.* (2006) (Early Triassic Bjorne Formation sandstone from the southern margin of the Sverdrup Basin). Røhr *et al.* (2008) interpreted the sediment to be derived from the Greenland Shield, although they did concede that the presence of late Paleoproterozoic and Mesoproterozoic ages in these samples were difficult to explain from the Greenland-Canada Shield. Miller *et al.* (2006) interpreted the Bjorne Formation sample to be derived from the Greenland-Canada Shield.

Arctic region tectonic evolution

Figure 7.5 summarizes the sediment provenance findings presented in this study. The observation that the Uralian Orogen, Taimyr Peninsula and Siberian Trap areas were an important Arctic region sediment source prior to the opening of the Amerasia Basin has important implications for the validity of Arctic Ocean opening models. In particular, a Uralian sediment source to the Sverdrup Basin and the East Siberian Shelf is not consistent with a rotational opening model for the entire Amerasia Basin, as suggested by many workers (Fig. 2.5). In this model, the source areas mentioned would be far removed from Arctic basins where this sediment is found (Fig. 7.6).

Instead, an alternative model is proposed, which better explains the location of clastic sediment derived from the Uralian Orogen, Taimyr Peninsula and Siberian Trap areas (Fig. 7.7). This model shares similarities with the model presented by Miller *et al.* (2006) in suggesting a complicated opening of the Central Arctic

Ocean. However, the model presented here reconstructs Chukotka closer to the Taimyr Peninsula. This model predicts that the Canada Basin opened by rotational opening, around a pole in the Mackenzie Delta region, but that the Central Arctic Ocean opened by a more complicated mechanism. This model depicts a continental Alpha-Mendeleev Ridge, reconstructing back to the Lomonosov Ridge. It is considered likely that the Alpha-Mendeleev and Lomonosov ridges are underlain by Baltica affinity crust. The model presented here calls for a mainly extensional opening of the Central Arctic Ocean. This can explain the extensional features seen in the Lomonosov Ridge, Alpha-Mendeleev Ridge and the Chukchi Borderland (Lawver *et al.*, 1990 and references therein).

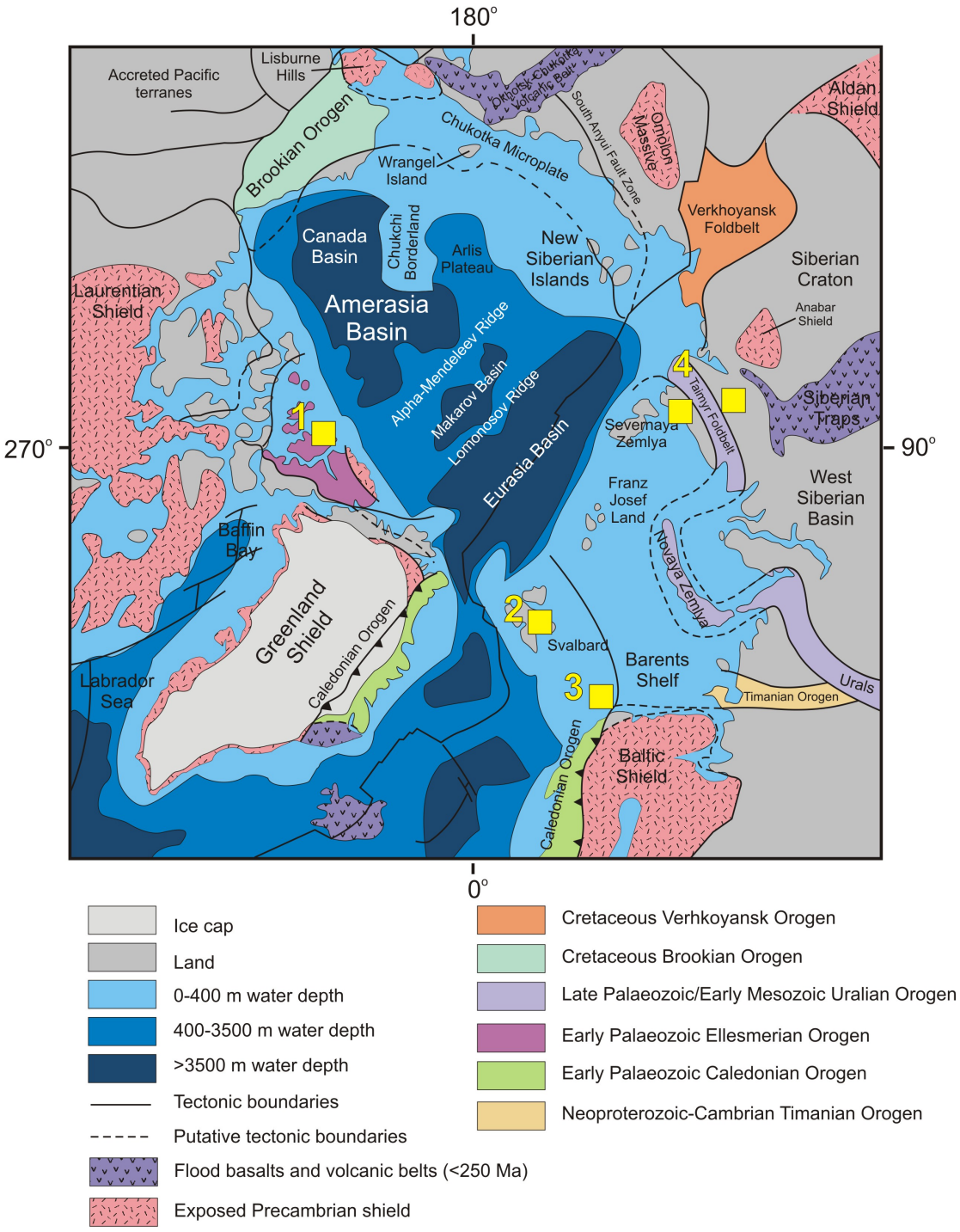

Figure 7.1: Project study areas on a tectonic map of the Arctic region. The areas studied are indicated by yellow boxes. 1: northern Sverdrup Basin, 2: Svalbard, 3: southwestern Barents Shelf and 4: Taimyr (north and south terranes). Bathymetry and topography are modified after the IBCAO Arctic Bathymetry database (Jakobsson *et al.*, 2008). Plate boundaries and geological features are modified after Harrison (2005). Neoproterozoic and younger orogenic belts on land are shown with different shadings.

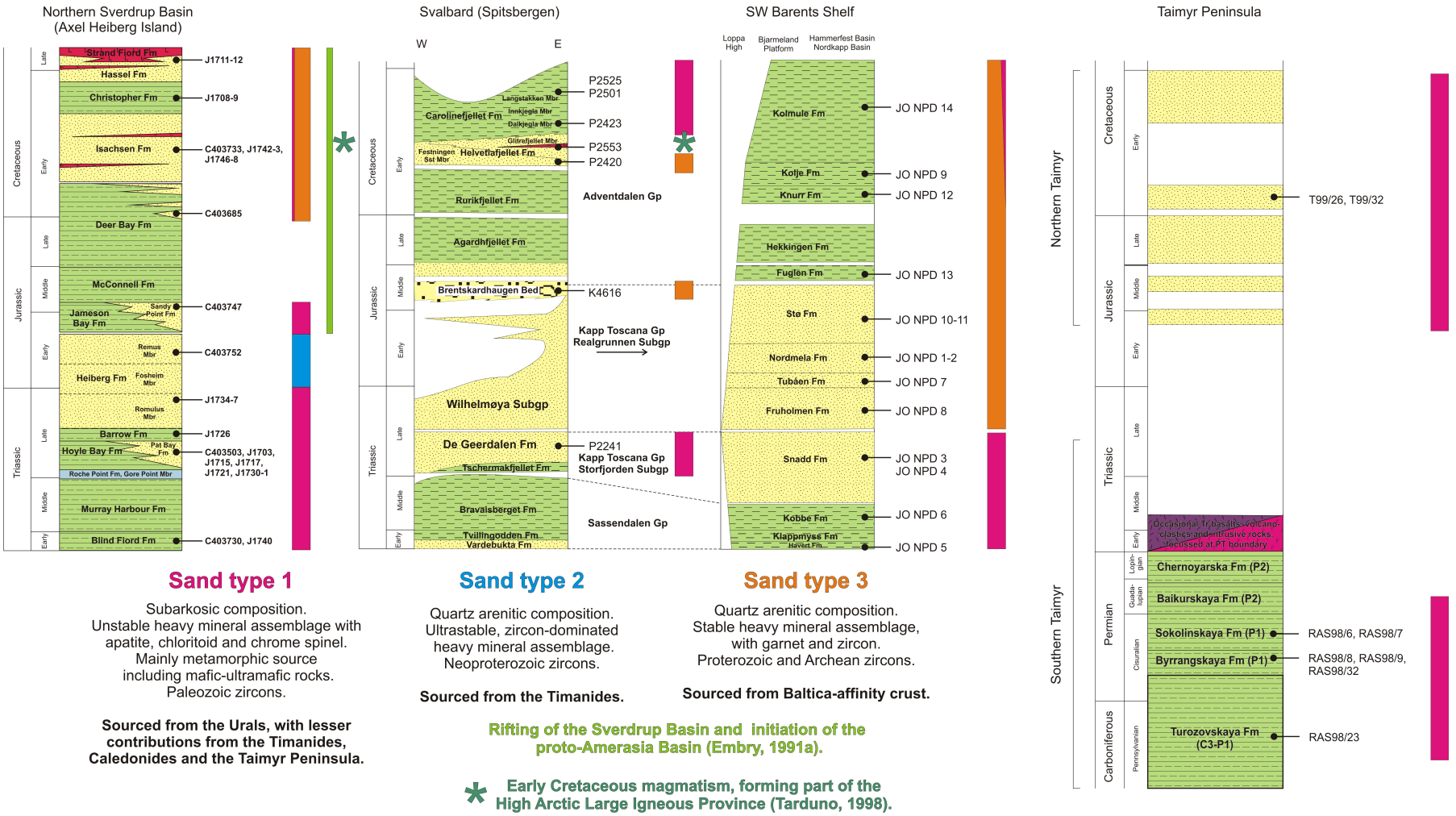

Figure 7.2: Stratigraphic columns for the northern Sverdrup Basin, Svalbard, the southwestern Barents Shelf and Taimyr. Three sand types are recognized: sand types 1, 2 and 3.

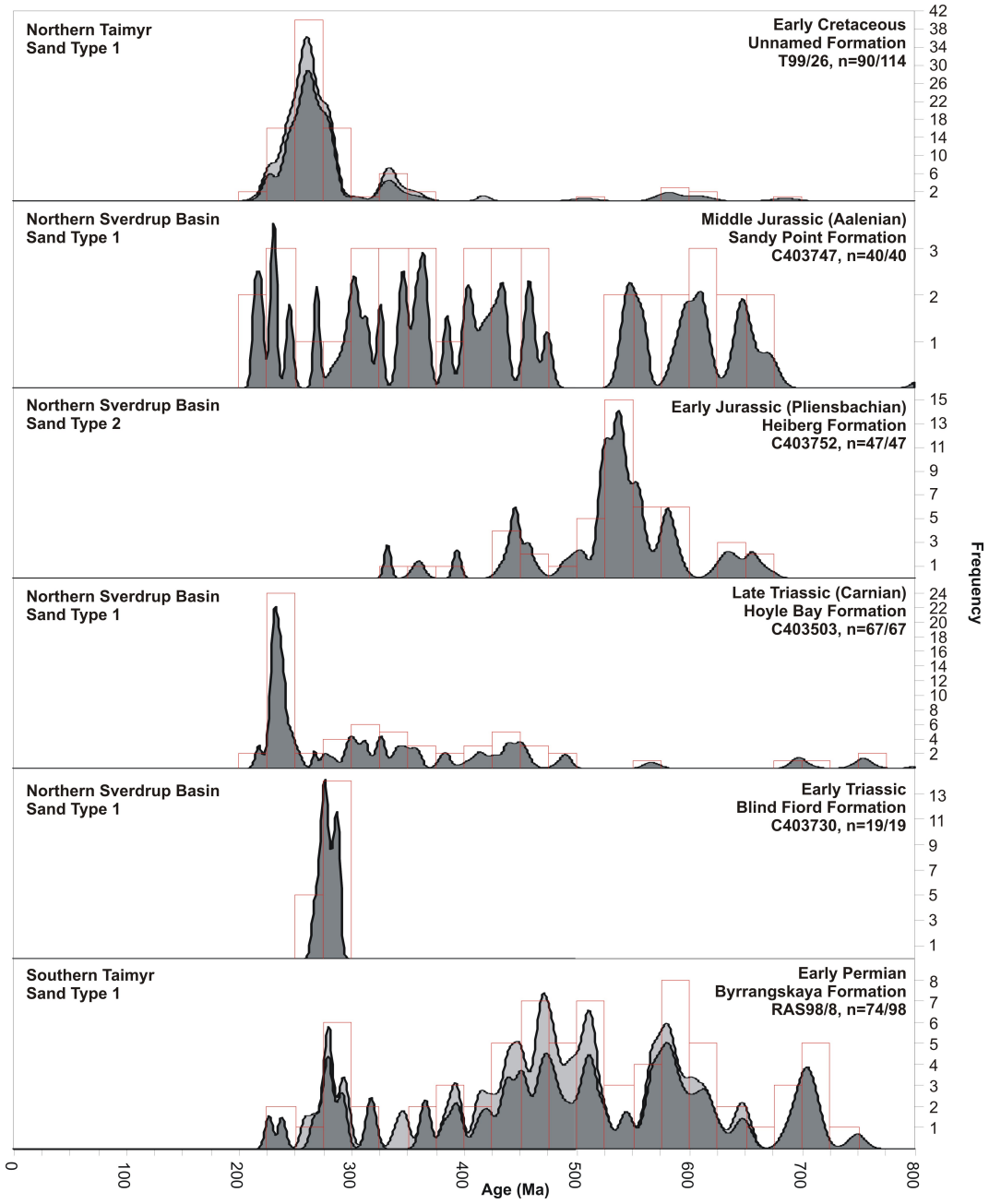

Figure 7.3: Sand types 1 and 2 cumulative frequency diagrams with histograms of U-Pb detrital zircon ages. Paleozoic-Neoproterozoic ages are shown for samples from northern Taimyr, northern Sverdrup Basin and southern Taimyr. The samples are shown in stratigraphic order. U-Pb age with 1σ uncertainty is shown. Ages younger than 1200 Ma are $^{206}Pb/^{238}U$ ages. Ages older than 1200 Ma are $^{207}Pb/^{206}Pb$ ages. Ages with 90-110% concordancy are shown by histograms and dark grey cumulative frequency curves. More discordant data are shown by pale grey cumulative frequency curves. N denotes the number of analyses with 90-110% concordancy relative to all analyses.

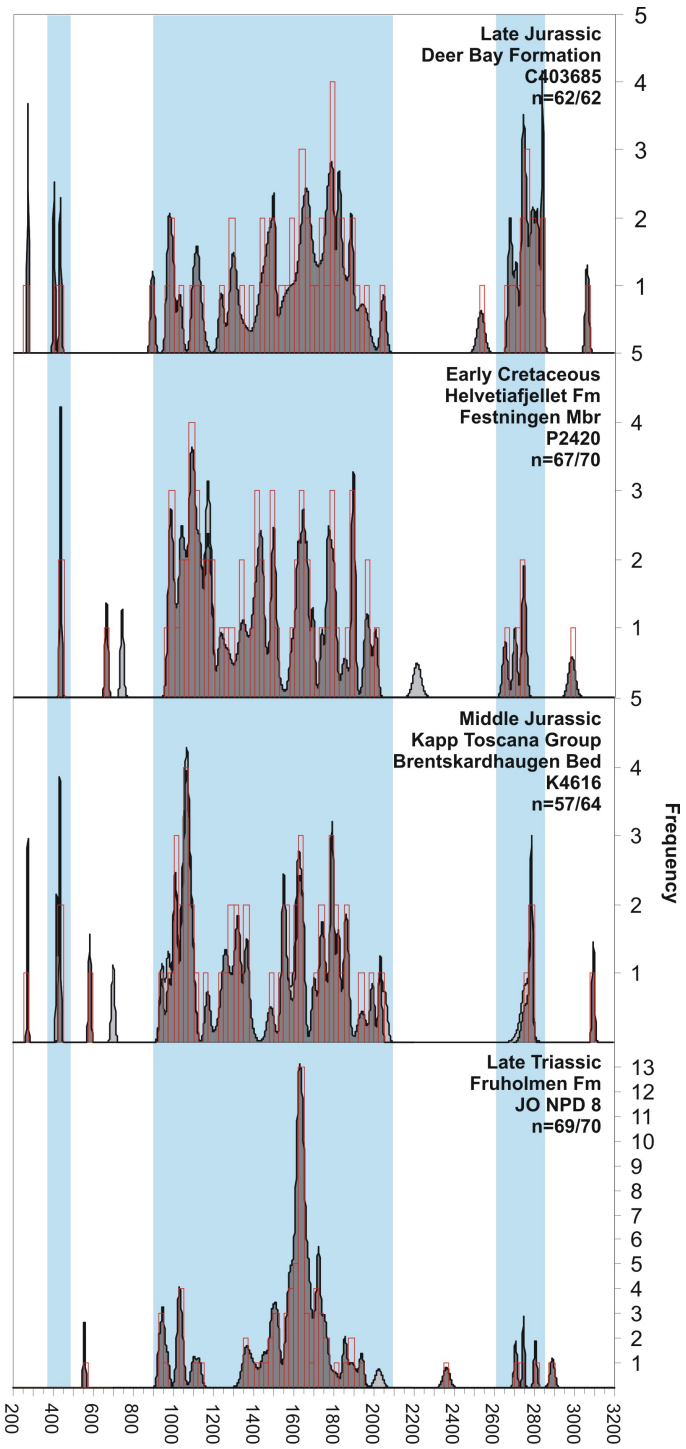

Figure 7.4: Sand type 3 cumulative frequency diagrams with histograms of U-Pb detrital zircon ages from the southwestern Barents Shelf, Svalbard and Axel Heiberg Island, northern Sverdrup Basin. U-Pb age with 1σ uncertainty is shown. Ages younger than 1200 Ma are $^{206}Pb/^{238}U$ ages. Ages older than 1200 Ma are $^{207}Pb/^{206}Pb$ ages. Ages with 90-110% concordancy are shown by histograms and dark grey cumulative frequency curves. More discordant data are shown by pale grey cumulative frequency curves. N denotes the number of analyses with 90-110% concordancy relative to all analyses. The similarities in zircon ages between the four samples are striking.

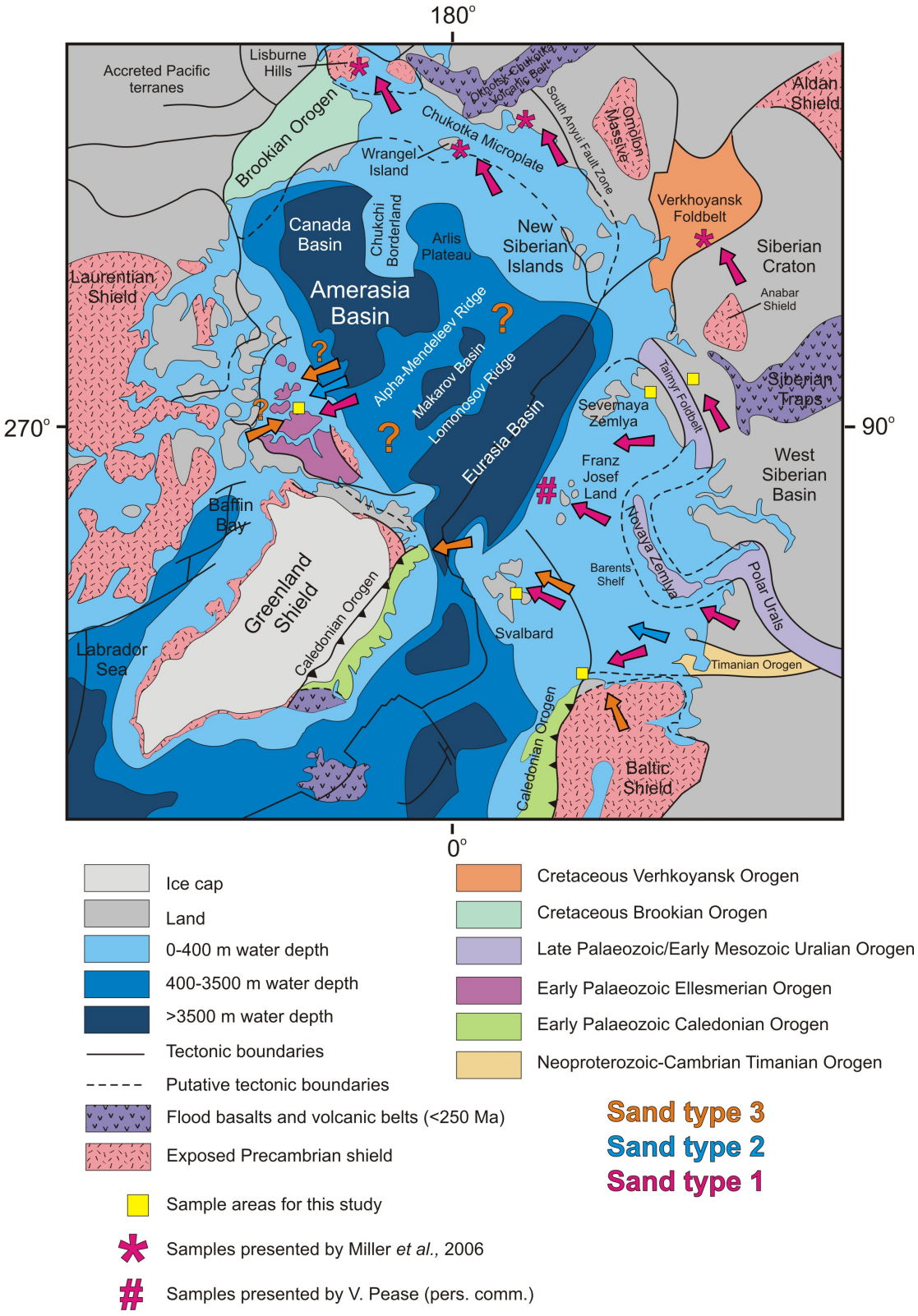

Figure 7.5: Putative sediment transport pathways of sand types 1, 2 and 3. Bathymetry and topography are modified after the IBCAO Arctic Bathymetry database (Jakobsson *et al.*, 2008). Plate boundaries and geological features are modified after Harrison (2005).

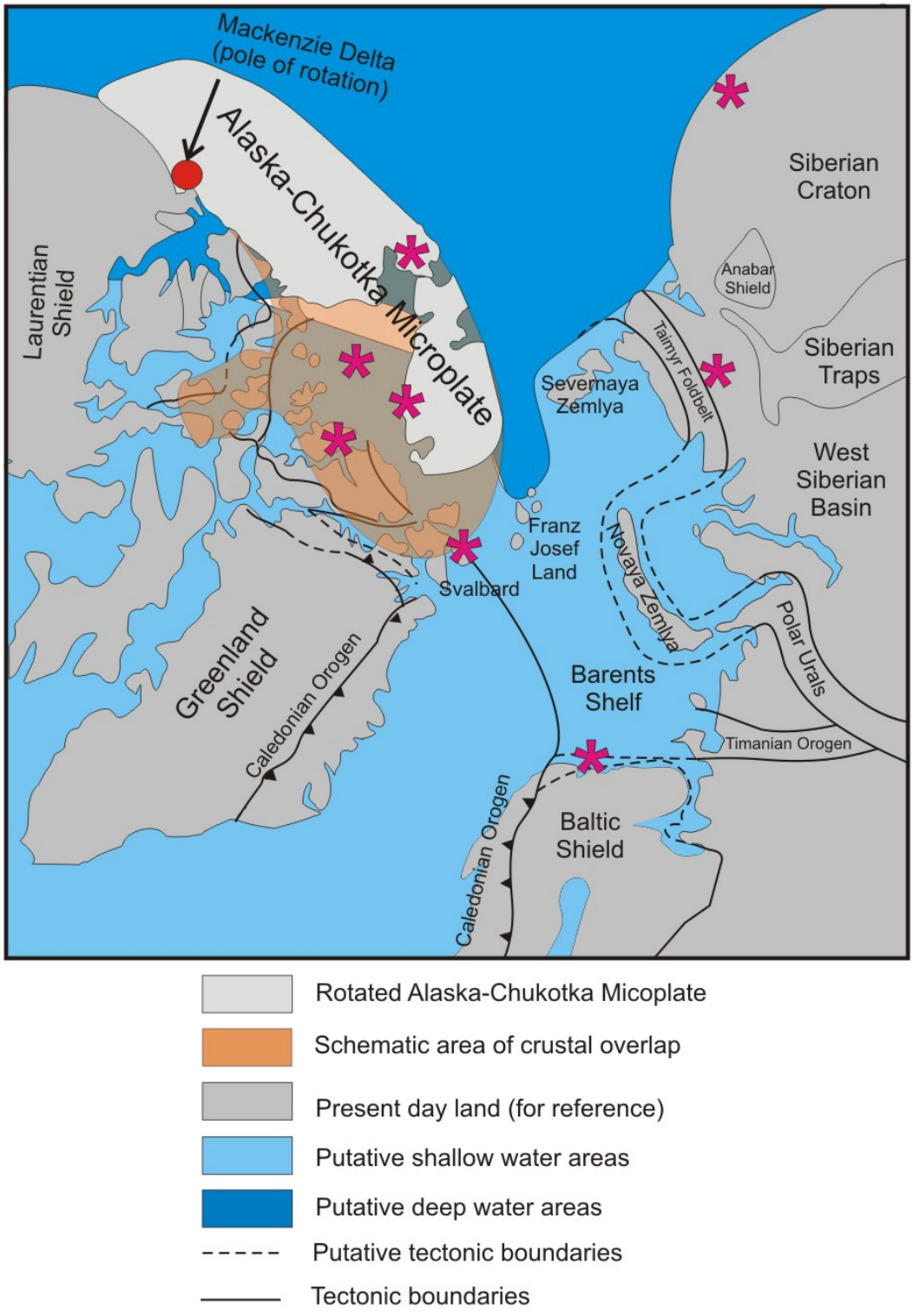

Figure 7.6: Localities and interpreted localities of sand type 1 (shown with pink stars) on a reconstructed Middle Jurassic Arctic region using the Alaska rotation model.

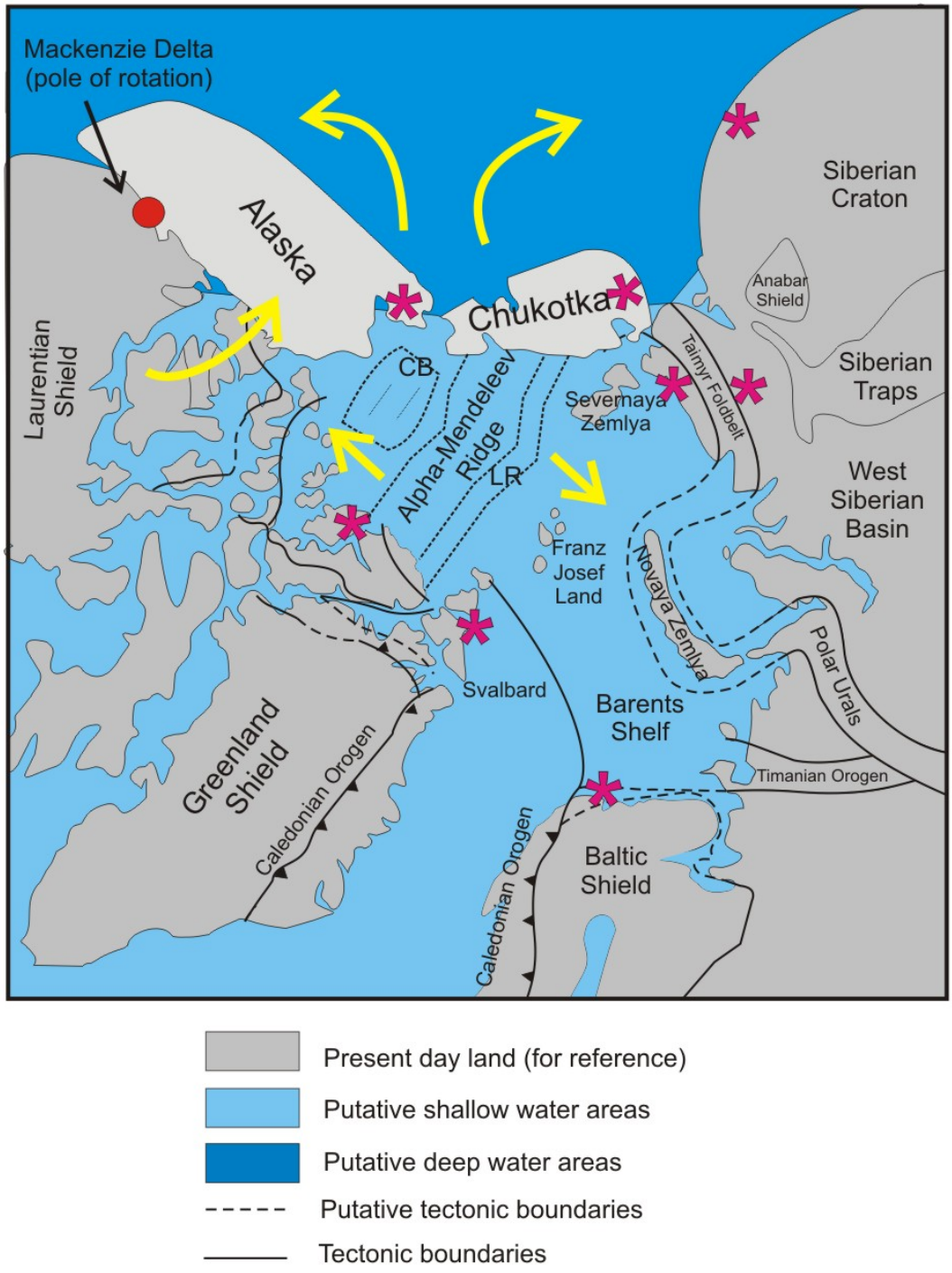

Figure 7.7: Proposed Arctic Ocean opening model. Localities and interpreted localities of sand type 1, shown with pink stars on a reconstructed Middle Jurassic Arctic region using the new model proposed by this thesis. LR = Lomonosov Ridge. CB = Chukchi Borderland. The yellow areas show the suggested opening directions for Arctic terranes during Late Jurassic-Cretaceous time.

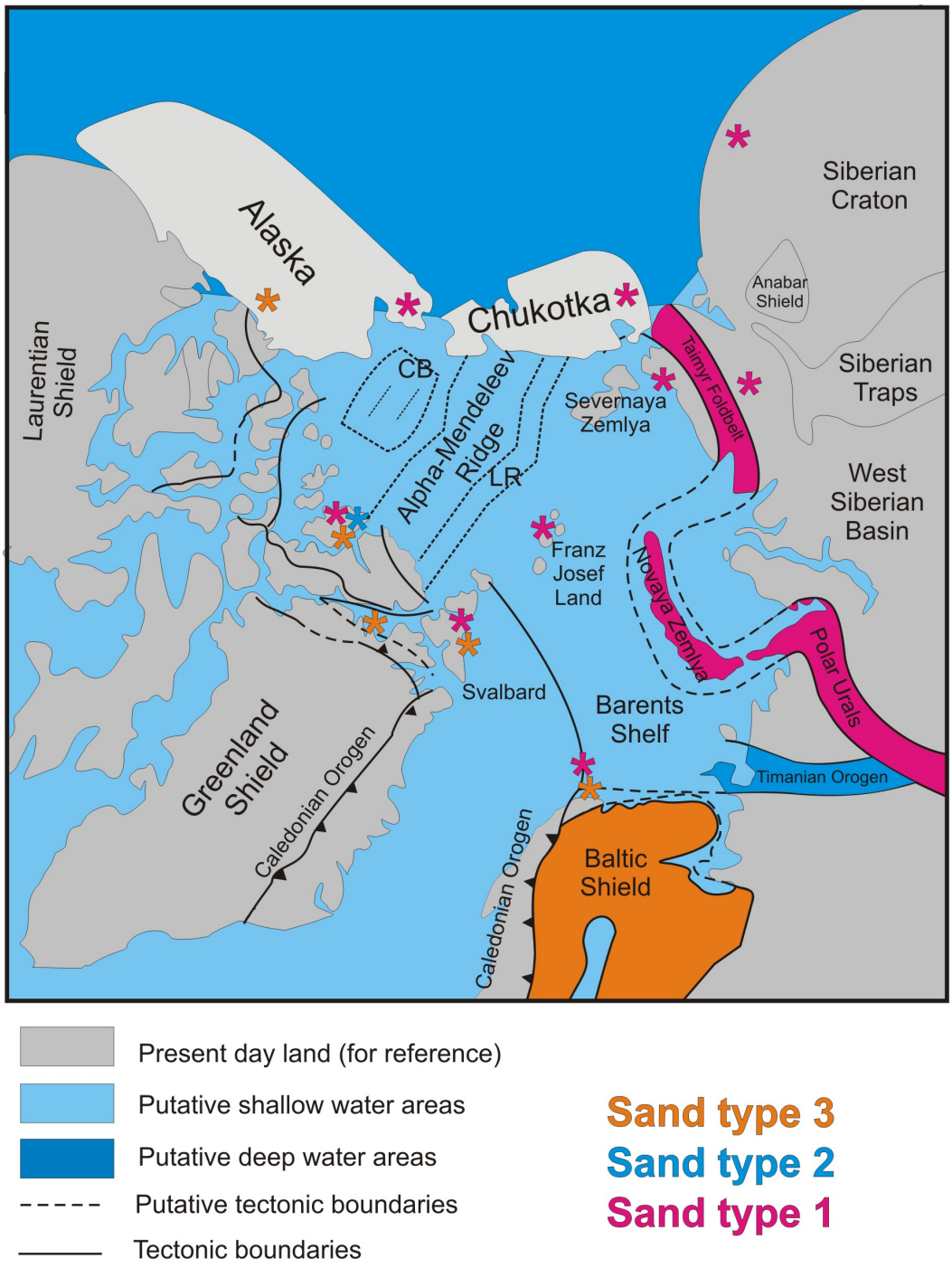

Figure 7.8: Middle Jurassic Arctic reconstruction proposed by this thesis showing the sediment source areas of sand types 1, 2 and 3, along with sampled localities of sand types 1, 2 and 3 shown with stars. The localities shown include samples from this thesis (Taimyr, western Barents Shelf, Svalbard and northern Sverdrup Basin), in addition to samples from Franz Josef Land (V. Pease, pers. comm.), North Greenland (Røhr *et al.*, 2008), the Verkhoyansk Foldbelt, Chukotka and Western Alaska (Miller *et al.*, 2006) and Arctic Alaska (J. Omma, unpublished data). LR = Lomonosov Ridge. CB = Chukchi Borderland.

Chapter 8

Conclusions

The Uralian Orogen, including the Taimyr Peninsula and the area of the Siberian Traps was an important sediment source to Arctic basins during Triassic time, following uplift of the area during Permo-Carboniferous time (Uralian orogeny) and around the Permo-Triassic boundary (Siberian Trap Magmatic event). Uralian/Siberian Trap-derived compositionally immature, first-cycle Triassic age clastic sediment was encountered in the northern Sverdrup Basin, southwestern Barents Shelf and Svalbard (this study) and is interpreted to be present on Franz Josef Land (V. Pease, pers. comm.), Chukotka, Wrangel Island and the Lisburne Hills of western Alaska and possibly the Verkhoyansk Mountains (Miller *et al.*, 2006).

During Jurassic and Cretaceous time, a compositionally mature, recycled clastic sediment of Baltic Shield provenance emerged as the dominant sediment source for the northern Sverdrup Basin, southwestern Barents Shelf and Svalbard. This sediment was encountered in the northern Sverdrup Basin, southwestern Barents Shelf and Svalbard (this study) and is interpreted to be present in the Wandel Sea Basin in North Greenland (Røhr *et al.*, 2008) and possibly beyond.

The observation that the Uralian Orogen, Taimyr Peninsula and Siberian Trap areas were an important Arctic region sediment source prior to the opening of the Amerasia Basin has important implications for the validity of Arctic Ocean opening models. In particular, a Uralian sediment source is not consistent with a rotational opening model for the entire Amerasia Basin, as suggested by many workers (see Lawver *et al.* (1990) for review). In this model, the source areas mentioned would be far removed from Arctic basins where this sediment is found (for example, the Sverdrup Basin and the east Siberian Shelf).

This study does not favour a rotational opening mechanism for the entire Amerasia Basin but considers a rotational opening for the Canada Basin to be likely. The sediment provenance data presented in this study suggest that the Uralian Orogen, Taimyr Peninsula and Siberian Trap area were proximal to several key

Arctic depocentres prior to the opening of the Amerasia Basin. It is uncertain whether crust of this affinity stretches into the Central Arctic Region. The Baltic Shield source for sediment in the Arctic also argues for the proximity of the Barents Shelf region to a restored Arctic region. The ultimate source of the Baltic Shield sediment is uncertain and it is considered equally possible that putative continental crust forming the seafloor of the Central Arctic region may have Baltica affinity. This idea is supported by the observation that Baltica plate structural trends (for example the Caledonian deformation front and suture) cross the Barents Shelf and in to the Central Arctic Ocean, where they cannot be traced. A revised model for Arctic Ocean opening is proposed, hypothesizing that the Canada Basin formed by rotational opening, but that the Central Arctic region formed in a mainly extensional regime.

Appendix A

Barents Shelf sedimentary logs

This section contains summary logs of Barents Shelf cores logged at the Norwegian Petroleum Directory during August 2007. Sample positions and are shown, together with selected photographs.

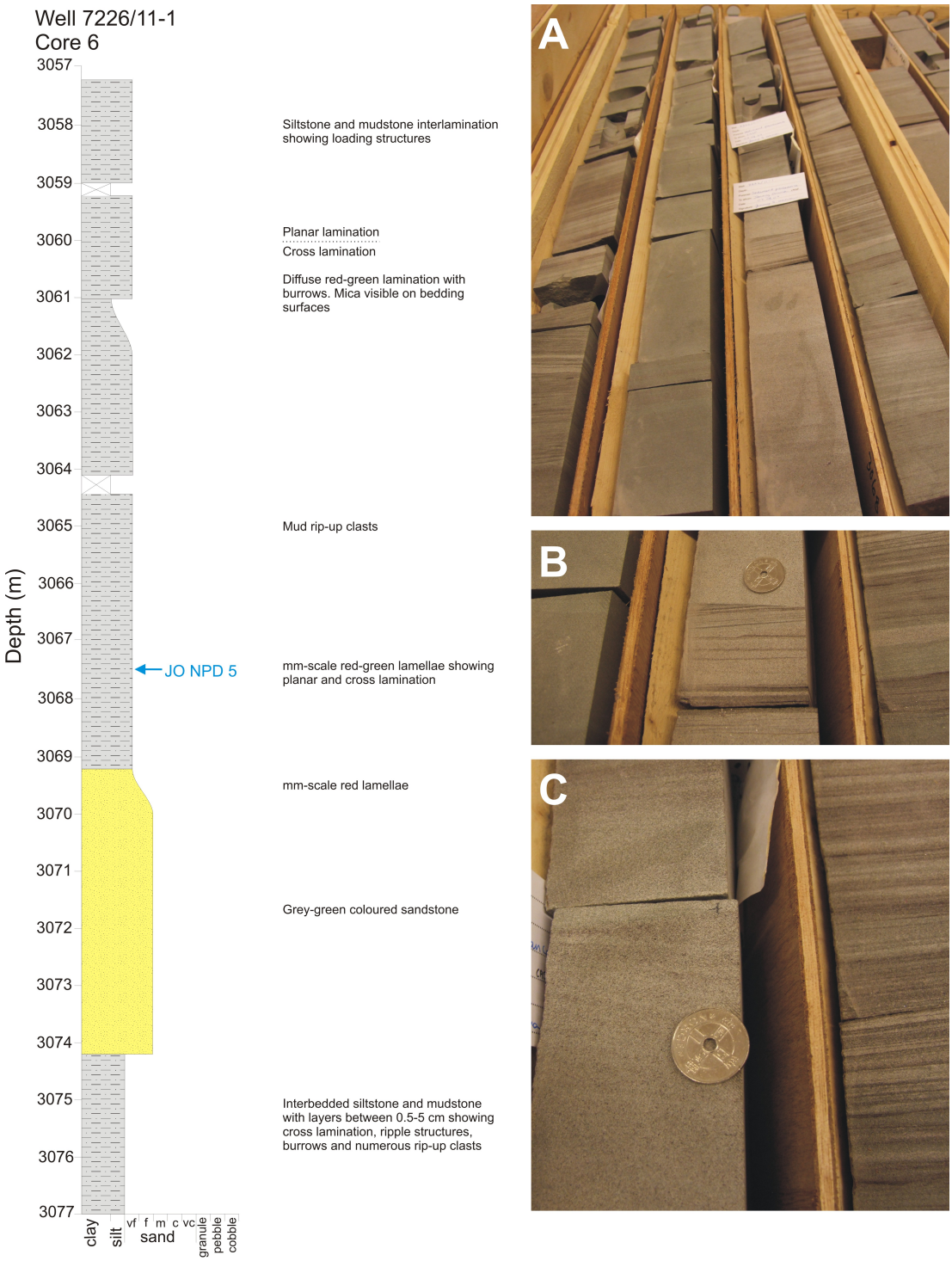

Figure A.1: Well 7226/11-1 Core 6 sedimentary log showing the position of sample JO NPD 5, Early Triassic (Induan) Havert Formation. (A) Overview 3069-3073 m. (B-C) Sample JO NPD 5 details.

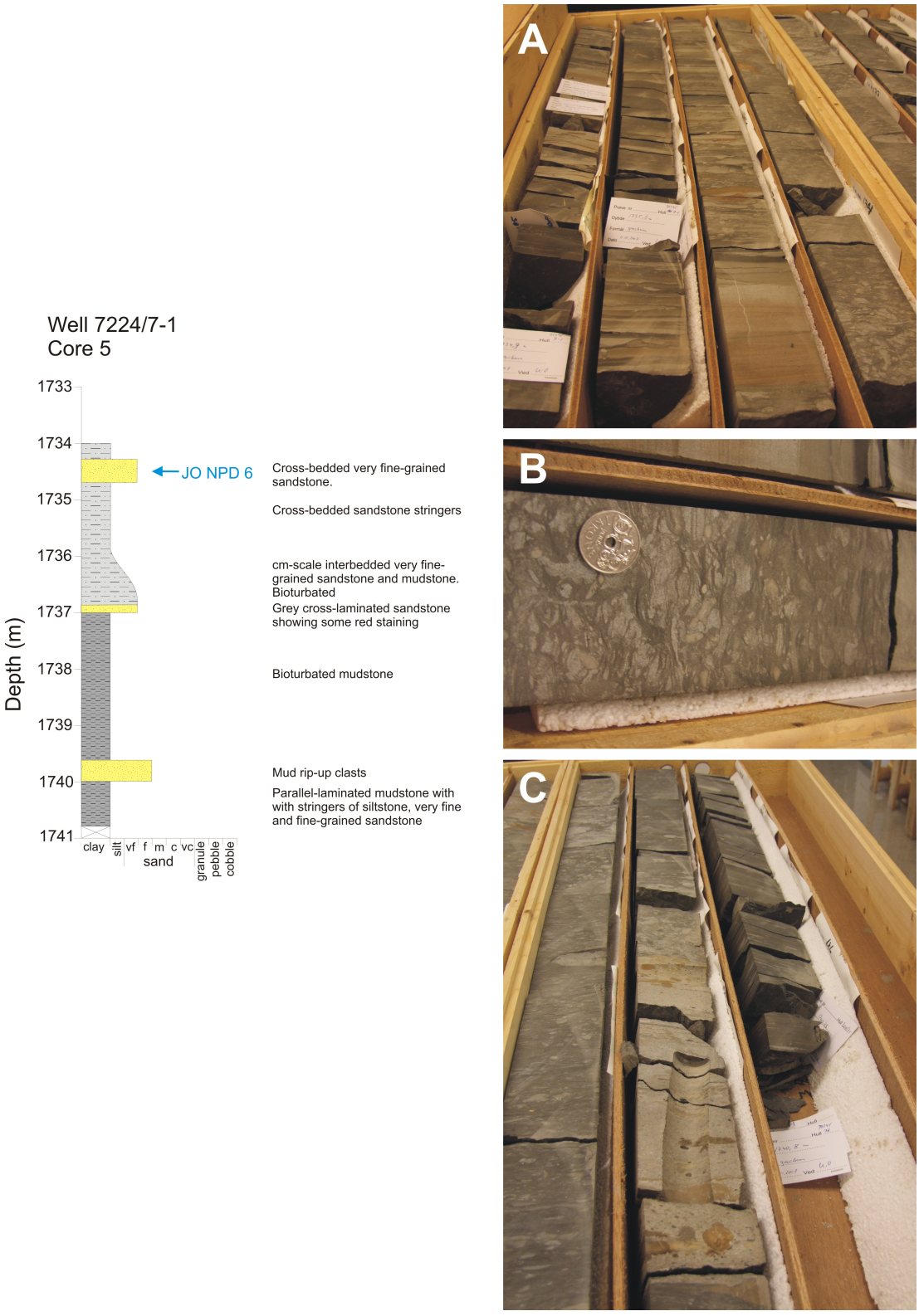

Figure A.2: Well 7224/7-1 Core 5 sedimentary log showing the position of sample JO NPD 6, Middle Triassic (Anisian) Kobbe Formation. (A) Overview of 1734-1738 m. (B) Bioturbated mudstone and sandstone. (C) Overview of 1738-1741 m.

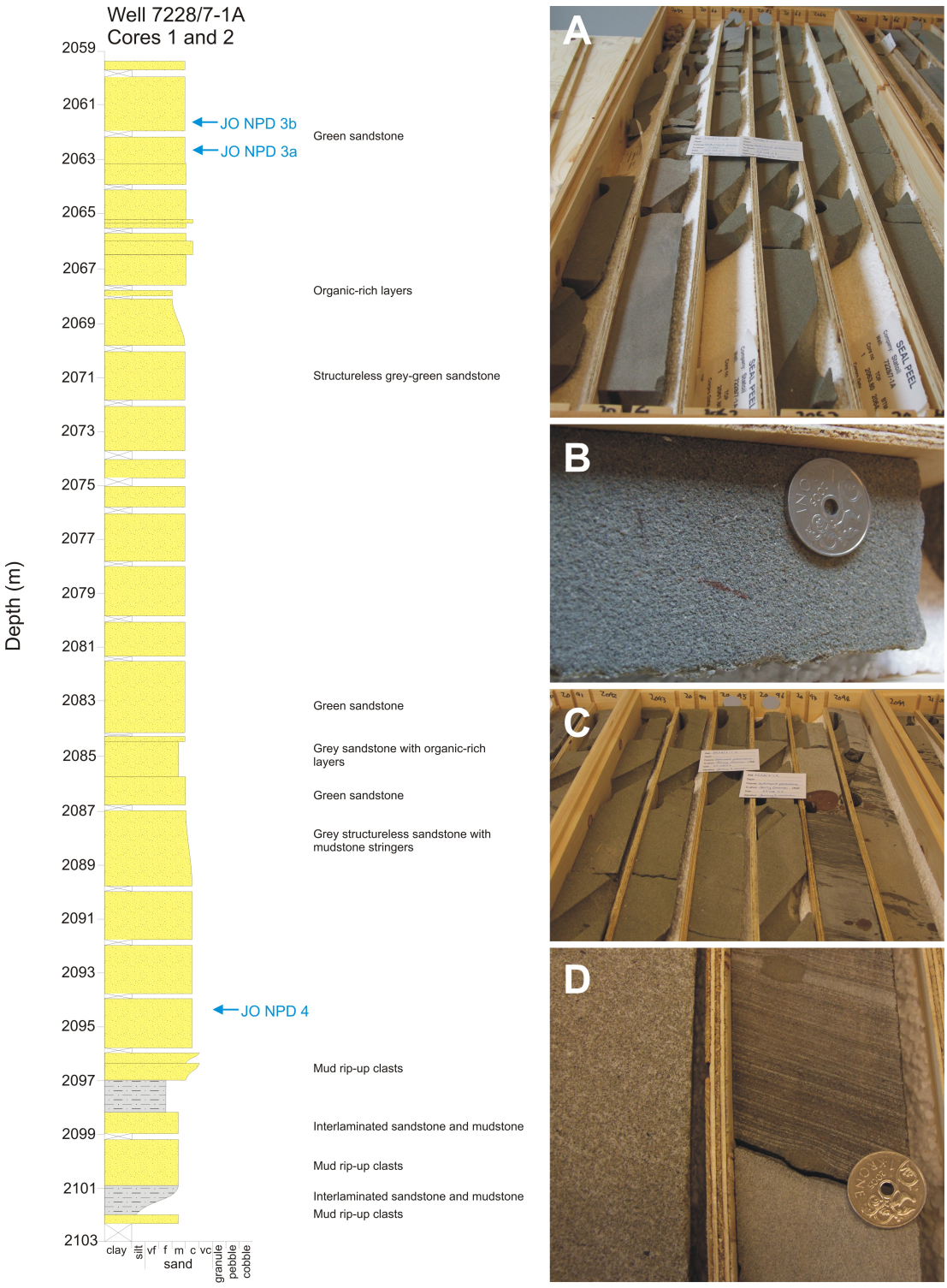

Figure A.3: Well 7228/7-1A Cores 1 and 2 sedimentary log showing the position of samples JO NPD 3a, 3b and 4, Middle-Late Triassic (Ladinian-Norian) Snadd Formation. (A) Overview 2059-2064 m. (B) Sample JO NPD 3. (C) Overview 2093-2098 m. (D) Mud-sand interbeds.

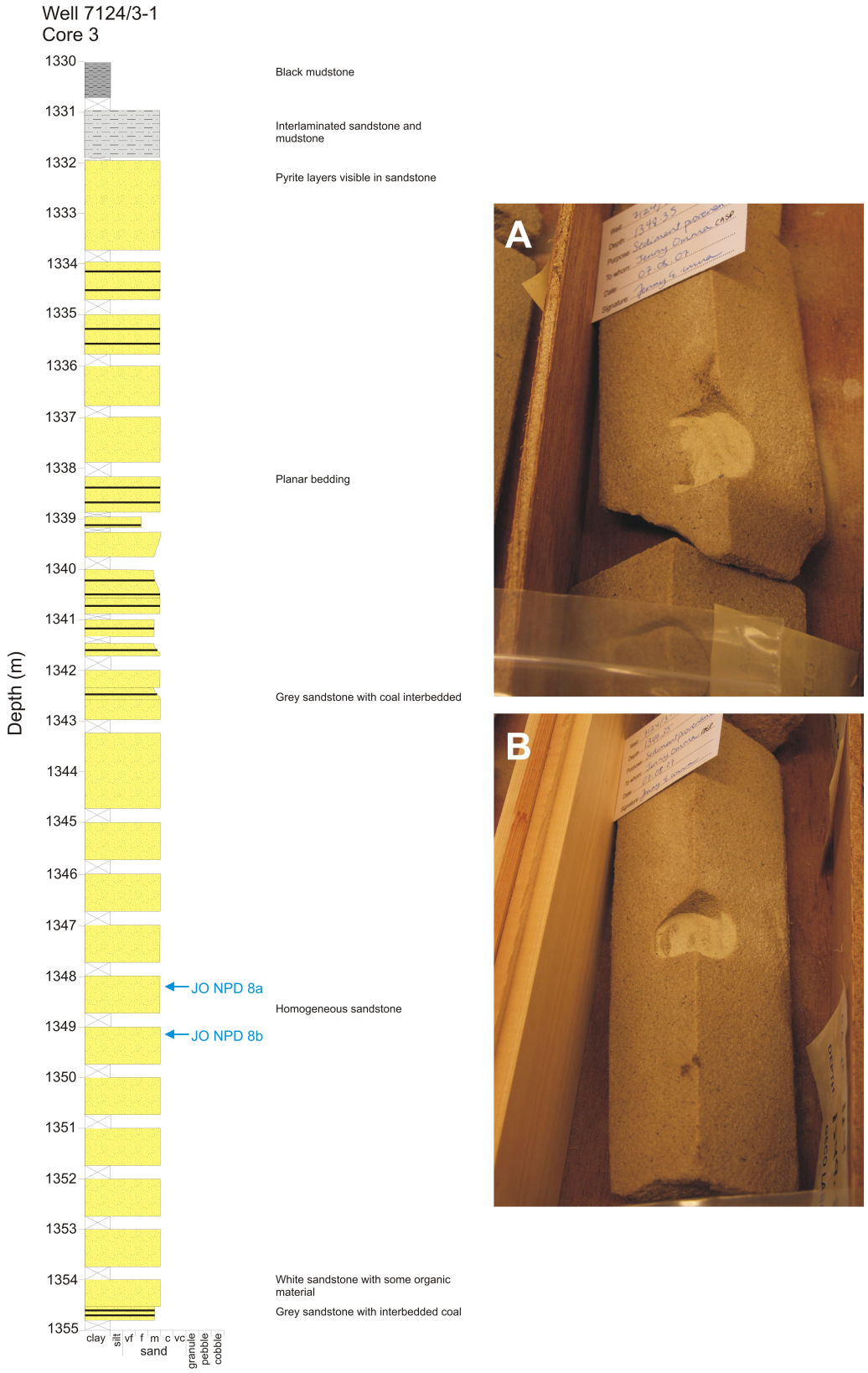

Figure A.4: Well 7124/3-1 Core 3 sedimentary log showing the position of samples JO NPD 8a and 8b, Late Triassic (Norian-Rhaetian) Fruholmen Formation. (A-B) Samples JO NPD8a and 8b.

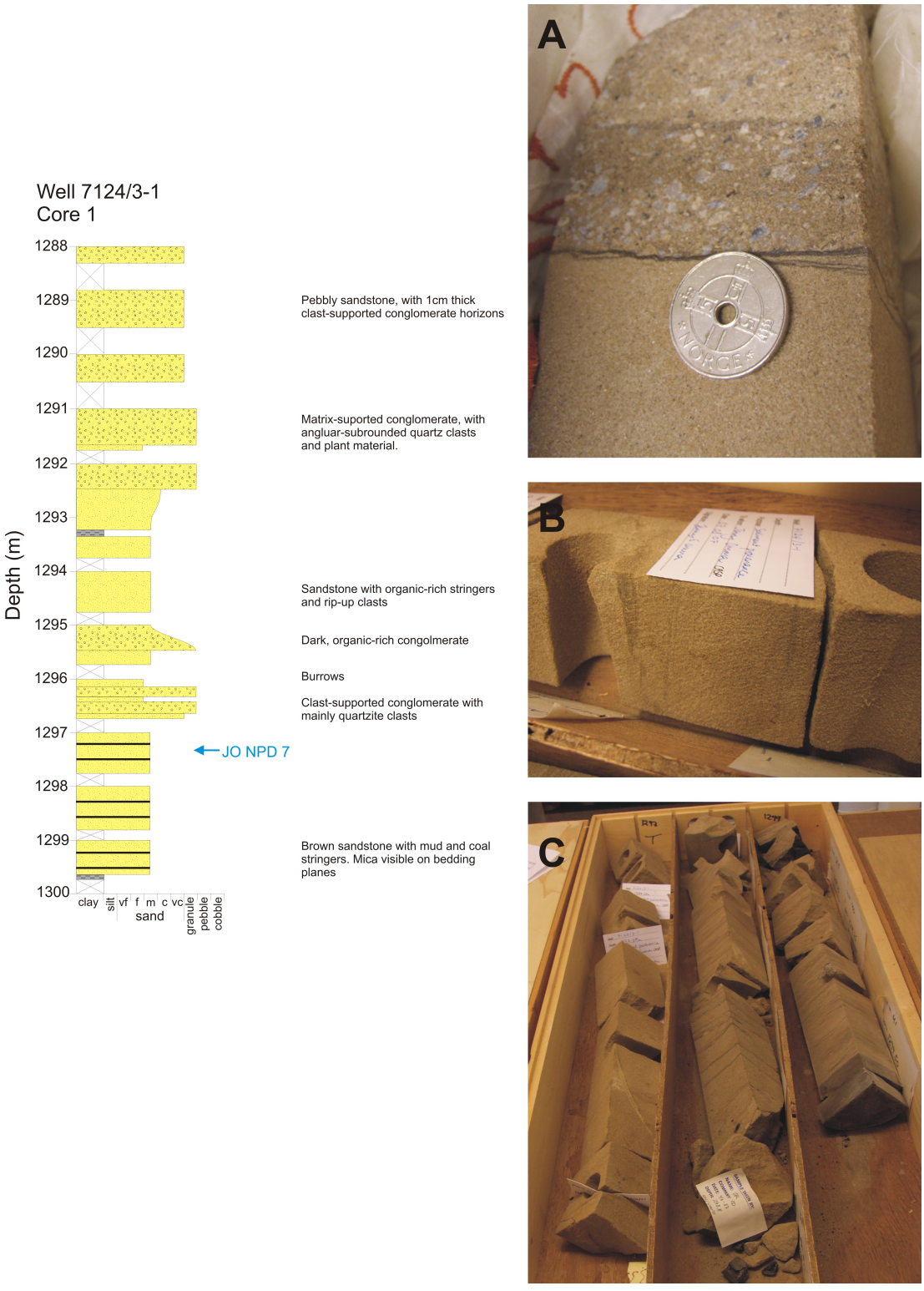

Figure A.5: Well 7124/3-1 Core 1 sedimentary log showing the position of sample JO NPD 7, Late Triassic-Early Jurassic (Rhaetian-Sinemurian) Tubåen Formation. (A) Conglomerate layer approximately 1296 m. (B) Sample JO NPD 7. (C) Overview of 1297-1300 m.

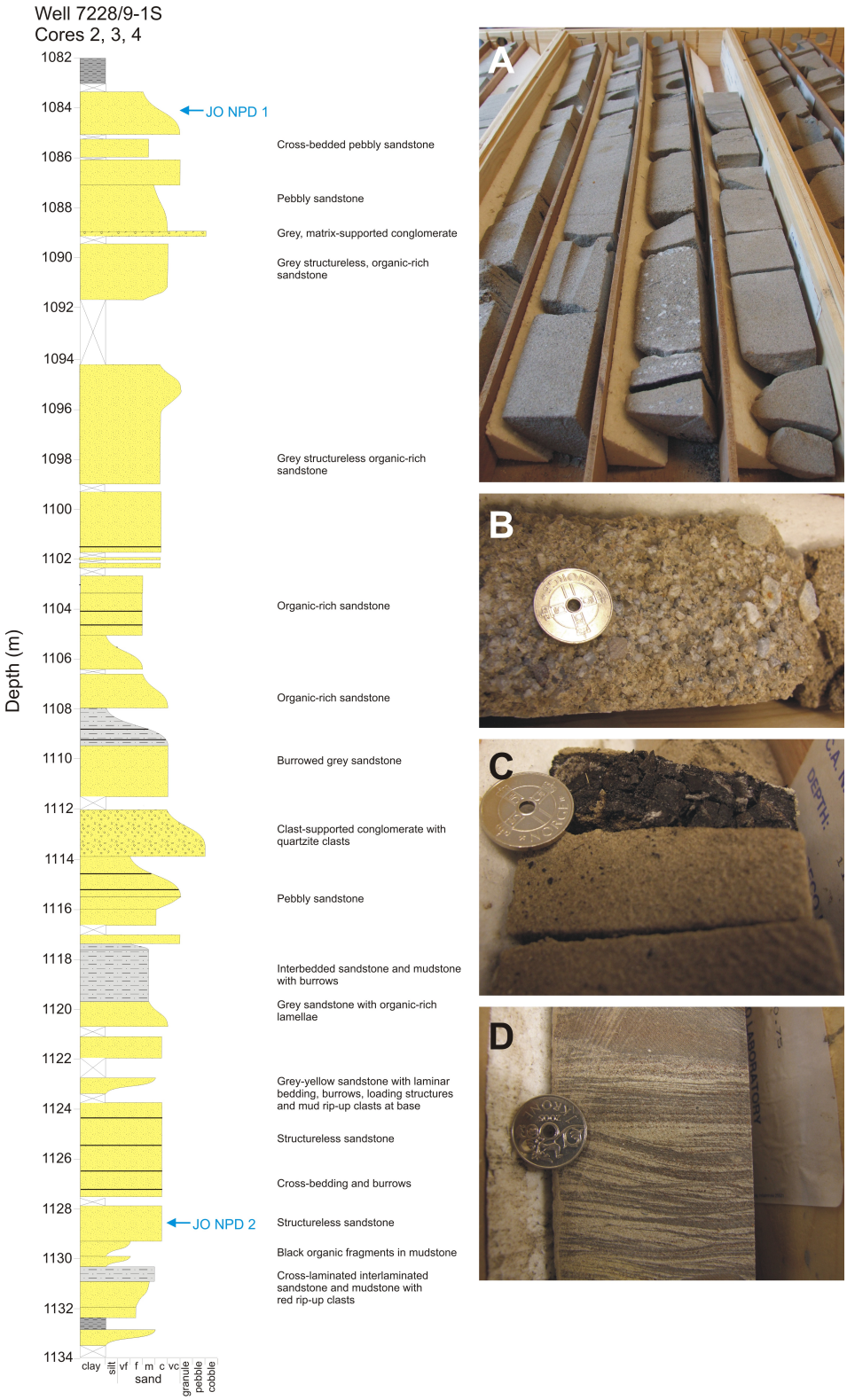

Figure A.6: Well 7228/9-1S Cores 2, 3 and 4 sedimentary log showing the position of samples JO NPD 1 and 2, Early Jurassic (Sinemurian-Pliensbachian) Nordmela Formation. (A) Core 2 overview. (B-C) Core 3 conglomerate and coal layer. (D) Core 4 sand-mud interbedding.

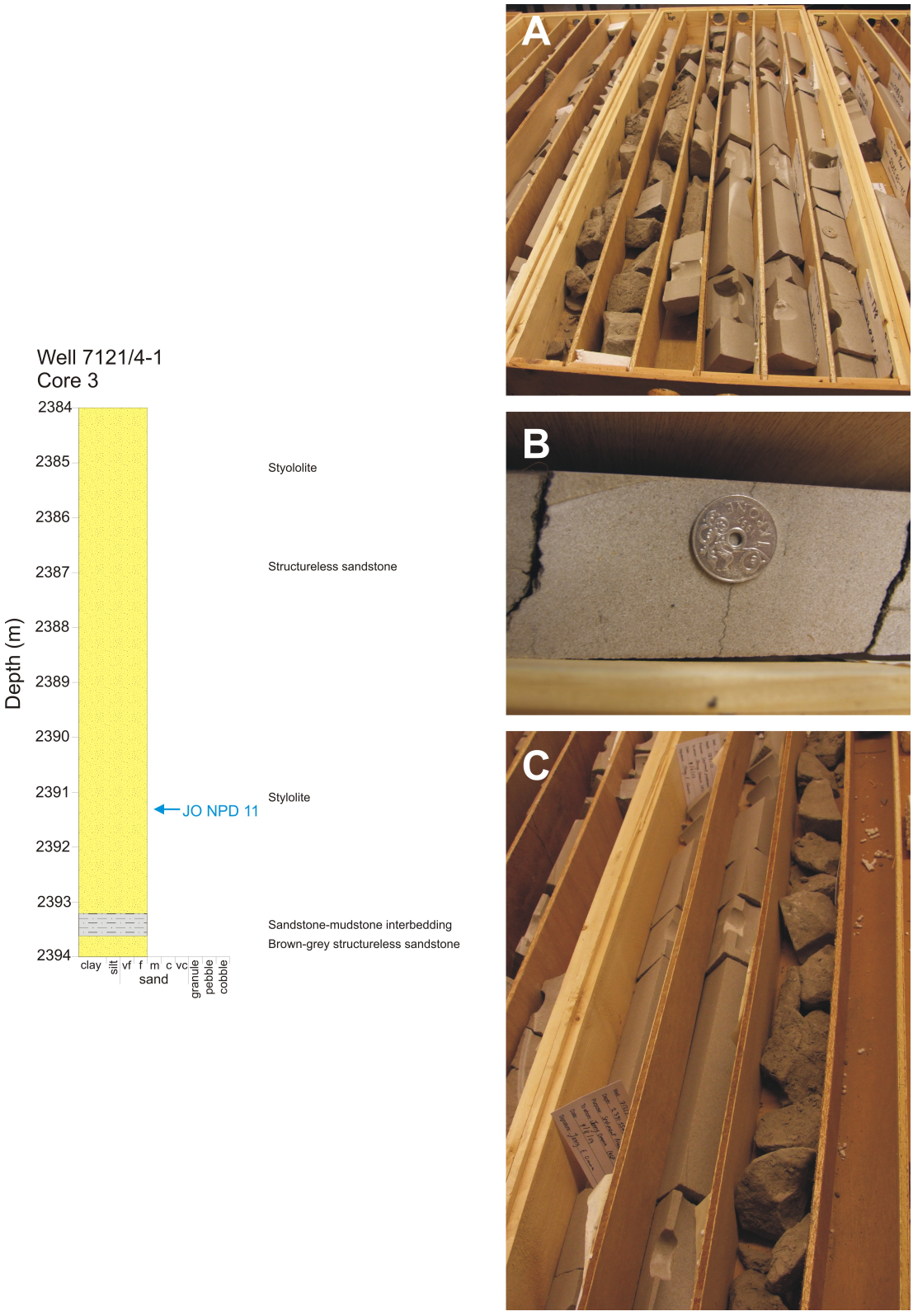

Figure A.7: Well 7121/4-1 Core 3 sedimentary log showing the position of sample JO NPD 11, Early-Middle Jurassic (Pliensbachian-Bajocian) Stø Formation. (A) Overview of 2378-2384 m. (B) Clean sand with stylolite. (C) Sand at base of section showing muddier layers.

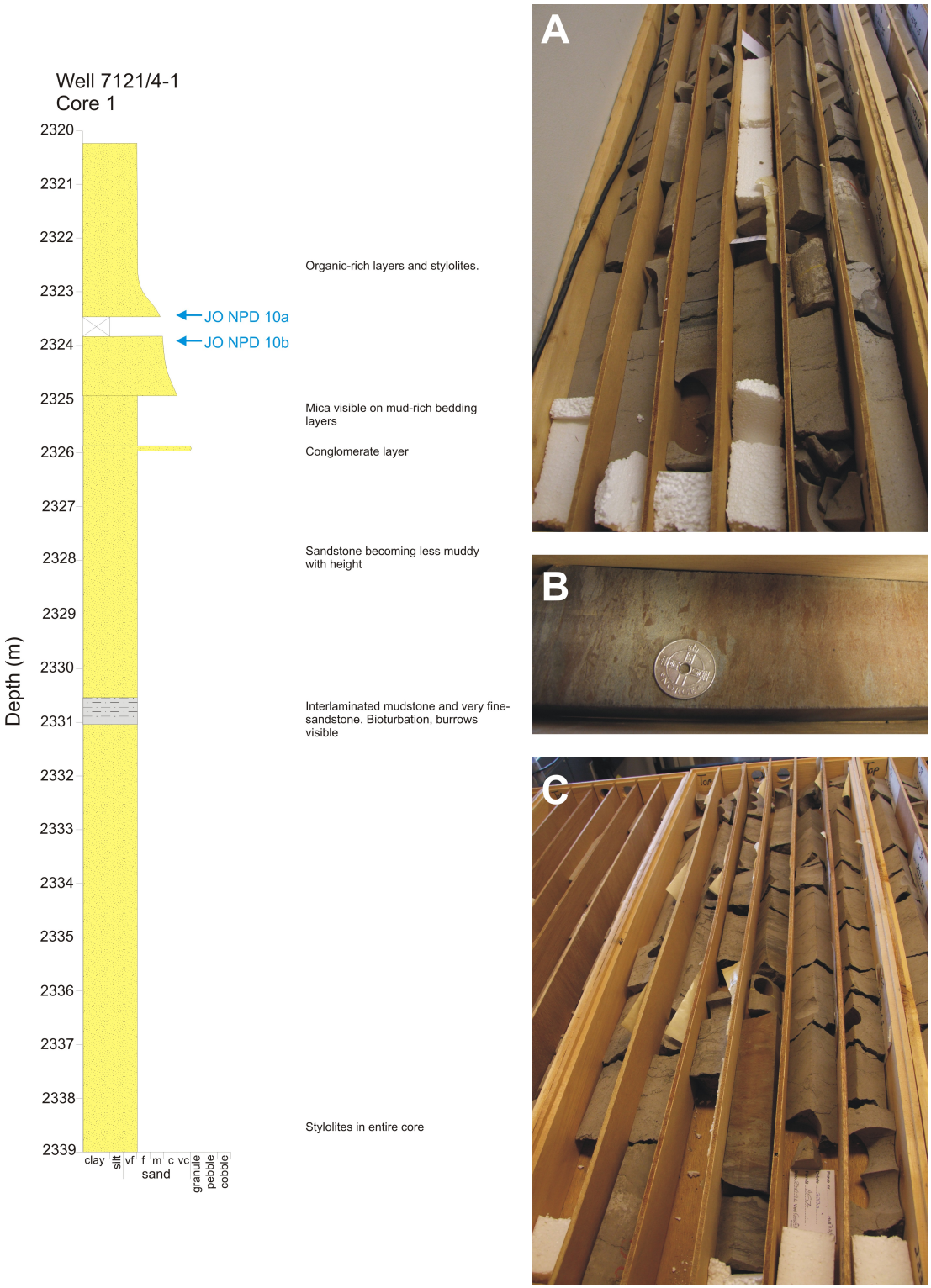

Figure A.8: Well 7121/4-1 Core 1 sedimentary log showing the position of samples JO NPD 10a and 10b, Early-Middle Jurassic (Pliensbachian-Bajocian) Stø Formation. (A) Overview of 2320-2327 m. (B) mud-sand interbeds at 2330 m. Younging to right. (C) Overview of 2333-2339 m.

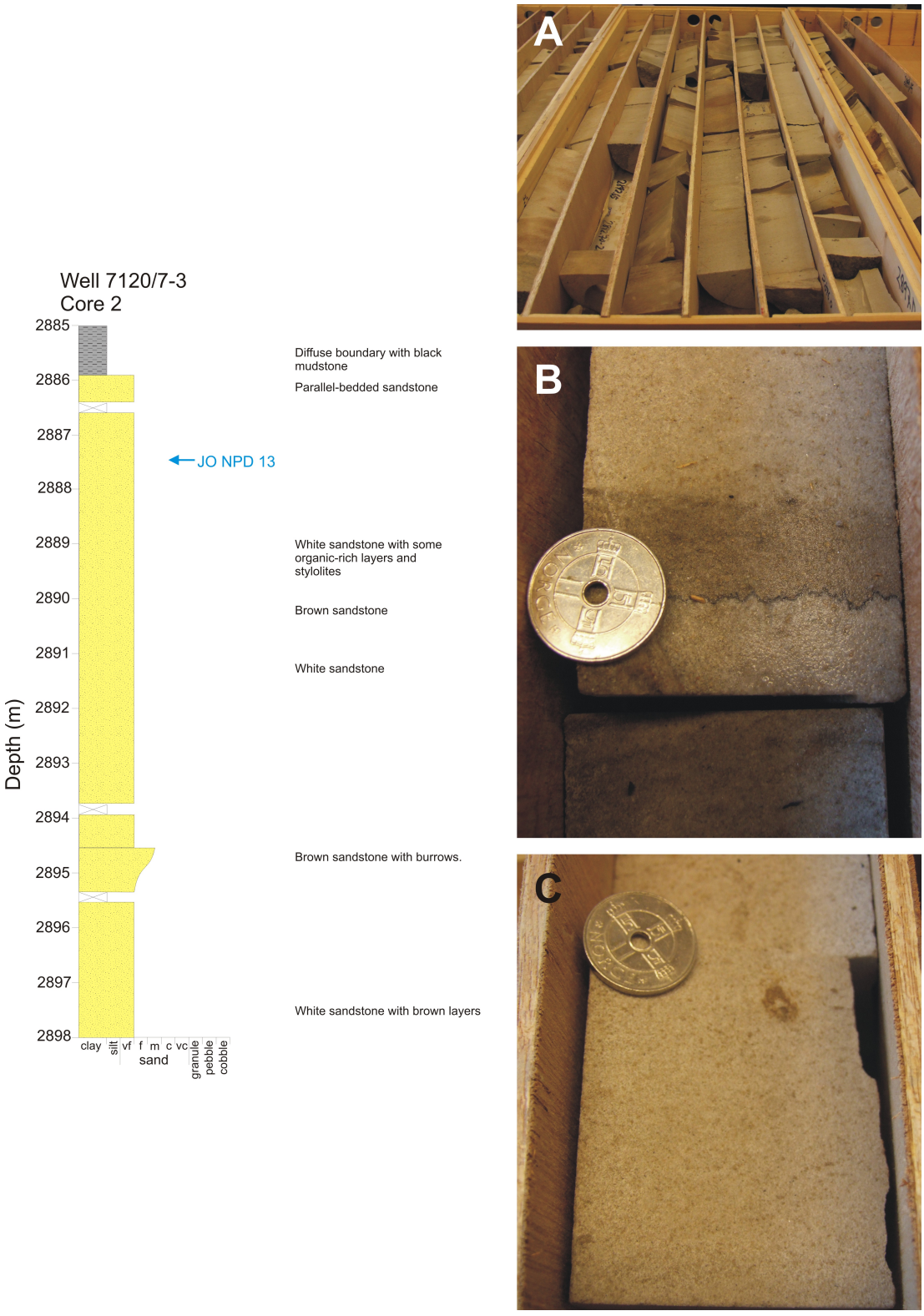

Figure A.9: Well 7120/7-3 Core 2 sedimentary log showing the position of sample JO NPD 13, Middle Jurassic (Bathonian-Callovian) Fuglen Formation. (A) General overview. (B) Stylolite. (C) Sample JO NPD 13.

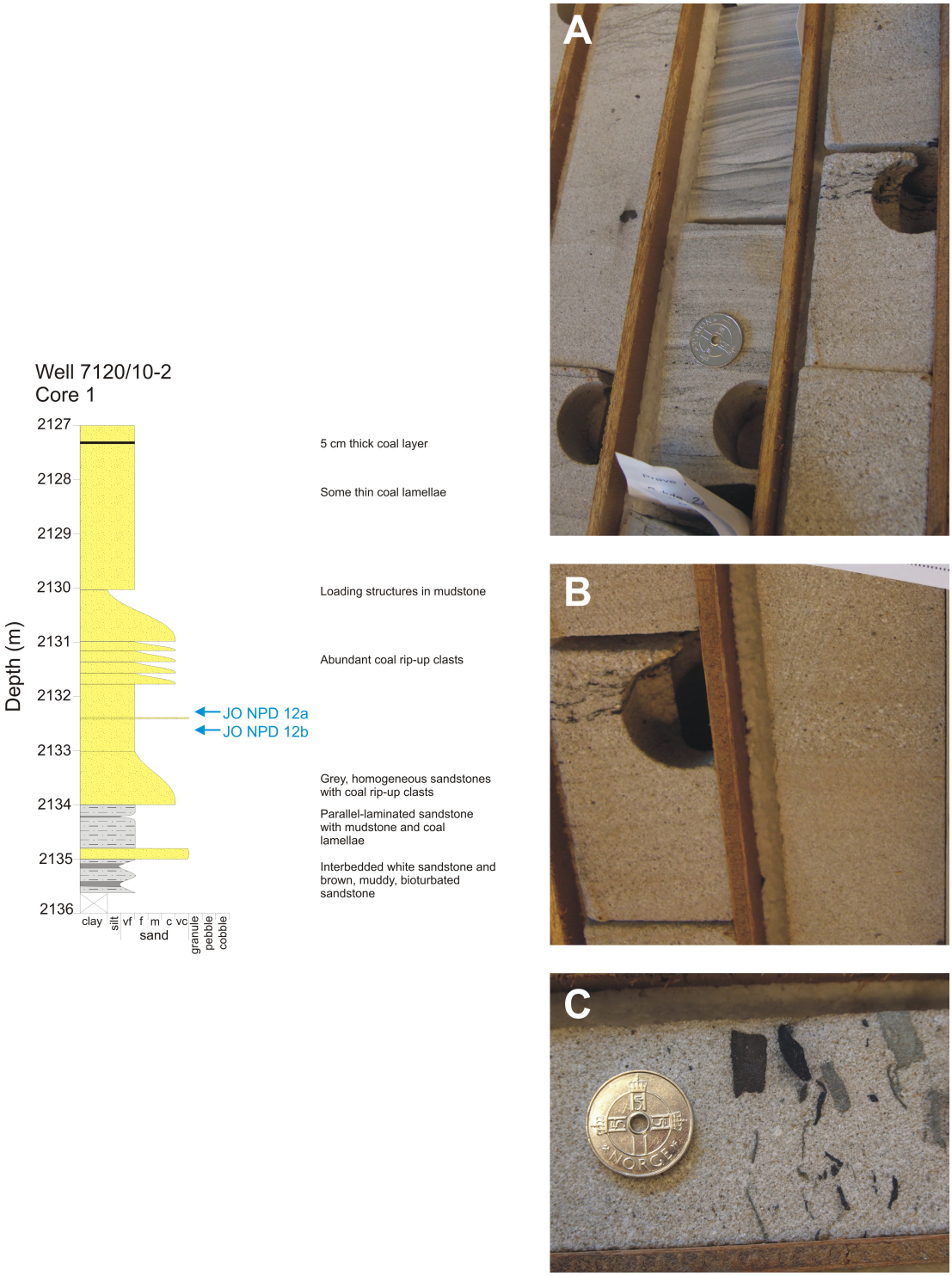

Figure A.10: Well 7120/10-2 Core 1 sedimentary log showing the position of samples JO NPD 12a and 12b, Early Cretaceous (Berriasian-Valangian) Knurr Formation. (A) General overview of sediment. (B) Samples 12a-b were collected here. (C) mud and coal rip-up clasts.

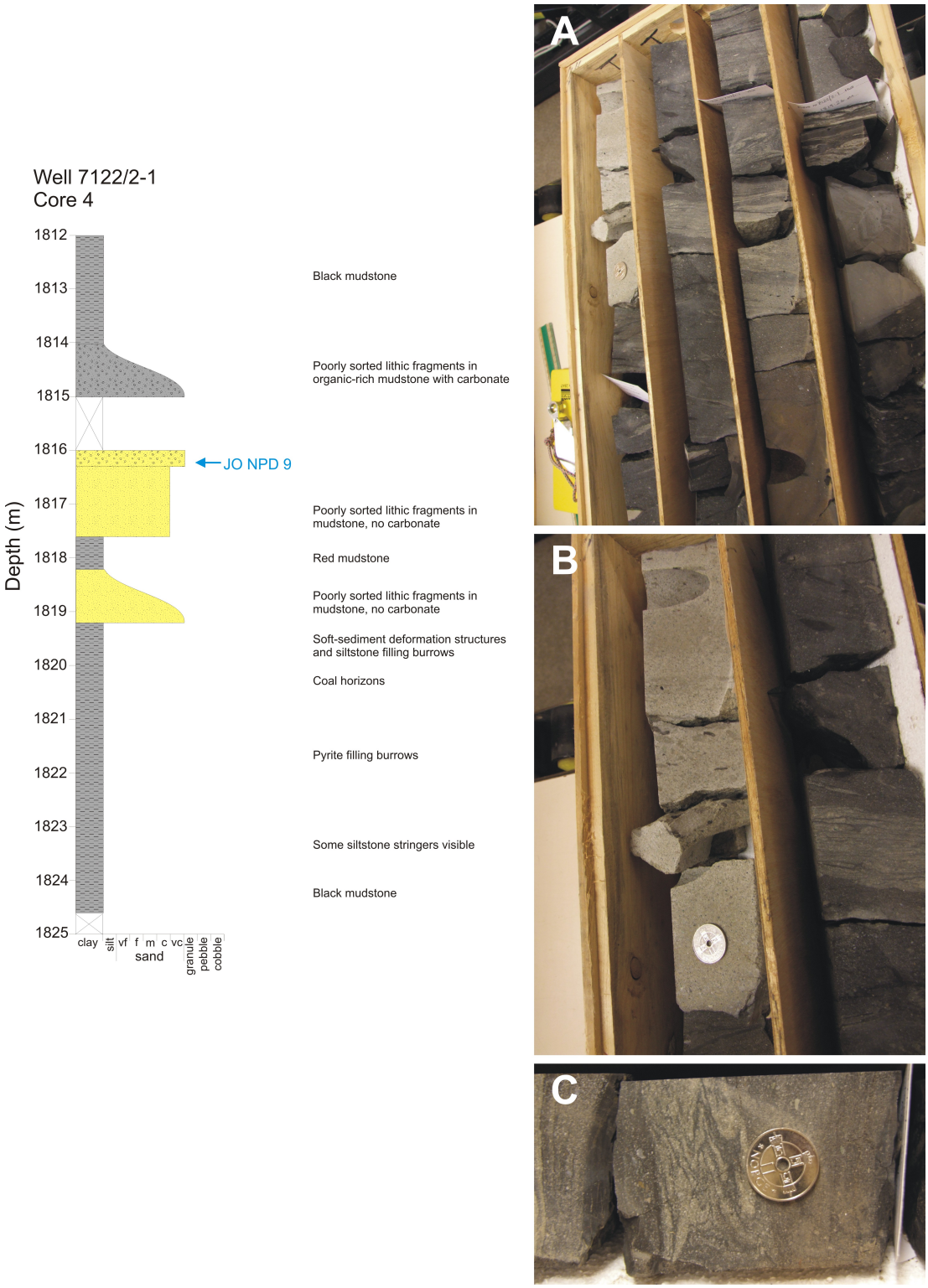

Figure A.11: Well 7122/2-1 Core 4 sedimentary log showing the position of sample JO NPD 9, Early Cretaceous (Hauterivian-Barremian) Kolje Formation. (A) Box from 1816-1820 m. (B) around 1816 m where sample JO NPD 9 was collected. (C) Approximately 1818 m showing soft-sediment deformation.

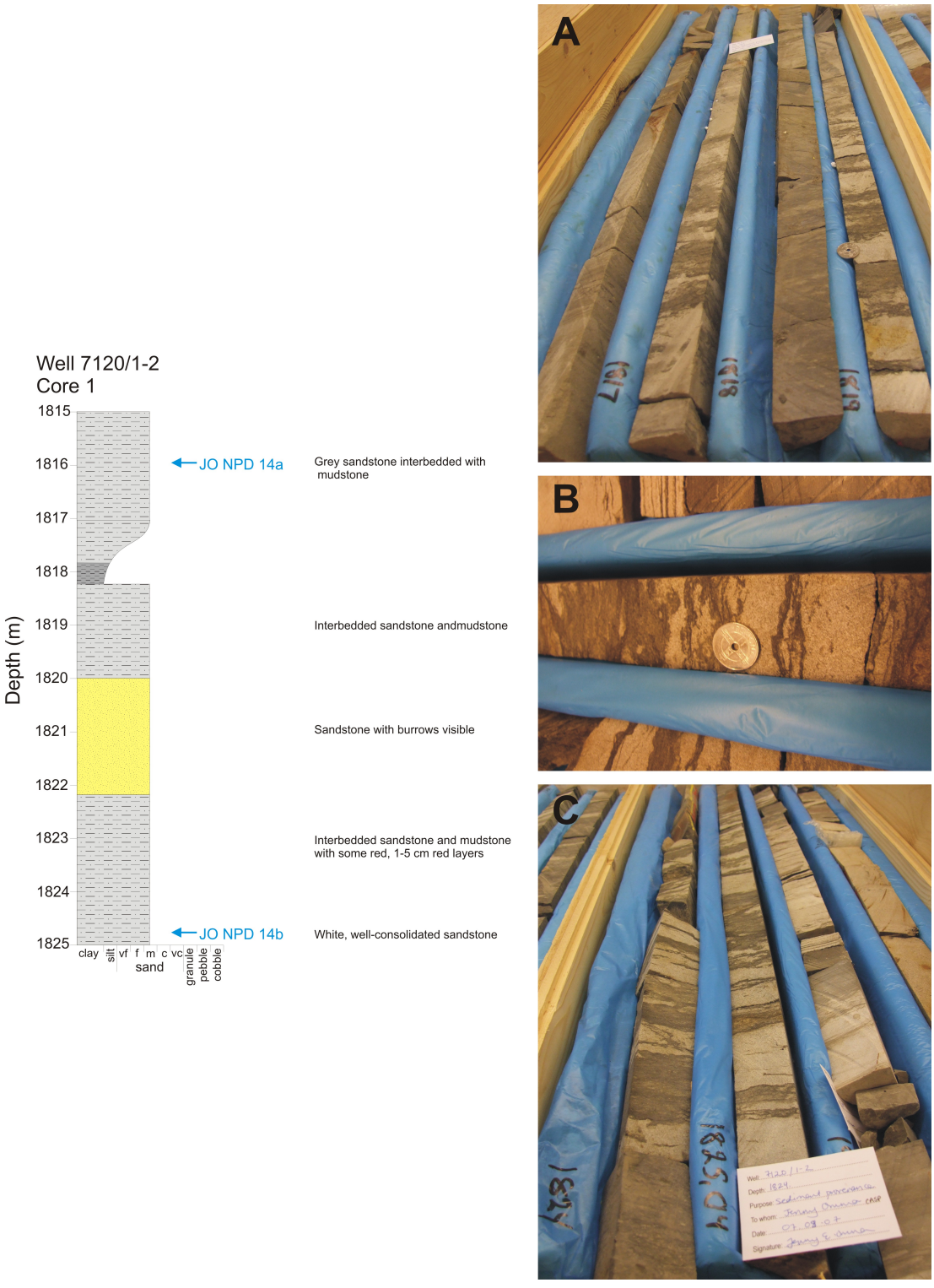

Figure A.12: Well 7120/1-2 Core 1 sedimentary log showing the position of samples JO NPD 14a and 14b, Early-Late Cretaceous (Barremian-Cenomanian) Kolmule Formation. (A) General overview showing the lithology of sample 14a. (B) Close-up photograph showing lithology. (C) General overview showing the lithology of sample 14b.

References

Astafurova, E., Glebovsky, V. & Fedorov, V. (2003). Results of density modelling of the major structural elements of the Arctic Ocean (Abstract). In *Fourth International Conference on Arctic Margins Abstracts, Dartmouth, Nova Scotia*, P–25. 16

Basu, A. (1985). Influence of climate and relief on compositions of sands released at source areas. In G. Zuffa, ed., *Provenance of Arenites*, 1–18, Reidel, Dordrecht. 29, 30

Bateman, R.M. & Catt, J.A. (1985). Modification of heavy mineral assemblages in English coversands by acid pedochemical weathering. *Catena*, **12**, 1–12. 29

Bezzubtsev, V., Malitch, N., Markov, F. & Pogrebitsky, Y. (1983). Geological map of mountainous Taimyr, 1:500 000. Ministry of Geology of the USSR, Ministry of Geology of the Russian Federation, (RFSFR), Krasnoyarskgeologia, Krasnoyarsk (in Russian). 144, 145, 146, 147, 150

Bezzubtsev, V., Zalyaleyev, R. & Sakovich, A. (1986). Geological map of mountainous Taimyr, 1:500 000: explanatory notes. Krasnoyarskgeologia, Krasnoyarsk (in Russian). 142, 145

Bird, K.J., Charpentier, R.R., Gautier, D.L., Houseknecht, D.W., Klett, T.R., Pitman, J.K., Moore, T.E., Schenk, C.J., Tennyson, M.E. & Wandrey, C.J. (2008). Circum-Arctic Resource Appraisal: Estimates of Undiscovered Oil and Gas North of the Arctic Circle. U.S. Geological Survey Fact Sheet 2008-3049. 1

Brozena, J., Kovacs, L.C. & Lawver, L.A. (1998). An aerogeophysical study of the southern Canada Basin. *Third International Conference on Arctic Margins Abstracts, Celle, Germany*, 36–37. 20

Brozena, J.M. (2003). New aerogeophysical study of the Eurasia Basin and the Lomonosov Ridge: implications for basin development. *Geology*, **31**, 825–828. 11, 12

Carey, S.W. (1955). The orocline concept in geotectonics. *Royal Society of Tasmania Proceedings*, **89**, 255–288. 18

Carey, S.W. (1958). The tectonic approach to continental drift. In *Proceedings, Continental drift; A symposium, Hobart, March, 1956*, 177–355, University of Tasmania, Hobart. 18

Carter, C. & Laufield, S. (1975). Ordovician and Silurian fossils in well cores from North Slope of Alaska. *American Association of Petroleum Geologists Bulletin*, **59**, 457–464. 9

Cecile, M.P., Lane, L.S., Khudoley, A.K. & Kos'ko, M.K. (2001). Lower Paleozoic rocks around today's Arctic Ocean: two ancestral continents and associated plates: Alaskan rotation unnecessary and unlikely. *Polarforschung*, **69**, 235–241. 21

Colpron, M. & Nelson, J. (2009). A Palaeozoic Northwest Passage: incursion of Caledonian, Baltican and Siberian terranes into eastern Panthalassa, and the early evolution of the North American Cordillera. In *Geological Society, London, Special Publications*, vol. 318, 177–355. 177

Condie, K.C. & Rosen, O.M. (1994). Laurentia-Siberia connection revisited. *Geology*, **22**, 168–170. 6

Cumming, G. & Richards, J. (1975). Ore lead isotope ratios in a continously changing earth. *Earth and Planetary Science Letters*, **28**, 155–171. 42

Damaske, D. & Estrada, S. (2003). Volcanic rocks of northern Greenland and the adjacent Lincoln Sea. In *Fourth International Conference on Arctic Margins Abstracts, Dartmouth, Nova Scotia*, P–33. 16

Davies, G. & Nassichuk, W. (1991). Carboniferous and Permian history of the Sverdrup Basin, Arctic Islands. In H. Trettin, ed., *Geology of the Innutian Orogen and Arctic Platform of Canada and Greenland*, 343–368, Geological Survey of Canada. 47, 92

Deer, W.A., Howie, R.A. & Zussman, J. (1992). *An introduction to the rock forming minerals, second edition*. Prentice Hall. 30, 33, 34, 38, 39, 156

Dickinson, W.R. (1970). Interpreting detrital modes of greywackes and arkose. *Journal of Sedimentary Petrology*, **63**, 695–707. 28

Dickinson, W.R. & Suczek, C. (1979). Plate tectonics and Sandstone Compositions. *American Association of Petroleum Geologists Bulletin*, **63**, 2164–2182. 34, 35, 69, 70, 110, 152

Dietz, V. (1973). Experiments on the influence of transport on shape and roundness of heavy minerals. *Contributions to Sedimentology*, **1**, 103–125. 35

Doré, A.G. (1991). The structural foundation and evolution of Mesozoic seaways between Europe and the Arctic. *Palaeogeography, Palaeoclimatology, Palaeoecology*, **87**, 441–492. 9

Dorsey, R. (1988). Provenance evolution and unroofing history of a modern arc-continent collision: evidence from petrography of Plio-Pleistocene sandstones, Eastern Taiwan. *Journal of Sedimentary Petrology*, **58**, 208–218. 31

Eldholm, O., Karasik, A.M. & Reknes, P.A. (1990). The North American plate boundary. In A. Grantz, G.L. Johnson & J.F. Sweeney, eds., *The Arctic Ocean Region: The Geology of North America*, 171–184, Geological Society of America, Boulder, Colorado. 11

Embry, A. (1982). The Upper Triassic-Lower Jurassic Heiberg Deltaic Complex of the Sverdrup Basin. In A.F. Embry & H.R. Balkwill, eds., *Arctic Geology and Geophysics*, 189–217, Memoir of the Canadian Society of Petroleum Geologists, 8. 22, 63, 176

Embry, A. (1984). The Schei Point and Blaa Mountain Groups (Middle-Upper Triassic), Sverdrup Basin. *Current Research, Part B. Geological Survey of Canada, Paper*, **83-1B**, 327–336. 50, 58, 59

Embry, A. (1986). Stratigraphic subdivision of the Blind Fiord and Bjorne formations (Lower Triassic), Sverdrup Basin, Arctic Islands. *Current Research, Part B. Geological Survey of Canada, Paper*, **86-1B**, 329–340. 50, 58

Embry, A. (1989). Correlation of Upper Palaeozoic and Mesozoic Sequences between Svalbard, Canadian Arctic Archipelago and northern Alaska. In J.D. Collinson, ed., *Correlation in Hydrocarbon Exploration*, 89–98, Norwegian Petroleum Society, Graham and Trotman, London. 21, 22

Embry, A. (1990). Geological and geophysical evidence in support of anticlockwise rotation of northern Alaska. *Marine Geology*, **93**, 317–329. 18, 21

Embry, A. (1991a). Mesozoic history of the Arctic Islands. In H. Trettin, ed., *Geology of the Innutian Orogen and Arctic Platform of Canada and Greenland*, 371–433, Geological Survey of Canada. 44, 47, 49, 50, 51, 52, 58, 59, 92, 178

Embry, A. (1991b). Middle-Upper Devonian clastic wedge of the Arctic Islands. In H. Trettin, ed., *Geology of the Innutian Orogen and Arctic Platform of Canada and Greenland*, 369–434, Geological Survey of Canada. 44

Embry, A. (1992). Crockerland - the northwest source area for the Sverdrup Basin, Canadian Arctic Islands. In T.O. Vorren, E. Bergsager, Ø.A. Dahl-Stamnes, E. Holter, B. Johansen, E. Lie & T.B. Lund, eds., *Arctic Geology and Petroleum Potential*, 205–216, NPF Special Publication 2. 24, 26, 47, 49, 50, 52

Embry, A. & Osadetz, K.F. (1988). Stratigraphy and tectonic significance of Cretaceous volcanism in the Queen Elizabeth Islands, Canadian Arctic Archipelago. *Canadian Journal of Earth Sciences*, **25**, 1209–1219. 52

Finch, R. & Hanchar, J. (2003). Structure and Chemistry of Zircon and Zircon-Group Minerals. *Reviews in Mineralogy and Geochemistry*, **53**, 1–25. 42

Forsberg, R. & Kenyon, S. (2004). Gravity and geoid in the Arctic region - the Northern Polar gap now filled. In *Proceedings of the GOCE Workshop, ESA-ESRIN*. 14

Forsyth, D.A., a l'Huissier, P.M., Asudeh, I. & Green, A.G. (1986). Alpha Ridge and Iceland - products of the same plume? *Journal of Geodynamics*, **6**, 197–214. 15

Gee, D.G. & Pease, V.L. (2004). The Neoproterozoic Timanide Orogen of eastern Baltica: introduction. In D.G. Gee & V.L. Pease, eds., *The Neoproterozoic Timanide Orogen of Eastern Baltica*, 1–3, Geologoical Society, London, Memoirs, 30. 9, 93, 101, 170

Glebovsky, V.Y., Kovacs, L.C., Mashenkov, S.P. & Brozena, J.M. (2000). Joint compilation of Russian and US Navy Aeromagnetic data in the central Arctic seas. *Polarforschung*, **68**, 35–40. 11

Glodny, J., Pease, V., Montero, P., Austrheim, H. & Rusin, A. (2004). Protolith ages of eclogites, Marun-Keu Complex, Polar Urals, Russia: implications for the pre- and early Uralian evolution of the northeastern European continental margin. In D.G. Gee & V. Pease, eds., *The Neoproterozoic Timanide Orogen of Eastern Baltica*, 87–105, Geologoical Society, London, Memoirs, 30. 170

Gradstein, F.M., Ogg, J.G. & Smith, A.G. (2004). *A Geologic Time Scale 2004*. Cambridge University Press. 43

Grantz, A., May, S.D., Mullen, M.W., Gray, L.B., Lull, J.S., Clark, D.L. & Stevens, C.H. (1993). Northwind Ridge: A continental fragment isolated by Tertiary rifting in the Amerasia Basin, Arctic Ocean. In *Eos, transactions, American Geophysical Union 74*, 614. 17

Grantz, A., Clark, D.L., Phillips, R.L., Srivastava, S.P., Blome, C.D., Gray, L.B., Haga, H., Mamet, B.L., McIntyre, D.J., McNeil, D.H., Mickey, M.B., Mullen, M.W., Murchey, B.L., Ross, C.A., Stevens, C.H., Silberling, N.J., Wall, J.H. & Willard, D.A. (1998). Phanerozoic stratigraphy of Northwind Ridge, magnetic anomalies in the Canada Basin, and the geometry and timing of rifting in the Amerasia Basin, Arctic Ocean. *Geological Society of America Bulletin*, **110**, 801–820. 15, 17, 18

Grantz, A., Pease, V.L., Willard, D.A., Phillips, R.L. & Clark, D.L. (2001). Bedrock cores from 89° North: implications for the geologic framework and Neogene paleoceanography of Lomonosov Ridge and a tie to the Barents Shelf. *Bulletin of the Geological Society of America*, **113**, 1272–1281. 13, 15, 27

Grantz, A., Scott, R., Drachev, S., Moore, T. & Howard, J. (2009). Map showing the sedimentary successions of the Arctic region (58°-64° to 90°N) that may be prospective for hydrocarbons (GIS format with legend and explanatory notes). 1:6,760,000. AAPG (GIS UDRIL), Houston. 4, 99

Green, A.R., Kaplan, A.A. & Vierbuchen, R.C. (1984). The geological framework and hydrocarbon potential of sedimentary basins in northern seas. In *Proceedings of the Offshore Northern Seas Conference*, E/1/1–1.53, Stavanger. 16

Gudlaugsson, S.T., Faleide, J.I., Johansen, S.E. & Breivik, A.J. (1998). Late Palaeozoic structural development of the southwestern Barents Sea. *Marine and Petroleum Geology*, **15**, 73–102. 9

Halgedahl, S.L. & Jarrad, R.D. (1987). Paleomagnetism of the Kuparuk River Formation from oriented drill core - evidence for rotation of the Arctic Alaska plate. In I.L. Tailleur & P. Weimar, eds., *Alaskan North Slope Geology*, 581–620, Society of Economic Paleontologists/Alaska Geological Society, Bakersfield, California. 20

Hall, J.K. (1970). Arctic Ocean Geophysical Studies, the Alpha Cordillera and Mendeleyev Ridge. 15

Hamilton, W. (1967). Continental drift in the Arctic. In *Symposium on Continental Drift Abstracts, Montevideo, Uruguay, 16-19 October, 1967*, 192–193, Paris, UNESCO, International Union of Geological Sciences. 18

Hamilton, W. (1968). Continental drift in the Arctic. *Geological Society of America Special Paper*, **121**, 510. 18

Hamilton, W. (1970). The Uralides and the motion of the Russian and Siberian platforms. *Geological Society of America Bulletin*, **81**, 2553–2576. 10, 101

Harland, W.B. (1997). *The Geology of Svalbard*. Geological Society of London, Memoirs, 17. 26, 44

Harrison, J.C. (2005). Geological evolution of the Arctic. In M. Nuttall, ed., *Encyclopedia of the Arctic*, 711–722, Routledge, New York. 4, 5, 6, 7, 8, 11, 12, 97, 140, 173, 180, 184

Harrison, J.C., Hall, J.H., Brent, T.A., Poulton, T.P. & Davies, E.H. (1999). Rift-related structures in Jurassic and Lower Cretaceous strata near the Canadian polar margin, Yukon Territory, Northwest Territories, and Nunavut. *Geological Survey of Canada, Current Research*, **1999-E**, 47–58. 17

Hartley, A. & Otava, J. (2001). Sediment provenance and dispersal in a deep marine foreland basin: the Lower Carboniferous Culm Basin, Czech Republic. *Journal of the Geological Society of London*, **158**, 137–150. 38

Hawthorne, F. & Henry, D. (1999). Classification of the minerals of the tourmaline group. *European Journal of Mineralogy*, **11**, 201–215. 41

Henry, D.J. & Dutrow, B.L. (1992). Tourmaline in a low grade clastic metasedimentary rock: an example of the petrogenic potential of tourmaline. *Contributions to Mineralogy and Petrology*, **112**, 203–218. 41

Henry, D.J. & Guidotti, C.V. (1985). Tourmaline as a petrogenic indicator mineral: an example from the staurolite-grade metapelites of NW Maine. *American Mineralogist*, **70**, 1–15. 41, 83, 84, 85, 122, 123, 124, 125, 126, 160, 161, 162

Herron, E.M., Dewey, J.F. & Pitman, W.C.I. (1974). Plate tectonic model for the evolution of the Arctic. *Geology*, **2**, 377–380. 15, 21

Higgins, A.K., Soper, N.J. & Leslie, A.G. (2000). The Ellesmerian and Caledonian Orogenic Belts of Greenland. *Polarforschung*, **68**, 141–151. 9, 47

Hoffman, P.F. (1989). Precambrian geology and tectonic history of North America. In A.W. Bally & A.R. Palmer, eds., *The Geology of North America - An overview. Geology of North America, v. A*, 447–512, Geological Society of America. 92, 95

Hoskin, P. & Schaltegger, U. (2003). The Composition of Zircon and Igneous and Metamorphic Petrogenesis. *Reviews in Mineralogy and Geochemistry*, **53**, 27–62. 41

Hubbard, R.J., Edrich, S.P. & Rattey, R.P. (1987). Geological evolution and hydrocarbon habitat of the 'Arctic Alaska Microplate'. *Marine and Petroleum Geology*, **4**, 2–34. 17

Inger, S. & Scott, R. (1999). Tectonic evolution of the Taimyr Peninsula; field data and preliminary interpretations. CASP Report, Regional Arctic Project, no. 689. 145, 147, 150

Inger, S., Scott, R. & Golinko, B. (1999). Tectonic evolution of the Taimyr Peninsula, northern Russia: implications for Arctic continental assembly. *Journal of the Geological Society of London*, **156**, 1069–1072. 10, 44, 101, 143, 144, 145, 146

Jakobsson, M., Cherkis, N., Woodward, J., Macnab, R. & Coakley, B. (2000). New grid of Arctic bathymetry aids scientists and mapmakers. *EOS*, **81**, 89–96. 13, 14

Jakobsson, M., Macnab, R., Mayer, M., Anderson, R., Edwards, M., Hatzky, J., Schenke, H.W. & Johnson, P. (2008). An improved bathymetric portrayal of the Arctic Ocean: Implications for ocean modeling and geological, geophysical and oceanographic analyses. *Geophysical Research Letters*, **35**, L07602. 3, 5, 13, 46, 97, 99, 100, 140, 142, 173, 180, 184

Johnson, G.L., Pogrebitsky, Y. & Macnab, R. (1994). Arctic structural evolution: relationship to paleoceanography. *American Geophysical Union Geophysical Monographs*, **85**, 285–294. 16

Johnsson, M.J., Stallard, R.F. & Meade, R. (1988). First-cycle quartz arenites in the Orinoco River drainage basin, Venezuela and Columbia. *Journal of Geology*, **96**, 263–277. 33

Johnsson, M.J., Stallard, R.F. & Lundberg, N. (1991). Controls on the composition of fluvial sands from a tropical weathering environment: Sands of the Orinoco River basin, Venezuela and Columbia. *Geological Society of America Bulletin*, **103**, 1622–1647. 29

Jokat, W. (2003). Seismic investigations along the western sector of Alpha Ridge, Central Arctic Ocean. *Geophysical Journal International*, **152**, 185–201. 15

Jokat, W., Uenzelmann-Neben, G., Kristoffersen, Y. & Rasmussen, T.M. (1992). Lomonosov Ridge - a double sided continental margin. *Geology*, **20**, 887–890. 13, 15

Jokat, W., Weigelt, E., Kristoffersen, Y., Rasmussen, T.M. & Shone, T. (1995). New geophysical results from the south-western Eurasian Basin (Morris Jessup Rise, Gakkel Ridge, Yermak Plateau) and the Fram Strait. *Geophysical Journal International*, **123**, 601–610. 13, 15

Kaban'kov, V.Y., Andreeva, I.A., Grikurov, G.E., Ivanov, V.N., Petrova, V.I., Sergeev, M.B. & Zatzepin, E.N. (2003). Genesis of bottom sediments in the Amerasia Basin and their importance for identifying geotectonic nature of bathymetric highs in the central Arctic Ocean. In *Morphology and Geological Nature of Deep Seabed and Submarine Elevations in the Arctic Basin: Controversial Issues in Context of UNCLOS/Arcticle 76*, 13, Ministry of Natural Resourses of the Russian Federation, St. Petersburg. 16

Kaminsky, V.D., Poselov, V.A., Butsenko, V.V., Glebovsky, V.Y., Pavelenkin, A.D., Daragan-Suchov, Y.J. & Puselova, L.G. (2003). Geophysical study of main Arctic Ocean geological structures and validity of relevant geological hypotheses. In *Morphology and Geological Nature of Deep Seabed and Submarine Elevations in the Arctic Basin: Controversial Issues in Context of UNCLOS/Arcticle 76*, 3–4, Ministry of Natural Resourses of the Russian Federation, St. Petersburg. 16

Kamo, S.L., Czamanske, G.K. & Krogh, T.E. (1996). A minimum u-pb age for siberian flood basalt volcanism. *Geochimica et Cosmochimica Acta*, **60**, 3505–3311. 170

Kamo, S.L., Czamanske, G.K., Amelin, Y., Fedorenko, V.A., Davis, D.W. & Trofimov, V.R. (2003). Rapid eruption of Siberian flood-volcanic rocks and evidence for coincidence with the Permian-Triassic boundary and mass extinction at 251 Ma. *Earth and Planetary Science Letters*, **214**, 75–91. 10, 101

Karasik, A.M. (1968). Magnetic anomalies of the Gakkel Ridge and origin of the Eurasian subbasin of the Arctic Ocean. In *Geophysical methods of prospecting in the Arctic*, 8–25, NIIGA, Leningrad. 11

Kelly, S.R.A., Braham, B., Jolley, D.W., Smyth, H.R. & Scott, R.A. (2008). Mesozoic and Cenozoic biostratigraphic studies on samples collected during Sverdrup Basin fieldwork 2007 (Ellesmere and Axel Heiberg islands), Canadian Arctic Islands, CASP Report, 2006-2007 Arctic Research and Database Project, Module 10. 55, 58, 59, 61

King, E.R., Zietz, I. & Alldredge, L.R. (1966). Magnetic data on the structure of the central Arctic region. *Bulletin of the Geological Society of America*, **77**, 619–646. 16

Kirkland, C., Pease, V., Whitehouse, M.J. & Ineson, J. (2009). Provenance record from Mesoproterozoic-Cambrian sediments of Peary Land, North Greenland: Implications for the ice-covered shield and Laurentian palaeogography. *Precambrian Research*, **170**, 43–60. 95

Kos'ko, M.K., Cecile, M.P., Harrison, J.C., Ganelin, V.G., Khandoshko, N.V. & Lopatin, B.G. (1993). *Geology of Wrangel Island, between Chukchi and East Siberian seas, northeastern Russia*. Geological Survey of Canada Bulletin, 461. 9

Kristoffersen, Y. (1990). Eurasia Basin. In A. Grantz, G.L. Johnson & J.F. Sweeney, eds., *The Arctic Ocean Region: The Geology of North America*, 365–378, Geological Society of America, Boulder, Colorado. 11

Kristoffersen, Y. (2000). The Eurasia Basin: an update from a decade of geoscientific research. *Polarforschung*, **68**, 11–18. 11

Kuzmichev, A. & Pease, V. (2007). Siberian trap magmatism on the New Siberian Islands: constraints for Arctic Mesozoic plate tectonic reconstructions. *Journal of the Geological Society, London*, **164**, 959–968. 92, 146, 170, 171, 174

Lane, L.S. (1997). Canada Basin, Arctic Ocean: evidence against a rotational origin. *Tectonics*, **13**, 363–387. 21, 22, 23

Lawver, L.A. & Muller, R.D. (1994). Iceland hotspot track. *Geology*, **22**, 311–314. 15, 16

Lawver, L.A., Grantz, A. & Meinke, L. (1984). The tectonics of the Arctic Ocean. In I. Dyer & C. Chryssostomos, eds., *Arctic Technology and Policy: an Assessment and Review for the Next Decade*, 147–158, Hemisphere, New York. 15

Lawver, L.A., Muller, R.D., Srivastava, S.P. & Roest, W.R. (1990). The opening of the Arctic Ocean. In U. Bleil & J. Thiede, eds., *Geological History of the Polar Oceans: Arctic Versus Antarctic*, 29–62, Dordrecht, Kluwer. 4, 15, 179, 188

Lawver, L.A., Grantz, A. & Gahagan, L.M. (2002). Plate kinematic evolution of the present Arctic region since the Ordovician. *Special Papers of the Geological Society of America*, **360**, 333–358. 9, 10, 11, 15, 16, 101

Laxon, S. & McAdoo, D. (1994). Arctic Ocean gravity field derived from ERS-1 satellite altimetry. *Science*, **265**, 621–624. 17, 18, 20

Lebedeva-Ivanova, N.N., Zamansky, Y.Y., Langinen, A.E. & Sergeyev, M.B. (2003). A seismic model of the Earth's crust along the 'East-Siberian Continental Margin - Podvodnikov Basin - Arlis Rise' geotraverse. In *Fourth International Conference on Arctic Margins Abstracts, Dartmouth, Nova Scotia*, P–20. 15

Li, Z.X., Bogdanova, S.V., Collins, A.S., Davidson, A., Waele, B.D., Ernst, R.E., Fitzsimons, I.C.W., Fuck, R.A., Gladkochub, D.P., Jacobs, J., Karlstrom, K.E., Lu, S., Natapov, L.M., Pease, V., Pisarevsky, S.A., Thrane, K. & Vernikovsky, V. (2008). Assembly, configuration, and break-up history of Rodinia: A synthesis. *Precambrian Research*, **160**, 179–210. 6, 7, 170

Lorenz, H., Gee, D. & Whitehouse, M. (2007). New geochronological data on Palaeozoic igneous activity and deformation in the Severnaya Zemlya Archpelago, Russia, and implications for the development of the Eurasian Arctic margin. *Geological Magazine*, **144**, 105–125. 93, 146

Ludwig, K. (2003). Isoplot 3.00 - A Geochronological Toolkit for Microsoft Excel. Berkeley Geochronological Center. 42

Lundshein, B., Høy, T., Riis, F., Mørk, A. & Mørk, M.B. (2008). Middle and Late Triassic Palaeogeography of the western Barents Sea and Svalbard based on new data from the northern Barents Sea. In *33rd International Geological Conference Abstracts, Oslo, Norway*, 1–1. 93

Maher, H.D. (2001). Manifestations of the Cretaceous high Arctic large igneous province in Svalbard. *Journal of Geology*, **109**, 91–104. 12, 13, 16, 103, 105, 138

Mange, M. & Maurer, F. (1992). *Heavy Minerals in Colour*. Chapman and Hall, London. 35

Mange, M.A. & Morton, A.C. (2007). Geochemistry of heavy minerals. In A. van Loon, ed., *Developments in Sedimentology, 58, Heavy minerals in Use*, 345–392, Elsevier. 38

Mayr, U., Beauchamp, B., Embry, A.F. & Harrison, J.C. (2002). Geology of Upper Paleozoic and Mesozoic formations of northern Axel Heiberg Island, parts of NTS 560D, Cape Stallworthy and 560A, Bukken Fiord, Nunavut. 48, 54, 55, 59, 61

McKerrow, W.S., MacNiocaill, C. & Dewey, J.F. (2000). The Caledonian Orogeny redefined. *Journal of the Geological Society of London*, **157**, 1149–1154. 9, 10

McNicoll, V.J., Harrison, J.C., Trettin, H.P. & Thorsteinsson, R. (1995). Provenance of the Devonian clastic wedge of Arctic Canada: evidence provided by detrital zircon ages. *SEPM Special Publication*, **52**, 77–93. 27, 95, 137, 177, 178

Miller, E.L., Toro, J., Gehrels, G., Amato, J.A., Prokopiev, A., Tuchkova, A.I., Akinin, V.V., Dumitru, T.A., Moore, T.E. & Cecile, M.P. (2006). New insights into Arctic paleogeography and tectonics from U-Pb detrital zircon geochronology. *Tectonics*, **25**, TC3013. 19, 22, 27, 93, 94, 95, 176, 178, 187, 188

Moore, T.E., Wallace, W.K., Bird, K.J., Karl, S.M., Mull, C.G. & Dillon, J.T. (1994). Geology of northern Alaska. In G. Plafker & H.C. Berg, eds., *The Geology of Alaska, The Geology of North America G-1*, 535–554, Geological Society of America, Boulder, Colorado. 9, 21

Mørk, A., Dallmann, W., Dypvik, H., Johannessen, E., Larssen, G., Nagy, J., Nøttvedt, A., Olaussen, S., Pčelina, T. & Worsley, D. (1999). Mesozoic Lithostratigraphy. In W. Dallmann, ed., *A Lithostratigraphic Lexicon for Svalbard*, 127–214. 27, 101, 102, 103, 104, 105, 106, 137, 138, 177

Mørk, M.B.E. (1999). Compositional variations and provenance of Triassic sandstones from the Barents Shelf. *Journal of Sedimentary Research*, **69**, 690–710. 38

Morton, A.C. (1984). Stability of detrital heavy minerals in Tertiary sandstones of the North Sea Basin. *Clay Mineralogy*, **19**, 287–308. 36, 38, 39

Morton, A.C. (1985). A new approach to provenance studies: electron microprobe analysis of detrital garnets from Middle Jurassic sandstones of the northern North Sea. *Sedimentology*, **32**, 553–566. 37, 38

Morton, A.C. & Hallsworth, C.R. (1994). Identifying provenance-specific features of detrital heavy mineral assemblages in sandstones. *Sedimentary Geology*, **90**, 241–256. 30, 37

Morton, A.C. & Hallsworth, C.R. (1999). Processes controlling the composition of heavy mineral assemblages in sandstones. *Sedimentary Geology*, **124**, 3–29. 29, 35, 36, 42

Morton, A.C. & Hallsworth, C.R. (2007). Stability of detrital heavy minerals during burial diagenesis. In A. van Loon, ed., *Developments in Sedimentology, 58, Heavy minerals in Use*, 215–245, Elsevier. 29, 36, 37, 38, 39

Morton, A.C. & Smale, D. (1991). The effects of transport and weathering on heavy minerals from the Cascade River, New Zealand. *Sedimentary Geology*, **68**, 117–123. 35

Morton, A.C., Hallsworth, C.R. & Chalton, B. (2004). Garnet compositions in Scottish and Norwegian basement terranes: a framework for interpretation of North Sea sandstone provenance. *Marine and Petroleum Geology*, **21**, 393–410. 38, 39, 40, 82, 91, 120, 121, 159

Natapov, L.M., Paraketsov, K.V., Kulikova, L.I. & Kononov, M.N. (1997). Jurassic-Cretaceous tectonostratigraphy of northern Russia. CASP Report, Arctic and Russian Studies, Regional Arctic Project, 663. 146, 150

Nøttvedt, A., Cecchi, M., Gjelberg, J., Kristensen, S., Lønøy, A., Rasmussen, A., Rasmussen, E., Skott, P. & van Veen, P. (1992). Svalbard-Barents Sea correlation: a short review. In T.O. Vorren, E. Bergsager, Ø.A. Dahl-Stamnes, E. Holter, B. Johansen, E. Lie & T.B. Lund, eds., *Arctic Geology and Petroleum Potential*, 363–375, NPF Special Publication 2. 137

Nutman, A.P., McGregor, V.R., Friend, C.R.L., Bennett, V.C. & Kinnyd, P.D. (1996). The Itsaq Gneiss Complex of southern West Greenland; the world's most extensive record of early crustal evolution (3900-3600 Ma). *Precambrian Research*, **78**, 1–39. 6

Okulitch, A. & Trettin, H. (1991). Late Cretaceous- Early Tertiary Deformation, Arctic Islands. In H. Trettin, ed., *Geology of the Innutian Orogen and Arctic Platform of Canada and Greenland*, 469–489, Geological Survey of Canada. 49

Ostenso, N.A. & Wold, R.J. (1971). A seismic and gravity profile across the Arctic Ocean Basin. *Tectonophysics*, **37**, 1–24. 15

Parker, J.R. (1966). *The Mesozoic History of Central Vestspitzbergen*. Ph.D. thesis, University of Cambridge. 106, 107

Patchett, P.J., Embry, A.F., Ross, G.M., Beauchamp, B., Harrison, J.C., Mayr, U., Isachsen, C.E., Rosenberg, E.J. & Spence, G.O. (2004). Sedimentary Cover of the Canadian Shield through Mesozoic Time Reflected by Nd Isotopic and Geochemical Results for the Sverdrup Basin, Arctic Canada. *The Journal of Geology*, **112**, 39–57. 49

Pearce, N., Perkins, W., Westgate, J., Gordon, M., Jackson, S., Neal, C. & Chenery, S. (1997). A compilation of new and published major and trace element data for NIST SRM 610 and NIST SRM 612 glass reference materials. *Geostandards Newsletter*, **21**, 115–144. 42

Pease, V. (2001). East European Craton Margin source for the allochthonous northern terrane of Taimyr, Arctic Siberia. *EOS Transaction AGU*, **82**, F1181. 92, 93, 145, 146, 169, 170

Pease, V. & Persson, S. (2006). Neoproterozoic island arc magmatism of northern Taimyr. In R. Scott & D. Thurston, eds., *Proceedings of the Fourth International Conference on Arctic Margins*, 31–49, US Department of the Interior, Minerals Management Service. 169

Pease, V. & Scott, R.A. (2009). Crustal affinities in the Arctic Uralides, northern Russia: significance of detrital zircon ages from Neoproterozoic and Palaeozoic sediments in Novaya Zemlya and Taimyr. *Journal of the Geological Survey of London*, **166**, 1–10. 93, 143, 145, 170, 172

Pettijohn, F., Potter, P. & Siever, R. (1987). *Sand and Sandstone*. Springer-Verlag, New York. 34, 66, 107, 151

Plafker, G. & Berg, H.C. (1994). Overview of the geology and tectonic evolution of Alaska. In G. Plafker & H.C. Berg, eds., *The Geology of Alaska, The Geology of North America G-1*, 989–1021, Geological Society of America, Boulder, Colorado. 11, 12

Rainbird, R., Heaman, L.M. & Young, G.M. (1992). Sampling Laurentia; detrital zircon geochronology offers evidence for an extensive Neoproterozoic river system originating from the Grenville Orogen. *Geology*, **20**, 351–354. 95

Reichow, M., Pringle, M., Al'Mukhamedov, A., Allen, M., Andreichev, V., Buslov, M., Davies, C., Fedoseev, G., Fitton, J., Inger, S., Medvedev, A., Mitchell, C., Puchov, V., Safonova, I., Scott, R. & Saunders, A. (2009). The timing and extent of the eruption of the Siberian Trap Large Igneous Province: implications for the end-Permian environmental crisis. *Earth and Planetary Science Letters*, **277**, 9–20. 10, 93, 101, 143, 146

Ricketts, B., Osadetz, K.G. & Embry, A. (1984). Volcanic style in the Strand Fiord Formation (Upper Cretaceous), Axel Heiberg Island, Canadian Arctic Archipelago. *Norsk Polarinstitutt*, 107–122. 63

Rivers, T. (1997). Lithotectonic elements of the Grenville Province: review and tectonic implications. *Precambrian Research*, **86**, 117–154. 6, 92, 94, 170

Roberts, D. (2003). The Scandinavian Caledonides: event chronology, palaeogeographic settings and likely modern analogues. *Tectonophysics*, **365**, 283–299. 93, 94

Roest, W.R. & Srivastava, S.P. (1991). Kinematics of the plate boundaries between Eurasia, Iberia and Africa in the north Atlantic from the Late Cretaceous to the Present. *Geology*, **19**, 613–616. 22

Røhr, T.S., Andersen, T. & Dypvik, H. (2008). Provenance of Lower Cretaceous sediments in the Wandel Sea Basin, North Greenland. *Journal of the Geological Society of London*, **165**, 755–767. 27, 178, 187, 188

Rubey, W. (1933). The size distribution of heavy minerals within a water-lain sandstone. *Journal of Sedimentary Petrology*, **3**, 3–29. 29, 35

Savage, K. & Potter, P. (1991). Petrology of modern sands of the Rios Guaviare and Inirida, Southern Columbia: tropical climate and sand composition. *Journal of Geology*, **99**, 289–298. 29

Savage, K., Cesero, P.D. & Potter, P. (1988). Mineralogical maturity of modern sand along a high energy tropical coast; Brixada de Jacarepagua, Rio de Janeiro, Brazil. *Journal of South American Earth Sciences*, **1**, 317–328. 29

Scarrow, J., Hetzel, R., Gorozhanin, V., Dinn, M., Glodny, J., Gerdes, A., Ayala, C. & Montero, P. (2002). Four decades of geochronological work in the Southern and Middle Urals: A Review. In D. Brown, C. Juhlin & V. Puchkov, eds., *Mountain Building in the Uralides: Pangea to the Present, American Geophysical Union Geophysical Monograph 132*, 233–255, Geological Society of America, Boulder, Colorado. 92, 93, 94, 136

Scott, R.A., Sample, J. & Sinclair, S. (2004). Opening of the Arctic Ocean. CASP Report, GIS Database of Arctic Tectonics and Stratigraphy, Module 2. 11, 12, 14, 15, 16, 18

Sears, J.W. & Price, R.A. (2003). Tightening the Siberian connection to western Laurentia. *Geological Society of America Bulletin*, **115**, 943–953. 6

Siedlecka, A., Roberts, D., Nystuen, J.P. & Olovyanishnikov, V.G. (2004). Northeastern and northwestern margins of Baltica in Neoproterozoic time: evidence from the Timanian and Caledonian Orogens. In D.G. Gee & V.L. Pease, eds., *The Neoproterozoic Timanide Orogen of Eastern Baltica*, 169–190, Geologoical Society of London, Memoirs, 30. 7, 101

Sircombe, K.N. (2004). AgeDisplay: an EXCEL workbook to evaluate and display univariate geochronological data using binned frequency histograms and probability density distributions. *Computers and Geoscience*, **30**, 21–31. 42

Sláma, J., Košler, J., Condon, D., Crowley, J., Gerdes, A., Hanchar, J., Horstwood, M., Morris, G., Nasdala, L., Norberg, N., Schaltegger, U., Schoene, B., Tubrett, M. & Whitehouse, M. (2008). Plešovice zircon - A new natural reference material for U-Pb and Hf isotopic microanalysis. *Chemical Geology*, **249**, 1–35. 42

Smyth, H., Hall, R. & Nichols, G. (2008). Significant volcanic contribution to some quartz-rich sandstones, East Java, Indonesia. *Journal of Sedimentary Research*, **78**, 335–356. 30, 32, 150

Stacey, J. & Kramers, J. (1975). Approximation of terrestrial lead isotope evolution by a two-stage model. *Earth and Planetary Science Letters*, **26**, 207–221. 42

Steiger, R. & Jäger, E. (1977). Subcommission on geochronology: convention on the use of decay constants in geo- and cosmochronology. *Earth and Planetary Science Letters*, **36**, 359–362. 42

Sweeney, J.F. (1990). Eurasia Basin. In M.W. McElhinny & D.A. Valencio, eds., *Geodynamic Series, Paleoreconstruction of continents*, 55–64, American Geophysical Union and Geological Society of America, Washington D. C. and Boulder Colorado. 16

Tailleur, I.L. (1973). Probable rift origin of Canada Basin, Arctic Ocean. *Memoirs of the American Association of Petroleum Geologists*, **19**, 526–535. 18, 22

Takeuchi, M. (1994). Changes in garnet chemistry show a progressive denudation of the source areas for Permian-Jurassic sandstones, southern Kitakami Terrane, Japan. *Sedimentary Geology*, **93**, 85–105. 38

Tarduno, J.A. (1998). The high Arctic large igneous province. In *Third International Conference on Arctic Margins Abstracts, Celle, Germany*. 12

Tarduno, J.A. (2003). Multidisciplinary studies of Cretaceous sequences on Axel Heiberg and Ellesmere Islands: implications for the geodynamics and magmatism of the Amerasian Basin. In *Fourth International Conference on Arctic Margins Abstracts, Dartmouth, Nova Scotia*, 46. 16

Thiel, G. (1940). The relative resistance to abration of mineral grains of sand size. *Journal of Sedimentary Petrology*, **10**, 103–124. 35

Thiel, G. (1945). Mechanical effects of stream transportation in mineral grains of sand size. *AAPG Bulletin*, **56**, 1207. 35

Thorsteinsson, R. & Tozer, E.T. (1970). Geology of the Arctic Archipelago. In R.J.W. Douglas, ed., *Geology and Economic Minerals of Canada, Geological Survey of Canada Economic Geological Report vol 1*, 547–590, Geological Survey of Canada. 9, 13, 47

Torsvik, T. & Andersen, T. (2002). The Taimyr fold belt, Arctic Siberia: timing of prefold remagnetisation and regional tectonics. *Tectonophysics*, **352**, 335–348. 143

Trettin, H.P. (1991). Late Silurian-Early Devonian deformation, metamorphism and granitic plutonism, Northern Ellesmere and Axel Heiberg Islands. In H.P. Trettin, ed., *Geology of the Innutian Orogen of Arctic Platform of Canada and Greenland*, 295–320, Geological Society of America, Boulder, Colorado. 9, 10, 13, 21, 50

Turner, G. & Morton, A.C. (2007). The effects of burial diagenesis on detrital heavy mineral grain surface textures. In A. van Loon, ed., *Developments in Sedimentology, 58, Heavy minerals in Use*, 393–412, Elsevier. 39

Uflyand, A., Natapov, L., Lopatin, V. & Chernov, D. (1991). To the Taimyr tectonic nature (in Russian). *Geotektonika*, **6**, 76–93. 143

van Andel, T.H. (1950). *Provenance, Transport and Deposition of Rhine Sediments*. Veenman, Wageningen. 29, 35

van Andel, T.H. (1959). Reflections on the interpretation of heavy mineral analyses. *Journal of Sedimentary Petrology*, **29**, 153–163. 29, 35

Vernikovskaya, V.V.A. (2001). Central Taimyr accretionary belt (Arctic Asia): Meso-Neoproterozoic tectonic evolution and Rodinia breakup. *Precambrian Research*, **110**, 127–141. 169

Vernikovsky, V., Neimark, L., Ponomarchuk, V., Vernikovskaya, A., Kireev, A. & Kuzmin, D. (1995). Geochemistry and age of collision granitoids and metamorphites of the Kara microcontinent (Northern Taimyr). *Russian Geology and Geophysics*, **36**, 46–60. 92, 142, 143, 145, 146, 169, 170

Vernikovsky, V., Pease, V., Vernikovskaya, A., Romanov, A., Gee, D. & Travin, A. (2003). First report of early Triassic A-type granite and syenite intrusions from Taimyr: product of the northern Eurasian superplume? *Lithos*, **66**, 23–36. 93, 143, 146, 171, 174

Villeneuve, M. & Williamson, M.C. (2003). ^{40}Ar-^{39}Ar dating of mafic magmatism from the Sverdrup Basin Magmatic Province. In *Fourth International Conference on Arctic Margins Abstracts, Dartmouth, Nova Scotia*, 45–46. 16

Villeneuve, M. & Williamson, M.C. (2006). ^{40}Ar-^{39}Ar dating of mafic magmatism from the Sverdrup Basin magmatic province. In D. Thurston & R. Scott, eds., *Fourth International Conference on Arctic Margins, Darthmouth, Nova Scotia, Canada*, 206–215, Mineral Management Service, United States Department of the Interior. 49, 51

Vogt, P.R. & Ostenso, N.A. (1970). Magnetic and gravity profiles across the Alpha Cordillera and their relation to Arctic sea-floor spreading. *Journal of Geophysical Research*, **75**, 4925–4937. 15

Vogt, P.R., Kovacs, L.C., Johnson, G.L. & Feden, R.H. (1979a). The evolution of the Arctic Ocean with emphasis on the Eurasia Basin. In *Proceedings of the Norwegian Sea Symposium*, 1–29, Norwegian Petroleum Society, Oslo. 11

Vogt, P.R., Taylor, P.T., Kovacs, L.C. & Johnson, G.L. (1979b). Detailed aeromagnetic investigation of the Arctic Basin. *Journal of Geophysical Research*, **84**, 1971–1089. 15

Walderhaug, H.J., Eide, E.A., Scott, R.A., Inger, S. & Golinko, E.G. (2005). Palaeomagnetism and ^{40}Ar-^{39}Ar geochronology from the South Taimyr igneous complex, Arctic Russia: a Middle-Late Triassic magmatic pulse after Siberian flood-basalt volcanism. *Geophysics Journal International*, **163**, 501–517. 143, 146

Weber, J.R. & Sweeney, J.F. (1990). Ridges and basins in the central Arctic Ocean. In A. Grantz, G.L. Johnson & J.F. Sweeney, eds., *The Arctic Ocean Region: The Geology of North America*, 305–336, Geological Society of America, Boulder, Colorado. 15, 16

Whitehouse, M.J. & Kamber, B. (2005). Assigning Dates to Thin Gneissic Veins in High-Grade Metamorphic Terranes: A Cautionary Tale from Akilia, Southwest Greenland. *Journal of Petrology*, **46**, 291–318. 42

Whitehouse, M.J., Kamber, B. & Moorbath, S. (1999). Age significance of U-Th-Pb zircon data from early Archaean rocks of west Greenland - a reassessment based on combined ion-microprobe and imaging studies. *Chemical Geology*, **160**, 201–224. 42

Wiedenbeck, M., Allé, P., Corfu, F., Griffin, W., Meier, M., Oberli, F., von Quadt, A., Roddick, J. & Spiegel, W. (1995). Three natural zircon standards for U-Th-Pb, Lu-Hf, trace elements and REE analysis. *Geostandards Newsletter*, **19**, 1–23. 42

Zamanskii, Y.Y., Ivanova, N.N., Langinen, A.E. & Sorokin, M.Y. (2003). Seismic studies on the Arktida-2000 geotraverse. *Investiya Physics of Solid Earth*, **39**, 453–463. 16

Zatzepin, E.N., Zamansky, Y.Y., Ivanova, N., Kaminsky, V.D., Pavlenik, A.D. & Poselov, V.A. (2003). Crustal structure of the Mendeleev Rise from results of Russian investigations. In *Morphology and Geological Nature of Deep Seabed and Submarine Elevations in the Arctic Basin: Controversial Issues in Context of UNCLOS/Arcticle 76*, 23–24, Ministry of Natural Resourses of the Russian Federation, St. Petersburg. 16

Ziegler, P.A. (1988). Evolution of the Arctic-North Atlantic and the Western Tethys. *American Association of Petroleum Geologists Memoir*, **43**, 1–193. 9, 10

Ziegler, P.A. (1989). *Evolution of Laurussia*. Kluwer Academic Publishers, Dordrecht, Netherlands. 9, 10

Zonenshain, L.P. & Natapov, L.M. (1987). Tectonic History of the Arctic. In Y.M. Pusharovsky, ed., *Actual Problems of the Tectonics of the Oceans and Continents*, 31–57 (in Russian), Nauka, Moscow. 22, 25

Zonenshain, L.P. & Natapov, L.M. (1989). Tectonic History of the Arctic Region from the Ordovician through the Cretaceous. In Y. Harman, ed., *The Arctic Seas, Climatology, Oceanography, Geology and Biology*, 829–862, Van Nostrand Reinhold Company, New York. 22, 25, 143

Zonenshain, L.P., Korinevsky, V.G., Kazmin, V.G., Pechevsky, D.M., Khain, V.V. & Matveenkov, V.V. (1984). Plate tectonic model of the South Urals development. *Tectonophysics*, **109**, 95–135. 10, 101

Zonenshain, L.P., Kuzmin, M.I. & Natapov, L.M. (1990). *Geology of the USSR: a plate tectonic synthesis*. American Geophysical Union, Washington D. C. 7, 16